Award Number: W81XWH-13-1-0016

TITLE: Underbody Blast Models of TBI Caused by Hyper- Acceleration and Secondary Head Impact

PRINCIPAL INVESTIGATOR: Dr. Gary Fiskum

CONTRACTING ORGANIZATION: University of Maryland
Baltimore, MD 21201

REPORT DATE: February 2016

TYPE OF REPORT: Annual

PREPARED FOR: U.S. Army Medical Research and Materiel Command
Fort Detrick, Maryland 21702-5012

REPORT DOCUMENTATION PAGE

Form Approved
OMB No. 0704-0188

1. REPORT DATE *(DD-MM-YYYY)*	**2. REPORT TYPE**	**3. DATES COVERED** *(From - To)*
February 2016	Annual	6Jan2015 - 5Jan2016

4. TITLE AND SUBTITLE

Underbody Blast Models of TBI Caused by Hyper-Acceleration and Secondary Head Impact

5a. CONTRACT NUMBER
W81XWH-13-1-0016

5b. GRANT NUMBER
PT110675

5c. PROGRAM ELEMENT NUMBER

6. AUTHOR(S)
Dr. Gary Fiskum

Dr. William Fourney

email: gfiskum@anes.umm.edu

5d. PROJECT NUMBER
0010224806

5e. TASK NUMBER

5f. WORK UNIT NUMBER

7. PERFORMING ORGANIZATION NAME(S) AND ADDRESS(ES)

University of Maryland
620 W. Lexington Street, 4D02
Baltimore, MD 21201

8. PERFORMING ORGANIZATION REPORT NUMBER

9. SPONSORING / MONITORING AGENCY NAME(S) AND ADDRESS(ES)
U.S. Army Medical Research and Materiel Command
Fort Detrick, Maryland 21702-5012

10. SPONSOR/MONITOR'S ACRONYM(S)

11. SPONSOR/MONITOR'S REPORT NUMBER(S)

12. DISTRIBUTION / AVAILABILITY STATEMENT

Approved for Public Release; Distribution Unlimited

13. SUPPLEMENTARY NOTES

14. ABSTRACT

There is a high incidence of TBI among warfighter occupants of vehicles targeted by underbody blasts but little is known about the unique forces involved or the pathophysiology.

We hypothesize:

- Acceleration experienced during survivable underbody blasts produces dose-dependent, TBI.
- Underbody blast-induced acceleration combined with secondary head impact is also military relevant and can be modeled.
- Neurologic outcome following underbody blast-induced TBI can be improved by force-modifying vehicle hull desig
- We will expand our underbody blast animal model of TBI to establish full dose-response relationships and to model the combination of acceleration plus head impact. This research will promote development of engineering- and biomedical-based neuroprotective interventions translatable to warfighter TBI.

15. SUBJECT TERMS					
Nothing listed					
16. SECURITY CLASSIFICATION OF:			17. LIMITATION OF ABSTRACT	18. NUMBER OF PAGES	19a. NAME OF RESPONSIBLE PERSO USAMRMC
a. REPORT	b. ABSTRACT	c. THIS PAGE			19b. TELEPHONE NUMBER *(include are code)*
U	U	U	UU	175	

Standard Form 298 (Rev. 8-98)
Prescribed by ANSI Std. Z39.18

INTRODUCTION:

There is a high incidence of TBI among warfighter occupants of vehicles targeted by underbody blasts but little is known about the unique forces involved or the pathophysiology. Our goal is to utilize small animal modeling of brain injury caused by underbody blasts to understand the pathophysiology of this uniquely military relevant form of TBI. Through this understanding, we aim to develop engineering- and biomedical-based neuroprotective interventions translatable to warfighter TBI.

Anesthetized and conscious animals have been used in experiments where the peak vertical acceleration elicited by an underbody blast varied between approximately 20 and 2800 Gs. Rats will be used in additional experiments combining blast-induced acceleration with the Tortella TBI model of projectile concussive impact (Ann Biomed Eng. 2014 Aug;42(8):1618-30; See Appendix 1). This combined model of acceleration and impact is unique but a better model of what occurs to occupants of vehicles targeted by IEDs than either model alone.

Comprehensive histopathology are being performed at 2 hr to 30 days after these blasts ± impact to provide spatiotemporal quantification of diffuse axonal injury, vascular damage, cellular inflammatory responses, cell death, and neurologic outcome that are necessary for understanding and mitigating underbody blast TBI.

We have also made substantial progress demonstrating that survival can be improved by modification to vehicle hull designs, including the use of hull materials that reduce the rate and extent of blast-induced acceleration.

BODY:

ALL PROGRESS IS LISTED UNDER ORIGINAL SOW TECHNICAL REQUIREMENTS AND IS BOLDED AND ITALICISED

1. Statement of Work

1.0 Introduction: The principal purpose of this agreement is to expand development of our novel, small animal model of TBI induced by the hyperacceleration associated with underbody blasts, with the long-term goal of supporting improved primary and secondary preventive strategies. All animal experiments and animal outcome measurements work will be carried out at University of Maryland School of Medicine. Experimental vehicle hull design and construction will be conducted at the University of Maryland School of Engineering.

1.1 Summary of Specific Aims/Objectives:

1.1.1. Establish dose-dependent relationships between G-force/JERK, neuronal/axonal injury, neurochemical alterations, and inflammation in different brain regions at different times after the underbody blast in the absence and presence of secondary head impact.

1.1.2. Eludicate the neurobehavioral alterations that occur after underbody blasts and establish their temporal relationships with the nature and extent of neuropathology present in different brain regions.

1.1.3. Determine if alterations in vehicle hull design, particularly those that reduce both maximal G-force and JERK, reduce histologic, neurochemical, or behavioral indices of brain injury.

2.0 Technical Requirements:

2.1. Quantify physiologic, neurochemical, and neuro-histopathologic TBI outcomes after exposure of rats to underbody blast-induced hyperacceleration. Compare these outcomes to direct measurements of acceleration (G-force) and acceleration rate (JERK) to determine minimal and maximal survivable loads associated with TBI, to establish dose-dependence relationships, and to identify the neurobiologic alterations most closely linked with the pathophysiology of this form of TBI. (Aligned with Objective 1)

2.1.1. Expose anesthetized test animals (rats) to defined degrees of blast-associated acceleration forces while secured on a metal structure that simulates a closed armored vehicle.

Approximately 65 ketamine-anesthetized rats have been subjected to underbody blasts resulting in peak vertical accelerations ranging from 100 G to 2800 G. All rats survived blasts ranging from 100 to 2000 Gs. Five of six rats exposed to 2800 G died immediately or within 30 min post-blast. .

2.1.2 Utilize a subset of animals for MRI and MRS measurements performed at one day prior to blast exposure (baseline) and again at several times post-blast.

Eight of the rats exposed to approximately 2000 G (1734 ± 90G) underbody blast were used for MRI/MRS measurements performed at baseline (one day prior to blast), and 2 hr, 24 hr and 7 days post-blast. Results obtained from diffusion tensor imaging (DTI) and magnetic resonance spectroscopy (MRS) are provided in the manuscript included as Appendix 2. Mean diffusivity of water was reduced at 2 hr post-blast in the hippocampus at 2 hr and 7 days and in the thalamus at 2 hr post-blast (Manuscript Table 1 and Fig. 2). Axial diffusivity was also reduced at both 24 hr and 7 days in the hippocampus and at in the internal capsule at 24 hr (Table 1 and Fig. 3 and 4). These changes could represent intraxonal molecular alterations which are consistent with the silver staining observed in the internal capsule of animals subjected to underbody blasts (Proctor et al., 2014; J Trauma Acute Care Surgery Sep;77(3 Suppl 2):S83-7)Appendix 3). MRS measurements of glutamate plus glutamine indicate a significant reduction in these metabolites in the cerebral cortex at both 2 hr and 7 days post-blast. These changes could represent metabolic alterations in either neurons or astrocytes since most glutamate is present in neurons and most glutamine is in astrocytes. The

significance of these results is that they provide evidence from non-invasive measurements that exposure of rats to underbody blasts results in both neurochemical and physiological abnormalities.

2.1.3. Euthanize anesthetized rats by perfusion fixation within 2 hr after blast exposure, remove brains, and process for electron microscopic analysis of cyto- and axonal ultrastructure and for histochemical evidence of acute neurochemical and neuroanatomic alterations.

Four ketamine-anesthetized rats exposed to 700G blast were perfusion fixed at 20 min post-blast and their brains processed for electron microscopy. We obtained quantitative evidence for perivascular swelling of astrocyte end-feet and swelling of vascular endothelial cells at 2 hr post-blast compared to 2 hr following sham blast (anesthesia alone). See Appendix 4.

2.1.4 Euthanize anesthetized rats by perfusion fixation at < 2hr and 24 hr, and at 7 and 30 days post-blast, and process brains for quantitative histochemical and biochemical evidence of subacute and chronic neurochemical and neuroanatomic alterations.

Qualitative findings obtained at relatively low G forces (30 – 50G) were reported earlier and are described in our manuscript that followed our invited presentation at the 2013 MHSRS meeting. See Appendix 3; Proctor et al (2014), J Trauma Acute Care Surgery Sep;77(3 Suppl 2):S83-7). The conclusions reported in this study are that 50G blast exposure results in axonal injury in the internal capsule and cerebellum that is evident at 7 days post injury. Exposure to this low level of blast-induced acceleration also results in astrocyte activation in the internal capsule and hypothalamus. No neuronal cell death was observed at 7 days post-blast, based upon lack of tissue staining with FluoroJade B.

We then embarked on a series of G-force dose escalation experiments. Results obtained from anesthetized rats subjected to underbody blasts of ≥ 100G are summarized here, accompanied by individual figures present in the Appendix. Rats were perfusion fixed at 2 and 24 hr post-blast and at 7 and 30 days post-blast. There was a significant increase in silver staining (de Olmos method) of axon fibers present in the internal capsule of rats 7 days following exposure to 100 and 700 G underbody blasts, compared to ketamine-anesthetized shams (Appendix 5). There was also a significant difference between axonal injury in the internal capsule of rats subjected to 700 Gs compared to 100 Gs or to shams. Immunohistochemistry for immunoglobulin G was used as a measure of blood-brain barrier (BBB) disruption since normally IgG is present at only very low levels within the brain parenchyma of sham animals with an intact BBB. A significant increase was observed in cerebral cortex following 100 G underbody and 700G blasts, with 700G blasts resulting in greatest IgG immunostaining (Appendix 6).

We also conducted preliminary gene expression assays on RNA extracted from the hippocampus at 24 hr following exposure to only 100G blasts. RNA was amplified and biotin labeled using the two-cycle target labeling kit (Affymetrix) and hybridized to the GeneChip® Rat Gene 2.0 ST arrays (Affymetrix). Samples were processed by the Biopolymer-Genomics Core Facility at the University of Maryland Baltimore. Samples were hybridized using a GeneChip hybridization oven 640 (Affymetrix), processed using a GeneChip Fluid Station 450 (Affymetrix), and scanned using a GeneChip Scanner system 3000 7G (Affymetrix).

Microarray data normalization was performed with Affymetrix® Console™ software. CEL data files were analyzed using Partek Genomics Suite version 6.4 (Partek GS, Partek, Inc.). Data were subjected to filtering by the detection of p-value and Z-normalization. Genes were identified as differentially expressed after calculating the Z-ratio, which indicates the fold-difference between experimental groups, as well as false discovery rate (FDR), which controls for the expected proportion of false rejected hypotheses. ANOVA was performed to evaluate the significance in gene expression alteration between experimental groups.

Of the over 7500 genes identified as changing in expression in the hippocampus at 24 hr after 100 G underbody blast, 12 genes were identified as changing in expression very significantly, using rigorous criteria of p value ≤ 0.05, absolute value of z-ratio ≥ 2.0 and FDR ≤ 0.05. Of these 12 genes, only 4 were identified as coding for known proteins. Rps20 codes for a protein that is part of the 40S subunit of mammalian ribosomes. In comparison to Shams, Rps20 RNA increased 2.5 fold at 24 hr following blasts. Fbxw8 encodes a member of the F-box protein family. These proteins constitute one of the four subunits of an ubiquitin protein ligase complex, which tags proteins for degradation by the proteosome. Blast exposure resulted in a 2.9 fold increase in Fbxw8 gene expression. Vwa5b2 codes for von Willebrand Factor (vWF), which is essential for platelet adhesion and is a sensitive marker of damage to vascular endothelial cells. Blast exposure resulted in a 2.2 fold increase in vWF gene expression. Bcl2 codes for the protein Bcl-2, which is the best studied of all anti-apoptotic molecules. The finding that blast exposure resulted in a 2.6 fold decrease in Bcl2 gene expression may contribute to underbody blast-induced TBI.

While microarrays are very useful for detecting changes in gene expression, their ability to accurately quantify the changes in expression is limited. We therefore decided to quantify the changes in expression of Bcl2 and Vwa5b2 using quantitative rtPCR. The results shown in Appendix 7 indicate that the more accurate change in Bcl2 gene expression was an approximately 4-fold reduction. The change in expression of Vwa5b2 was a 10-fold increase. Further validation of these results came from immunohistochemical measurements of vWF immunostaining and Bcl2 immunoblots. Hippocampal vWF immunostaining was greater with ketamine-anesthetized rats at 7 days following exposure to 100G blasts, compared to Shams (Appendix 8). Hippocampal and cerebellar Bcl2 immunoreactivity was greater with conscious rats at 24 hr following exposure to either 700G or 2400G blasts, compared to Shams (Appendix 8).

2.1.5. Compare quantitative histopathologic measurements of brain injury with accelerometer measurements of maximal G-force and JERK.

Evidence that brain injury is more closely dependent on JERK, which is the first derivative of acceleration, compared to maximal acceleration comes from experiments performed with rats that were fully conscious when exposed to underbody blasts (See 2.3 below).

2.1.6. Milestone: Complete all histopathologic marker/G-force correlations (*timing = 24 months*).

While we have made considerable progress using histopathology to understand the pathophysiology of underbody blast-induced TBI, many more experiments and histologic tests are necessary, primarily due to a shift in our paradigm from using ketamine-anesthetized to

using fully conscious rats. Taken together with the new experiments that will combine blast-induced acceleration with head impact, the histopathology measurements will likely continue during the duration of the project.

2.1.6.1. Deliverable 1: Determination of whether histopathologic markers of brain injury display a dose-dependent relationship to underbody blast-associated G-forces and whether maximal Gs, JERK or HIC is the best predictor of TBI.
2.1.4.2. Deliverable 2: Determination of minimum G-force associated with any degree of measurable neurohistopathology; determination of the maximum survivable G-force in this experimental system.

At this juncture, for ketamine anesthetized rats, the minimum acceleration that yields quantifiable histopathological evidence for brain injury is 100G. The maximum survivable acceleration associated with both histologic and neurologic evidence for TBI is 2000G, for ketamine-anesthetized rats. For conscious rats, the maximum survivable acceleration is 2400G. At a force of 2800G, 6 out of 8 rats died immediately, apparently due to pulmonary hemorrhaging.

2.2. Quantify neurobehavioral alterations after underbody blast-associated acceleration injury, including any evidence of G-force and JERK dose-dependence. (Aligned with Objective 2)

2.2.1. Apply these tests to experiments described by 2.1.1.
2.2.2. In animals surviving to 30 days post-injury, perform behavioral testing with standard methods
2.2.3. Correlate results of neurobehavioral testing with measured G-force and JERK.
2.2.4 Compare results of neurobehavioral testing with MRI/MRS and histologic measurements.
2.2.5. Milestone: Complete all neurobehavioral testing/G-force correlations (*timing = 24 months*).

2.2.5.1. Deliverable: Determination of whether neurobehavioral testing results display a dose-dependent relationship to blast-associated G-force or JERK.
2.2.5.2 Deliverable: Identification of the physiologic, neuroanatomic, and neurochemical outcome measures that are most closely related to neurobehavioral indicators of TBI, thus providing insight into the pathophysiology of this form of TBI.

Within the first 24 months of this project, we performed a variety of behavioral tests on rats that were ketamine anesthetized during exposure to underbody blasts. These tests included those for motor function (balance beam and composite neuroscore), cognition and memory (novel object recognition), and anxiety (forced swim test). Following either sham procedure (ketamine anesthesia) or blasts at 100 or 700G with anesthetized rats, we detected no statistically significant differences in any of the behavioral outcomes between shams and either 100G or 700G blast rats. As explained below, once we started detecting behavioral changes in rats that were completely conscious during the underbody blasts, we completely shifted our attention to experiments performed with awake animals, particularly since they better model exposure to blasts by occupants within military vehicles targeted by land mines.

2.3 Perform a limited number of experiments and outcome measures described in 2.1 and 2.2 with rats that are fully-awake but restrained during the underbody blast. (Aligned with Objectives 1 and 2)

2.3.1. In addition to standard outcome measurements, determine if rats lose consciousness or ability to walk or right themselves after moderate G force underbody blasts.
2.3.2. Quantitatively compare both short and long-term outcome measurements obtained from rats that are anesthetized and those that are conscious.
2.3.3. Milestone: Complete all blasts and outcome measurements with rats wide-awake during the blasts (*timing = 30 months*).

Approval was obtained from the Univ. of Maryland, Baltimore IACUC and the ACURO to expose conscious rats to blasts. We then purchased standard plexiglass rat restraints from Braintree Scientific and bolted two of these to the top hull of our blast device, in place of the aluminum tubes used previously for the ketamine-anesthetized rats. The rats fit tight within these restrains allowing for normal breathing but very little movement of the head or body that could cause external or internal injuries. To eliminate the stress of placing the rats into the restraints, we exposed them to 5% isoflurane for 5 min and then secured them in the restraints while they were briefly anesthetized. Within 2 min of removing them from the isoflurane chamber, the rats began to move. They appeared completely awake 5 min after cessation of anesthesia, which is when the explosive was detonated. Three different G forces were used. The lowest was approximately 1200G with a JERK equal to 0.5 x 10^8 meter/sec/sec. The next higher level was approximately 2400G and 1.1 x 10^8 meter/sec/sec. All rats survived these two G forces. The highest level used was 2800G and 1.8 x 10^8 meter/sec/sec. Six of 8 animals died immediately after the 2800G blasts. All results from these blasts, including behavior, histology, and neurochemistry is included in the manuscript included in the Appendix, which will be submitted for publication within the next few weeks. This manuscript is now attached as Appendix 9 and is currently under review for publication in the Journal of Neurotrauma.

2.3.3.1. Deliverable: Determination of whether rats that are conscious during exposure to underbody blasts demonstrate immediate neurobehavioral alterations and if they exhibit evidence for greater short-term and long-term TBI compared to animals anesthetized during the blast.

The following results are provided in the manuscript by Tchantchou et al., (Appendix 9)

A. *Figure 2 – The Y maze is a test of working memory. Normal rats move from one of the 3 arms of the Y maze to the next with a spontaneous alternation of approximately 70%. The spontaneous alternation for rats within 2hr following exposure to 2400G blasts was greatly reduced (5%) and was also significantly reduced to the level of 30% at 6 days post-blast.*
B. *Figure 2 – The elevated plus maze is a test of anxiety or fear. Normal rats are inquisitive and will spend significant time in two of the arms of the plus maze that have no walls and therefore expose the rats to the environment. The time spent in the open arms by rats exposed to either 1200 or 2400G blasts was significantly lower than shams at day 1, 8, 14, and 28 days post-blast.*

C. *Figure 3 – F4/80 is an antibody to a protein that is a marker of inflammatory activation of either macrophages or microglia. At one day post-blast generating either 1200 or 2400G, F4/80 immunoreactivity in was significantly higher than in the brains of sham rats. This marker of inflammation was also higher after 2400G blasts compared to 1200G blasts at one day post-blast. F4/80 immunostaining at 7 days post-blast was not different than that of shams.*
D. *Figure 4 – Molecular markers of vascular injury include occludin and ZO-1, which decline following injury, and vWF, which increases with injury, as explained earlier. Occludin and ZO-1 immunoblot levels declined significantly in the hippocampus and cortex at 24 hr post-2400G blasts. vWB immunoeactivity increased significantly in the cerebellum following either 1200 or 2400G blasts.*
E. *Figure 5 – Hsp70 is a protein that increases follow oxidative and other forms of cellular stress. At 24 hr following either 1200 or 2400G blasts, Hsp70 levels increased in both the hippocampus and cerebellum, in comparison to shams.*
F. *Figure 5 – As mentioned earlier, Bcl-2 is a protein that protects against apoptotic and other forms of cell death. At 24 hr following either 1200 or 2400G blasts, Bcl-2 levels decreased in both the hippocampus and cerebellum, in comparison to shams.*
G. *Figure 6 – The proteolytic cleavage of caspase 3 is a broadly used marker of caspase-dependent apoptotic cell death. The tissue immunostaining for cleaved caspase 3 was significantly higher in the hippocampus at 24 hr post-1200G or 2400G blasts compared to shams.*
H. *Figure 7 – A common approach to quantifying cell death is to count the number of cells that stain positive for TUNEL (terminal deoxynucleotidyl transferase dUTP nick end labeling) Hippocampal TUNEL-stained cells 24 hr following 1200 or 2400G blasts were significantly greater than those of shams. TUNEL staining was also greater following 2400G blasts compared to 1200G blasts.*
I. *Figure 8 – The neurobehavioral alterations that accompany TBI can be the consequence of neuronal death or to loss of synaptic connections between neurons. PSD-95, synaptophysin, and synaptophilin are three proteins crucial for maintaining functional synapses. Immunoblot measurements of these proteins revealed a significant decrease in all three in the hippocampus at 24 hr following either 1200 or 2400G blasts.*

2.4. Establish a modified version of the animal model that includes a controlled secondary head impact during the underbody blast-induced hyperacceleration. (Aligned with Objectives 1 and 2)

2.4.1. Develop an articulated rat head holder that allows for the top of the skull to impact the "roof" of the vehicle during the underbody blast.
2.4.2. Expose *anesthetized* rats to a moderate G force underbody blast, allowing for secondary head impact.
2.4.3. Perform all outcome measurements described in 2.1 and 2.2.
2.4.4. Quantitatively compare outcomes obtained from rats with secondary head impact to those without secondary head impact.
2.4.5. Milestone: Complete all blast experiments and outcome measurements with rats exposed to underbody blast plus secondary head impact (*timing = 36 months*).

We decided that the model briefly described by 2.4.1 would not be reproducible enough for this project and therefore changed the impact model to the Tortella projectile concussive impact (PCI) model (Appendix 1). These experiments will now be performed in collaboration with Dr. Deborah Shear and coworkers at WRAIR. We have obtained both IACUC and ACURO approval for these experiments and will perform our first experiment on March 23, 2016 at the University of Maryland School of Medicine.

2.4.5.1. Deliverable: A small animal model of TBI caused by the combination of underbody blast-induced hyperacceleration plus secondary head impact that is particularly relevant to many of the warfighters who survive underbody blasts.

We did not meet the 36 month projected date for this deliverable but are confident it will be met by month 46.

2.5. Test the effects of different vehicle hull designs on the loads imparted to the vehicle and to the test animals and determine which design is most effective at reducing TBI. (Aligned with Objective 3)

2.5.1. Test 3 different hull designs (e.g., multiple V-hull and inverted V-hull) for mitigation of maximal G force and JERK loads on the vehicle alone.
2.5.2. Test 3 of these design modifications with *anesthestized* rat occupants at a blast stand-off distance that imparts a moderate G-force with the standard hull design.
2.5.3. Perform all outcome measurements described in 2.1 and 2.2.
2.4.4. Quantitatively compare outcomes obtained from tests using the modified hull designs to those using the standard hull design.
2.4.5. Milestone: Complete all blast experiments and outcome measurements with the modified hull designs (*timing = 44 months*).

Substantial progress has been made toward this objective, as shown below. We now project that these experiments will be completed by 46 months.

2.4.5.1. Deliverable: Identification of a hull design that both mitigates loads on the vehicle and its occupants and that reduces TBI after underbody blast.

1. **Improving survival from underbody blasts by a double hull separated by compressible cylinders**

Dr. Fourney's Dynamic Effects Laboratory at the University of Maryland College Park School of Engineering has for many years been using small scale simulated vehicle models and subjected them to a variety of blast conditions http://www.cecd.umd.edu/projects/dynamic-effects-lab.html. He has tested a wide variety of vehicle hull designs for their ability to withstand blasts. His work has been validated with full scale vehicles and helped lead to the double V-hull design used in "mine resistant, ambush protected military vehicles (MRAPs) that have dramatically reduced the number of mortalities associated with vehicles targeted by IEDs. As an integral part of this project, Dr. Fourney and his associates, Dr. Leiste and Dr. Bonsmann, have tested the ability of compressible cylinders located between top and bottom hulls to reduce the load and therefore the acceleration of the top hull, i.e., farthest away from an underbelly blast. As mentioned in a previous progress report, they have found that the

placement of compressible polyurea-coated aluminum cylinders between two hulls can reduce the load imparted to the top hull by approximately 90%, compared to the acceleration measured when only a thin rubber mat was present between the two hulls. Given this result, we tested the compressible can design in our underbody blast model with ketamine-anesthetized rats secured within restraints bolted to the top of the upper hull (Appendix 10).

For these tests, we used a relatively large, 2.3 g level of pentaerythritol tetranitrate as the explosive and a stand-off distance between the charge and the bottom of the lower plate that would give a peak acceleration of the top hull of 2800G in the absence of the compressible cylinders. As shown in Appendix 10, a maximum force of 2800G was indeed obtained, using an accelerometer located directly next to the head end of tubes in which the ketamine anesthetized rats were placed In the presence of 4 compressible cylinders located just inside the edge of the hulls halfway between each corner plus one located between the centers of each hull, the maximum acceleration measured on the top hull was reduced to between 150 and 300G. Using two rats for each blast, 5 out of 6 that were subjected to the 2800G force died either immediately or within 30 min later due to massive internal hemorrhaging to the lungs, liver, and other organs (Appendix 10). In contrast, all 8 rats survived that were subjected to the same conditions except that the cylinders were present between the top and bottom hulls. These rats appeared healthy and gained normal weight during the 7 days they were kept alive before perfusion fixation. At the time of fixation, all internal organs appeared normal. We consider these results to be highly significant as they represent strong evidence that a relatively simple modification of a vehicle hull design can dramatically reduce the load on occupants during an underbody blast, thereby saving lives. As previously communicated, Dr. Fourney submitted a hull design patent application based on results he obtained in his Dynamic Effects laboratory. Hopefully, he can partner with the US Army and or military contractors to translate this design into a new and much safer class of MRAPs. The following provides additional details regarding the previous and ongoing tests performed at the Dynamic Effects Laboratory that are supported by this research award.

2. Testing of Multiple Mitigation Techniques on a Simulated Vehicle Undergoing Blast Loading

Significant progress has been made testing two different mitigation techniques on a simulated vehicle. By testing a V-shaped hull and polyurea cans individually, as well as together, we can gain a fuller understanding of just how much energy can be mitigated from the blast.

Dr. Jarrod Bonsmann and the Dynamic Effects Lab tested two methods of mitigation to reduce peak acceleration experienced by a blast loaded vehicle. To do these tests we used two round plates and kept the distance between them constant. The bottom plate would represent the hull of a vehicle and it was kept at a constant distance above the surface of the saturated sand in which the explosive was buried beneath the center of the plate. The second (top) plate would represent the floor of the passenger compartment and it was connected to the bottom plate by the mitigating structural element. We have run numerous tests with no mitigating mechanism between the two plates so as to be able to measure the effect of the mitigation technique being tried. In the first picture on the left in Appendix 11, the two plates are separated by four long slender hollow tubes. When the detonation occurs these four tubes buckle globally, that is a single buckle occurs at the center of the tubes. The buckled tubes can be seen in the photo at the top right. In the picture on the bottom left we have placed four

soda cans (which have a large outer diameter and thin walls) between the hull and the passenger compartment. As shown in the photograph on the bottom right of Appendix 11, all cans are locally buckled with many buckling sites. That is, they are crushed by the very dynamic load. A typical acceleration signal for the control group is shown in Appendix 12.

Appendix 13 shows that aluminum cans are an effective way of mitigation the peak acceleration experienced by a blast loaded vehicle. In regards to Traumatic Brain Injury (TBI), the most important piece of data is the peak acceleration recorded on the plate. The peak acceleration of Appendix 13 is the highest value recorded above, or approximately 2500 g's. Since the test is done at small scale. The scaling factor for this particular test is 10, meaning that a person on a full sized vehicle would experience 250 g's.

To enhance the effect of using aluminum cans as mitigation, the cans have been coated in polyurea to further reduce the peak acceleration experienced by the vehicle. Appendix 14 shows the effect of polyurea coated cans on peak acceleration. Different amounts of polyurea coating, measured in mass ratio, have different reductions in peak acceleration on the blast loaded plate. As the amount of polyurea coating increases, the reduction in peak acceleration increases.

As can be seen above, the polyurea coated aluminum cans have the lowest peak acceleration of all tests, so they will be used in the current study alongside the V-shaped hull. In our current test matrix, there are four different test plate set ups: flat bottom hull with rigid connectors, V-shaped hull with rigid connectors, flat bottom hull with polyurea coated can connectors, and V-shaped hull with polyurea coated can connectors. Appendix 15 provides examples of flat bottom and V-shaped bottom hulls, with the rigid hull connectors.

Each test will be conducted at a constant Stand-off Distance (SOD), meaning that the distance between the bottom of the bottom plate and the top of the sand test bed is held constant. While the Dynamic Effects Lab chooses to use Stand-off Distance as a test parameter, some choose to use the distance to the floor board where the vehicle's passengers would theoretically be sitting. This is a factor that could affect the results and is something that could possibly be explored in future testing.

Each of the four different test set-ups will be tested at five different charge locations to see the effects of the mitigation in less idealized settings. The charge will be buried at the center of the plate, a quarter of the plate width to the right of the center, half of the plate width to the right of the center, a quarter of the plate length forward of the center, and half of the plate length forward of the center.

To date, all of the center charge tests have been completed, as well as four of the five tests at the quarter front charge location. The results for reduction in peak acceleration are shown in Appendix 16.

In the center charge location case, the peak acceleration is reduced from 1406G in the baseline case to 111G when utilizing the V-hull and polyurea coated cans. In the quarter front charge location, the peak acceleration is reduced from 1611G in the baseline case to 127G when utilizing the V-hull and reused polyurea coated cans. With a scaling factor of 10 on the acceleration signals, both test cases become survivable at large scale when using the v-hull with the polyurea coated cans. Appendix 17 provides examples of the total energy, or the total of linear and rotational kinetic energy, of the system.

Future work includes completing the test matrix outlined above by testing at the three remaining charge locations. Once the test matrix is complete, attempts will be made to shorten the height of the polyurea coated cans from 1.5 inches to a shorter distance of around 0.5

inches. Since the scaling factor on these tests is 10, a 1.5 inch polyurea coated can translates to a 15 inch can on a full sized vehicle. Adding such a considerable height to the vehicle has many negative effects, including a higher center of gravity and increased chance of rollover.

KEY RESEARCH ACCOMPLISHMENTS:

- Quantitative histochemical evidence for damage to brain white matter axon fibers following exposure of rats to underbody blasts resulting in peak vertical accelerations of 100 and 700 Gs, with significant increase in axon injury at 700 compared to 100 Gs.
- Quantitative immunohistochemical evidence for blood brain disruption in the cerebral cortex of rats following exposure to 700 G underbody blasts.
- Quantitative immunohistochemical evidence for a large elevation in vascular levels of von Willebrand Factor 7 days after 100G underbody blasts.
- Quantitative immunohistochemical evidence for an increase in the number of either perivascular or periventricular macrophages or microglia at 24 hr following 700G blast.
- Quantitative molecular biological evidence for significant differences in hippocampal gene expression following exposure to 100 G underbody blasts. A significant reduction in expression of Bcl2 was observed, which could promote brain cell death, and a significant increase in expression of von Willebrand Factor was observed, which is indicative of vascular injury.
- Qualitative histological evidence for axonal injury in several brain regions, including the internal capsule, the corpus callosum, and the cerebellum. Also evidence for astrocyte activation.
- Preliminary evidence for hippocampal neuronal death and cerebellar Purkinje neuronal death at 24 hr after exposure to 700G blast.
- Neurobehavioral evidence for acute and chronic fear and anxiety in conscious rats exposed to 2400G blasts.
- Quantitative evidence that the levels of proteins associated with neuronal synapses are reduced following 700 and 1200G blasts.
- Demonstration that the use of crushable cylinders separating an outer and inner hull can dramatically reduce the G force load on the inner hull. Further demonstrations that application of a poly-urea covering to the cylinders can provide further protection at high G forces and allow for at least partial reinstatement of shock-absorbing cylinder structures. This rebound characteristic could increase the chance of the blast-targeted vehicle to remain in operation.
- Demonstration that the presence of these cylinders results in a load on anesthetized rats of 300G with no mortality at a charge size and standoff distance that result in a load of 2800G and 80% mortality when the cylinders are not present.

REPORTABLE OUTCOMES:

1. Manuscript published in the Journal of Trauma and Acute Care Surgery providing qualitative histologic evidence for brain injury to rats in our underbody blast TBI model. J Trauma Acute Care Surg. 2014 Sep;77(3 Suppl 2) Appendix 1.

2. Results obtained from this project were presented in a poster session at the MHSRS meeting in Ft. Lauderdale, FL in August of 2015 and as a poster at the National Capitol TBI symposium in March of 2015. Appendix 18 and 19

3. Intellectual property disclosure to the University of Maryland College Park for vehicle hull designs that can mitigate injury caused by underbody blasts. Appendix 20

4. Manuscript submitted to J Neurotrauma in Year 4, titled "Neuropathology and Neurobehavioral Alterations in a Rat Model of Traumatic Brain Injury to Occupants of Vehicles Targeted by Underbody Blasts" Appendix 9

5. Manuscript to be submitted to J Neurotrauma in Year 4, titled "Central Nervous System Changes Induced by Underbody Blast-induced Hyper-acceleration: an in vivo Diffusion Tensor Imaging and Magnetic Resonance Spectroscopy Study" Appendix 2

CONCLUSIONS: (Red highlights conclusions made during Year 3)

- At this stage of the project we can conclude with confidence that underbody blast induced G forces of as little as 100 Gs cause white matter and vascular damage in the brains of rats.
- We also conclude that in the absence of secondary head impact, ketamine-anesthetized rats survive blast-induce force of at least 1700 G but have a high mortality rate after exposure to 2800G blasts.
- MRI brain imaging provides verification that water diffusivity in several brain locations is altered within at least 2 hr and maintained for at least 7 days following 1700G accelerations. These results are consistent with diffuse axonal injury. Reduction in brain creatine and glutamine for at least 24 hr post-blast is consistent with astrocyte activation.
- Rats that are conscious during 2400G blasts survive but exhibit acute and chronic fear and anxiety. Most rats that are conscious during 2800G blasts die immediately afterwards due to pulmonary hemorrhaging.
- Exposure to blast-induced accelerations between 1200 and 2400G compromises the blood brain barrier, leading to increased accumulation of inflammatory microglia/macrophages in the brain.
- Blast-induced brain trauma also causes neuronal cell loss in the hippocampus, associated with reduced expression of pre- and post-synaptic proteins and a decrease in the level of the anti-death protein, Bcl2.
- Finally, our vehicle hull design efforts have been very successful at demonstrating an unexpectedly large reduction in load placed on the floor of a vehicle, using inner and outer hulls separated by polyurea-coated, crushable cylinders. Application of such a design to military vehicles could dramatically reduce the extent of injuries to the occupants and even allow the vehicle to keep operating, thus increasing the successful completion of the military mission.

LITERATURE CITED

Leung LY, Larimore Z, Holmes L, Cartagena C, Mountney A, Deng-Bryant Y, Schmid K, Shear D, Tortella F. The WRAIR projectile concussive impact model of mild traumatic brain injury: re-design, testing and preclinical validation. Ann Biomed Eng. 2014 Aug;42(8):1618-30.

APPENDIX 1

Leung et al., Ann Biomed Eng. 2014 Aug;42(8):1618-30

Annals of Biomedical Engineering, Vol. 42, No. 8, August 2014 (© 2014) pp. 1618–1630
DOI: 10.1007/s10439-014-1014-8

The WRAIR Projectile Concussive Impact Model of Mild Traumatic Brain Injury: Re-design, Testing and Preclinical Validation

LAI YEE LEUNG,[1] ZACHARY LARIMORE,[2] LARRY HOLMES,[2] CASANDRA CARTAGENA,[1] ANDREA MOUNTNEY,[1] YING DENG-BRYANT,[1] KARA SCHMID,[1] DEBORAH SHEAR,[1] and FRANK TORTELLA[1]

[1]Brain Trauma Neuroprotection and Neurorestoration Branch, Center for Military Psychiatry and Neuroscience, Walter Reed Army Institute of Research (WRAIR), 503 Robert Grant Avenue, Silver Spring, MD 20910, USA; and [2]Composites and Hybrid Materials Branch, United States Army Research Labs, Aberdeen, MD, USA

(*Received 26 November 2013; accepted 11 April 2014; published online 23 April 2014*)

Associate Editor Stefan M Duma oversaw the review of this article.

Abstract—The WRAIR projectile concussive impact (PCI) model was developed for preclinical study of concussion. It represents a truly non-invasive closed-head injury caused by a blunt impact. The original design, however, has several drawbacks that limit the manipulation of injury parameters. The present study describes engineering advancements made to the PCI injury model including helmet material testing, projectile impact energy/head kinematics and impact location. Material testing indicated that among the tested materials, 'fiber-glass/carbon' had the lowest elastic modulus and yield stress for providing an relative high percentage of load transfer from the projectile impact, resulting in significant hippocampal astrocyte activation. Impact energy testing of small projectiles, ranging in shape and size, showed the steel sphere produced the highest impact energy and the most consistent impact characteristics. Additional tests confirmed the steel sphere produced linear and rotational motions on the rat's head while remaining within a range that meets the criteria for mTBI. Finally, impact location testing results showed that PCI targeted at the temporoparietal surface of the rat head produced the most prominent gait abnormalities. Using the parameters defined above, pilot studies were conducted to provide initial validation of the PCI model demonstrating quantifiable and significant increases in righting reflex recovery time, axonal damage and astrocyte activation following single and multiple concussions.

Keywords—Concussion, Mild TBI, Projectile, Helmet, Impact energy, Head kinematics, Gait.

INTRODUCTION

A concussion is defined as a mild form of traumatic brain injury (TBI), usually caused by a blow to the head. Approximately 75% of TBIs that occur each year are concussions or other forms of mild TBIs (mTBI). In the United States, the annual incidence of sports-related concussion is estimated at 300,000.[3] In the military, there have been over 230,000 service members diagnosed with mTBI since 2000, which has distinguished it as the "signature injury" of the military conflicts in the Middle East.[10]

Preclinical research models have been developed to study the neurobiology of concussion. The majority of these mTBI models were modified from existing, gold standard models of moderate/severe TBI such as the controlled cortical impact (CCI)[24,25] and fluid percussion injury (FPI)[15,26] models where, for mTBI, the force of impact is simply reduced but the intact dura is still exposed *via* craniotomy to allow for the direct impact of the cortical tissue. The weight drop model has also been used to study mTBI[7] but typically requires a scalp incision and the attachment of a metal disc to the exposed skull prior to impact by a free falling weight. Alternative 'non-impact' models such as rotational acceleration/deceleration[11,27] and blast[4,13] have also been designed for the purpose of evaluating coup-contrecoup and blast wave energies potentially associated with mTBI.

Although researchers have successfully demonstrated clinically relevant pathology of mTBI using these classically refined models, there are certain caveats with regards to replicating "true" closed-head concussive impact injury. First, CCI and FPI involve a craniotomy procedure which itself can trigger proinflammatory

Address correspondence to Lai Yee Leung, Brain Trauma Neuroprotection and Neurorestoration Branch, Center for Military Psychiatry and Neuroscience, Walter Reed Army Institute of Research (WRAIR), 503 Robert Grant Avenue, Silver Spring, MD 20910, USA. Electronic mail: laiyee.leung@us.army.mil

responses and related behavioral changes.[6] Even the weight drop model of mTBI involves an invasive incision that may result in inflammatory and possibly behavioral effects. Second, the majority of concussions are caused by impact which cannot be represented by non-impact models of brain trauma. Thus the absence of a true closed-head impact model of mTBI remains a critical research gap in the field of TBI. The WRAIR projectile concussive impact (PCI) model was developed to address this gap and to provide a truly non-invasive, closed-head impact model of mTBI.[5] The initial, proof-of-concept, PCI injury device utilized a simple design that consisted of heating a small, torque-sealed, microcentrifuge tube packed with dry ice to launch a targeted projectile (microcentrifuge cap), and a prototype stainless steel helmet to prevent skull fracture and subdural hematoma. However, this proof-of-concept PCI model had several limitations.[5] The stainless steel helmet was thick and rigid, and it left empty, irregular gaps between the helmet and the rats head. The prototype helmet was also too heavy with respect to the weight of the rats head, and it thus restricted head motion upon impacts. Besides, the impact energy was limited by the microcentrifuge tube and sublimation of the dry ice such that neither the impact force nor the projectile velocity could be titrated (i.e., it was an all-or-none effect regardless of the amount of dry ice packed into the tube). Therefore, a second generation device has been developed that utilizes compressed nitrogen to launch a projectile (Fig. 1). The primary advantage of using compressed gas vs. dry ice sublimation is that the mechanical forces used to induce the injury are far more controllable, reproducible and quantifiable. In addition, several modifications were made to the engineering components in the PCI model including (1) custom fabricated helmet material construction and design, (2) the testing of different PCI projectiles and (3) the evaluation of different angles/locations of the projectile impact to the surface of the rat head. Finally, pilot studies were conducted to provide further neurobiological validation of the PCI-mTBI model.

MATERIALS AND METHODS

Animals

Male adult Sprague–Dawley rats (280–320 g; Charles River Labs, Raleigh, VA, USA) were used in these experiments. All procedures involving animal use were reviewed and approved by the Institutional Animal Care and Use Committee (IACUC) of Walter Reed Army Institute of Research. Research was conducted in compliance with the animal welfare act, Guide for the Care and Use of Laboratory Animals (National Research Council) and other federal statutes and regulations. Animals were housed individually under a 12 h light/dark cycle in a facility accredited by the Association for Assessment and Accreditation of Laboratory Animal Care International.

PART I: HELMET

Helmet Material Preparation and Tensile Test

Three composite materials were chosen for the rat helmet. (1) *Fiber glass/Carbon*: 4 ply lay-up with the bottom layer constructed of Cycom 7781 plain weave fiber glass, the second layer with Cycom IM7 unidirectional carbon at 90°, the third layer with Cycom IM7 unidirectional carbon at 0°, and the top layer with Cycom 7781 plain weave fiber glass. All layers were pre-impregnated fibers with Cycom 381 resin system. The material was prepared under vacuum at ~94.81 kPa, and cured at 104 °C for 6 h. (2) *S-2 Fiber glass*: 4 ply lay-up with all layers constructed from Cycom 7781 plain weave S-2 fiber glass pre-impregnated with Cycom 381 resin. The material was prepared under vacuum at ~94.81 kPa and cured at 104 °C for 6 h. (3) *Dyneema/carbon fiber*: 6 ply lay-up with the bottom 4 ply constructed from Dyneema HB26 with a thermoplastic binder, and the top two ply constructed from plain woven IM7 carbon fiber which was bonded to the Dyneema *via* a wet lay-up process utilizing SC-15 toughened epoxy resin. The samples were prepared under vacuum at ~94.81 kPa, and cured and 127 °C for 6 h. All the samples were prepared for and tested under ASTM Standard D3039_D3039M-08 "Standard Test Method for Tensile Properties of Polymer Matrix Composite Materials" using an Instron 1125 testing machine with a 10 kN load cell at a loading rate of 2 mm/min (Fig. 2a). Six samples were tested for each composite material. Maximum stress and strain and elastic modulus were calculated from the tensile loading curves of each sample.

Helmet Fabrication and Selection

The helmets were fabricated using a 3-D mold of an adult Sprague–Dawley rat (~300 g) with the aforementioned composite materials. Sections of string were used to secure the helmet on the rat head. Three types of helmets were fabricated: Helmet A (Fiber glass/carbon), Helmet B (S-2 Fiber glass) and Helmet C (Dyneema/carbon fiber).

For helmet testing, animals were randomly assigned into 3 helmet groups ($n = 3$ per helmet). PCI injury was performed as previously described.[5] Briefly, animals

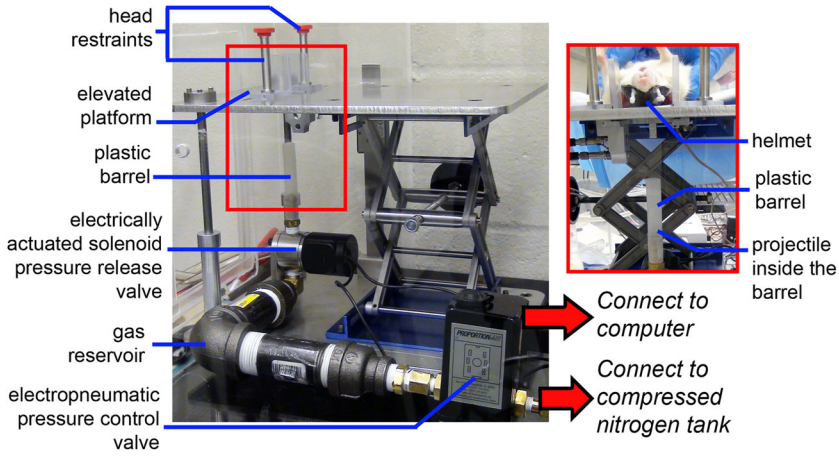

FIGURE 1. Second generation of WRAIR PCI Device (compressed nitrogen driven). The inset shows the side view of the device with a helmet-protected rat.

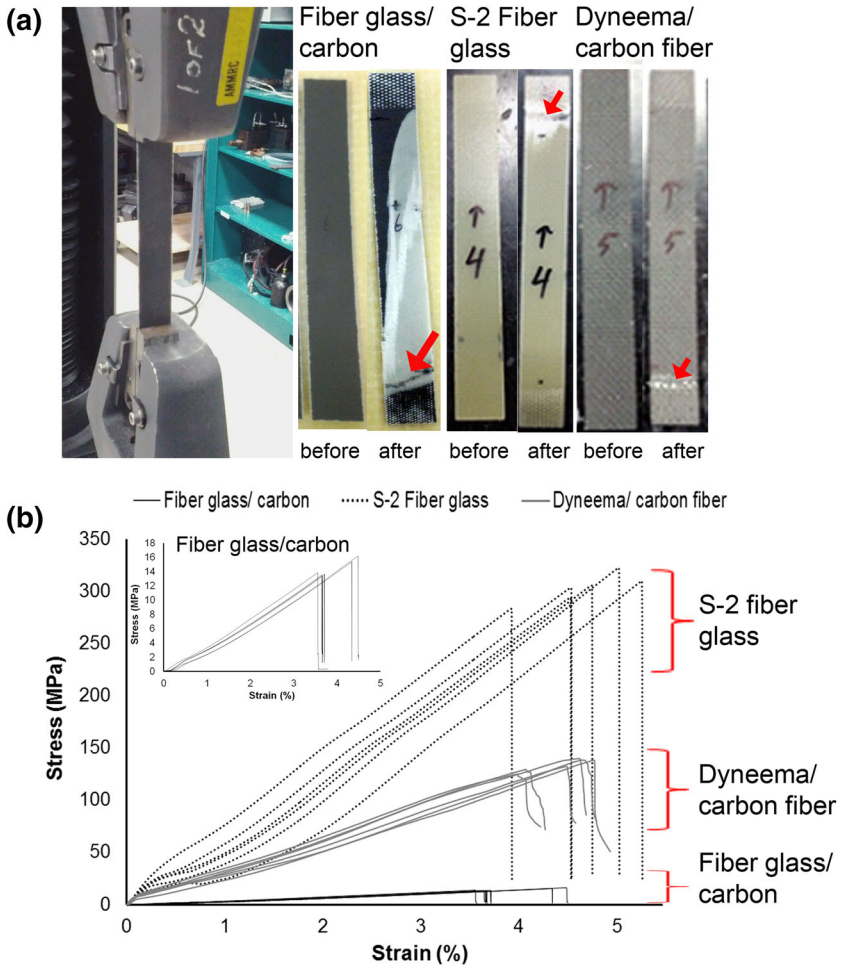

FIGURE 2. Helmet material tensile test: (a) Instron 1125 testing machine and composites materials before and after testing (red arrow indicates fracture); (b) stress–strain curves of all tested samples. The inset shows the stress–strain curves of the fiber glass/ carbon samples.

were anesthetized with 5% isoflurane and the helmet was securely fastened onto the rat's head. Pressure sensor films (Fujifilm pre-scale pressure sensitive film) were adhered to the inner and outer surfaces of the helmet and recorded the distribution and magnitude of pressure from the impact of the projectile. The animal

was placed in a dorsal lateral position on the elevated platform with the head positioned over an opening of the platform. The rat was lightly restrained with an elastic band placed 50 mm above the rat's head that allowed the rat's head and cervical spine to move freely yet maintained the position of the body on the PCI platform. The rats were subjected to a single PCI injury targeted at the temporoparietal surface of the helmet covering the rat's head. The inner/outer pressure sensor films were removed from the helmets and scanned for analysis with the Topaq Pressure Analysis System using a specially calibrated densitometric scanner (Sensor Products, Inc., NJ). The magnitudes of contact pressure, force and contact area were quantified from film sections for both the inner and outer surfaces of each helmet. For histopathological comparison, a sham control group ($n = 3$) was exposed to all the same procedures except the projectile impact.

At 24 h after injury, the rats were fully anesthetized with an overdose of ketamine/xylazine (70 and 6 mg/kg, i.p., respectively) and were transcardially perfused with 0.1 M phosphate buffer saline (PBS) followed by 4% paraformaldehyde (PFA). Brains were removed and post-fixed for 6 h in 4% PFA-PBS then placed in 20% sucrose. Serial sections (40 μm) were cut coronally through the whole cerebrum from +4.0 to −7.0 mm anterior-posterior (AP) from Bregma at 960-μm intervals. Free floating sections were washed with 0.01 M PBS, pH 7.4, blocked with vector blocking reagent, and then incubated for 24 h at 4 °C with glial fibrillary acidic protein (GFAP) (1:40,000; DAKO, Carpinteria, CA). Sections were rinsed with PBS, and then incubated for 2 h at room temperature with biotin conjugated secondary antibody and detected by Vector ABC system. After three washes in PBS, sections were mounted with Permont (EMD, NJ). Images of the slides were digitized using a BX61 microscope (Olympus, PA) at uniform criteria for sensitivity and exposure time. The computerized threshold was performed using ImageJ software (NIH, Version 1.44) and set in order to pick up maximal positive staining of reactive GFAP-labeled astrocytes in the hippocampus (3 sections per brain; approximately −2.6 to −3.6 mm AP from Bregma) with minimal artifacts. To ensure objective quantification, the same threshold was applied to all brain sections. Positive-stained cells were quantified as a ratio of the number of pixels above the threshold to the total pixels in the selected area.

Final PCI helmet selection was based on several criteria including elastic modulus, load transfer characteristics and the ability to detect an appropriate injury response in the brain. The selected helmet should have low elastic modulus allowing deformation with a small amount of stress, good load transfer reflected by a relatively high ratio of pressure or force on the inner surface to the outer surface of the helmet (i.e., how much pressure was being transferred from the projectile impact to the rat head), and an significant increase in astrocyte activation.

PART II: PROJECTILE

Impact Testing of Projectiles

To measure the impact energy, a surrogate head and a test stand were built (Fig. 4a). The mass of the surrogate head was similar to that of an actual adult rat head/neck. A section of helmet material (fiber glass/carbon) was mounted to the front of the surrogate. An elastomer between the helmet material and the surrogate head served as a surrogate skin/flesh. The surrogate head was instrumented with four high fidelity accelerometers (Dytran, CA) that provide impact acceleration data *via* a Nicolet Pro60 acquisition system (Nicolet, MN) for energy calculations as below:

$$F = ma \tag{1}$$

$$E(t) = \int_0^t F(t)\mathrm{d}t \tag{2}$$

where F is force, m is mass of the surrogate, a is acceleration, E is energy absorbed and t is time. The surrogate head was supported by two wires about a calculated axis of rotation to provide deflection characteristics similar to that of an actual rat being tested in a typical fashion. The injury device was aligned with the front of the surrogate as shown in Fig. 1. The following device/projectile combinations were tested: (1) the dry ice-driven injury device with microcentrifuge cap, (2) compressed nitrogen-driven injury device operating at 552 kPa with (a) microcentrifuge cap, (b) steel sphere, (c) brass sphere, (d) ceramic sphere, (e) steel cylinder, (f) nylon cylinder, (g) aluminum cylinder. Ten trials for each device/projectile combination were recorded. To estimate the projectile velocity, high speed video was taken using Photoron FASTCAM-APX RS cameras (Photron, CA) operated at 1000 Hz for each impact trial.

Head Kinematics

The dry-ice driven PCI device and nitrogen-driven PCI device were used to compare kinematic data using the original microcentrifuge cap projectile (0.37 g; tested using both PCI devices) vs. the 3.52 g steel sphere and the 5.22 g steel cylinder (tested using the nitrogen-driven PCI device). Rats were anesthetized, fitted with helmets and positioned on the PCI platform as previously described. High speed videos were captured

using two Phantom Miro cameras and software (Vision Research Inc., New Jersey) operated at 5.4 kHz. The motion of rat head was assessed by tracking the snout (Fig. 5a) using the Phantom Cine Viewer v2.14 software. All subsequent processing and calculations of displacement, velocity and acceleration were carried out in Matlab (MathWorks, MA).

PART III: IMPACT LOCATION

To examine the effect of impact location, rats ($n = 10$ per group) were subjected to PCI targeting either parietal (bilateral), temporoparietal (unilateral, right side) or temporal (unilateral, right side) region/surface of the fiber glass/carbon helmet using the nitrogen-driven device with steel sphere projectile. Sham animals were exposed to the same procedures with the exception of the projectile impact. Gait performance was assessed 7 days prior to the injury (baseline measures) and at 2 h, 1, 3 and 7 days post-PCI using the CatWalk automated gait analysis system (Noldus Information Technology Inc, Leesburg, VA). Prior to testing for each time point, rats were first acclimated in a dark goal box positioned at one end of the runway for 5 min. Following acclimation, the animals were placed at another end of the walkway and completed 3 consecutive runs with 2 min inter-trial intervals in the box between runs. Runs with walking velocities >30% variation were excluded from analysis. Images from each trial were processed using CatWalk XT 9.1 software. Following footprint identification and labeling, data pertaining to static and dynamic gait parameters were quantified and the mean scores from three consecutive trials (per animal per time points) were analyzed for statistical significance.

PART IV: PILOT STUDY USING THE REFINED MODEL

A pilot study using the optimal parameters defined by the above experiments was conducted using the compressed nitrogen-driven PCI device operating at 522 kPa. Outcome metrics consisted of righting reflex measures (preclinical index corresponding to loss of consciousness; LOC) and the degrees of positive beta-amyloid precursor protein (β-APP; marker for axonal injury) and GFAP staining. Briefly, all animals ($n = 3$–6 per group) were anesthetized with 4% isoflurane for 4 min in an induction chamber. After securing the helmets and pressure sensor films onto the rat head, the rat was transferred to the PCI chamber that was prefilled with 2% isoflurane. Immediately following PCI injury the rat was placed on its back in the home cage and timing was initiated to record the latency to return the righting reflex. In rats exposed to multiple PCI injury (4 hits, 1 h apart), righting reflex was recorded after each impact. At 6 and 24 h following PCI the rats were sacrificed with an overdose of ketamine/xylazine (70 and 6 mg/kg, i.m., respectively) and were transcardially perfused as previously described. Coronal free floating brain sections (40 μm) were immunostained for β-APP and GFAP with Vector ABC system. Images of the slides were digitized and examined using a BX61 microscope (Olympus, PA). β-APP accumulation was quantified by direct cell counting (10 sections per brain including the cerebrum and cerebellum; ipsilateral to PCI). Reactive GFAP-labeled astrocytes (ipsilateral and contralateral hippocampi) were quantified using threshold analysis as described in Part I.

Statistical Analysis

Statistical analysis was performed using SPSS v19.0 (IBM Corp, Somers, NY) and SigmaPlot 12.0 (Systat Software Inc, San Jose, California). Material property, impact testing and histopathology data was analyzed using one-way analysis of variance (ANOVA). Two-way repeated measures ANOVA with Fisher LSD *post hoc* tests were used to identify potential differences in gait parameters between groups. The significance criterion was set at $p < 0.05$. Data are presented as the mean ± SEM.

RESULTS

Part I: Helmet

Figure 2b shows the stress–strain curves obtained for the composite materials (a) fiber glass/carbon (weighs 2.92 g), (b) S-2 fiber glass (weighs 5.78 g) and (c) Dyneema/carbon fiber (weighs 5.89 g). Fiber glass/carbon was found to exhibit the lowest tensile modulus ($E = 362.9 \pm 2.3$ MPa) and yield stress ($\varepsilon = 14.3 \pm 0.5$ MPa) compared to S-2 fiber glass ($E = 6525.7 \pm 174.9$ MPa; $\varepsilon = 303.2 \pm 5.5$ MPa) and Dyneema/carbon fiber ($E = 2922.5 \pm 32.2$ MPa; $\varepsilon = 133.9 \pm 2.4$ MPa). Pressure and force measurements were obtained from the pressure sensor films and the ratios of inner to outer surfaces of the helmets were calculated (Fig. 3a). The pressure and impact force on the inner and outer surfaces, as well as the force ratio of Helmet C (Dyneema/carbon fiber) were significantly lower than that of Helmet A (fiber glass/carbon), possibly due to the high energy absorption characteristic of Dyneema in Helmet C. Helmet B (S-2 fiber glass) had significantly lower ratio of pressure on the

inner surface to outer surface indicating lesser load transfer from the projectile impact to the rat head, compared to Helmet A and C ($p < .05$). Overall, Helmet A appeared to have a good load transfer likely due to its relatively low elastic modulus compared to Helmets B and C.

All helmets effectively protected the rat against skull fracture, subarachnoid hemorrhage and contusion. However, GFAP-positive astrocytes in the brains of animals from the Helmet A group appeared to be more hypertrophic compared to the other groups (Fig. 3b). Moreover, GFAP immunoreactivity in the right hippocampus (Fig. 3c) was significantly higher in Helmet A group compared to that in sham control group ($p < 0.01$) and Helmet C group ($p < .05$).

Part II: Projectile

The weight, average velocity and peak energy of the projectiles obtained from the impact tests are summarized in Table 1. The microcentrifuge caps launched by the dry ice-driven device (Fig. 4b) and by the compressed nitrogen device (Fig. 4c) had the lowest impact energy but with a relatively high variance. The impact characteristics were more consistent (low inter-trial variance) with the nitrogen-driven injury device (operating at 552 kPa) and the spherical projectiles (Figs. 4d, 4e, and 4f) compared to the cap and the cylindrical projectiles (Figs. 4b, 4c, 4g, 4h, and 4i). Steel spheres yielded the highest impact energy (14.6 ± 0.6 J) among all the projectiles. In general, impact energy increases with the mass of the projectile but it was also limited by other configurations of the device such as the operating pressure and the barrel length.

Head kinematics data quantified from the high speed videos revealed the trajectory of the rat head on the sagittal plane during impact (Fig. 5). The impact caused linear and rotational acceleration with a backward rotation and a marked hyperextension of the neck. Head motions of the anesthetized rat during impact by the steel ball or cylinder were more vigorous and of greater displacement in x and y directions, compared to the cap (Fig. 5b). The maximum y-displacements range from 40 to 50 mm with the microcentrifuge cap and 50–60 mm with the steel sphere/cylinder (Fig. 5c). Peak linear velocity and acceleration of the rat head during impact were calculated from the

(a)

	Helmet A	Helmet B	Helmet C
Outer surface (between projectile and helmet)			
Pressure (kPa)	4895 ± 87	5209 ± 149	4481 ± 106
Contact area (mm^2)	115 ± 8	114 ± 9	118 ± 9
Force (N)	507 ± 46	593 ± 47	528 ± 47
Inner surface (between helmet and rat head)	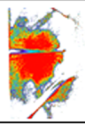		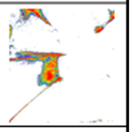
Pressure (kPa)	449 ± 6	431 ± 9	416 ± 9
Contact area (mm^2)	399 ± 81	328 ± 77	160 ± 21
Force (N)	160 ± 21	136 ± 30	54 ± 10
Ratio of Inner to Outer surfaces of the helmet (%)			
Pressure	9.2 ± 0.1	8.3 ± 0.3	9.3 ± 0.2
Contact area	358 ± 83	327 ± 104	293 ± 189
Force	29.0 ± 4.2	25.2 ± 7.3	9.9 ± 1.1

(b)

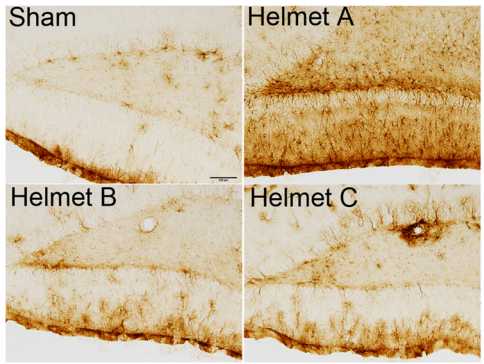

(c)

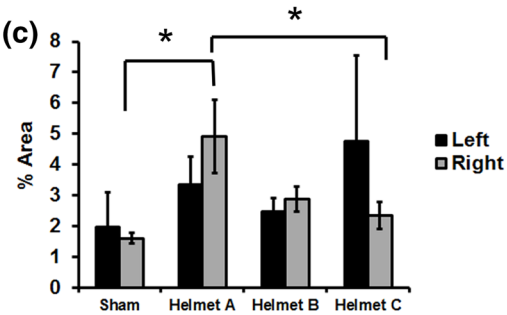

FIGURE 3. (a) Pressure sensor films with pseudo color showing the pressure magnitude and distribution. Pressure, contact area and force of the impact on the outer and inner surfaces of the helmets were quantified based on the colorimetric scale; Ratios of the inner to outer surfaces of the helmets were summarized; (b) GFAP immunoreactivity in the right hippocampus following sham procedures or PCI with Helmet A (fiber glass/carbon), Helmet B (S-2 fiber glass) and Helmet C (Dyneema/carbon fiber); Scale bar: 100 μm (magnification: 10× objective); and (c) quantification of the hippocampal GFAP immunoreactivity (thresholded area). *$p < 0.05$ (one-way ANOVA; Fisher's LSD *post hoc* tests).

TABLE 1. Projectile mass, average velocity and peak energy.

Device	Projectile	Mass (g)	Velocity (m/s)	Peak energy (J)
Dry ice driven	Microcentrifuge cap	0.37	44.27 ± 3.28	0.97 ± 0.1
Compressed N_2 driven	Microcentrifuge cap	0.37	49.46 ± 1.43	0.53 ± 0.04
	Steel sphere	3.52	21.61 ± 0.09	14.6 ± 0.59
	Brass sphere	3.82	20.29 ± 0.17	13.81 ± 0.59
	Ceramic sphere	1.47	27.18 ± 0.35	6.13 ± 0.25
	Steel cylinder	5.22	10.69 ± 0.09	7.97 ± 0.31
	Aluminum cylinder	1.82	19.07 ± 0.07	2.75 ± 0.10
	Nylon cylinder	1.19	25.14 ± 0.23	1.30 ± 0.07

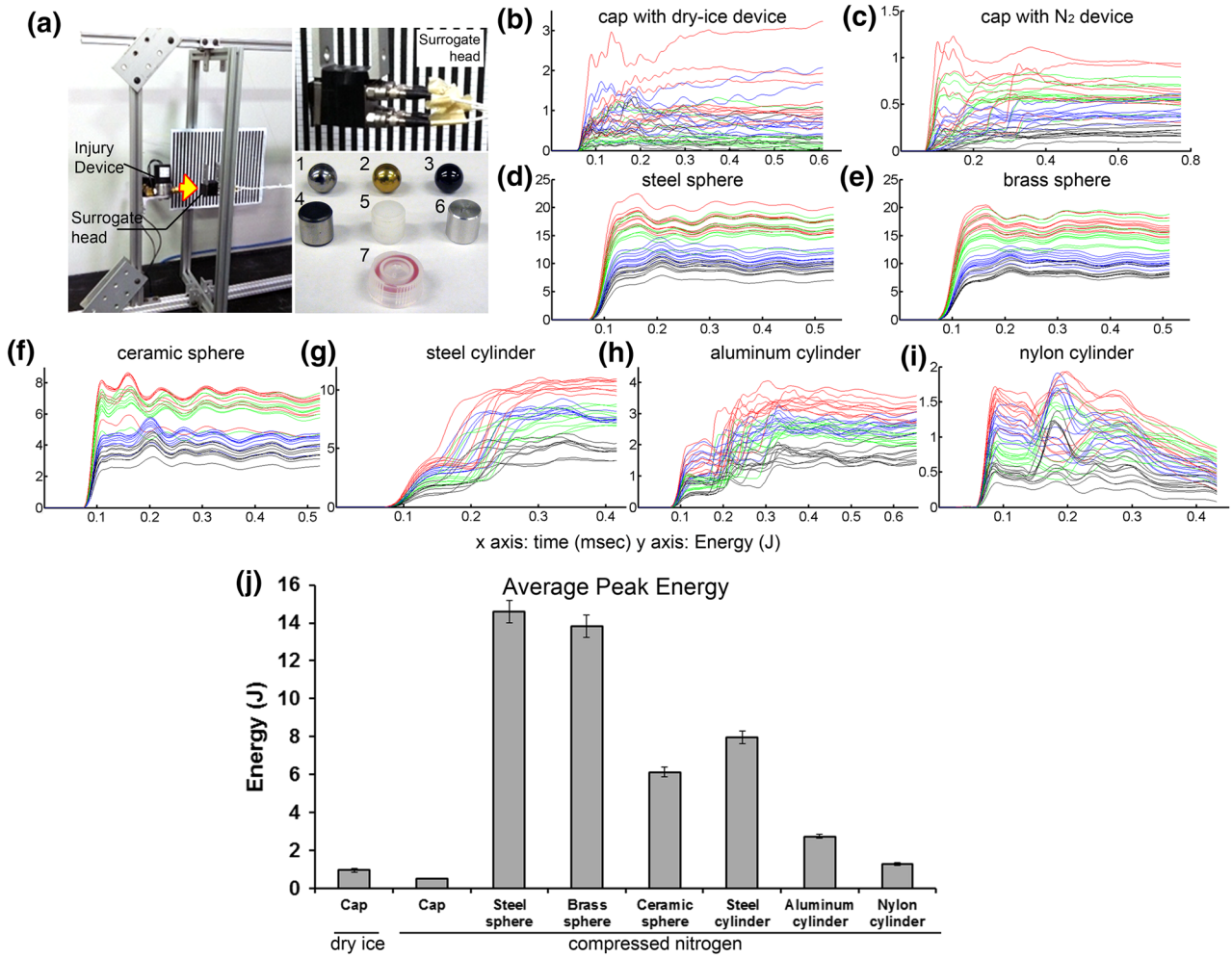

FIGURE 4. Impact testing of projectile: (a) Instrumentation including the injury device and the surrogate head with four accelerometers, and projectiles—1. steel sphere, 2. brass sphere, 3. ceramic sphere, 4. steel cylinder, 5. nylon cylinder, 6. aluminum cylinder, 7. microcentrifuge cap; (b–i) Impact energy profiles (energy vs. time) of each projectile; Blue, black, red and green lines represent data obtained from the accelerometers on the top left, top right, bottom left and bottom right corners respectively. (j) the average peak energy of each projectile.

displacement–time graphs. The caps with the dry ice device produced a head movement at a linear velocity of 2.8 ± 0.5 m/s and linear acceleration of 0.7 ± 0.3 m/s whereas with the compressed nitrogen device, the linear velocity and acceleration were 1.8 ± 0.1 and 0.3 ± 0.1 m/s respectively. Steel sphere and cylinder resulted in head movement of higher velocity (sphere = 6.4 ± 1.2 m/s; cylinder = 6.6 ± 1.1 m/s) and acceleration (sphere = 1.2 ± 0.1 ms^{-2}; cylinder = 1.4 ± 0.4 ms^{-2}).

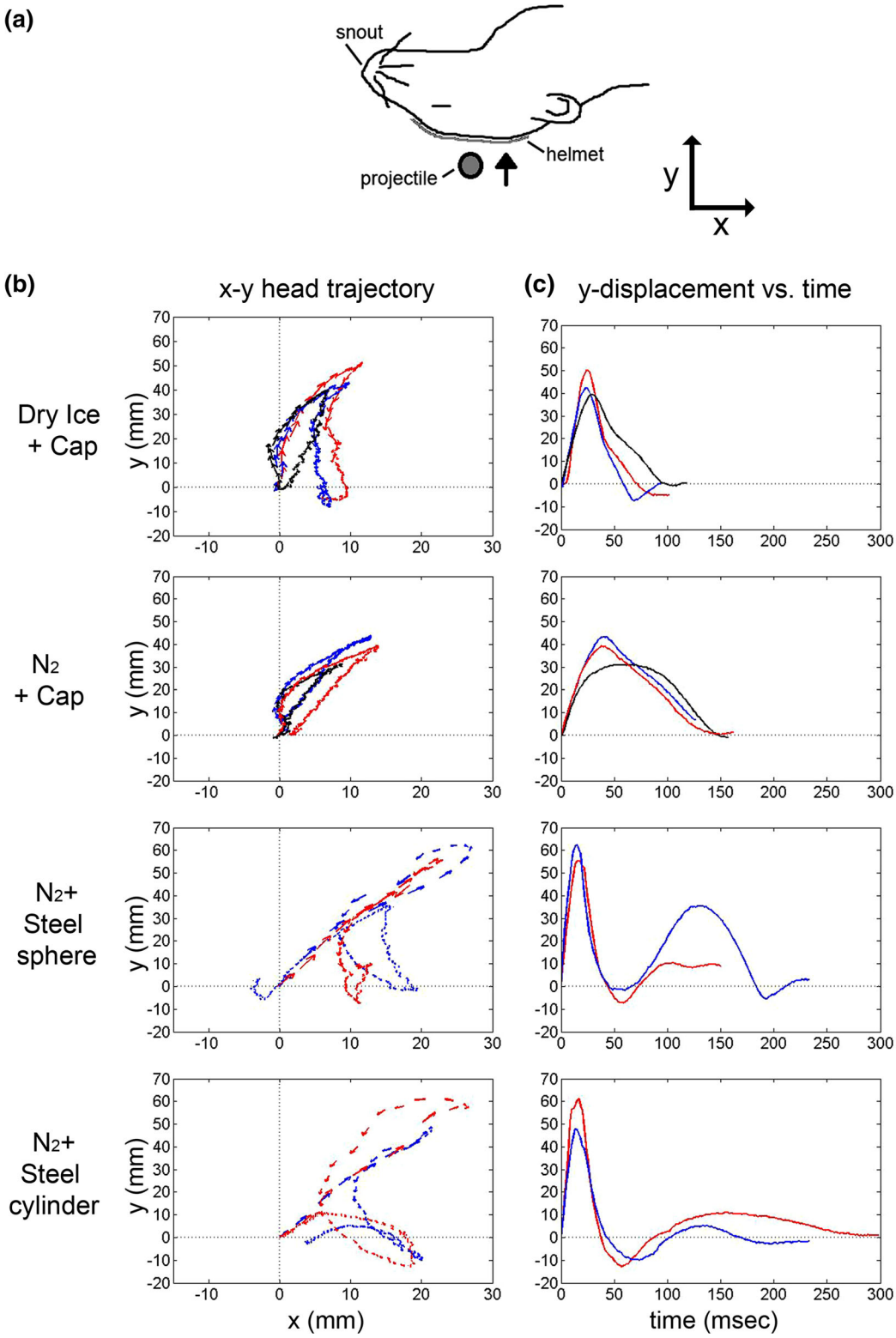

FIGURE 5. Head kinematics during projectile impact: (a) schematic drawing of a helmet-protected rat subjected to PCI; the trajectory of the snout was tracked frame by frame from the high speed videos; (b) Head trajectories on the *x–y* plane and; (c) *y*-displacement vs. time, during impact with different projectiles. Different colors represent different impact trials.

Part III: Impact location

Table 2 summarizes selected gait parameters that were altered significantly (compared to sham control) at 2 h, 1, 3, and 7 day following PCI. Overall, unilateral PCI caused significant alterations in 46 (temporoparietal hit) or 32 (temporal hit) gait parameters whereas bilateral (parietal hit) PCI affected only 18 gait parameters. Significant increases in mean intensities of both front and hind paw prints were observed in rats subjected to unilateral hits (temporoparietal and parietal hits) at 1, 3 or 7 day post-injury ($p < .05$ vs. sham). Further, at 3 day post-injury, significant increases in other static parameters such as contact area, print area and print length of the hind paws were detected following temporoparietal unilateral PCI ($p < .05$ vs. sham) but the effects of bilateral (parietal hit) PCI were limited to left hindpaw print-length. Notably, both parietal and temporoparietal PCI caused a significant decrease in single support at 3 day post-injury.

Part IV: Pilot Study

Based on the aforementioned results, we made the following refinements to the PCI model: (1) helmets constructed from fiber glass/carbon, (2) steel sphere projectile, and (3) temporoparietal contact as the impact location. Using these parameters in conjunction with the compressed nitrogen-driven PCI device, we conducted a pilot study which assessed the injury-induced loss of righting reflex (indicative of LOC), axonal injury and astrocyte activation. A significant increase in time to return of righting reflex ($p < .05$ vs. sham) was observed after a single impact (394 ± 16 s). The recovery time remained significantly higher than controls after the second (529 ± 42 s), third (523 ± 65 s) and fourth (473 ± 42 s) impact. Similar delayed recovery was absent in the sham controls when exposed to repeated anesthesia (Fig. 6a). Six hours following a single PCI, axonal damage was detected in

TABLE 2. Gait parameters altered at different time points following PCI at different locations (parietal, temporoparietal and temporal regions).

		Parietal					Temporoparietal					Temporal				
		-7d	2h	1d	3d	7d	-7d	2h	1d	3d	7d	-7d	2h	1d	3d	7d
Mean Intensity (A.U.)	LF									●						
	LH															●
	RF															
	RH										●			●		
	FP									●						
	HP										●			●		
Max. Contact Area (cm2)	LF															
	LH									●						
	RF															
	RH									●						
	FP															
	HP									●						
Print Area (cm2)	LF									●						
	LH									●						
	RF															
	RH									●						
	FP															
	HP									●						
Print Length (cm)	LF															
	LH				●					●						
	RF															
	RH															
	FP															
	HP				●					●						
Support	Single %				O					O						

O Decrease ● Increase

LF left front paw, *LH* left hind paw, *RF* right front paw, *RH* right hind paw, *FP* front paws, *HP* hind paws.

corpus callosum and cerebral cortex revealed by accumulation of β-APP and the formation of axonal bulbs. The amount of axonal damage and axonal bulbs increased following multiple PCI (Figs. 6b and 6d). As shown in Fig. 6c and d, hippocampal GFAP immunoreactivity increased significantly at 24 h following a single PCI ($p < .05$ vs. sham), suggestive of astrocyte activation. Multiple PCI significantly increased GFAP expression at 6 h post-injury (Fig. 6d).

DISCUSSION

This study described the advancements made to the engineering components in the PCI injury model including a fiber glass/carbon helmet, a steel spherical projectile and temporoparietal region as the impact target. The pilot study using this refined PCI model showed a prolonged righting reflex suppression, acute axonal damage as indicated by the accumulation of β-APP in corpus callosum, as well as hippocampal astrocyte activation.

The primary purpose of the helmet in our PCI model is to absorb and distribute impact energy elicited by the projectile in order to replicate the effects of closed-head concussion leading to mTBI, yet protecting the rat against skull fracture and cerebral laceration. In keeping with this, the helmet testing procedures were designed to identify which material construct transfers sufficient energy during impact to produce a mild concussive injury. Critically, the mass of the helmet reduces the velocity imparted to the head and thus reduces potential linear/angular acceleration caused by the projectile impact.[17] Thus, one of the goals was to achieve a lighter helmet in order to minimize the effect of additional mass on the head kinematics. The fiber glass/carbon helmet (Helmet A) was the lightest among the helmets we tested (2.92 vs. 11.83 g metal helmet in the original PCI model). It also had the lowest elastic modulus, allowing deformation with a relatively small load thus facilitating contact (and load transfer) between the inner surface of the helmet and the rat head. Moreover, the helmet was fabricated using a rat head mold to maximize the contact area and thus the load distribution on the rat head during impact. The effective transfer of energy onto the head protected by Helmet A was revealed by the larger helmet-to-head contact area and pressure magnitude indicated on the pressure sensor films, compared to the other helmets. The robustness of injury response in animals wearing Helmet A was evident from the observation of significant upregulation of GFAP in the hippocampus following PCI. Elevated GFAP is a hallmark of reactive astrocytes that are essential to preserve neural tissue and restrict infiltration of inflammatory cells into viable neural tissue after brain injury.[20] Both material testing and immunohistological data suggest that Helmet A (fiber glass/carbon) produces mTBI in the absence of any overt pathology that would be indicative of more severe forms of TBI.

The type of projectile is another factor determining the impact energy in our PCI model. At an operating pressure of 552 kPa, cylindrical projectiles and the caps were unstable and tumbled, limiting the consistency of impact characteristics. In contrast, the spherical projectiles produced more precise, consistent impacts of higher energy at the same operating pressure, due to their relatively low drag coefficient and small point of contact with the impact surface. In addition, the impact energy was reflected by the head movement such that steel spheres and cylinders produced greater displacement of the rat head at a higher rate compared to the caps. Existing animal models involving head impact use blunt impactors of heavier weight (50–600 g) at lower velocity (4–11 m/s), producing a head velocity of 3–5 m/s and focal contusion primarily under the impact site.[22,30] Our approach of using a spherical projectile of lower mass results in a higher impact velocity (>20 m/s) that theoretically induces larger stress and produces more severe injury without causing local tissue deformation (contusion).[21] The type of projectile also affects the head acceleration which is a critical factor predictive of brain injury severity. However, while the center of gravity of the rat head is not known and in this study the animals were not instrumented to record head acceleration (linear or angular), the interpretation of the acceleration data obtained solely from the high speed videography is limited.

Impact location in the PCI model affected the gait/locomotor performance. A PCI at the temporoparietal region of the rat head produced the most robust gait abnormalities, compared to the targeted temporal or parietal regions. This can be, in part, explained by the functional organization of the cerebral cortex in rats. The temporoparietal hit (point of impact at approximately −0.5 to −1.5 mm posterior to Bregma) targeted directly at the hindlimb and forelimb regions of the right primary somatosensory cortex.[23] The somatosensory system adjusts and fine-tunes the limb parameters by receiving and processing sensory information from muscles, skin and joint receptors.[8] Previous studies have demonstrated that damage or age-related degeneration of the primary somatosensory cortex led to gait disturbance including asymmetric use of the limbs[1] and increased paw print/pressure.[12] Using the CatWalk gait analysis system, Vandeputte *et al.*[29] observed acute alterations of gait metrics (increased paw intensity, print area and print width) in a rat

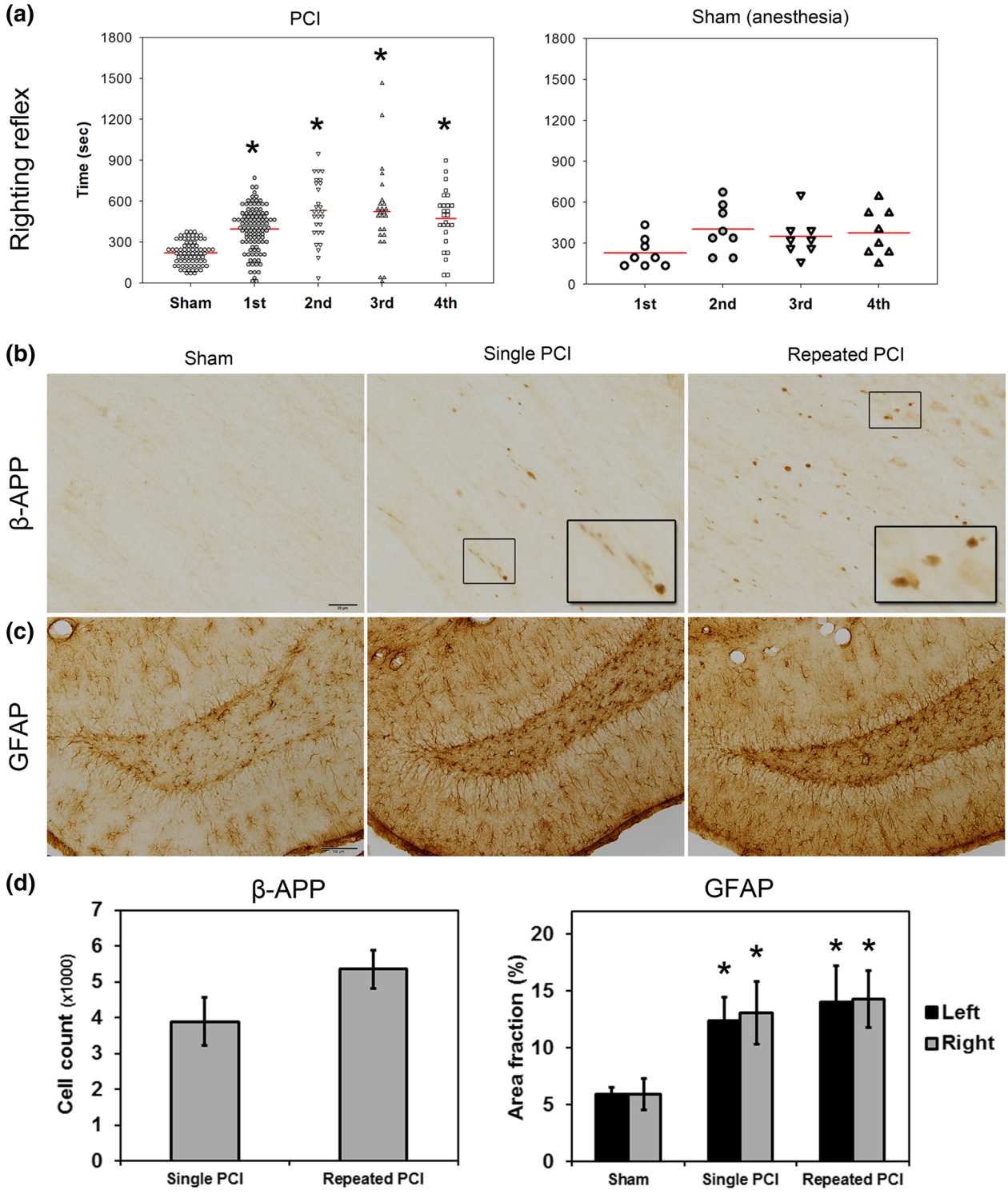

Figure 6

FIGURE 6. Preliminary data obtained from the refined PCI injury model: (a) Time to return righting reflex of sham control, single and repeated PCI (top left) and repeated sham control (top right). *$p < 0.05$ compared to sham control (one-way ANOVA with Dunn's *post hoc* tests); (b) axonal injury indicated by the accumulation of β-APP and bulb formation in the corpus callosum of animals subjected to PCI(s); Scale bar: 20 μm (magnification: 40x objective); (c) astrocyte activation indicated by the increased immunoreactivity of GFAP in the hippocampus following PCI(s); scale bar: 100 μm (magnification: 10× objective); (d) quantification of the β-APP and GFAP immunoreactivity. *$p < 0.05$ vs. sham (one-way ANOVA; Fisher's LSD *post hoc* tests).

model of temporoparietal stroke. These gait changes are similar to those seen in the present study and in our previous study using the dry ice-driven PCI device.[5] More importantly, they mirrored the conservative gait strategy adopted by young adults with concussion.[19] In contrast, temporal PCI targeted at the right barrel cortex and upper lip region of the right primary somatosensory cortex, whereas a parietal (bilateral) injury encompassed both left and right cingulate areas and secondary motor cortices.[23] The barrel cortex may indirectly affect the gait since it receives sensory information from the whiskers that may guide locomotion, particularly in darkness.[14] Other affected areas by the temporal or parietal PCI might have little or no effect on the locomotor performance.

The dynamic responses of the rat head resulting from different impact locations might also account for the more prominent changes produced by temporoparietal PCI (vs. temporal or parietal PCIs). A study using non-human primates reported that the head acceleration by a temporoparietal impact was the highest among the frontal, occipital and cranial impacts, resulting in longer duration of unconsciousness. The high acceleration was suggested to be associated with the low mechanical impedance at the temporoparietal blow due to the oval shape of the head.[16] Although these findings cannot be directly translated into rat as the head geometry is different, they provide a plausible mechanism of how the impact location affects the head kinematics and thus injury severity. Examining such a hypothesis requires comprehensive biomechanical analysis of the PCI model that is beyond of the scope of the current study.

The refined model resulted in delayed righting reflex recovery, accumulation of β-APP and astrocyte activation. In both clinical and experimental TBI, the loss of righting reflex indicates LOC that is associated with the injury severity. In general, loss of righting reflex of 15–30 min in animal TBI models is considered moderate-severe TBI, and <15 min is considered mild.[9] In our PCI model, the righting reflex suppression ranges from 6 to 9 min thereby meeting the 'mild' criteria. PCI also produced axonal injury without gross pathology. Axonal injury identified by β-APP accumulation and retraction balls (axonal swelling) have been observed in mild closed-head injury, both experimentally[18] and clinically.[2] It was suggested to be associated with head acceleration/deceleration.[28] In our PCI model, the rat head sustains a combined linear and angular acceleration. This suggests that the observation of acute increases in β-APP staining in the current study may be due to tissue deformation/axonal injury resulting from an intracerebral pressure gradient generated by linear acceleration and transient deformation of skull, as well as the shear and tensile strains generated by angular acceleration. In keeping with our previous findings, hippocampal GFAP level increased significantly following a single PCI (vs. sham) indicating that the refined PCI model is capable of inducing regional-specific astrocyte activation comparable to that detected in the original model.

To conclude, the WRAIR PCI model was refined to provide a consistent and highly reproducible closed-head concussion in rats. Clinically relevant signs such as LOC and axonal injury were evident in this refined concussion model. Because the PCI model is fully non-invasive and does not involve any surgical procedures, it provides a unique and valuable tool for studying the injury mechanism of closed-head impacts, particularly repeated concussion. Moreover, by virtue of its reproducibility, high throughput capacity (12 animals can be injured in an hour), simple design and relative ease of fabrication, the model will provide an optimal exploratory platform for future diagnostic and therapeutic preclinical studies that can be readily implemented in other research laboratories.

ACKNOWLEDGMENTS

The views of the authors do not purport or reflect the position of the Department of the Army or the Department of Defense (para 4-3, AR 360-5). The authors declare that there are no conflicts of interest in this study. This research is funded by Combat Casualty Care Research Program and Congressionally Directed Medical Research Program (Contract #: W81XWH-12-2-0134). The authors would like to thank Weihong Yang, Francis Bustos, Megan Winter, David Miles and SGT Shawn McLoughlin for technical supports.

REFERENCES

[1]Blaszczyk, J. W., and C. Dobrzecka. Effects of unilateral somatosensory cortex lesion upon locomotion in dogs. *Acta Neurobiol. Exp. (Wars)* 55:133–140, 1995.

[2]Blumbergs, P. C., G. Scott, J. Manavis, H. Wainwright, D. A. Simpson, and A. J. McLean. Staining of amyloid precursor protein to study axonal damage in mild head injury. *Lancet* 344:1055–1056, 1994.

[3]CDC. Sports-related recurrent brain injuries—United States. *MMWR Morb. Mortal. Wkly. Rep.* 46:224–227, 1997.

[4]Cernak, I., Z. Wang, J. Jiang, X. Bian, and J. Savic. Ultrastructural and functional characteristics of blast injury-induced neurotrauma. *J. Trauma* 50:695–706, 2001.

[5]Chen, Z., L. Y. Leung, A. Mountney, Z. Liao, W. Yang, X. C. Lu, J. Dave, Y. Deng-Bryant, G. Wei, K. Schmid, D. A. Shear, and F. C. Tortella. A novel animal model of closed-head concussive-induced mild traumatic brain

injury: development, implementation, and characterization. *J. Neurotrauma*. 29:268–280, 2012.
[6]Cole, J. T., A. Yarnell, W. S. Kean, E. Gold, B. Lewis, M. Ren, D. C. McMullen, D. M. Jacobowitz, H. B. Pollard, J. T. O'Neill, N. E. Grunberg, C. L. Dalgard, J. A. Frank, and W. D. Watson. Craniotomy: true sham for traumatic brain injury, or a sham of a sham? *J. Neurotrauma*. 28:359–369, 2011.
[7]Creeley, C. E., D. F. Wozniak, P. V. Bayly, J. W. Olney, and L. M. Lewis. Multiple episodes of mild traumatic brain injury result in impaired cognitive performance in mice. *Acad. Emerg. Med*. 11:809–819, 2004.
[8]Deliagina, T. G., G. N. Orlovsky, P. V. Zelenin, and I. N. Beloozerova. Neural bases of postural control. *Physiology (Bethesda)* 21:216–225, 2006.
[9]Dewitt, D. S., R. Perez-Polo, C. E. Hulsebosch, P. K. Dash, and C. S. Robertson. Challenges in the development of rodent models of mild traumatic brain injury. *J. Neurotrauma* 30:688–701, 2013.
[10]DVBIC. DoD Worldwide Numbers for TBI. 2013. http://www.dvbic.org/dod-worldwide-numbers-tbi.
[11]Gennarelli, T. A., L. E. Thibault, J. H. Adams, D. I. Graham, C. J. Thompson, and R. P. Marcincin. Diffuse axonal injury and traumatic coma in the primate. *Ann. Neurol*. 12:564–574, 1982.
[12]Godde, B., T. Berkefeld, M. David-Jurgens, and H. R. Dinse. Age-related changes in primary somatosensory cortex of rats: evidence for parallel degenerative and plastic-adaptive processes. *Neurosci. Biobehav. Rev*. 26:743–752, 2002.
[13]Goldstein, L. E., A. M. Fisher, C. A. Tagge, X. L. Zhang, L. Velisek, J. A. Sullivan, C. Upreti, J. M. Kracht, M. Ericsson, M. W. Wojnarowicz, C. J. Goletiani, G. M. Maglakelidze, N. Casey, J. A. Moncaster, O. Minaeva, R. D. Moir, C. J. Nowinski, R. A. Stern, R. C. Cantu, J. Geiling, J. K. Blusztajn, B. L. Wolozin, T. Ikezu, T. D. Stein, A. E. Budson, N. W. Kowall, D. Chargin, A. Sharon, S. Saman, G. F. Hall, W. C. Moss, R. O. Cleveland, R. E. Tanzi, P. K. Stanton, and A. C. McKee. Chronic traumatic encephalopathy in blast-exposed military veterans and a blast neurotrauma mouse model. *Sci. Transl. Med*. 4:134ra160, 2012.
[14]Grant, R. A., B. Mitchinson, and T. J. Prescott. The development of whisker control in rats in relation to locomotion. *Dev. Psychobiol*. 54:151–168, 2012.
[15]Hicks, R. R., V. B. Martin, L. Zhang, and K. B. Seroogy. Mild experimental brain injury differentially alters the expression of neurotrophin and neurotrophin receptor mRNAs in the hippocampus. *Exp. Neurol*. 160:469–478, 1999.
[16]Hodgson, V., L. Thomas, and T. Khalil. Twenty-seventh stapp car crash conference proceedings (P-134) with International Research Committee on Biokinetics of Impacts (IRCOBI), San Diego, California, October 17–19, 1983.
[17]Hong, Y., and R. Bartlett. Routledge handbook of biomechanics and human movement science. New York: Routledge, 2010.
[18]Lewen, A., G. L. Li, P. Nilsson, Y. Olsson, and L. Hillered. Traumatic brain injury in rat produces changes of beta-amyloid precursor protein immunoreactivity. *Neuroreport* 6:357–360, 1995.
[19]Martini, D. N., M. J. Sabin, S. A. DePesa, E. W. Leal, T. N. Negrete, J. J. Sosnoff, and S. P. Broglio. The chronic effects of concussion on gait. *Arch. Phys. Med. Rehabil*. 92:585–589, 2011.
[20]Myer, D. J., G. G. Gurkoff, S. M. Lee, D. A. Hovda, and M. V. Sofroniew. Essential protective roles of reactive astrocytes in traumatic brain injury. *Brain* 129:2761–2772, 2006.
[21]Nahum, A. M., and J. Melvin. Accidental injury: biomechanics and prevention. Berlin: Springer, 2002.
[22]Nilsson, B., U. Ponten, and G. Voigt. Experimental head injury in the rat. Part 1: mechanics, pathophysiology, and morphology in an impact acceleration trauma model. *J. Neurosurg*. 47:241–251, 1977.
[23]Paxinos, G., and C. Watson. The rat brain in stereotaxic coordinates: hard cover edition. New York: Elsevier, 2006.
[24]Prins, M. L., A. Hales, M. Reger, C. C. Giza, and D. A. Hovda. Repeat traumatic brain injury in the juvenile rat is associated with increased axonal injury and cognitive impairments. *Dev. Neurosci*. 32:510–518, 2010.
[25]Shitaka, Y., H. T. Tran, R. E. Bennett, L. Sanchez, M. A. Levy, K. Dikranian, and D. L. Brody. Repetitive closed-skull traumatic brain injury in mice causes persistent multifocal axonal injury and microglial reactivity. *J. Neuropathol. Exp. Neurol*. 70:551–567, 2011.
[26]Shultz, S. R., F. Bao, V. Omana, C. Chiu, A. Brown, and D. P. Cain. Repeated mild lateral fluid percussion brain injury in the rat causes cumulative long-term behavioral impairments, neuroinflammation, and cortical loss in an animal model of repeated concussion. *J. Neurotrauma* 29:281–294, 2012.
[27]Smith, D. H., X. H. Chen, M. Nonaka, J. Q. Trojanowski, V. M. Lee, K. E. Saatman, M. J. Leoni, B. N. Xu, J. A. Wolf, and D. F. Meaney. Accumulation of amyloid beta and tau and the formation of neurofilament inclusions following diffuse brain injury in the pig. *J. Neuropathol. Exp. Neurol*. 58:982–992, 1999.
[28]Smith, D. H., D. F. Meaney, and W. H. Shull. Diffuse axonal injury in head trauma. *J. Head Trauma Rehabil*. 18:307–316, 2003.
[29]Vandeputte, C., J. M. Taymans, C. Casteels, F. Coun, Y. Ni, K. Van Laere, and V. Baekelandt. Automated quantitative gait analysis in animal models of movement disorders. *BMC Neurosci*. 11:92, 2010.
[30]Viano, D. C., A. Hamberger, H. Bolouri, and A. Saljo. Evaluation of three animal models for concussion and serious brain injury. *Ann. Biomed. Eng*. 40:213–226, 2012.

APPENDIX 2

RESEARCH MANUSCRIPT

Tang et al., Nervous System Changes Induced by Underbody Blast-induced Hyper-acceleration: an *in vivo* Diffusion Tensor Imaging and Magnetic Resonance Spectroscopy Study (To be submitted to J. Neurotrauma)

Journal of Neurotrauma

Journal of Neurotrauma: http://mc.manuscriptcentral.com/neurotrauma

Central Nervous System Changes Induced by Underbody Blast-induced Hyper-acceleration:an in vivo Diffusion Tensor Imaging and Magnetic Resonance Spectroscopy Study

Journal:	*Journal of Neurotrauma*
Manuscript ID	NEU-2016-4650
Manuscript Type:	Regular Manuscript
Date Submitted by the Author:	17-Jun-2016
Complete List of Authors:	Tang, Shiyu; University of Maryland School of Medicine, Magnetic Resonance Research Center Xu, Su; University of Maryland School of Medicine, Diagnostic Radiology and Nuclear Medicine Fourney, William; University of Maryland at College Park Leiste, Ulrich; University of Maryland at College Park Proctor, Julie; University of Maryland School of Medicine, Magnetic Resonance Research Center Fiskum, Gary; University of Maryland School of Medicine, Gullapalli, Rao; University of Maryland School of Medicine, Magnetic Resonance Research Center; University of Maryland School of Medicine, Department of Diagnostic Radiology & Nuclear Medicine
Keywords:	ANIMAL STUDIES, Diffusion Tensor Imaging, MRI SPECTROSCOPY, MODELS OF INJURY

Central Nervous System Changes Induced by Underbody Blast-induced Hyper-acceleration: an *in vivo* Diffusion Tensor Imaging and Magnetic Resonance Spectroscopy Study

Shiyu Tang[1,2], Su Xu[1,2], William L Fourney[3,4], Ulrich H Leiste[3,4], Julie L Proctor[5,6], Gary Fiskum[5,6], Rao P Gullapalli[1,2]

[1]Department of Diagnostic Radiology and Nuclear Medicine, University of Maryland, Baltimore, MD, United States
[2]Core for Translational Research in Imaging @ Maryland, University of Maryland, Baltimore, MD, United States
[3]Department of Mechanical Engineering, University of Maryland, College Park, MD, United States
[4]Center of Energetics Concepts Development, University of Maryland, College Park, MD, United States
[5]Department of Anesthesiology, University of Maryland, Baltimore, MD, United States
[6]Shock, Trauma, and Anesthesiology Research Center, University of Maryland, Baltimore, MD, United States

Shiyu Tang, Department of Diagnostic Radiology & Nuclear Medicine, University of Maryland School of Medicine, 22 S Greene St, Baltimore, MD 21201; Phone: 410-706-5418; sytang317@gmail.com

Su Xu, Ph.D, Department of Diagnostic Radiology & Nuclear Medicine, University of Maryland School of Medicine, 22 S Greene St, Baltimore, MD 21201; Phone: 410-706-5419; sxu@umm.edu.

William L Fourney, Ph.D, Department of Aerospace Engineering, 1131 Glenn L. Martin Hall, University of Maryland, College Park, MD; Phone: 301-405-5339; uleiste@umd.edu.

Julie L Proctor, MS, Department of Anesthesiology, University of Maryland School of Medicine, 22 S Greene St, Baltimore, MD 21201; Phone: 410-706-4711; jproctor@anes.umm.edu

Gary Fiskum, Ph.D, Department of Anesthesiology, University of Maryland School of Medicine, 22 S Greene St, Baltimore, MD 21201; Phone: 410-706-4711; gfiskum@anes.umm.edu.

Running Title:*CNS changes following Blast Induced Hyperacceleration*

Conflict of Interest: We declare no conflict of interest

Corresponding Author
Rao P Gullapalli, Ph.D.
Department of Diagnostic Radiology & Nuclear Medicine
University of Maryland School of Medicine
22 S Greene St, MD 21201
Phone: 410-328-2099
Fax: 410=328=5937
Email: rgullapalli@umm.edu

Abstract

Background: Blast related traumatic brain injury (bTBI) resulting from improvised explosive devices is the hallmark injury of recent wars and affects many returning veterans who experienced either direct or indirect exposure. Many of these veterans suffer from long term neuro-cognitive symptoms. However, there is very little evidence to show whether blast-induced acceleration alone, in the absence of secondary impacts, can cause mild TBI.

Purpose: In this study, we examine the effect of under-vehicle blast-induced hyperacceleration (uBIH) of approximately 1700G on the biochemical and microstrucutral changes in the brain using diffusion tensor imaging (DTI) and magnetic resonance spectroscopy (MRS).

Materials and Methods: Two groups of adult male Sprague-Dawley (SD) rats were subjected to a sham procedure and uBIH respectively. Axonal and neurochemical alterations were assessed using *in vivo* DTI and MRS at 2 hours, 24 hours and 7 days after uBIH.

Results: Significant reduction in mean diffusivity, axial diffusivity and radial diffusivity were observed in the hippocampus, thalamus, internal capsule and corpus callosum as early as 2 hours and sustained up to 7 days post uBIH. Total creatine (Cr) and glutamine (Gln) were reduced in the internal capsule at 24 hours post uBIH.

Conclusions: The reductions in DTI parameters, Cr and Gln *in vivo* suggests significant activation of astrocytes and diffuse axonal injury following a single underbody blast confirming previous histology reports.

Key Words: Under body blast, hyper-acceleration, MR spectroscopy, diffusion tensor imaging

Introduction

Accumulating clinical evidence as well as experience from contemporary military operations suggests that substantial short- and long-term neurologic deficits can result from blast exposure in the absence of a mechanical hit to the head. [1–5] Although the biological mechanisms underlying blast-induced traumatic brain injury (bTBI) are not completely understood, interaction with a fast-moving, transient pressure wave is generally accepted as the primary cause of brain injury that results from blast exposure. [3,6–8] Over the last few decades, a number of experimental blast models have been implemented to study the mechanisms of blast overpressure impact in rodents and larger animals such as sheep. [9–11] A common methodology is to use a shock tube where a gas-driven pressure wave is delivered directly to the immobilized animal's head or body. Experimental studies in rodents have demonstrated a correlation between memory dysfunction and distribution of neuropathological damage in the brain after exposure to blast overpressure. [12,13]However, in addition to blast overpressure, a multitude of other physical forces may play a role in bTBI, including thermal components and hyper-acceleration. Recently we described the development of a new device [14]that can be used to induce underbody blast-induced hyper-acceleration(uBIH) in rodents. Our uBIH paradigm models what occurs to occupants of vehicles targeted by land mines, rather than what occurs when an explosion occurs in the vicinity of an unmounted soldier. Using this device, we demonstrated that exposure of rats to uBIH results in histopathological evidence of diffuse axonal injury and astrocyte activation under conditions resulting in an accelerative load of 50G, indicating that hyper-acceleration alone in the absence of significant blast pressure can cause mild TBI. Whether these subtle changes are discernible*in vivo* through advanced imaging has not been examined.Indeed, the ability to accurately diagnose changes in the brain *in vivo* can have a profound impact on the appropriate therapeutic management of the patient.

Several advanced *in vivo* imaging techniques, including diffusion tensor imaging (DTI) and proton magnetic resonance spectroscopy (MRS), have been explored to study TBI in preclinical animal models in order to better understand the temporal microstructural and biochemical changes following TBI. [15–

[21]Commonly used DTI parameters include mean diffusivity (MD) and fractional anisotropy (FA). MD measures the average water diffusion within the brain tissue, whereas FA measures the degree of diffusion anisotropy present within a voxel as would be in the case of axons where water diffuses preferentially along the axon. Alterations in MD reflect pathological changes in the brain tissue due to changes in the diffusion characteristics of the intra- and extra-cellular water compartments, including restricted diffusion (cytotoxic edema) and water exchange across permeable boundaries. [22] Changes in the FA on the other hand are indicative of the structural integrity of the tissue. The sub-parameters of FA include axial diffusivity (AD) and radial diffusivity (RD). Diffusion along the axon is measured by AD and is a measure of axonal integrity, whereas RD measures diffusion across the axonand is reflective of myelin integrity. [23]Previous TBI studies on both humans and animals have shown altered MD [24–27]and FA in white matter regions [19,28–33] anywhere from 24 hours to several days followinginjury, reflecting pathological conditions such as edema, fiber degeneration, cellular membrane disruption and cell death. [20,32,34,35]High-resolution *in vivo*MRS provides complementary information and assesses metabolic irregularities following injury. Several metabolites such as N-acetylaspartate (NAA), choline (Cho) and lactate (Lac) are highly sensitive to the pathology that contributes to TBI.Reductionin concentration of NAA, glutamate (Glu),creatine (Cr), myo-inositol (Ins) and taurine (Tau) in tissues and increased concentrations of lactate, phosphocholine (PCho) and glutamine (Gln) at either acute or sub- acute stages have beenreported, indicating conditions including ischemia, mitochondrial dysfunction and imbalance of excitatory/inhibitory and astrocyte activation. [20,21,36,37]In this study we use both *in vivo* DTI and MRS to evaluate early microstructural and biochemical alterations caused by uBIH in the rat brain.

Materials and Methods

Animal Preparation

Six adult male Sprague-Dawley (SD) rats weighing 300 to 350g underwent the uBIH procedure as described in Proctor et al. [14]and another group of six male SD rats at the same weight range were assigned to

be the sham group.[14] Briefly, all rats were initially anesthetized with ketamine (80mg/kg) and xylazine (10 mg/kg). Each rat belonging to the uBIH group was wrapped in 2 cm thick cotton blankets to minimize movement and placed inan aluminumcylinder, 37 cm long by 3 cm wide thatwas bolted onto a 38 cm square and 5 cm thick aluminum platform. This platform was located immediately above a second 38 cm square aluminum platform that was 2.5 cm thick. A 0.6 cm thick hard rubber pad was placed between the two platforms to dampen oscillatory accelerations. Both platforms had 2.5 cm wide holes located inside each of the four corners. Aluminum rods 90 cm high were inserted through each of the holes and secured to a steel base on which the platforms rested, thus allowing for only direct movement of the platforms vertically following the blasts. The steel base was bolted to the edges of a steel tank filled with water to a stand-off distance of from the bottom platform of 0.25 cm. An explosive charge of 1.5g pentaerythritoltetranitrate was placed in the water 5 cm under the center of the plate, that when detonated, generated maximal G forces of 1734 ± 90 G (mean ±sem; n= 6) as measured by an accelerometer attached to the top plate near the head ends of the cylinder. . The explosion caused the plate to accelerate vertically to heights of approximately 70 cm and then drop back down to the original location. During two experiments, we also attached pressure sensors to the top plate near the accelerometer. An increase of only less than one pound per square inch (psi) was observed. Following the uBIH exposure, the rats were removed from the assembly and allowed to recover from the anesthesia. All animals recoverednormal activity within one hour and exhibited no signs of distress. Following the imaging measurements performed on day 7 after sham or blast exposure, the rats were euthanized.

In vivo DTI and ^{1}H MRS

MR experiments were performed prior to the uBIH/sham procedure (baseline), 2 hours, 24 hours and 7 days post-uBIH on a Bruker BioSpec 7.0 Tesla 30 cm horizontal bore scanner (Bruker Corporation, Ettlingen, Germany) equipped with a BGA12S gradient system and interfaced to a Bruker ParaVision 5.1

console. A Bruker 72 mm linear-volume coil was used as the transmitter and a Bruker ^{1}H 4-channel surface coil array was used as the receiver. The rat was under 2–3% isoflurane anesthesia and 1 L/min oxygen administration during the MR experiment. An MR compatible small-animal monitoring and gating system (SA Instruments, Inc., New York, USA) was used to monitor the animal's respiration rate and body temperature. The animal's body temperature was maintained at 35–37 °C using a warm water bath circulation. Ear pins and bite bars were used to fix the animal's head to minimize head motion.

A three-slice (axial, mid-sagittal, and coronal) scout image using rapid acquisition with fast low angle shot (FLASH) [38,39]was used to localize the rat brain. A fast shimming procedure (FASTMAP) was used to improve the B_0 homogeneity covering the brain. [40] Both proton density (PD) and T_2-weighted images were obtained for anatomic reference using a two-dimensional rapid acquisition with relaxation enhancement (RARE) sequence covering the entire brain. [41] Imaging was performed over a 3.5 cm field of view (FOV) in the coronal plane with an in-plane resolution of 137 μm using 24 slices at 1 mm thickness, at an effective echo-time of 18.94 ms for the proton density weighted images and an effective echo-time (TE) of 56.82 ms for the T_2-weighted images. The repeat time (TR) was 3500 ms.

Diffusion-tensor images were acquired with a single shot, spin-echo echo-planar imaging sequence. An encoding scheme of 30 gradient directions was used with the duration of each of the diffusion gradients being 4 ms with a temporal spacing of 20 ms between the two diffusion gradients. Three b-values (1000 s/mm^2, 1500 s/mm^2 and 2000 s/mm^2) were acquired for each direction following the acquisition of five images acquired at b= 0 s/mm^2. The DTI images were obtained using a single average over the same FOV as the coronal PD/T2 images but at an in-plane resolution of 0.273 mm at a TR/TE of 6000/49.90 ms respectively.

^{1}H MRS datawas obtained from voxels that covered left internal capsule (3 x 3 x 3 mm^3), left hippocampus (1.5 x 3.5 x 3 mm^3) and left cortex (1.5 x 4 x 3 mm^3) respectively. These regions were chosen as they were implicated in a previous study using the same injury model and also based on reports using

other TBI models. [14,36]Prior to acquiring the spectra, adjustments of all first- and second-order shims over the voxel of interest were accomplished with the FASTMAP procedure. A custom modified short-echo-time Point-RESolved Spectroscopy (PRESS) pulse sequence (TR/TE = 2500/10 ms, number of averages = 360) [42]was used for MRS data acquisition covering the three regions of interest (ROI). The unsuppressed water signal from each of the prescribed voxels was obtained to serve as a reference for determining the specific metabolite concentrations. The total duration of the entire imaging experiment was approximately 2.5hour. All animal procedures were approved by the University of Maryland, Baltimore, Animal Care and Use Committee.

Data Processing and Analysis

DTI reconstruction was performed on each voxel using in-house MATLAB program (Mathworks, Natick, MA) to generate MD, FA, AD and RD maps. ROIs for each rat were manually drawn on the FA map within the cortex (left, right), hippocampus (left, right), thalamus (left, right), internal capsule (left, right), and the corpus callosum (genu, trunk, splenium) respectively as shown in Fig. 1.

^{1}H MRS data was fitted using the LCModel package.[43]Representative *in vivo* high resolution ^{1}H MRS from the internal capsule from one uBIH rat at its baseline is shown in Fig. 2B. The Cramer-Rao lower bounds were estimated by the LCModel to assess the reliability of the reported metabolite concentration, and only metabolites with standard deviations (SD) < 20 were included for further analysis.

DTI and MRS data from each region were normalized to its own baseline level (pre-uBIH). The ratio of post to pre-uBIH level was used to capture changes between the two time points. Statistical analysis was performed using SigmaPlot version 12.5 (Systat Software, Inc., San Jose, CA, USA). Both DTI and MRS data of sham and uBIH rats at 4 time points were analyzed using a two-way repeated measure ANOVA to examine temporal changes in each region and group comparisons were made at each observation point. Statistical significance was defined as $p < 0.05$.

Results

Microstructural Alterations following uBIH

Six rats were exposed to uBIH that generated maximal G forces ranging from 1500 to 1900 G, with a mean value of 1734 ± 90 G. All of these rats and the six sham rats that were similarly anesthetized but not subjected to uBIH survived to 7 days, at which time they were euthanized. No animal demonstrated any visible changes on T_2-weighted brain images at 2 h, 24 h, and 7 days post-blast or post-sham blast. However, broad reductions of DTI parameters were observed in the hippocampus, thalamus and the internal capsule of rats in the uBIH group compared to the sham group. Significant alterations of MDwere observed in the hippocampus (right: $F = 2.44$, $p = 0.017$), and the thalamus (left: $F = 7.092$, $p = 0.024$; right: $F = 5.257$, $p = 0.045$) (Table 1) in the uBIH rats compared to the sham group. The reductions of MD were significant at 2 hours ($p = 0.044$) and 7 days ($p = 0.025$) in the hippocampus (Fig. 2A) and at 2 hours in the thalamus (left: $p = 0.008$; right: $p = 0.018$) (Fig.2B, C) in the uBIH cohort compared to the sham cohort. AD was significantly reduced in the hippocampus (right: $F = 7.208$, $p = 0.023$) (Table 1) at 24 hours ($p = 0.006$) and 7 days ($p = 0.008$) (Fig.3A) and in the internal capsule (right: $F = 5.222$, $p = 0.045$) at 24 hours ($p = 0.006$) (Fig. 4B) in the uBIH group compared to the sham group.RD was significantly reduced in the thalamus (left: $F = 14.291$, $p = 0.004$; right: $F = 7.861$, $p = 0.019$) (Table 1) at 2 hours (left: $p < 0.001$; right: $p = 0.001$), 7 days (left: $p = 0.013$; right: $p = 0.041$) (Fig.4A, B) and in the genu of corpus callosum ($F = 8.407$, $p = 0.016$) at 2 hours ($p = 0.031$), 7 days ($p = 0.004$) (Fig.4C) after uBIH.

Biochemical Alterations following uBIH

Biochemical alterations were observed in the internal capsule where changes in the levels of Cr ($F =5.844$, $p =0.036$) were substantial and marginal Gln ($F =3.877$, $p = 0.077$) changes were also observed in the uBIH group compared to the sham group (Table 1). Both Cr ($p =0.005$) and Gln ($p =0.021$) levels were significantly reduced at 24 hours in the uBIH group compared to the sham group (Fig. 5). No other

significant biochemical alterations were detected in any other regions at any time points in the uBIH rats compared to the sham rats.

Discussion

To the best of our knowledge, this is the first *in vivo* study to apply a combination of DTI and MRS to detect biochemical and microstructural changes following hyper-acceleration from a blast in isolation from the overpressure from the blast (primary impact) or other secondary impact related injuries. We demonstrate early metabolic alterations and tissue microstructure following hyper-acceleration which persist until 7 days following the exposure.Our study reveals three main findings: (a) no visible brain injuries were observed on conventional T_2-weighted imaging even when the animals were exposed to an average of 1700G; (b)Cr and Gln levels decreased in the internal capsule at 24-hours post uBIH and returned to baseline values by seven days; and (c) shearing injuries as observed by changes in diffusion tensor parameters were observed in the internal capsule, hippocampus, and thalamus as late as 7 days following injury.When compared to the histologic findings from our previous study performed under conditions that generated much lower G forces (50G) and which resulted in diffuse axonal injury and astrocyte activation [14], the present study not only confirms these findings but provides further evidence that neuropathologychanges can be detected *in vivo*using DTI and MRS techniques.

In the present study, decreased AD level in the internal capsule at 24 hours and decreased MD and AD levels in the hippocampus at both 2 hours and 7 days post uBIH are indicative of mild diffuse axonal injuries which agree with the histology findings using the same uBIH model. [14] In addition to these changes, we also observed a decreased MD and RD in the thalamus at 2 hours post uBIH indicating cell swelling. These results indicate that the sequelae of pathological events occur at a different rate in each vulnerable brain which is well captured non-invasively from the longitudinal DTI data. The low Cr and Gln levels found in the uBIH rats at 24 hours in the internal capsule may indicate an imbalance in astrocytic function after exposure to uBIH. Synthesized in the liver and transported to the brain, it has been shown that Cr is

two- to four-fold more concentrated in glial cells than in neurons,[44] with quite large regional variations. Astroglial cells are virtually the sole site for Gln synthetase activity in brain to convert Glu to Gln.[45] A prior study using this injury model demonstrated astrocyte activation in the internal capsule at 7 days post uBIH.[14] It is quite likely that the depletions of Cr and Gln are due to this astrocyte activation. The *in vivo* longitudinal localized MRS findings in this study provide further evidence that gliosis in the internal capsule is a prominent pathology following uBIH.[14,36]

Various animal models have been developed to replicate different aspects of human TBI over the past several decades. The most widely-used ones are the controlled cortical impact (CCI) model,[46] the fluid percussion injury (FPI) model[47] and blast tube bTBI models.[48,49] CCI and FPI models result in direct brain deformation and neuronal cell death which is absent in the uBIH model. Depending on the severity of injury, tissue damage from CCI and FPI is focal and may be directly visible even with conventional MRI. Studies have shown that the changes from these focal injuries lead to various changes in local conditions including ischemia, mitochondrial dysfunction and imbalance of excitatory/inhibitory and astrocyte activation.[15,20,37,50]

Studies using blast overpressure primary bTBI models are more comparable to our uBIH model since they don't introduce direct impact on the brain and result in relatively mild injuries without severe tissue damage and broad biochemical disturbances. In primary bTBI models, injury is generated by blast overpressure waves or shock waves to the head and often to the chest and abdomen. Previous *in vivo* or *in vitro* primary bTBI studies using shock tube or direct cranial blast reported increased mean kurtosis (MK), Gln levels and expression of glial fibrillary acidic protein (GFAP), indicating astrocyte and microglial activation in subcortical regions such as the internal capsule, hippocampus and hypothalamus at the sub-acute stage following injury.[36,51,52] Diffuse axonal injury was also observed as increased FA in the internal capsule and decreased MD in the hippocampus up to 14 days post blast, indicating axonal swelling or a disruption of ionic homeostasis resulting in an imbalance in intra- and extra-cellular water.[18,19,36] A more

recent study assessed the value of manganese-enhanced magnetic resonance imaging (MEMRI) using manganese chloride ($MnCl_2$) at various time points following a 30 psig blast in a shock tube and found that manganese uptake to be a promising biomarker of TBI. [53] While future preclinical studies on hyper-acceleration may benefit form MEMRI, the use of manganese in humans has been shown to be neurotoxic and the translation of such studies may take some time as research continues to make less toxic manganese-based chelates.

The present study demonstrates that in uBIH, the changes are localized to the internal capsule and the hippocampus with changes occurring at different time points, depending on the parameter measured and the brain location. The resultsshow some consistency with previous primary bTBI reports. In a previous study on direct cranium only blast traumatic brain injury (dc-bTBI) rat model which was silent on conventional T_2-weighted imaging, diffusion kurtosis imaging (DKI) and proton MRSalso demonstrated impairments in the internal capsule and the hippocampuswith peak changes observed at about 21 days after dc-bTBI. [36]Significant microglial activation and neurodegeneration were observed even at 28 days in the hippocampus.

It is generally accepted that TBI without physical signs of head injury can potentially contribute to post-traumatic stress disorder (PTSD). [5,54]Thehippocampus and the internal capsule are reported to play a role in triggering the typical symptoms of PTSD. [55–62] PTSD patients with a history of combat traumashow a considerable reduction in the volume of the hippocampus and hippocampal dysfunction. [56–58]Treatments which resulted in neurogenesis in the hippocampus or increased hippocampal volume were shown to improve PTSD symptoms. [59,61,62]PTSD symptoms induced by mTBI are also associated with white matter damageto the internal capsule and uncinate fasciculus, inducing a loss of inhibitory control of the autonomic nervous system (ANS) which results in alterations in ANS driven defense and socially adaptive physiological states. [55]Significantly reduced FA in the internal capsule was also reported to be closely related to major depressive disorder (MDD) after mTBI. [60]While the present study did not assess the long term behavioral outcome on the rats, given the spatial locations that are implicated in this study and the dc-

bTBI model, the results suggest the possibility of vestibular dysfunction and memory impairment.[34] Our findings also suggest that both the cranium only blast injury and the hyper-acceleration associated injury may combine synergistically resulting in comorbidities that are worse than from a single type of injury. Indeed, this is a more likely scenario wherea person exposed to blast injury may also be exposed to certain amount of hyper-acceleration.

This study on microstructural and biochemical alterations after uBIH should be viewed in the context of certain limitations. First,no studies were performed to assess the long-term behavioral outcomes of these animals. While we expect similar behavior changes as in the dc-bTBI model given the similarity in the regions affected, future studies should include comprehensive behavioral testing and correlate with *in vivo* findings.Second,histological confirmation was not possible on these animals at this time. However, histologyresults from the previous study using the same uBIH model are supportive of the observed results in this study.[12]Third, this study only used male rats and so the results cannot be generalized across sex. The effect of sex on the outcomes and recovery of TBI has been emphasizedin multiple clinical and animal studies. [63–66]Given the limitation of this pilot study, future longitudinal studies should incorporate behavioral testing of the animals and histological confirmation incorporating both sexes.

Conclusion

In this study, we demonstrate for the first time that uBIH alone in the absence of the blast overpressure component results in acute mild TBI which continues to persist up to 7 days post-uBIH. These findings offer useful information in understanding the pathophysiology of uBIH induced mild TBI. uBIH induces diffuse axonal injury and astrogliosis in the internal capsule and hippocampus. Given that similar regions were implicated in dc-bTBI, it is likely that the hyper-acceleration along with the ensuing blast may synergistically lead to more comorbiditiesin the long term.The internal capsule and hippocampus may be potential therapeutic targets for treating bTBI and preventing delayed mental health problems.

Acknowledgments

This material is based on research sponsored by the U.S.Army grant W81XWH-13-1-0016 and by the U.S.AirForce711HPW/XPT under Cooperative Agreement number FA8650-11-2-6142 and FA8650-11-2-6D04.TheU.S. Government is authorized to reproduce and distribute reprints for Governmental purposes notwithstanding any copyright notation thereon.

The views expressed in this article are those of the authors and do not necessarily reflect the official policy or position of the Air Force, the Department of Defense, or the U.S. Government.

References

1. Trudeau, D.L., Anderson, J., Hansen, L.M., Shagalov, D.N.,Schmoller J.,, Nugent S., and Barton S. (1998). Findings of mild traumatic brain injury in combat veterans with PTSD and a history of blast concussion. JNeuropsychiatry Clinical Neurosci 10, 308–313.
2. Cernak, I.,Savic, J., Ignjatovic, D.,and Jevtic, M. (1999). Blast injury from explosive munitions. J Trauma 47, 96–103; discussion 103–104.
3. DePalma, R.G., Burris, D.G., Champion, H.R., and Hodgson, M.J. (2005). Blast injuries. N Engl J Med 352, 1335–1342.
4. Ling, G., Bandak, F., Armonda, R., Grant, G., and Ecklund, J. (2009). Explosive blast neurotrauma. J Neurotrauma 26, 815–825.
5. Elder, G.A., and Cristian, A. (2009). Blast-related mild traumatic brain injury: mechanisms of injury and impact on clinical care. Mt Sinai J Med 76, 111–118.
6. Elsayed, N.M. (1997). Toxicology of blast overpressure. Toxicology 121, 1–15.
7. Taber, K.H., Warden, D.L., and Hurley, R.A. (2006). Blast-related traumatic brain injury: what is known? J Neuropsychiatry Clin Neurosci 18, 141–145.
8. Przekwas, A., Somayaji, M.R., and Gupta, R.K. (2016). Synaptic Mechanisms of Blast-Induced Brain Injury. Front Neurol 7, 2.
9. Savić, J. (1991). [Primary blast injuries]. VojnosaniPregl48, 489–498.
10. Stuhmiller, J.H. (1997). Biological response to blast overpressure: a summary of modeling. Toxicology 121, 91–103.
11. Garman, R.H., Jenkins, L.W., Switzer, R.C., Bauman, R.A., Tong, L.C., Swauger, P.V., Parks, S.A., Ritzel, D.V., Dixon, C.E., Clark, R.S., Bayir, H., Kagan, V., Jackson, E.K., and Kochanek, P.M. (2011). Blast exposure in rats with body shielding is characterized primarily by diffuse axonal injury. J. Neurotrauma 28, 947–59.
12. Cernak, I., Wang, Z., Jiang, J., Bian, X., and Savic, J. (2001). Ultrastructural and functional characteristics of blast injury-induced neurotrauma. J Trauma 50, 695–706.
13. Cernak, I., Wang, Z., Jiang, J., Bian, X., and Savic, J. (2001). Cognitive deficits following blast injury-induced neurotrauma: possible involvement of nitric oxide. Brain Inj 15, 593–612.
14. Proctor, J.L., Fourney, W.L., Leiste, U.H., and Fiskum, G. (2014). Rat model of brain injury caused by under-vehicle blast-induced hyperacceleration. J Trauma Acute Care Surg 77, S83–S87.
15. Mac Donald, C.L., Dikranian, K., Bayly, P., Holtzman, D., and Brody, D. (2007). Diffusion tensor imaging reliably detects experimental traumatic axonal injury and indicates approximate time of injury. J Neurosci 27, 11869–11876.
16. Mayer, A.R., Ling, J., Mannell, M.V., Gasparovic, C., Phillips, J.P., Doezema, D., Reichard, R., and Yeo, R.A. (2010). A prospective diffusion tensor imaging study in mild traumatic brain injury. Neurology 74, 643–650.
17. Croall, I., Cowie, C., He, J., Peel, A., Wood, J., Aribisala, B., Mitchell, P., Mendelow, Smith, F., Millar, D., Kelly, T., and Blamire, A. (2014). White matter correlates of cognitive dysfunction after mild traumatic brain injury. Neurology 83, 494–501.
18. Wilde, E.A., McCauley, S.R., Hunter, J.V., Bigler, E.D., Chu, Z., Wang, Z.J., Hanten, G.R., Troyanskaya, M., Yallampalli, R., Li, X., Chia, J., and Levin, H.S. (2008). Diffusion tensor imaging of acute mild traumatic brain injury in adolescents. Neurology 70, 948–955.
19. Bazarian, J.J., Zhong, J., Blyth, B., Zhu, T., Kavcic, V., and Peterson, D. (2007). Diffusion tensor imaging detects clinically important axonal damage after mild traumatic brain injury: a pilot study. J. Neurotrauma 24, 1447–1459.
20. Xu, S., Zhuo, J., Racz, J., Shi, D., Roys, S., Fiskum, G., and Gullapalli, R. (2011). Early microstructural and metabolic changes following controlled cortical impact injury in rat: a magnetic resonance imaging and spectroscopy study. J. Neurotrauma 28, 2091–2102.

21. Sajja, V., Galloway, M., Ghoddoussi, F., Thiruthalinathan, D., Kepsel, A., Hay, K., Bir, C., and VandeVord, P. (2012). Blast-induced neurotrauma leads to neurochemical changes and neuronal degeneration in the rat hippocampus. NMR Biomed 25, 1331–1339.
22. Gass, A., Niendorf, T., and Hirsch, J.G. (2001). Acute and chronic changes of the apparent diffusion coefficient in neurological disorders--biophysical mechanisms and possible underlying histopathology. JNeurolSci 186 Suppl 1, S15–S23.
23. Song, S.K, Sun, S.W., Ju, W.K., Lin, S.J., Cross, A.H., and Neufeld, A.H. (2003). Diffusion tensor imaging detects and differentiates axon and myelin degeneration in mouse optic nerve after retinal ischemia. Neuroimage 20, 1714–1722.
24. Alsop, D.C., Murai, H., Detre, J.A., McIntosh, T.K., and Smith, D.H. (1996). Detection of acute pathologic changes following experimental traumatic brain injury using diffusion-weighted magnetic resonance imaging. JNeurotrauma 13, 515–521.
25. Huisman, T.A., Sorensen, A.G., Hergan, K., Gonzalez, R.G., and Schaefer, P.W. (2003). Diffusion-weighted imaging for the evaluation of diffuse axonal injury in closed head injury. JComputAssistTomogr 27, 5–11.
26. Liu, A.Y., Maldjian, J.A., Bagley, L.J., Sinson, G.P., and Grossman, R.I. (1999). Traumatic brain injury: diffusion-weighted MR imaging findings. AJNR. AmJNeuroradiol 20, 1636–1641.
27. Mamere, A.E., Saraiva, L.A., Matos, A.L., Carneiro, A.A., and Santos, A.C. (2009). Evaluation of delayed neuronal and axonal damage secondary to moderate and severe traumatic brain injury using quantitative MR imaging techniques. AJNR. AmJNeuroradiol 30, 947–952.
28. Arfanakis, K., Haughton, V.M., Carew, J.D., Rogers, B.P., Dempsey, R.J., and Meyerand, M.E. (2002). Diffusion tensor MR imaging in diffuse axonal injury. AJNR. AmJNeuroradiol 23, 794–802.
29. Huisman, T.A., Schwamm, L.H., Schaefer, P.W., Koroshetz, W.J., Shetty-Alva, N., Ozsunar, Y., Wu, O., and Sorensen, A.G. (2004). Diffusion tensor imaging as potential biomarker of white matter injury in diffuse axonal injury. AJNR. AmJNeuroradiol 25, 370–376.
30. Mac Donald, C.L., Dikranian, K., Song, S.K., Bayly, P.V., Holtzman, D.M., and Brody, D.L. (2007). Detection of traumatic axonal injury with diffusion tensor imaging in a mouse model of traumatic brain injury. ExpNeurol 205, 116–131.
31. Mayer, A.R., Ling, J., Mannell, M.V., Gasparovic, C., Phillips, J.P., Doezema, D., Reichard, R., and Yeo, R.A. (2010). A prospective diffusion tensor imaging study in mild traumatic brain injury. Neurology 74, 643–650.
32. Wilde, E.A., Chu, Z., Bigler, E.D., Hunter, J.V., Fearing, M.A., Hanten, G., Newsome, M.R., Scheibel, R.S., Li, X., and Levin, H.S. (2006). Diffusion tensor imaging in the corpus callosum in children after moderate to severe traumatic brain injury. JNeurotrauma 23, 1412–1426.
33. Wozniak, J.R., Krach, L., Ward, E., Mueller, B.A., Muetzel, R., Schnoebelen, S., Kiragu, A., and Lim, K.O. (2007). Neurocognitive and neuroimaging correlates of pediatric traumatic brain injury: a diffusion tensor imaging (DTI) study. ArchClinNeuropsychol 22, 555–568.
34. Salmond, C.H., Menon, D.K., Chatfield, D.A., Williams, G.B., Pena, A., Sahakian, B.J., and Pickard, J.D. (2006). Diffusion tensor imaging in chronic head injury survivors: correlations with learning and memory indices. Neuromage 29, 117–124.
35. Kraus, M.F., Susmaras, T., Caughlin, B.P., Walker, C.J., Sweeney, J.A., and Little, D.M. (2007). White matter integrity and cognition in chronic traumatic brain injury: a diffusion tensor imaging study. Brain 130, 2508–2519.
36. Zhuo, J., Keledjian, K., Xu, S., Pampori, A., Gerzanich, V., Simard, J.M., and Gullapalli, R.P. (2015). Changes in diffusion kurtosis imaging and magnetic resonance spectroscopy in a direct cranial blast traumatic brain injury (dc-bTBI) model. PloS one 10, e0136151.
37. Harris, J.L., Yeh, H.-W.W., Choi, I.-Y.Y., Lee, P., Berman, N.E., Swerdlow, R.H., Craciunas, S.C., and Brooks, W.M. (2012). Altered neurochemical profile after traumatic brain injury: (1)H-MRS biomarkers of pathological mechanisms. J Cereb Blood Flow Metab 32, 2122–2134.

38. Haase, A., Frahm, J., Matthaei, D., Hänicke W., and Merboldt, K.D. (2011). FLASH imaging: rapid NMR imaging using low flip-angle pulses. 1986. JMagnReson 213, 533–541.
39. Frahm, J., Haase, A., and Matthaei, D. (1986). Rapid NMR imaging of dynamic processes using the FLASH technique. MagnResonMed 3, 321–327.
40. Gruetter, R. (1993). Automatic, localized in vivo adjustment of all first- and second-order shim coils. MagnResonMed 29, 804–811.
41. Hennig, J., Nauerth, A., and Friedburg, H. (1986). RARE imaging: a fast imaging method for clinical MR. MagnResonMed3, 823–833.
42. Xu, S., Ji, Y., Chen, X., Yang, Y., Gullapalli, R., and Masri, R. (2013). In vivo high-resolution localized (1) H MR spectroscopy in the awake rat brain at 7 T. MagnResonMed 69, 937–943.
43. Provencher, S.W. (2001). Automatic quantitation of localized in vivo 1H spectra with LCModel. NMR Biomed 14, 260–264.
44. Urenjak, J., Williams, S.R., Gadian, D.G., and Noble, M. (1993). Proton nuclear magnetic resonance spectroscopy unambiguously identifies different neural cell types. JNeuroscience 13, 981–989.
45. Norenberg, M.D., and Martinez-Hernandez, A. (1979). Fine structural localization of glutamine synthetase in astrocytes of rat brain. Brain Res 161, 303–310.
46. Dixon, C.E., Clifton, G.L., Lighthall, J.W., Yaghmai, A.A., and Hayes, R.L. (1991). A controlled cortical impact model of traumatic brain injury in the rat. JNeurosciMethods 39, 253–262.
47. McIntosh, T.K., Vink, R., Noble, L., Yamakami, I., Fernyak, S., Soares, H., and Faden, A.L. (1989). Traumatic brain injury in the rat: characterization of a lateral fluid-percussion model. Neuroscience 28, 233–244.
48. Kuehn, R., Simard, P., Driscoll, I., Keledjian, K., Ivanova, S., Tosun, C., Williams, A., Bochicchio, G., Gerzanich, V., and Simard, J.M. (2011). Rodent model of direct cranial blast injury. JNeurotrauma 28, 2155–2169.
49. Shah, A.S., Stemper, B.D., and Pintar, F.A. (2012). Development and characterization of an open-ended shock tube for the study of blast mtbi. Biomedical sciences instrumentation 48, 393–400.
50. Budde, M.D., Janes, L., Gold, E., Turtzo, L.C., and Frank, J.A. (2011). The contribution of gliosis to diffusion tensor anisotropy and tractography following traumatic brain injury: validation in the rat using Fourier analysis of stained tissue sections. Brain 134, 2248–2260.
51. Kabu, S., Jaffer, H., Petro, M., Dudzinski, D., Stewart, D., Courtney, A., Courtney, M., and Labhasetwar, V. (2015). Blast-associated shock waves result in increased brain vascular leakage and elevated ROS levels in a rat model of traumatic brain injury. PLoS ONE 10, e0127971.
52. Miller, A.P., Shah, A.S., Aperi, B.V., Budde, M.D., Pintar, F.A., Tarima, S., Kurpad, S.N., Stemper, B.D., and Glavaski-Joksimovic, A. (2015). Effects of blast overpressure on neurons and glial cells in rat organotypic hippocampal slice cultures. Front Neurol 6, 20.
53. Rodriguez, O., Schaefer, M.L., Wester, B., Lee, Y.-C.C., Boggs, N., Conner, H.A., Merkle, A.C., Fricke, S.T., Albanese, C., and Koliatsos, V.E. (2016). Manganese-Enhanced Magnetic Resonance Imaging as a Diagnostic and Dispositional Tool after Mild-Moderate Blast Traumatic Brain Injury. J. Neurotrauma 33, 662–71.
54. Chen, Y., and Huang, W. (2011). Non-impact, blast-induced mild TBI and PTSD: concepts and caveats. Brain injury 25, 641–50.
55. Williamson, J.B., Heilman, K.M., Porges, E.C., Lamb, D.G., and Porges, S.W. (2013). A possible mechanism for PTSD symptoms in patients with traumatic brain injury: central autonomic network disruption. Frontiers in neuroengineering 6, 13.
56. Kitayama, N., Vaccarino, V., Kutner, M., Weiss, P., and Bremner, J.D. (2005). Magnetic resonance imaging (MRI) measurement of hippocampal volume in posttraumatic stress disorder: a meta-analysis. Journal of affective disorders 88, 79–86.
57. Wang, Z., Neylan, T.C., Mueller, S.G., Lenoci, M., Truran, D., Marmar, C.R., Weiner, M.W., and Schuff, N. (2010). Magnetic resonance imaging of hippocampal subfields in posttraumatic stress disorder.

Archives of general psychiatry 67, 296–303.
58. Shin, L.M., Shin, P.S., Heckers, S., Krangel, T.S., Macklin, M.L., Orr, S.P., Lasko, N., Segal, E., Makris, N., Richert, K., Levering, J., Schacter, D.L., Alpert, N.M., Fischman, A.J., Pitman, R.K., and Rauch, S.L. (2004). Hippocampal function in posttraumatic stress disorder. Hippocampus 14, 292–300.
59. Bremner, J.D., and Vermetten, E. (2005). Neuroanatomical changes associated with pharmacotherapy in posttraumatic stress disorder. Annals of the New York Academy of Sciences 1032, 154–7.
60. Maller, J.J., Thomson, R.H., Lewis, P.M., Rose, S.E., Pannek, K., and Fitzgerald, P.B. (2010). Traumatic brain injury, major depression, and diffusion tensor imaging: making connections. Brain research reviews 64, 213–40.
61. Vermetten, E., Vythilingam, M., Southwick, S.M., Charney, D.S., and Bremner, J.D. (2003). Long-term treatment with paroxetine increases verbal declarative memory and hippocampal volume in posttraumatic stress disorder. Biological psychiatry 54, 693–702.
62. Douglas Bremner, J., Mletzko, T., Welter, S., Siddiq, S., Reed, L., Williams, C., Heim, C.M., and Nemeroff, C.B. (2004). Treatment of posttraumatic stress disorder with phenytoin: an open-label pilot study. The Journal of clinical psychiatry 65, 1559–64.
63. Farace, E., and Alves, W.M. (2000). Do women fare worse: a metaanalysis of gender differences in traumatic brain injury outcome. Journal of neurosurgery 93, 539–45.
64. Berry, C., Ley, E.J., Tillou, A., Cryer, G., Margulies, D.R., and Salim, A. (2009). The effect of gender on patients with moderate to severe head injuries. The Journal of trauma 67, 950–3.
65. Mychasiuk, R., Hehar, H., Farran, A., and Esser, M.J. (2014). Mean girls: sex differences in the effects of mild traumatic brain injury on the social dynamics of juvenile rat play behaviour. Behavioural brain research 259, 284–91.
66. Mychasiuk, R., Hehar, H., and Esser, M.J. (2015). A mild traumatic brain injury (mTBI) induces secondary attention-deficit hyperactivity disorder-like symptomology in young rats. Behavioural brain research 286, 285–92.

Legends

Figure 1. (A) Placement of DTI ROIs (white contours) on coronal FA maps.1. left cortex ; 2. right cortex ; 3. left hippocampus; 4. right hippocampus; 5. left thalamus; 6. right thalamus; 7.left internal capsule; 8. Right internal capsule; 9. corpus callosum (genu and splenium corpus callosum are on the most anterior and posterior slices respectively; corpus callosum on other slices are grouped to trunk corpus callosum). (B) Representative *in vivo* high resolution ^{1}H MRS from the internal capsule (white box) from one uBIH rat at its baseline. creatine+phospocreatine (Cr+PCr); gamma aminobutyric acid (GABA) ; Glucose (Glc), ; glutamine (Gln); glutamate (Glu); Glu+Gln (Glx); myo-inositol (Ins); lactate (Lac); macromolecules (MM) ; N-acetylaspartate (NAA); N-acetylaspartylglutamic acid (NAAG); taurine (Tau).

Figure 2.Mean diffusivity alterations (ratio to baseline level) in right hippocampus (HP)(A), left (B) and right (C) thalamus (Tha) from 2 hours to 7 days post-uBIH. *=p<0.05, **=p<0.01.

Figure 3.Axial diffusivity alterations (ratio to baseline level) in right hippocampus (HP) (A) and right internal capsule (IC) (B) across three time points. **=p<0.01.

Figure 4.Radial diffusivity alterations (ratio to baseline level) in left (A) and right (B) thalamus (Tha), genu of corpus callosum (CC_gn), (C) across three time points. *=p<0.05, **=p<0.01, ***=<0.001

Figure 5.Changes in creatine (A) and glutamine (B) relative to baseline in the internal capsule across three time points. *=p<0.05, **=p<0.01.

DTI	Right_HP	Left_Tha	Right_Tha	Right_IC
Mean Diffusivity	F = 8.244 p = 0.017	F = 7.029 p = 0.024	F = 5.257 p = 0.045	
Axial Diffusivity	F = 7.208 p = 0.023			F = 5.222 p = 0.045
Radial Diffusivity		F = 14.291 p = 0.004	F = 7.861 p = 0.019	

MRS	Left_IC
Creatine	F = 5.844 p = 0.036
Glutamine	F = 3.877 p = 0.077

Table 1: Brain regions with significant changes in diffusion and spectroscopy parameters
198x123mm (72 x 72 DPI)

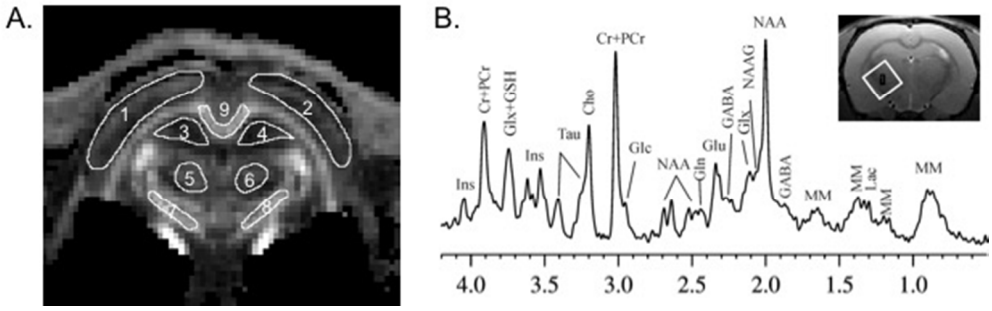

Figure 1. (A) Placement of DTI ROIs (white contours) on coronal FA maps.1. left cortex ; 2. right cortex ; 3. left hippocampus; 4. right hippocampus; 5. left thalamus; 6. right thalamus; 7.left internal capsule; 8. Right internal capsule; 9. corpus callosum (genu and splenium corpus callosum are on the most anterior and posterior slices respectively; corpus callosum on other slices are grouped to trunk corpus callosum). (B) Representative in vivo high resolution 1H MRS from the internal capsule (white box) from one uBIH rat at its baseline. creatine+phospocreatine (Cr+PCr); gamma aminobutyric acid (GABA) ; Glucose (Glc), ; glutamine (Gln); glutamate (Glu); Glu+Gln (Glx); myo-inositol (Ins); lactate (Lac); macromolecules (MM) ; N-acetylaspartate (NAA); N-acetylaspartylglutamic acid (NAAG); taurine (Tau).
219x69mm (72 x 72 DPI)

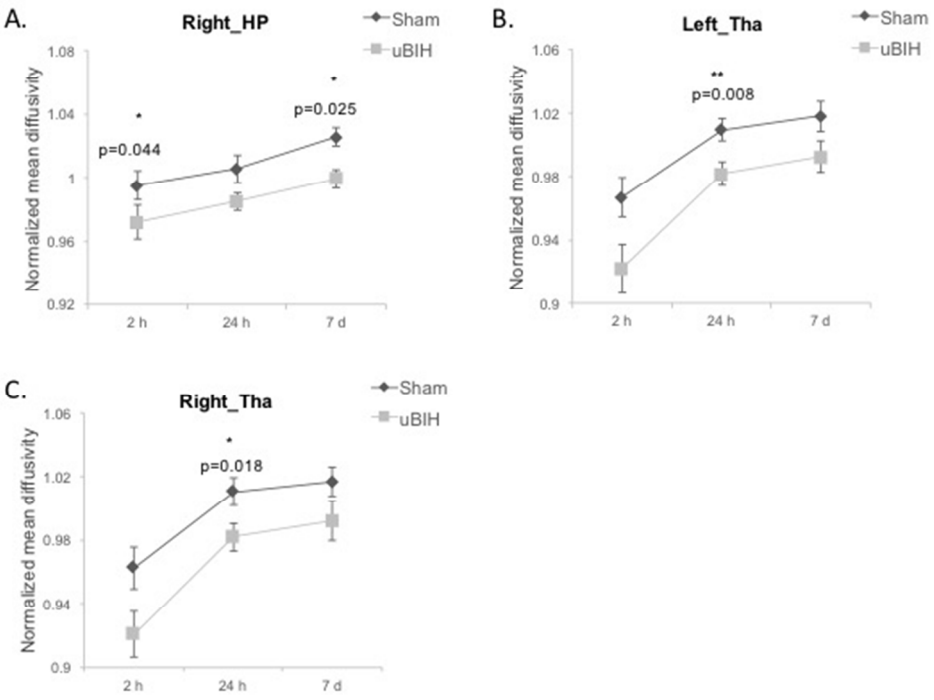

Figure 2.Mean diffusivity alterations (ratio to baseline level) in right hippocampus (HP)(A), left (B) and right (C) thalamus (Tha) from 2 hours to 7 days post-uBIH. *=p<0.05, **=p<0.01.
218x161mm (72 x 72 DPI)

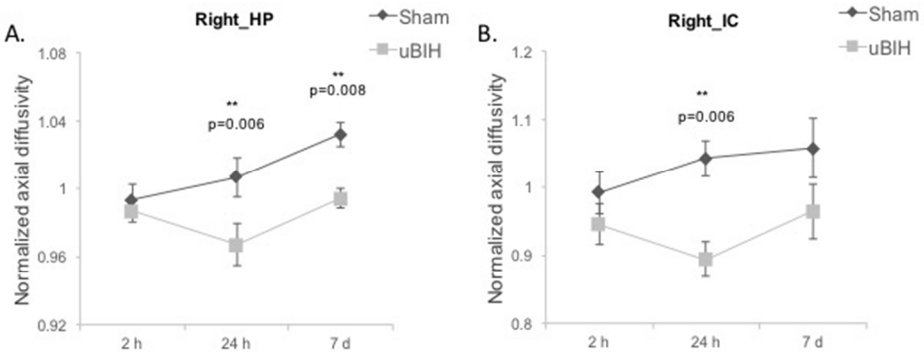

Figure 3.Axial diffusivity alterations (ratio to baseline level) in right hippocampus (HP) (A) and right internal capsule (IC) (B) across three time points. **=p<0.01.
241x98mm (72 x 72 DPI)

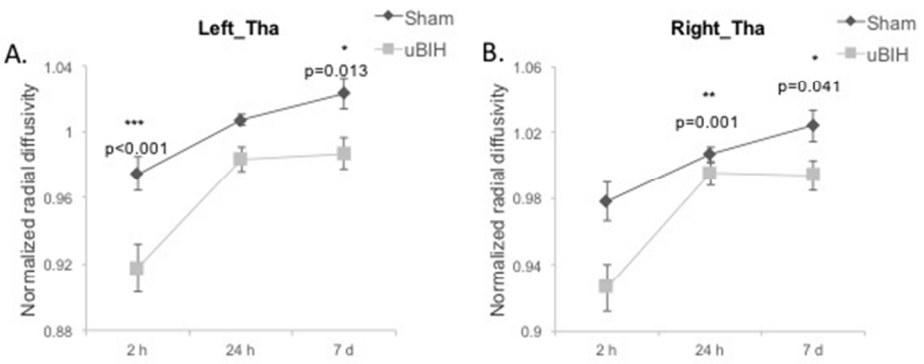

Figure 4.Radial diffusivity alterations (ratio to baseline level) in left (A) and right (B) thalamus (Tha), genu of corpus callosum (CC_gn), (C) across three time points. *=p<0.05, **=p<0.01, ***=<0.001
215x84mm (72 x 72 DPI)

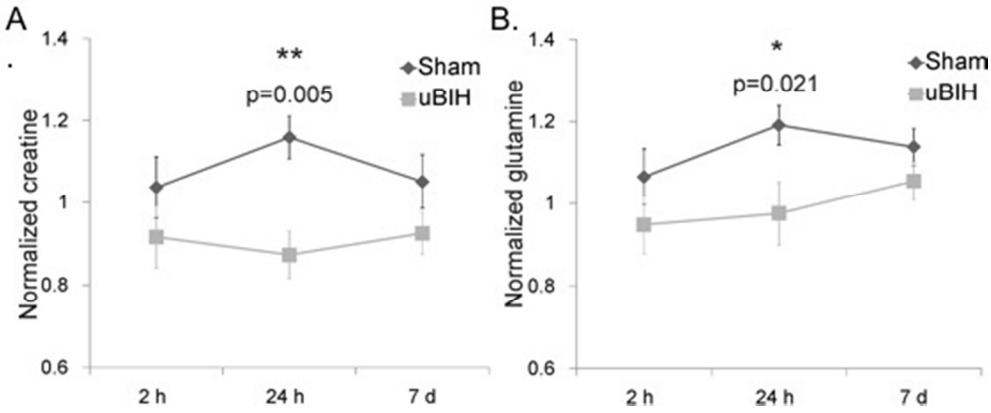

Figure 5.Changes in creatine (A) and glutamine (B) relative to baseline in the internal capsule across three time points. *=p<0.05, **=p<0.01.
200x83mm (72 x 72 DPI)

APPENDIX 3

PUBLISHED MANUSCRIPT

Proctor et al., Rat model of brain injury caused by under-vehicle blast-induced hyperacceleration. J Trauma Acute Care Surg. 2014 Sep;77(3 Suppl 2):S83-7.

Rat model of brain injury caused by under-vehicle blast-induced hyperacceleration

Julie L. Proctor, MS, William L. Fourney, PhD, Ulrich H. Leiste, PhD, *and* **Gary Fiskum, PhD,** *Baltimore, Maryland*

BACKGROUND: More than 300,000 US war fighters in Operations Iraqi and Enduring Freedom have sustained some form of traumatic brain injury (TBI), caused primarily by exposure to blasts. Many victims are occupants in vehicles that are targets of improvised explosive devices. These underbody blasts expose the occupants to vertical acceleration that can range from several to more than 1,000 G; however, it is unknown if blast-induced acceleration alone, in the absence of exposure to blast waves and in the absence of secondary impacts, can cause even mild TBI.

METHODS: We approached this knowledge gap using rats secured to a metal platform that is accelerated vertically at either 20 G or 50 G in response to detonation of a small explosive (pentaerythritol tetranitrate) located at precise underbody standoff distances. All rats survived the blasts and were perfusion fixed for brain histology at 4 hours to 30 days later.

RESULTS: Robust silver staining indicative of axonal injury was apparent throughout the internal capsule, corpus callosum, and cerebellum within 24 hours after blast exposure and was sustained for at least 7 days. Astrocyte activation, as measured morphologically with brains immunostained for glial fibrillary acidic protein, was also apparent early after the blast and persisted for at least 30 days.

CONCLUSION: Exposure of rats to underbody blast-induced accelerations at either 20 G or 50 G results in histopathologic evidence of diffuse axonal injury and astrocyte activation but no significant neuronal death. The significance of these results is that they demonstrate that blast-induced vertical acceleration alone, in the absence of exposure to significant blast pressures, causes mild TBI. This unique animal model of TBI caused by underbody blasts may therefore be useful in understanding the pathophysiology of blast-induced mild TBI and for testing medical and engineering-based approaches toward mitigation. (*J Trauma Acute Care Surg*. 2014;77: S83–S87. Copyright © 2014 by Lippincott Williams & Wilkins)

KEY WORDS: Axonal injury; astrocyte; inflammation; internal capsule; cerebellum.

Approximately 25% of all US combat casualties in Operation Iraqi Freedom and Operation Enduring Freedom have been caused by traumatic brain injury (TBI), with most of these injuries caused by explosive munitions such as bombs, land mines, improvised explosive devices (IEDs), and missiles.[1,2] Little is known regarding the pathophysiology of "blast TBI." The majority of animal research on blast TBI has focused on one aspect of these explosions, the blast overpressure.[3–6] Most of these studies use a model in which a gas-driven pressure wave was delivered via a long shock tube, directly to the immobilized animal's head or body. A multitude of physical forces may play a role in blast TBI, including blast overpressure, thermal and chemical components, shockwave, and hyperacceleration of the brain. We hypothesize that this extreme hyperacceleration, with subsequent rapid deceleration, is responsible for many aspects of blast TBI.

Acceleration may be particularly important for the large number of soldiers and others injured while being occupants of armored vehicles targeted by IEDs. Such explosions result in a very short but very intense acceleration of the vehicle and its occupants. The Dynamic Effects Laboratory at the University of Maryland School of Engineering has used small-scale testing to evaluate the loads applied to personnel carriers when a buried explosive detonates beneath them.[7,8] Adaptation and scaling of this model to allow animal injury in a similar explosive environment could provide a completely new, clinically relevant model of blast TBI that encompasses many of the physical forces including the extreme hyperacceleration. As a first step toward this goal, this study tested the hypothesis that relatively low underbody blast-induced accelerations of 20 G and 50 G result in histologic evidence for mild TBI in the absence of obvious injury to other vital organs.

MATERIALS AND METHODS

Underbody Blast-Induced Hyperacceleration

The device used to induce underbody blast-induced acceleration consists of an aluminum water tank 3 ft long × 2 ft wide × 2 ft deep in which a platform is located that supports two thick aluminum plates, each 15 in square and 1.5 in thick (Fig. 1). The two plates are separated by a styrofoam pad of the same dimensions, which absorbs some of the force transmitted between the plates. The plates and pad travel vertically in response to a blast in the water tank, guided by poles located in

Submitted: December 13, 2013, Revised: March 6, 2014, Accepted: March 17, 2014.

From the Department of Anesthesiology (J.L.P., G.F.), and Shock, Trauma, and Anesthesiology Research Center (STAR) (J.L.P., G.F.), School of Medicine, and Department of Mechanical Engineering (W.L.F., U.H.L.), School of Engineering, and the Center of Energetics Concepts Development (W.L.F., U.H.L.), University of Maryland, Baltimore, Maryland.

This work was presented at the 2013 Military Health System Research Symposium, August 12–15, 2013, in Fort Lauderdale, Florida.

Address for reprints: Gary Fiskum, PhD, Department of Anesthesiology, School of Medicine, University of Maryland, 685 W Baltimore St, 534 MSTF, Baltimore, MD; email: gfiskum@anes.umm.edu.

DOI: 10.1097/TA.0000000000000340

holes in each corner of the plates and pad. The two cylinders secured to the top of the plate each house an anesthetized rat that is wrapped in a thick cotton "blanket" to minimize secondary movement within the cylinders. An explosive charge of 0.75-g pentaerythritol tetranitrate is placed in the water precisely under the center of the plate at distances that generate precise, maximal G forces in these experiments of between 20 G and 50 G. Standoff distances were determined previously at the Dynamics Effects Laboratory and measured during the animal experiments, using accelerometers. When detonated, the explosion causes the plate containing the two rats to accelerate upward extremely rapidly to heights of less than 4 in, followed by a return down to the original location. Pressure sensors located immediately next to the rat heads indicated that they were exposed to less than 1-psi increase in pressure following the explosion. Figure 1 provides examples of the accelerometer measurements performed during these tests, demonstrating reproducibility between two different blasts at both 20 G and 40 G and differences observed at 20, 40, and 60 G, with peak accelerations occurring at 5, 4, and 3 milliseconds, respectively.

Animal Experiments

All animal procedures were performed in accordance with the University of Maryland School of Medicine Institutional Animal Care and Use Committee, the US Army Animal Care and Use Review Office, and the US Air Force Animal Use Program Office of Research Oversight and Compliance. At approximately 10 minutes before each blast, two adult male Sprague-Dawley rats (300–350 g) were deeply anesthetized by intraperitoneal injection of ketamine (80 mg/kg) and xylazine (10 mg/kg). Immediately following the underbody blast, the rats were removed from the cylinders, and their respiratory rates were compared with those recorded before the blast. No changes in respiration were observed. All animals were fully conscious within 90 minutes after the blast and appeared unharmed. In addition to the 25 anesthetized rats subjected to blast-induced hyperacceleration, 10 sham rats were anesthetized but not used in blast experiments.

Tissue Preparation

At different times following the blasts or sham anesthetization, rats were heavily reanesthetized by intraperitoneal injection of ketamine (160 mg/kg) and xylazine (20 mg/kg) and transcardially perfused with 4% paraformaldehyde plus 2.5% acrolein.[9] Brains were removed from the skull and transferred into 30% sucrose. Once brains sunk to the bottom of the container, they were cut (40 μm) on a freezing sliding microtome, yielding 12 series per animal, and were kept in cryoprotectant (−20°C) until further processing was initiated.

Pathology

None of the 25 rats used in the blast experiments exhibited any evidence of injury to the lungs, heart, liver, or spleen upon inspection following thoracotomy during perfusion fixation.

Staining of brain sections with Fluoro-Jade B (FJB) was used to detect dead or dying neurons.[9,10] Free floating brain sections were rinsed free of cryoprotectant with KPBS, mounted on Vectabond-treated PLUS superfrost glass slides and dried overnight at 50°C. Slides were sequentially dipped in the following: 100% EtOH (3 minutes), 70% EtOH (1 minute), deionized H_2O (1 minute), 0.06% $KMnO_4$ (15 minutes), H_2O (2 minutes), and 0.0005% solution of FJB (30 minutes). Slides were then dipped in H_2O four times to five times and were allowed to dry for 30 minutes at 50°C before being cleared in xylene and coverslipped with DPX mounting media.

The amino cupric silver method of de Olmos was used to stain free-floating 40-μm tissue for the identification of damaged and degenerating axons. Our staining procedure closely followed the detailed protocol described by Tenkova and Goldberg.[11] Before staining, all glassware was cleaned in 50% nitric acid. Sections were rinsed free from cryoprotectant and incubated in 4% paraformaldehyde (4°C) for 1 week before staining to block nonspecific labeling of neurons. Sections were then rinsed with deionized H_2O and incubated in preimpregnation buffer (cupric silver) for 1 hour at 50°C then at room temperature overnight. The next day, sections were exposed to the following solutions at room temperature: 100% acetone (30 seconds), impregnation buffer (silver diamine) solution for 35 minutes, reduction agent (formaldehyde with citric acid) for 2 minutes, bleaching solution (potassium ferricyanide) for 20 minutes, deionized H_2O for 3 minutes, and stabilization buffer (thiosulfate solution) for 10 minutes. All solutions were made fresh immediately before use, and sections were carefully shielded from direct light during all staining procedures. After staining, sections were mounted in

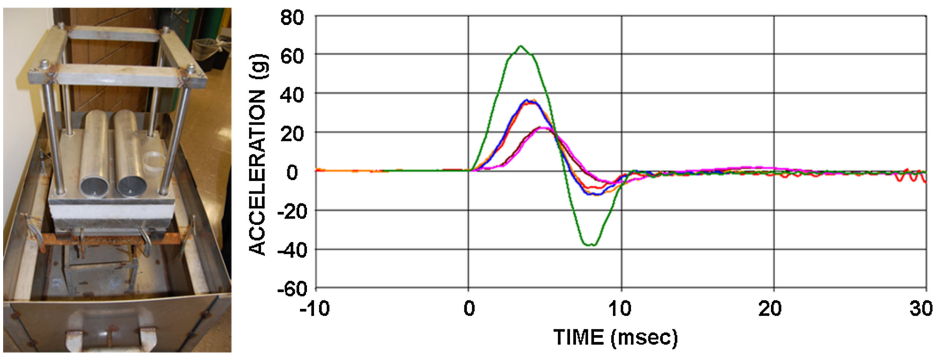

Figure 1. Device used for underbody blast-induced hyperacceleration experiments and accelerometer recordings obtained during the blasts. Tracings show highly reproducible accelerations generated by duplicate blasts at both 20 G and 40 G as well as a single blast at 60 G.

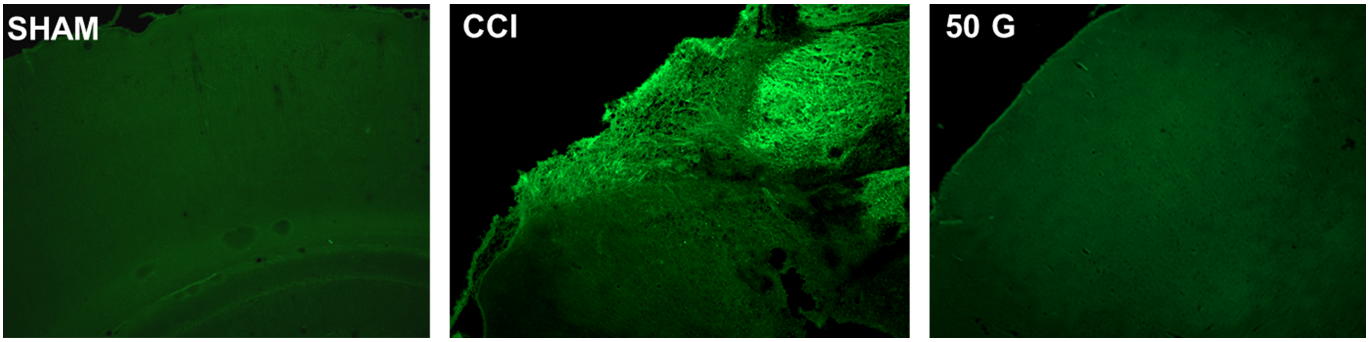

Figure 2. FJB staining for dead or dying cortical neurons after exposure of rats to head impact or underbody blast. Sham animal was anesthetized with ketamine and perfusion fixed 7 days later. One rat was used in a CCI model of moderate TBI and perfused 7 days later. One ketamine-anesthetized rat was subjected to a 50-G underbody blast and perfused 7 days later.

50% ethanol onto subbed PLUS slides, dehydrated with ethanol and xylene, and subsequently coverslipped with DPX mounting media.

Immunohistochemistry

Free-floating sections were single labeled with antibodies against the astrocyte marker, glial fibrillary acidic protein (GFAP),[9] by rinsing multiple times in 0.05-M KPBS buffer before and after exposure to the following: 1% solution of sodium borohydride for 20 minutes; primary antibody diluted in 0.05-M KPBS + 0.4% Triton-X for 48 hours (Dako Anti-GFAP; 1:150K); biotinylated secondary antibody diluted in 0.05-M KPBS + 0.4% Triton-X 1:600 for 1 hour; and incubation in Vectastain A/B solution (1:222) for 1 hour. Tissue was then rinsed before and after 12-minute incubation in Ni-DAB solution with 0.175-M sodium acetate buffer. After a final rinse in KPBS buffer, slices were mounted on slides, dehydrated, and coverslipped with DPX mounting media. The sections were examined with Nikon Eclipse E800 microscope and captured using StereoInvestigator software.

RESULTS

Neuronal death is typically observed within 1 week of injury in most rodent TBI models. Neuronal death or degeneration that occurs in this period is often detected histologically, using a FJB stain, which selectively labels dead or dying neurons.[9,10] Figure 2 compares FJB staining present in the frontal cerebral cortex of a sham rat, perfusion fixed 7 days after ketamine anesthesia, to that observed 7 days following moderate injury induced using a controlled cortical impact (CCI) model, which uses a pneumatic device to directly impact the cortical surface.[12] Representative tissue from the CCI model was obtained from our rodent brain bank and not generated as part of this study. Extensive staining was apparent in the brain from the rat that underwent the CCI, whereas virtually no staining was detectable in the sham rat. In contrast to the staining exhibited by the positive control animal that was previously subjected to cortical impact, no FJB staining was observed at 7 days in a rat subjected to a 50-G underbody blast. Examination of 12 coronal sections representing the entire brain detected no FJB-stained neurons in 23 rats used in the 50-G underbody blast experiments or in 2 rats used in 20-G underbody blast experiments.

Diffuse axonal injury is often observed in rodent brain injury models and can be detected by staining of axons with silver-containing reagents.[10,13] With the use of the de Olmos silver staining method, widespread staining was evident at 7 days after 50-G blasts. Staining was most striking in the internal capsule, corpus callosum, and cerebellum (Fig. 3). Abnormal axon morphologic finding was represented by undulations and bulb-like swellings (Fig. 3, bottom panels). Additional axonal staining was observed in tracts serving the thalamus, while very few fibers in the olfactory bulb or anterior commissures showed evidence of axonopathy. Where silver staining was observed in superficial layers of the brain, it occurred more commonly in the ventral rather than dorsal cortical regions. Relatively little axonal silver staining was observed in noninjured sham animals.

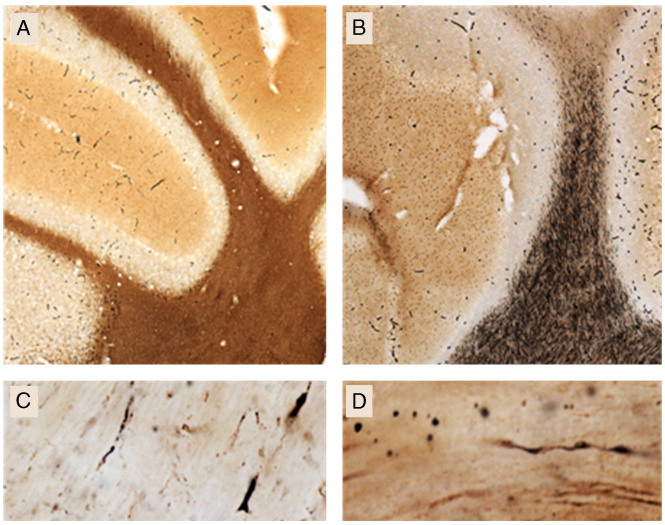

Figure 3. de Olmos silver staining of rat brain 7 days following a 50-G underbody blast. Widespread staining demonstrates axonopathy in white matter structures of the cerebellum in rats exposed to underbody blast (*B*) as compared with sham controls (*A*). High magnification confirms the presence of abnormal swellings and varicosities present in silver-stained axons within the internal capsule (*C* and *D*) following blast exposure.

Axonal silver staining was detectable in the internal capsule of animals subjected to 20-G underbody blasts and perfusion fixed at either 24 hours or 7 days. Evidence for even earlier axonal injury was obtained with brains fixed 3 hours after 50-G blasts (Fig. 4). In contrast, silver staining was much less obvious at 30 days after blast than at 3 hours or 7 days (Fig. 4).

Cellular inflammatory responses are another hallmark of TBI. These responses are characterized by proliferation, migration, and morphologic transformation of astrocytes and microglia, which constitute approximately 50% of the mass of the human brain.[14] Surprisingly, we obtained no convincing evidence for microglial activation following 20-G or 50-G blasts at any outcome times (not shown). Nevertheless, we consistently observed astrocyte accumulation near ventral cortical surfaces, hypothalamic regions, and the internal capsule (Fig. 5). In addition, many astrocytes present in different brain regions exhibited large cell bodies, indicative of activation. Unlike the silver staining of axons, which declined between 7 days and 30 days after the blast, these cellular inflammatory reactions persisted and possibly increased during this period.

DISCUSSION

To the best of our knowledge, these experiments represent the first to test for the effects of specifically underbody blast-induced hyperacceleration on the brains of laboratory animals. The blast paradigm was designed to test for the effects of this form of acceleration on the brains of rats in the absence of exposure to any significant blast overpressure. Several conclusions can be made. (1) Adult rats can be subjected to blast-induced hyperacceleration at maximal G forces of at least 50 G with a 100% survival rate, provided they are protected against secondary impact injuries. (2) FJB-detectable neuronal death does not occur following exposure of rats to either 20-G or 50-G underbody blasts. (3) Diffuse axonal injury occurs in several brain regions, as early as 4 hours after 20-G or 50-G underbody blasts and is still evident at 7 days, based on silver staining of axonal fibers. (4) Despite the lack of evidence for substantial microglial activation, astrocyte activation occurs within 7 days and persists for 30 days following 20-G or 50-G underbody blasts. 5. Based on these qualitative histologic findings, we conclude that rats subjected to 50-G blasts and possibly even 20-G blasts experience mild TBI.

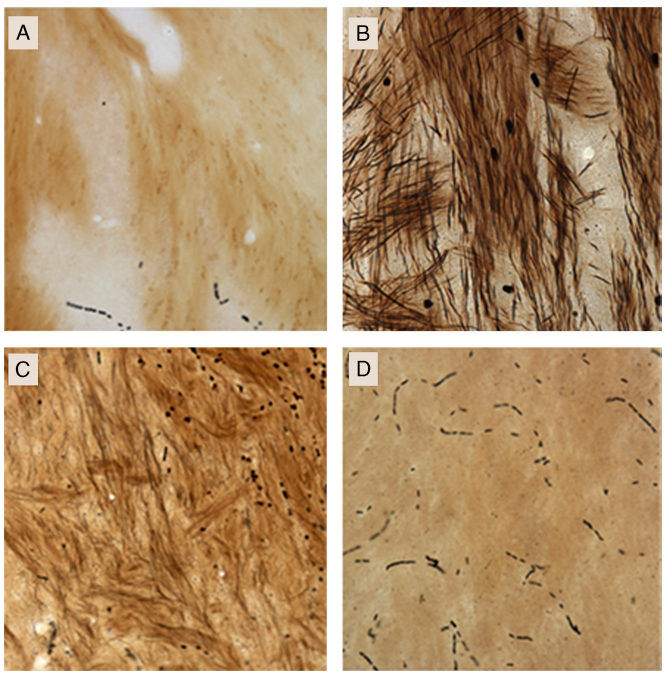

Figure 4. de Olmos silver staining of rat brain internal capsule at early and late time points following 50-G generated blasts. Intense internal capsule staining is induced with 50-G forces (*B–D*), which appears to dissipate with time as compared with ketamine-anesthetized sham controls (*A*). *A*, Sham; *B*, 50 G at 3 hours after blast; *C*, 50 G at 7 days after blast; *D*, 50 G at 30 days after blast.

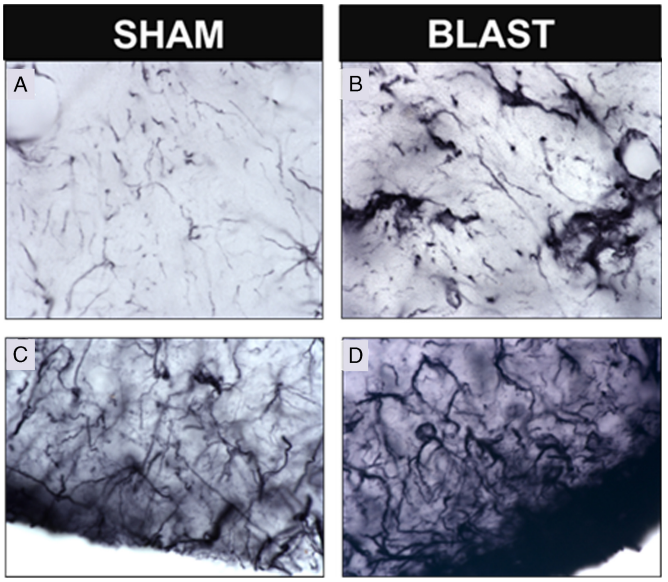

Figure 5. Astrocyte activation near hypothalamic regions at 7 days after a 50-G underbody blast. Intensities of GFAP-stained astrocytes were greater in animals exposed to underbody blasts compared with sham-treated rats. Astrocyte activation was observed in the internal capsule (*B*) and regions of the hypothalamus (*D*) as compared with these regions in shams (*A* and *C*).

This unique initial approach to understanding the effects of underbody blasts on the brain has several limitations. (1) We specifically designed the device for exposing rats to underbody blasts to test specifically for the effects of acceleration, without secondary effects of potential head impact. Clearly, many victims of TBI who are occupants of vehicles targeted by IEDs detonated underneath the vehicles are subjected to both acceleration, head impact, and other injuries. Therefore, polytrauma animal models may be more clinically relevant.[5,15] (2) Only two maximal G forces were used, which are much lower than maximum survivable G forces experienced by occupants within targeted vehicles. We purposely used relatively low loads in this initial study to avoid mortality and injury to other vital organs. Studies are in progress exposing rats to underbody blasts at much higher G forces in the range of 100 G to 2,000 G. Recently, one study published evidence of head acceleration exceeding 3,000 G in a

blast tube, porcine model of survivable free field blast exposure.[16] (3) Neuronal death was only measured using one method, that is, FJB tissue staining. It is therefore possible that other methods, such as active caspase 3 immunostaining, could detect neuronal death not detected by FJB. (4) Diffuse axonal injury was only evaluated using the de Olmos silver staining method. Although this approach is used extensively, additional procedures, for example, immunohistochemical detection of phosphorylated tau protein and beta-amyloid precursor protein, could provide helpful validation.[17,18] 5. The results obtained from the silver staining of degenerative neurons and the GFAP immunostaining of astrocytes demonstrating activated morphology are at this juncture purely qualitative. Studies are in progress to obtain quantitative results for these and other histologic outcome measures. (6) No quantitative assessment of behavior was performed. Now that we have obtained histologic evidence for mild TBI following low-G underbody blasts, we are developing neurobehavioral tests sensitive enough to detect neurologic alterations at these and higher G forces.

AUTHORSHIP

J.L.P. performed all of the histology and generated all of the results presented in the article. W.L.F. and U.H.L. designed and built the device used for the underbody blast TBI model, were present at every experiment, and conducted the blasts and performed the accelerometer measurements. G.F. is the principal investigator of the grants that supported the work and conceived the study design. He was also present at every experiment. All authors contributed to the writing of this manuscript.

DISCLOSURE

There are no financial, consultant, institutional, or relationship conflicts declared by any author. This work was supported in part by US Air Force grant FA8650-11-2-6D04 and the US Army grant W81XWH-13-1-0016.

REFERENCES

1. Okie S. Traumatic brain injury in the war zone. *N Engl J Med*. 2005;352:2043–2047.
2. Hoge CW, McGurk D, Thomas JL, Cox AL, Engel CC, Castro CA. Mild traumatic brain injury in U.S. Soldiers returning from Iraq. *N Engl J Med*. 2008;358:453–463.
3. Magnuson J, Leonessa F, Ling GS. Neuropathology of explosive blast traumatic brain injury. *Curr Neurol Neurosci Rep*. 2012;12:570–579.
4. Cernak I, Radosevic P, Malicevic Z, Savic J. Experimental magnesium depletion in adult rabbits caused by blast overpressure. *Magnes Res*. 1995; 8:249–259.
5. Garman RH, Jenkins LW, Switzer RC 3rd, Bauman RA, Tong LC, Swauger PV, Parks SA, Ritzel DV, Dixon CE, Clark RS, et al. Blast exposure in rats with body shielding is characterized primarily by diffuse axonal injury. *J Neurotrauma*. 2011;28:947–959.
6. Long JB, Bentley TL, Wessner KA, Cerone C, Sweeney S, Bauman RA. Blast overpressure in rats: recreating a battlefield injury in the laboratory. *J Neurotrauma*. 2009;26:827–840.
7. Fourney WL, Leiste U, Bonenberger R, Goodings D. Explosive impulse on plates. *FRAGBLAST*. 2005;9:1–17.
8. Fourney WL, Leiste U, Bonenberger RJ, Goodings D. Mechanism of loading on plates due to explosive detonation. *FRAGBLAST*. 2005;9:205–217.
9. Hazelton JL, Balan I, Elmer GI, Kristian T, Rosenthal RE, Krause G, Sanderson TH, Fiskum G. Hyperoxic reperfusion after global cerebral ischemia promotes inflammation and long-term hippocampal neuronal death. *J Neurotrauma*. 2010;27:753–762.
10. Hall ED, Bryant YD, Cho W, Sullivan PG. Evolution of post-traumatic neurodegeneration after controlled cortical impact traumatic brain injury in mice and rats as assessed by the de Olmos silver and fluorojade staining methods. *J Neurotrauma*. 2008;25:235–247.
11. Tenkova TI, Goldberg MP. A modified silver technique (de Olmos stain) for assessment of neuronal and axonal degeneration. *Methods Mol Biol*. 2007;399:31–39.
12. Robertson CL, Puskar A, Hoffman GE, Murphy AZ, Saraswati M, Fiskum G. Physiologic progesterone reduces mitochondrial dysfunction and hippocampal cell loss after traumatic brain injury in female rats. *Exp Neurol*. 2006;97:235–243.
13. Kochanek PM, Dixon CE, Shellington DK, Shin SS, Bayır H, Jackson EK, Kagan VE, Yan HQ, Swauger PV, Parks SA, et al. Screening of biochemical and molecular mechanisms of secondary injury and repair in the brain after experimental blast-induced traumatic brain injury in rats. *J Neurotrauma*. 2013;30:920–937.
14. Kumar A, Loane DJ. Neuroinflammation after traumatic brain injury: opportunities for therapeutic intervention. *Brain Behav Immun*. 2012;26:1191–1201.
15. Hicks RR, Fertig SJ, Desrocher RE, Koroshetz WJ, Pancrazio JJ. Neurological effects of blast injury. *J Trauma*. 2010;68:1257–1263.
16. Shridharani JK, Wood GW, Panzer MB, Capehart BP, Nyein MK, Radovitzky RA, Bass CR. Porcine head response to blast. *Front Neurol*. 2012;3:70.
17. Goldstein LE, Fisher AM, Tagge CA, Zhang XL, Velisek L, Sullivan JA, Upreti C, Kracht JM, Ericsson M, Wojnarowicz MW, et al. Chronic traumatic encephalopathy in blast-exposed military veterans and a blast neurotrauma mouse model. *Sci Transl Med*. 2012;4(134):134ra60.
18. Risling M, Plantman S, Angeria M, Rostami E, Bellander BM, Kirkegaard M, Arborelius U, Davidsson J. Mechanisms of blast induced brain injuries. Experimental studies in rats. *Neuroimage*. 2011;54(Suppl 1):S89–S97.

APPENDIX 4

ELECTRON MICROSCOPY OF CERBROVASCULAR INJURY FOLLOWING UNDERBODY BLASTS

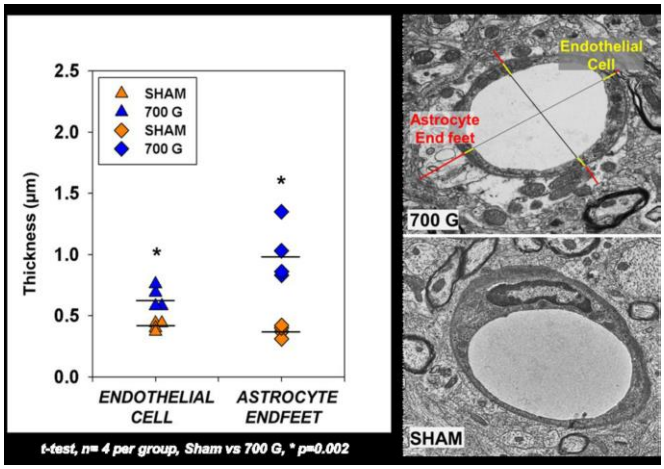

Fig 1. Quantification of neurovascular injury was performed by random sampling of transverse cut blood vessels from the cerebral cortex 30 min following blast. The thickness perpendicular to the vessel wall was measured for the endothelial cell and astrocyte end feet at four randomly oriented points in each blood vessel.

APPENDIX 5

SILVER STAINING EVIDENCE FOR INCREASED AXONAL INJURY FOLLOWING 700G COMPARED TO 100G BLAST EXPOSURE

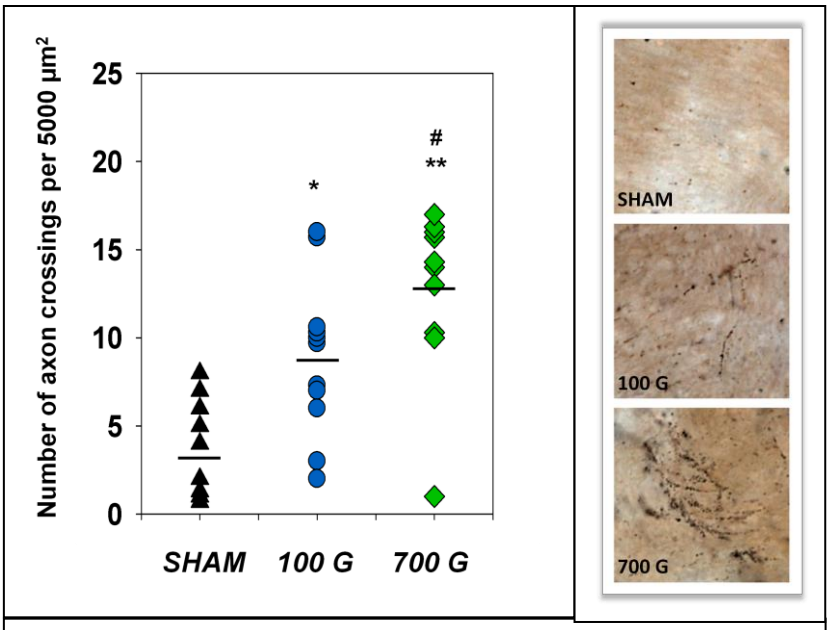

Silver staining of damaged axonal fibers present in the internal capsule at 7 days after 100 or 700 G blasts or sham anesthesia. *p<0.05 compared to sham. #p<0.05 compared to 100 G. N=8-11 animals per group.

APPENDIX 6

IgG IMMUNOSTAINING EVIDENCE FOR INCREASED BLOOD BRAIN BARRIER DISRUPTION FOLLOWING 700G COMPARED TO 100G BLAST EXPOSURE

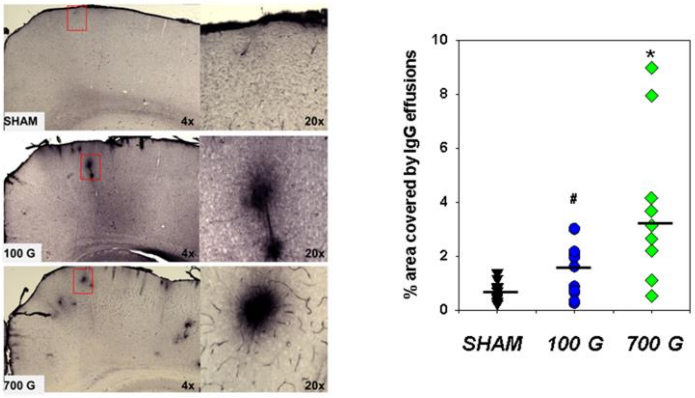

Rat cortex immunostained for IgG demonstrating perivascular effusions at 24 hr following underbody blast TBI. Quantification demonstrated significant increase in percent area staining for IgG after either 100G or 700G blasts.

APPENDIX 7

IDENTITY OF GENES WHOSE EXPRESSION CHANGED IN THE HIPPOCAMPUS BY MORE THAN TWO-FOLD AT 24 HR FOLLOWING EXPOSURE TO 100G BLASTS IN COMPARISON TO KETAMINE ANESTHETIZED SHAM RATS

Fold change ≥ 2, $p \leq 0.05$, FDR ≤ 0.05

Gene Symbol	RefSeq	p-value	Fold-Change	Description (100G vs. sham)
Novel miRNA*	ENSRNOT000043523	1.01E-05	-2.06438	down
Bcl2	ENSRNOT00000003768	4.07E-05	-2.59557	down
Fbxw8	reviewed	8.99E-05	2.86312	up
Novel miRNA**	ENSRNOT000000063683	0.000312	2.13415	up
RAB1B	ENSRNOT00000027486	0.000617	2.47881	up
Rps20	NM_001007603	0.000589	2.50095	up
snoRNA##	ENSRNOT000000069073	0.000631	2.00346	up
snoRNA##	ENSRNOT000000069073	0.000631	2.00346	up
-	---	0.000991	2.83156	up
snoRNA#	ENSRNOT000000054102	0.000652	2.28636	up
-	---	0.000988	-2.94326	down
Vwa5b2	NM_001134535	0.001112	2.22691	up

Affymetrix microarray detected 12 genes whose expression changed by more than 2-fold. Only 4 of these genes code for known proteins (Bcl2, Fbxw8, Rps20, and Vwa5b2)

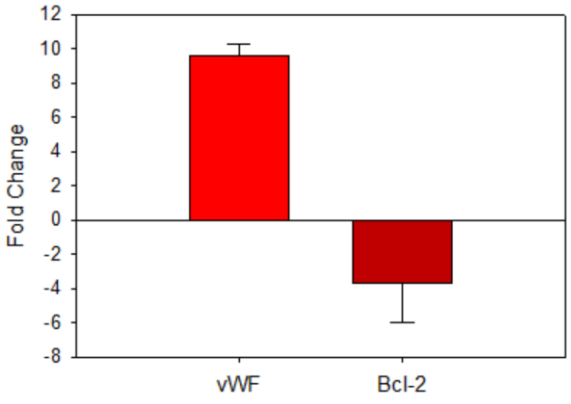

Quantitative rtPCR measurements of mRNA coding for von Willebrand Factor and Bcl-2.

APPENDIX 8

HIPPOCAMPAL VON WILLEBRAND FACTOR IMMUNOSTAINING AT 7 DAYS FOLLOWING EXPOSURE TO BLAST-INDUCED 100G ACCELLERATION

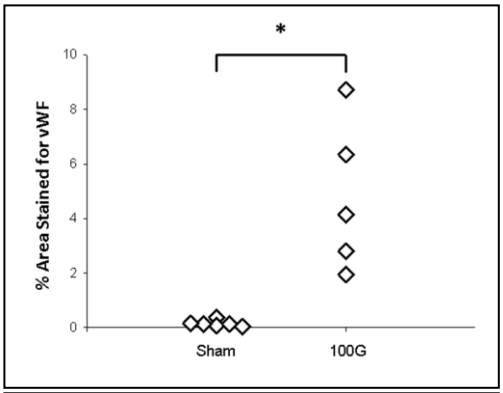

Brains were perfusion fixed at 7 days post 100G blast and immunostaining was quantified as percent area stained with antibodies to vWF. * $p<0.05$ n=5-6

HIPPOCAMPAL BCL2 IMMUNOREACTIVITY 24 HR FOLLOWING EXPOSURE TO BLAST-INDUCED ACCELERATIONS OF 700 AND 2400G

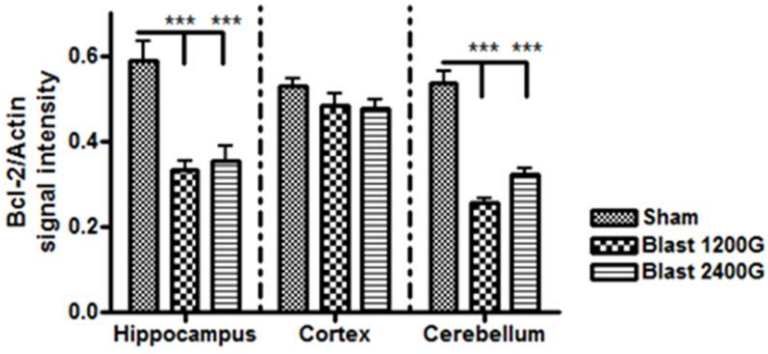

Conscious rats were exposed to blasts that produced either 1200 or 2400G accelerations. Brains were removed and dissected at 24 hr post-blast and immediately frozen and stored at -80°. Bcl2 densitometry revealed significant reductions in the hippocampus and cerebellum but not cortex at either blast level. *** $p<0.01$ n=6-8

Journal of Neurotrauma

Journal of Neurotrauma: http://mc.manuscriptcentral.com/neurotrauma

Neuropathology and Neurobehavioral Alterations in a Rat Model of Traumatic Brain Injury to Occupants of Vehicles Targeted by Underbody Blasts

Journal:	*Journal of Neurotrauma*
Manuscript ID	NEU-2016-4654
Manuscript Type:	Regular Manuscript
Date Submitted by the Author:	23-Jun-2016
Complete List of Authors:	Tchantchou, Flaubert; University of Maryland School of Medicine Fourney, William; University of Maryland at College Park, Engiineering Leiste, Ulrich; University of Maryland at College Park Vaughan, Joshua; University of Maryland School of Medicine, Anesthesiology Rangghran, Parisa; University of Maryland School of Medicine, Anesthesiology Puche, Adam; University of Maryland School of Medicine, Anatomy and Neurobiology Fiskum, Gary; University of Maryland School of Medicine,
Keywords:	ADULT BRAIN INJURY, Apoptosis, BLOOD-BRAIN BARRIER DYSFUNCTION, COGNITIVE FUNCTION, INFLAMMATION

TITLE

Neuropathology and Neurobehavioral Alterations in a Rat Model of Traumatic Brain Injury to Occupants of Vehicles Targeted by Underbody Blasts

TABLE OF CONTENTS TITLE

Underbody Blast-Induced Traumatic Brain Injury

RUNNING TITLE

Blast Traumatic Brain Injury

AUTHORS

Flaubert Tchantchou, PhD, University of Maryland School of Medicine, Department of Anesthesiology, Center for Shock, Trauma, and Anesthesiology Research (STAR), 685 W. Baltimore St., Baltimore, MD 21201; Phone: 410-706-3418; Email: ftchantchou@anes.umm.edu

William Fourney, Ph.D., University of Maryland School of Engineering, Department of Aerospace Engineering, 1131 Glenn L. Martin Hall, College Park, MD 20742; Phone: 301-405-1129; Email: four@umd.edu

Ulrich Leiste, Ph.D., University of Maryland School of Engineering, Department of Aerospace Engineering, 1131 Glenn L. Martin Hall, College Park, MD 20742; Phone: 301-405-1129; Email: uleiste@umd.edu

Joshua Vaughan, B.S., University of Maryland School of Medicine, Department of Anesthesiology, STAR, 685 W. Baltimore St., Baltimore, MD 21201; Phone: 410-706-3418; Email: vaughan1009@gmail.com

Parisa Rangghran, M.S., University of Maryland School of Medicine, Department of Anesthesiology, STAR, 685 W. Baltimore St., Baltimore, MD 21201; Phone: 410-706-3418; Email: prangghran@anes.umm.edu

Adam Puche, Ph.D., University of Maryland School of Medicine, Department of Anatomy and Neurobiology, Health Science Facility-2, Room 255, Baltimore, MD 21201; (410) 706-3530; Email: apuche@umaryland.edu

Gary Fiskum, Ph.D., (Corresponding Author) University of Maryland School of Medicine, Department of Anesthesiology, STAR, 685 W. Baltimore St., Baltimore, MD 21201; Phone: 410-706-4711; Email: gfiskum@anes.umm.edu

KEY WORDS: Acceleration-force, apoptosis, inflammation, anxiety, synapse

ACKNOWLEDGMENTS: Support from US Dept. of Defense W81-xWH-13-1-0016 and the US Air Force Medical Service FA8650-11-2-6D04

ABSTRACT

Many victims of blast-induced traumatic brain injury are occupants of military vehicles targeted by land mines. Recently improved vehicle designs protect these individuals against blast overpressure, leaving acceleration as the main force potentially responsible for brain injury. This study tested the hypothesis that underbody blast-induced acceleration force alone is sufficient to cause TBI. Adult male rats were restrained on a platform that was propelled vertically by blasts generating acceleration forces of 1200 to 2800Gs, and evaluated over 28 days for working memory (Y maze) and anxiety (elevated plus maze). The brains from rats obtained at one, and seven days post-injury were used for neuropathology and neurochemical assays. Rats exposed to acceleration only injury exhibited deficits in working memory at 6 days with recovery by four weeks post-injury; however, increased anxiety was persistent throughout the entire testing period. This injury was associated with acute neuroinflammatory microglia activation, hippocampal neuronal death, reductions in blood brain barrier-associated molecular markers, and decreased synaptic protein expression. Taken together, these results demonstrate that exposure of rats to underbody blast-induced G forces results in significant traumatic brain injury that is similar but not identical to brain injury caused by blast overpressure.

Introduction

Brain injuries resulting from direct or indirect exposure to explosions represent up to 68% of more than 300,000 U.S. military neurotrauma victims who served in the recent wars in Iraq and Afghanistan.[1-6] Blast-induced traumatic brain injuries (bTBI) are mainly classified in four sub-categories: 1. Primary injury, which results from blast overpressure. 2. Penetrating injuries caused by debris propelled by the explosion. 3. "Coup-countercoup" head injury resulting from secondary head impact 4. Exposure to intensive heat, toxic chemicals, and electromagnetic radiation.[7, 8] Missing from these classifications is TBI induced by sudden acceleration force without significant exposure to blast overpressure, as is experienced by occupants of vehicles targeted by land mines, where the V-shaped armored hulls deflect the bulk of blast overpressure laterally, away from the occupants.

Clinical research and epidemiological studies suggest that the majority of all bTBI victims suffer from mild TBI.[3, 9] Although most victims of mild-bTBI pass the Acute Concussion Evaluation,[10, 11] many return to the hospital later, exhibiting cognitive and memory impairments, increased anxiety, and depression.[11-13] Thus, a better knowledge of the pathophysiology of different forms of bTBI is needed to improve both short and long-term outcomes for bTBI casualties.

A number of different animal models of bTBI have been developed,[14, 15] with the goal of improving treatment for bTBI.[16, 17] Such models have focused primarily on brain injuries caused by exposure to blast overpressure and shock waves, such as those experienced by "unmounted" warfighters on foot patrol. These models typically utilize rodents restrained within or just outside the end of a shock tube that exposes the

animals to these forces. The results of these experiments demonstrate that exposure of laboratory animals to a single blast can cause significant pathological changes in the brain including the disruption of the blood brain barrier integrity,[6, 18] increased accumulation of inflammatory microglia/macrophages, neuronal cell death, and neurobehavioral deficits.[6, 19, 20]

Since the combination of forces experienced by bTBI victims during open-field compared to underbody blasts is quite different, we developed an underbody blast model, using rats exhibiting histologic evidence of TBI at blast-induced acceleration forces of as low as 50G.[21] The current study investigates the impact of much higher underbody blast-induced acceleration force of 1200 – 2800G on the blood brain barrier integrity, neuroinflammation, neuronal death, synaptic protein levels, behavioral impairment, and mortality at periods ranging from one hour to 30 days post-injury.

Materials and Methods

Animals and their environment

All animal research protocols were approved by the University of Maryland, Baltimore Animal Use and Care Committee and the US Army Animal Care and Use Review Office. Male Sprague-Dawley rats (Harlan Laboratories, CA), 300-350 g were maintained under a controlled environment with an ambient temperature of 23 ± 2°C, a 12 hr light/dark cycle, and continuous access to food and water *ad libitum*. Experimental groups consisted of 10 to 14 rats for behavioral studies, 4 to 8 rats for immunohistochemistry or biochemical analyses, and 6 – 14 rats for mortality incidence.

Exposure of rats to underbody blast-induced hyperacceleration force

Exposure of rats to underbody blast-induced hyperacceleration force was performed following scaling analysis to develop parameters to guide the design by a procedure modified from what we described previously.[21,22] In brief, two rats were anesthetized simultaneously with 4% isoflurane in room air for 5 min. Anesthesia was discontinued and the rats were secured, while still unconscious, within two fiberglass restrainers (Stoeling Inc., IL), with a custom addition of metallic cone to restrain the head and minimize secondary acceleration and head impact. The restrainers were bolted onto a 38 cm square and 1.5 cm thick aluminum platform. This platform was located immediately above a second 38 cm square aluminum platform that was either 3.0 cm thick (for 1200G acceleration force) or 1.5 cm thick (for 2800G acceleration). A 0.25 in thick hard rubber pad was present between the two platforms to dampen oscillatory acceleration forces. Both platforms had 2.5 cm wide holes located inside each of the four corners. Aluminum rods 90 cm high were inserted through each of the holes and secured to a steel base on which the platforms rested, thus allowing for only direct movement of the platforms vertically following an underbody blast. The steel base was bolted to the edges of a steel tank filled with water to different stand-off distances from the bottom platform, resulting in relatively low acceleration force at large distances and relatively high acceleration force at short distances.

An explosive charge of pentaerytritol tetranitrate (PETN) was secured in the water at a fixed 5 cm depth of burial from the water line. The explosives weighing 0.75 g, for 1200G blasts, and 2.00 g, for 2400G and 2800G blasts, were detonated electromagnetically at exactly 5 min after anesthesia was discontinued, when the rats

were fully conscious. Explosion within the water ensured a non-compressible transfer of the explosive energy onto the bottom of the lower platform and subsequently to the upper platform where the rats were located. Accelerometers were placed on the top of the higher platform near the front of the rat restraints and the velocity, acceleration force, and JERK (first derivative of acceleration force) measured using UERD-Tools software (U.S NAVY). The peak acceleration force reached in these blast experiments was in the range of 0.30 to 0.50 msec. Sham animals were also anesthetized with 4% isoflurane for 5 min, secured on the platform and removed 5 min later.

All blast and sham animals were returned to their cages immediately after the blast or sham procedure and examined for any physical injuries every 30 min for three hours. Necropsies were performed on all four animals that died immediately following the 2800G blasts.

Behavior

Y maze test

The Y maze is a Y-shaped platform that consists of three arms 50 cm long and 10 cm wide, each surrounded on three sides by 20 cm high walls. The open ends of the three arms are connected centrally and positioned radially at 120 degree angles (Stoelting Co., IL). The test was performed at approximately 1hr, and 6, 13 and 27 days post-injury, as previously described.[23] Each rat was placed at the center of the maze and allowed to explore for 5 min. Movement was recorded using an overhead camera and analyzed using the Any-maze software (SD instruments, CA). Arm visit sequences and number of entries to each arm were recorded. Working memory was defined by the

frequency of alternately exploring different arms and was determined using the formula: total number of alternations / (total number of arm entries - 2) X 100.

Elevated Plus maze

This plus sign-shaped device consists of four perpendicular arms measuring 90 cm long and 10 cm wide, connected by a 10 cm x 10 cm central platform. Two of the arms are bordered on three sides by 10 cm high black plastic walls, while the other two arms together with the center of the maze are open. The arms are located 50 cm above the floor.[24] The test was performed on days 1, 8, 14 and 28 post-blast, as previously described, with a minor modification.[24] In brief, rats were individually placed on the central area and allowed to explore the maze for 10 min. Movement was recorded by an overhead camera and the data were analyzed by Any-maze software (SD instruments, CA), to provide information including the time spent in each arm and the central area and the total distance travelled. Anxiety like behavior was determined by the time spent in the open arms.

Tissue collection and processing

At different times following blasts or sham anesthesia (Fig. 1), rats were deeply anesthetized by intraperitoneal injection of a mixture of ketamine (160 mg / kg) and xylazine (120 mg / kg), and euthanized by exsanguination via transcardial perfusion. Anesthetized rats were initially perfused for 5 min with oxygenated artificial CSF containing 148 mM NaCl, 5 mM glucose, 3.0 mM KCl, 1.85 mM $CaCl_2$, 1.7 mM $MgCl_2$ 1.5 mM Na_2HPO_4, 0.14 mM NaH_2PO_4 (pH 7.4). Rats were then perfused with 500 ml fixative consisting of 4% paraformaldehyde in 100 mM Na_2HPO_4 and 100 mM NaH_2PO_4

(pH 7.4). The brains were removed, maintained in fixative for 24 hr, and transferred to 30% sucrose. After a few days when the brains sank to the bottom of their containers, each was sectioned in serial sections of 40 μm, preserved in cryoprotectant (66mM NaH_2PO_4, 0.19M Na_2HPO_4, 0.87M sucrose, 30% ethylene glycol, and 1.25 mM povidone), and stored at -20°C for histology and immunohistochemistry.

For western blot analysis, anesthetized rats were decapitated with a guillotine. Their brains were rapidly removed and dissected to yield the hippocampus, cortex and cerebellum, which were immediately frozen on dry ice and stored at -80°C.

Immunostaining

Immunohistochemical analysis of fixed, frozen sections was performed to determine the expression of inflammation biomarkers F4/80 and inducible nitric oxide synthase (iNOS) and the apoptosis biomarker cleaved caspase 3. Visualization utilized either fluorescence immunostaining or nickel diaminobenzadine (DAB) immunostaining. The number of dead or dying cells was quantified using terminal deoxynucleotidyl transferase dUTP nick end labeling (TUNEL).

Immunofluorescence staining

Brain sections were co-stained for the expression of cleaved caspase 3 and neuronal nuclear antigen (NeuN) or F4/80 and iNOS as previously described.[25] In brief, free floating sections were rinsed in PBS, then blocked in 1% horse serum in phosphate buffered saline (PBS) containing 0.3% Triton X for 1 hr. Sections were then transferred in a solution containing rabbit anti-Cleaved caspase-3 polyclonal antibody (1:10,000; Millipore, Temecula, CA) and mouse anti-NeuN monoclonal antibody clone, A60 (1:2000; Millipore, Temecula, CA) or rat anti-F4/80 monoclonal antibody (1:500;

eBioscience, San Diego, CA) and rabbit anti-iNOS polyclonal antibody (1:3000; Millpore, Temecula, CA) and incubated at 4° C overnight. The sections were washed in PBS and incubated for 1 hr at room temperature in a mixture of corresponding secondary antibodies Alexa Fluor 488 or Alexa Fluor594 (1:1500; Invitrogen, NY). Sections were washed with PBS and counterstained with 4', 6-diamidino-2-phenylindole (DAPI).

Nickel DAB immunostaining

Brain sections were single labelled for the expression of F4/80 as previously described.[21] Free floating sections were rinsed in PBS, blocked with 1% horse serum, and incubated with rat anti-F4/80 monoclonal antibody (1:15,000; eBioscience, CA) overnight at 4°C. Sections were washed and incubated at room temperature in biotinylated rabbit anti-rat secondary antibody for 1 hr, followed by incubation in Vestastain solution and in nickel DAB and rinsed in PBS.

TUNEL assay

Floating sections were rinsed in PBS, transferred onto glass slides and allowed to air dry for 1 hr. They were rehydrated in PBS and stained to detect apoptotic cells marked by DNA fragmentation using a kit (Millipore, NY) and following manufacturer's instructions. DAPI used as a counterstain. All stained sections were mounted and examined under a Zeiss Axio-Imager microscope and images captured with x20 or x63 magnification objectives.

Western blot analysis

Western blotting was performed to determine the expression of Zona occluden (ZO-1), occludin, von Willebrand Factor (VWF), Bcl-2, heat shock proteins 70 (Hsp70), synaptophysin, PSD-95, spinophilin and beta-actin (used as loading control). The hippocampus, cortex and cerebellum were manually homogenized in lysis buffer containing 50 mM HEPES (pH 7.5), 6 mM $MgCl_2$, 1 mM EDTA, 75 mM sucrose, 1 mM dithiothreitol, 1% Triton X-100 and 1% protease/phosphatase inhibitor cocktail (Cell Signaling Technology, MA) and centrifuged at 12,000 rpm for 20 min. Proteins (20-30 µg) from each sample were separated by electrophoresis on 4-12% SDS-polyacrylamide gels (Invitrogen, CA), then transferred to a nitrocellulose membrane. Membranes were blocked with 1% BSA and incubated overnight at 4°C with rabbit polyclonal antibodies against VWF (1:400; Santa Cruz, CA), occludin (1:2000; Abcam, MA), spinophilin (1:500; Millipore, MA), synaptophysin (1:1000), PSD-95 (1:1000), Bcl-2 (1:750) all from Cell Signaling Technology, MA; a rat anti-ZO-1 monoclonal antibody (1:400, Millipore, MA) or mouse monoclonal antibodies against Hsp70 (1:750; Cayman chemical, MI) or β-actin (1:4000; Sigma, MO). Blots were washed in TBST and incubated for 1 hr at room temperature with corresponding HRP-conjugated secondary antibodies (1: 5000; Millipore, MA). Horseradish peroxidase labelled proteins was detected by enhanced chemilunescence (ECL, Thermo Scientific, IL) and protein bands were visualized using a digital blot scanner (LI-COR, NE).

Quantification and statistical analysis

The optical fractionator method of stereology was employed to quantify cleaved caspase 3 or TUNEL positive cells in 40 µM thick immune-stained sections, using the

stereo-investigator software (MBF Bioscience, VT). A total of 6 sections selected to cover the entire hippocampus region, -1.60 mm to -6.3 mm from bregma, corresponding to every 12 serial sections were analyzed for each brain. For quantification, the dendate gyrus and the Cornu Ammonis 2/3 (CA2/3) sub-regions in the hippocampus of each brain hemisphere was demarcated and using a grid spacing of 75 µm x 75 µm in the x and *y*-axis and guard zones of 2 µm at the top and bottom of each section, cell bodies were counted. The total number of cleaved caspase 3 or TUNEL positive cells in the hippocampal sub-region of interest was divided by the area to determine the cellular density per area unit, expressed as cells / mm^2.

Image J software (NIH) was used to measure immunoblot protein band signal intensity and the percent area of F4/80 immunostaining in brain tissue. Sections stained for F4/80 were optically segmented by threshold with the threshold greyscale value selected at 0.3 µM. These thresholded images were automatically measured for the relative percent containing positive F4/80 signal in ImageJ. This method is proportional to the percent area covered by F4/80 immuno-positive cells.

Statistical analyses were performed using GraphPad InStat 3 software (GraphPad Software, Inc., La Jolla, CA). Analysis of Variance [26] together with Tukey-Kramer multiple comparisons post-test was used to compare differences among the multiple groups. Results are expressed as mean ± standard error of the mean (SEM). Statistical significance was defined as $p < 0.05$.

Results

Blast-induced G force levels and mortality

Previous experiments were conducted with 0.75 g of the PETN explosive, generating maximum acceleration forces in the range of 50 – 100G, with histologic evidence of TBI, but no obvious behavioral abnormalities, external injuries or mortality.[21] In this study, the maximal blast-induced G force was escalated to determine the maximum survivable underbody blast induced acceleration force and characterize the effects of these higher blast levels on histologic and behavioral measures of TBI. The acceleration force target for the first set of experiments was 1200G. Based on calibration curves generated with blasts using 0.75 g of PETN explosive present at different stand-off distances in the absence of rats, we that a stand-off distance of 2.5 mm from the top of the water to the bottom of the lower platform would generate a peak acceleration force of approximately 1200G. The mean maximal force measured by accelerometers attached to the top plate near the head-end of the rat restraint was 1187 ± 115G (SEM) for n=10 blasts. The change in acceleration force with time, referred to as JERK, was 0.48×10^{7} meters sec^{-3}. All rats survived these blast-induced G and JERK levels with no apparent external injury.

The second acceleration force target was 2400G. In order to reach this level, we used the same stand-off distance of 2.5 mm that generated 1200G forces, but increased the amount of PETN to 2.0 g. The mean maximal force generated under these conditions was 2460 ± 76G for n=6 blasts. For these blasts, JERK was 1.09×10^{8} meters sec^{-3}. While these blasts doubled the G forces, the JERK increased ~20 fold. Although all animals survived these relatively high G forces, they exhibited shallow breathing, lethargy, and disorientation lasting several minutes immediately after the blast. These signs of acute insult indicated that the 2400G force was close to the

maximum survivable and therefore set a third target of 2800G to test this hypothesis. In order to reach this level, we used the same 2.0 g of PETN and a stand-off distance of 2.5 mm but the mass of the two platforms was reduced by a net 25%, which increases the peak acceleration. The mean maximal force generated under these conditions was 2851 ± 359G for n=3 blasts. The JERK level was 1.77 ± 0.33 x 10^8 meters sec^{-3}. Four of the six rats subjected to this blast force died either immediately or within a few minutes after the blast. Necropsies performed on these animals revealed severe pulmonary hemorrhaging and edema, without obvious damage to the heart, liver, or spleen. The two animals that survived this blast level were used for behavioral measurements through 28 days post injury and were relatively different from rats that experienced 2400G blasts. The time they spent in the open arms of the Plus maze on day 28 post-injury was 13.08 ± 13.08 s compared to 39.02 ± 11.93 s spent by the 2400G blast rats.

Behavioral outcomes

Previous underbody blast experiments where rats were subjected to mild G forces in the range of 50 – 100G showed no behavioral alterations, despite findings of white matter axonal injury and cerebrovascular damage.[21] In this study we used Y maze and Elevated Plus maze tests for hippocampus-dependent working memory and anxiety, respectively, as we have found them to be sensitive assays of functional injury in other TBI paradigms.

Hippocampus-dependent working memory

The Y maze tests the innate ability of a rodent to continuously alternate visits in the three arms during the maze exploration. Rats with a good “working” memory ‘recognize’ the most recently explored arm of the maze and will successfully alternate arm visits approximately 70% of the time.[27] The mean percent alternation for sham rats was only approximately 35% on day zero when tested one hour after anesthesia but improved to a normal range of between 65 and 75% on days 6, 13, and 27 days later. Rats subjected to 1200G blast force exhibited similar alternation deficit on day zero and recovery on the subsequent test days. There were no differences in alternation between 1200G blast rats and shams on any of the test days. In contrast, rats exposed to 2400G blast force displayed only 5% sucessful alternation on day zero, 30% on day 6, and between 50 and 65% on days 13 and 27. Spontaneous alternation by 2400G rats was significantly lower than that of shams on day zero and on day 6 (Fig. 2A), with a regression over time showing the 2400G blast animals are nearly three weeks slower to recovery compared with either sham or 1200G animals.

Anxiety-like behavior

The elevated plus maze was used to test anxiety like behaviors in rats subjected to blast-induced acceleration forces of both 1200G and 2400G. Normal rats spend most of their time in the plus maze in the close arms but display significant periods of inquisitive venture into the open arms. Rats that are interpreted as ‘fearful and anxious’ generally spend much less time in the open arms in comparison with normal rats. Animals that received either 1200G or 2400G both exhibited significant impairment. Both groups spent 33 to 80% less time in open arms throughout the one month testing period (days 8, 14 and 28 post-injury) compared to shams (Fig. 2B).

In this paradigm, the decision to explore either the open arms or enter in the adjacent close arm can only be made in the central zone where the arms cross. Rats subjected to both blast levels spent the same relative time in the central area (Fig. 2C). Total distance traveled was identical for sham and 1200G blasts, however 2400G blast rats exhibited approximately 50% to 80% of the total distance traveled in the other groups throughout the testing period (Fig. 2D). Although total travel was reduced in this group it was unchanged in the 1200G group. Thus, the relative time between open and closed arms was not hindered by their motor performance.

Accumulation of inflammatory cells

Activated microglia, macrophages, and astrocytes are commonly observed in other animal models of TBI.[28] To test whether our purely acceleration force-induced injury model produces inflammatory responses, we immunostained for activated microglia/macrophages present at one and seven days post-blast, using antibodies to the F4/80 marker protein. Although F4/80 immunostaining was observed primarily in perivascular and periventricular regions throughout the cortex (Fig. 2.A) and hippocampus (not shown), the staining was quantified by expressing the total stained area as a percentage of the total area present over a wide area in each coronal section as a measurement of total magnitude of F4/80. Compared to Shams that exhibited 1.65 ± 0.47% of brain area F4/80 immunoreactive, rats subjected to underbody blasts that generated 1200G accelerations exhibited almost 5 times greater F4/80 immunostaining at 24 hr post-blast (7.62 ± 1.35%) (Fig. 3B). Rats subjected to 2400G blasts exhibited 9 times as much staining for activated microglia/macrophages as sham (15.07 ± 1.28%).

These results indicate a rapid extensive microglial / macrophage inflammatory response. However, by seven days post-injury, neuroinflammation measured by F4/80 subsided in both the 1200G and 2400G blast groups (3.58 ± 0.88% and 2.83 ± 1.52%). Double labeling with antibodies to both F4/80 and inducible nitric oxide synthase (iNOS) confirm the pro-inflammatory identify of these cells (Fig. 3.C) as iNOS is highly specific for pro-inflammatory cells, e.g., activated microglia and macrophages.[29, 30]

Tight junction proteins and vascular endothelial cell damage

Brain injuries, including those resulting from explosive blast, have been associated with blood brain barrier dysfunction.[6, 31] In the underbody blast model, we compared western blot analysis of brain tissue from rats exposed to 1200G and 2400G acceleration forces with sham for changes in the expression levels of tight junction proteins occludin and ZO-1 and of von Willebrand Factor (VWF) (an endothelial cell injury marker) 24 hr post-insult (Figures 3A, B and C). This time was chosen to coincide with the peak of neuroinflammatory cellular responses seen in F4/80 immunohistochemistry. Compared to sham animals, the expression of occludin was reduced by ~40% in the hippocampus and cortex of rats subjected to 2400G acceleration force intensity (Fig. 4D), with no significant change in the cerebellum (figure 4D). Blasts that generated 1200G force levels did not result in significant alterations of occludin expression. Furthermore, the expression of ZO-1 was decreased in the cortex of 2400G blast rats compared to sham rats (Fig. 4E). Similar to occludin, ZO-1 expression levels were not affected in the cerebellum or after 1200G blasts (Fig. 4E). von Willebrand Factor is a protein produced and released from vascular endothelial

cells in response to stress. VWF expression was significantly increased in hippocampal and cerebellar tissues following blast (Fig. 4F). Although occluding/ZO-1 were altered in cortex, there were no changes in VWF, suggesting endothelial/perivascular responses to explosive acceleration force within the brain are non-uniform among different regions. Interestingly, the most significant alterations were in areas associated with working memory and cognition (hippocampus and cortex), where behavioral defects were observed, and less in the motor function associated cerebellum.

Oxidative stress and expression of the anti-apoptotic protein Bcl-2

In many models TBI and, neuroinflammatory activity is followed by oxidative stress, which can contribute to cell death cascades. We therefore examined the expression levels of oxidative stress response protein HSP70 and the anti-apoptotic protein Bcl-2 in different brain regions 24 hr following blast exposure. The expression of Hsp70 was significantly upregulated in the hippocampus (Fig. 5A) and cerebellum (Fig. 5C) following exposure of rats to underbody blast. Following both 1200G and 2400G blasts, there was a 50% increase in Hsp70 expression in the hippocampus and 30% increase in the cerebellum, compared to sham animals (Fig. 5E). In contrast, blast-induced acceleration forces of 1200 and 2400G dramatically reduced Bcl-2 immunoreactive protein levels in both the hippocampus, by 40%, and the cerebellum, by 50% (Fig. 5D). Surprisingly, Hsp70 and Bcl-2 levels were not affected by underbody blast in the cortex. Since a reduction in Bcl-2 can increase susceptibility to cell death, we quantified cell death in the hippocampus, using TUNEL staining, and immunohistostaining for active (cleaved) caspase 3.

Hippocampal cell death

The hippocampus is a brain region that is particularly vulnerable to neuronal damage and death following acute brain injury and is essential for learning and memory. We therefore determined if neuronal death occurred in the hippocampus at 24 hr following exposure to 1200G or 2400G blasts, using both immunohistochemical staining for cleaved caspase 3 and histochemical TUNEL staining, which have been associated with cognitive deficits in other blast TBI models.[32] Blast exposure at 1200G and 2400G acceleration forces increased the appearance of cleaved caspase 3 immunoreactive cells in the dentate gyrus (Fig. 6.A) and the CA2/CA3 areas (not shown) of the hippocampus; however, very sparse staining for either biomarker was observed in the CA1 area (not shown). The number of cleaved caspase 3 positive cells present in the dentate gyrus was 11 ± 2 per mm^2 for rats exposed to 1200G acceleration force and 13 ± 3 per mm^2 for 2400G blast rats, in comparison to 2 ± 1 per mm^2 for sham animals (Fig. 6B). In the Ca2/Ca3 area of the hippocampus, the cell count was 7 ± 1 per mm^2 for 1200G blast rats and 11 ± 2 per mm^2 for 2400G blast rats, as opposed to 1 ± 1 per mm^2 for sham rats (Fig. 6B). After counting 350 cleaved caspase 3 immunoreactive cells in the DG using a 63 x magnification objective, we found that 92% of these cells co-labeled with the neuronal marker NeuN (Fig. 6A).

Cleaved caspase 3 immunoreactivity reflects the presence of a caspase 3 dependent apoptotic pathway but is not a direct indicator of cell death. Additional evidence that exposure of rats to blast-induced acceleration forces of 1200 – 2400G came from quantification of TUNEL positive cells, which is a marker of DNA

fragmentation and late stage cell death. Tunnel positive cells count in the DG 24hrs post-injury was 8 ± 1 / mm^2 for rats exposed to 1200G blast intensity and 11 ± 2 / mm^2 for 2400G blast rats both versus 2 ± 1 / mm^2 for sham animals. Similar results were observed on the Ca2/Ca3 area where the count was 4 ± 1 / mm^2 for 1200G blast rats and 8 ± 1 / mm^2 for 2400G blast rats, compared to 2 ± 1 / mm^2 for shams (figure 6B).

Expression of neurosynaptic proteins

In addition to cerebrovascular damage, inflammation, and neuronal death, significant disruption to synaptic connectivity is a hallmark of mild forms of TBI. [33, 34] Immunoblot protein analyses revealed significant, 25 – 50% reductions in the expression levels of synaptic markers PSD95, synaptophysin and of the dendritic spine marker spinophilin in different brain regions 24 hr following exposure to underbody blast that produced either 1200 or 2400G acceleration forces (Fig. 8A-C). PSD-95 levels were reduced in the hippocampus, cortex, and cerebellum. Synaptophysin was reduced in the hippocampus and cerebellum but not the cortex. Synaptophilin immunoreactivity reduced in the hippocampus but not the cortex and was not measured in the cerebellum.

Discussion

This study describes quantitative changes in brain histology, neurochemistry, and behavior that occur within a few hours to several weeks following exposure of rats to sublethal acceleration loads that model those experienced by occupants of vehicles targeted by land mines. Several conclusions can be drawn from our observations. First, high blast loads result in a transient deficit in working memory and a chronic increase in anxiety, as measured using the Y maze and elevated plus maze, respectively. Second, a decrease in the levels of tight junction proteins taken together with an increase in VWF immunoreactivity indicate that high underbody blast loads result in cerebrovascular damage. Third, these blasts result in neuroinflammation, as reflected by increased perivascular and periventricular F4/80 immunopositive cells during the first week following injury. Fourth, underbody blasts cause significant neuronal death primarily within the hippocampus. Fifth, the significant reduction in both presynaptic and postsynaptic proteins that occurs within 24 hr following high blast loads suggests a rapid loss of functional neuronal synapses.

Impairments in Y and elevated maze tests could be impacted by motor deficits as well as by cognitive deficits. However, with the exception of the rats analyzed one day following 2400G blasts, there was no difference in the total distance traveled between sham and blast rats at 1 – 28 days post-blast in any of the behavioral metrics. Thus, motor impairments are unlikely to be complicating interpretation of behavioral alterations observed at 6 - 28 days after the blasts. The results obtained on day zero or one are possibly less reliable than those obtained at later times since the values in the

shams for both tests were lower than the values obtained a later times. Most likely, this is due to behavioral disruption from anesthesia or other stress in the first 24 hours.

The behavioral alterations apparent in our underbody blast model exhibit some of the characteristics observed in overpressure rodent models of TBI. For example, a single exposure of mice to open field overpressure blast causes significant deficits in cognition and spatial memory, both occurring seven days post-insult.[35] In other studies, rodents subjected to overpressure as well as blast shock waves showed significant deficits in learning, spatial memory and increased anxiety at up to at least one month following blast exposure.[7, 19, 36] Thus, either open field blast overpressure or underbody hull blast-induced acceleration is sufficient to cause mild to moderate, long-term behavioral alterations. Thus, it may not be sufficient to protect from overpressure in vehicle design without considering the acceleration injury caused by transfer of kinetic energy to the vehicle.

Neurobehavioral impairments observed following TBI are often associated with markers of neuroinflammation. Neuroinflammatory mechanisms are emerging as a potential common effector of TBI damage to the brain, as well as markers of injury. In our model, we observed a blast dose-dependent increase in F4/80-positive, activated microglia and / or macrophages in perivascular and periventricular regions of the brain. F4/80 positive cells co-labeled with antibodies to inducible nitric oxide synthase (iNOS), which contributes nitrous oxide dependent exacerbation of brain damage caused by inflammation [37]. F4/80 immunostaining returned to nearly normal levels by 7 days post-blast suggesting the microglial phase of acceleration induced injury peaks rapidly following the blast.

A range of evidence supports the role of inflammation in the pathogenesis of open field blast-induced TBI. Observations include the increased expression of inflammatory mediators including macrophage inflammatory proteins, monocytes chemotactic proteins, IL-1β, IL-6 TNF-α and INF-γ. [36, 38-40] cDNA microarray measurements indicate an increase in the mRNA levels of many pro-inflammatory genes including interleukins and TNF-α. [41] At the cellular level, microglia activation and increase macrophage levels have been reported in the rodent brains following blast exposure. [38, 40, 42, 43] In most of these studies, including ours, markers of inflammation responses from microglia occur acutely at 3-48 hours post-blast.

An elevation in the presence of inflammatory cells in the brain after TBI can be caused by endogenous microglial activation, migration, and proliferation. Systemically circulating macrophages can also invade the brain parenchyma, particularly if there is disruption in the blood brain barrier (BBB) and/or vascular endothelial cells. Two major components of tight junctions (Occludin and ZO-1), crucial in maintaining BBB integrity [6, 44] showed significant reductions in cortex and hippocampus. The mechanisms resulting in the reduction are unclear, but could be reduced synthesis rate or alterations in the proteolytic activity of enzymes such as the metalloproteinase-9, which is associated with effectors of BBB dysfunction following TBI [45]. In contrast, an increase in VWF was observed primarily in the cerebellum after either 1200 or 2400G blasts. VWF activation may represent a compensatory mechanism to promote blood coagulation after vascular injury that occurs after TBI. [46, 47] The reduction in Occludin and ZO-1 protein levels seen after underbody blasts is consistent with recent report by Abdul-Muneer and colleagues indicating that exposure of rats to a single blast-relevant shock

wave caused a downregulation of tight junction protein expression, associated with increased levels of the oxidative stress markers 3-nitrotyrosine (3-NT) and 4 – hydroxynonenal (4-HNE). [6] In contrast to downregulation of Occludin and ZO-1 proteins, the platelet adhesion regulating molecule VWF increased in the cerebellum only. VWF activation may represent a compensatory mechanism to promote blood coagulation after vascular injury [46, 47] and be protective of this brain region. Additional studies are needed, however, to test whether these molecular changes result in BBB disruption, and possible protection in cerebellar regions, in the underbody blast TBI model.

We previously reported the absence of significant cell death in the brains of rats following underbody blasts at low G forces (50G). However at the higher accellerations used in the present study (1200 – 2400G) there was significant cell death. Some studies have concluded apoptosis in different brain regions following exposure to blast that correlated with cognitive impairments associated with function of those regions. [19, 20, 48] We detected the presence of apoptotic cells in the hippocampus, amygdala and cerebellum of blast animals, which was coupled with a decrease in Bcl-2 expression and an upregulation of the anti-stress protein Hsp70. Although the increase expression of Hsp70 may represent an attempt to the deleterious effect of blast-induced oxidative stress,[49, 50] the downregulation of the anti-apoptotic protein Bcl-2 may be involved in the apoptotic process. Thus, while it can be speculated neuronal loss in the hippocampus and amygdala may contribute to deficits in working memory and anxiety like behavior in blast animals, additional studies of neural circuit processing are needed.

Adequate synaptic transmission is clearly required for the maintenance of neurobehavioral functions. [51, 52] Loss of synapses and dendritic spine has been reported

in models of focal brain injury shortly after trauma and affect learning and memory performance,[34, 53] Interestingly, in our blast model, we observed decreased expression of synaptic markers synaptophysin and PSD-95 and that of the dendritic spine marker spinophilin, which all suggest a deficit in synaptic transmission. However, similar to changes seen with the expression of tight junction proteins between shams and blast rats, their expression was heterogeneous in different regions of the brain with a decrease observed in the hippocampus and little or no change in the cortex. This heterogeneous expression pattern could be due to anatomical differences in various brain regions and differences in sensitivity to excitotoxic insult [54]. Prior studies in models of experimental brain trauma demonstrated increased vulnerability of hippocampal neurons and cerebellar purkinje cells to trauma. [55-57]

In summary, our results demonstrate that high acceleration force induced brain injury altered the integrity of the blood brain barrier endothelium, potentially leading to increased accumulation of inflammatory cells in the brain. Blast-induced brain trauma also caused neuronal cell loss in the hippocampus, amygdala and cerebellum associated with reduced expression of proteins which modulate synaptic transmission. The neurologic consequences of these neuropathological alterations are a transient deficit in working memory and a chronic change in behavior interpreted as anxiety or depression. Overall, findings from our unique model of underbody blasts indicate that exposure to acceleration force alone is sufficient to cause at least mild TBI relevant to what survivors of under-vehicle explosions often experience. Work is in progress to develop new vehicle hull designs that dramatically reduce the force that these blasts

transfer to the occupants, thus reducing both mortality and injury to the brain and other vital organs.

References

1. Okie, S. (2005). Traumatic brain injury in the war zone. N. Engl. J. Med. 352, 2043-2047.
2. DePalma, R.G., Burris, D.G., Champion, H.R. and Hodgson, M.J. (2005). Blast injuries. N. Engl. J. Med. 352, 1335-1342.
3. Hoge, C.W., McGurk, D., Thomas, J.L., Cox, A.L., Engel, C.C. and Castro, C.A. (2008). Mild traumatic brain injury in U.S. Soldiers returning from Iraq. N. Engl. J. Med. 358, 453-463.
4. Rosenfeld, J.V., McFarlane, A.C., Bragge, P., Armonda, R.A., Grimes, J.B. and Ling, G.S. (2013). Blast-related traumatic brain injury. Lancet neurology 12, 882-893.
5. Owens, B.D., Kragh, J.F., Jr., Wenke, J.C., Macaitis, J., Wade, C.E. and Holcomb, J.B. (2008). Combat wounds in operation Iraqi Freedom and operation Enduring Freedom. J. Trauma 64, 295-299.
6. Abdul-Muneer, P.M., Schuetz, H., Wang, F., Skotak, M., Jones, J., Gorantla, S., Zimmerman, M.C., Chandra, N. and Haorah, J. (2013). Induction of oxidative and nitrosative damage leads to cerebrovascular inflammation in an animal model of mild traumatic brain injury induced by primary blast. Free Radic. Biol. Med. 60, 282-291.

7. Cernak, I., Merkle, A.C., Koliatsos, V.E., Bilik, J.M., Luong, Q.T., Mahota, T.M., Xu, L., Slack, N., Windle, D. and Ahmed, F.A. (2011). The pathobiology of blast injuries and blast-induced neurotrauma as identified using a new experimental model of injury in mice. Neurobiol. Dis. 41, 538-551.

8. Mellor, S.G. (1988). The pathogenesis of blast injury and its management. Br. J. Hosp. Med. 39, 536-539.

9. Lange, R.T., Brickell, T.A., Ivins, B., Vanderploeg, R.D. and French, L.M. (2013). Variable, not always persistent, postconcussion symptoms after mild TBI in U.S. military service members: a five-year cross-sectional outcome study. J. Neurotrauma 30, 958-969.

10. Brenner, L.A., Vanderploeg, R.D. and Terrio, H. (2009). Assessment and diagnosis of mild traumatic brain injury, posttraumatic stress disorder, and other polytrauma conditions: burden of adversity hypothesis. Rehabilitation psychology 54, 239-246.

11. Elder, G.A., Mitsis, E.M., Ahlers, S.T. and Cristian, A. (2010). Blast-induced mild traumatic brain injury. Psychiatr. Clin. North Am. 33, 757-781.

12. Jaffee, M.S. and Meyer, K.S. (2009). A brief overview of traumatic brain injury (TBI) and post-traumatic stress disorder (PTSD) within the Department of Defense. The Clinical neuropsychologist 23, 1291-1298.

13. Rosenfeld, J.V. and Ford, N.L. (2010). Bomb blast, mild traumatic brain injury and psychiatric morbidity: a review. Injury 41, 437-443.

14. Kovacs, S.K., Leonessa, F. and Ling, G.S. (2014). Blast TBI Models, Neuropathology, and Implications for Seizure Risk. Frontiers in neurology 5, 47.

15. Goldstein, L.E., McKee, A.C. and Stanton, P.K. (2014). Considerations for animal models of blast-related traumatic brain injury and chronic traumatic encephalopathy. Alzheimer's research & therapy 6, 64.

16. Schultz, B.A., Cifu, D.X., McNamee, S., Nichols, M. and Carne, W. (2011). Assessment and treatment of common persistent sequelae following blast induced mild traumatic brain injury. NeuroRehabilitation 28, 309-320.

17. Chen, Y., Huang, W. and Constantini, S. (2013). Concepts and strategies for clinical management of blast-induced traumatic brain injury and posttraumatic stress disorder. J. Neuropsychiatry Clin. Neurosci. 25, 103-110.

18. Elder, G.A., Gama Sosa, M.A., De Gasperi, R., Stone, J.R., Dickstein, D.L., Haghighi, F., Hof, P.R. and Ahlers, S.T. (2015). Vascular and inflammatory factors in the pathophysiology of blast-induced brain injury. Frontiers in neurology 6, 48.

19. Vandevord, P.J., Bolander, R., Sajja, V.S., Hay, K. and Bir, C.A. (2012). Mild neurotrauma indicates a range-specific pressure response to low level shock wave exposure. Ann. Biomed. Eng. 40, 227-236.

20. Kwon, S.K., Kovesdi, E., Gyorgy, A.B., Wingo, D., Kamnaksh, A., Walker, J., Long, J.B. and Agoston, D.V. (2011). Stress and traumatic brain injury: a behavioral, proteomics, and histological study. Frontiers in neurology 2, 12.

21. Proctor, J.L., Fourney, W.L., Leiste, U.H. and Fiskum, G. (2014). Rat model of brain injury caused by under-vehicle blast-induced hyperacceleration. The journal of trauma and acute care surgery 77, S83-87.

22. Zhao, X., Tiwari, V., Sutton, M.A., Deng, X., Fourney, W.L. and Leiste, U. (2013). Scaling of the deformation histories for clamped circular plates subjected to blast loading by buried charges. International Journal of Impact Engineering 54, 31-50.

23. Tchantchou, F. and Zhang, Y. (2013). Selective Inhibition of Alpha/Beta-Hydrolase Domain 6 Attenuates Neurodegeneration, Alleviates Blood Brain Barrier Breakdown, and Improves Functional Recovery in a Mouse Model of Traumatic Brain Injury. J. Neurotrauma.

24. Budde, M.D., Shah, A., McCrea, M., Cullinan, W.E., Pintar, F.A. and Stemper, B.D. (2013). Primary blast traumatic brain injury in the rat: relating diffusion tensor imaging and behavior. Frontiers in neurology 4, 154.

25. Tchantchou, F., Xu, Y., Wu, Y., Christen, Y. and Luo, Y. (2007). EGb 761 enhances adult hippocampal neurogenesis and phosphorylation of CREB in transgenic mouse model of Alzheimer's disease. FASEB J. 21, 2400-2408.

26. Chanda, P.K., Gao, Y., Mark, L., Btesh, J., Strassle, B.W., Lu, P., Piesla, M.J., Zhang, M.Y., Bingham, B., Uveges, A., Kowal, D., Garbe, D., Kouranova, E.V., Ring, R.H., Bates, B., Pangalos, M.N., Kennedy, J.D., Whiteside, G.T. and Samad, T.A. (2010). Monoacylglycerol lipase activity is a critical modulator of the tone and integrity of the endocannabinoid system. Mol. Pharmacol. 78, 996-1003.

27. Maurice, T., Hippert, C., Serratrice, N., Dubois, G., Jacquet, C., Antignac, C., Kremer, E.J. and Kalatzis, V. (2009). Cystine accumulation in the CNS results in severe age-related memory deficits. Neurobiol. Aging 30, 987-1000.

28. Ramlackhansingh, A.F., Brooks, D.J., Greenwood, R.J., Bose, S.K., Turkheimer, F.E., Kinnunen, K.M., Gentleman, S., Heckemann, R.A., Gunanayagam, K., Gelosa, G. and Sharp, D.J. (2011). Inflammation after trauma: microglial activation and traumatic brain injury. Ann. Neurol. 70, 374-383.

29. Tchantchou, F., Tucker, L.B., Fu, A.H., Bluett, R.J., McCabe, J.T., Patel, S. and Zhang, Y. (2014). The fatty acid amide hydrolase inhibitor PF-3845 promotes neuronal survival, attenuates inflammation and improves functional recovery in mice with traumatic brain injury. Neuropharmacology 85, 427-439.

30. Loane, D.J., Stoica, B.A., Tchantchou, F., Kumar, A., Barrett, J.P., Akintola, T., Xue, F., Conn, P.J. and Faden, A.I. (2014). Novel mGluR5 positive allosteric modulator improves functional recovery, attenuates neurodegeneration, and alters microglial polarization after experimental traumatic brain injury. Neurotherapeutics : the journal of the American Society for Experimental NeuroTherapeutics 11, 857-869.

31. Walls, M.K., Race, N., Zheng, L., Vega-Alvarez, S.M., Acosta, G., Park, J. and Shi, R. (2015). Structural and biochemical abnormalities in the absence of acute deficits in mild primary blast-induced head trauma. J. Neurosurg., 1-12.

32. Itoh, T., Imano, M., Nishida, S., Tsubaki, M., Mizuguchi, N., Hashimoto, S., Ito, A. and Satou, T. (2013). Increased apoptotic neuronal cell death and cognitive impairment at early phase after traumatic brain injury in aged rats. Brain structure & function 218, 209-220.

33. Przekwas, A., Somayaji, M.R. and Gupta, R.K. (2016). Synaptic Mechanisms of Blast-Induced Brain Injury. Frontiers in neurology 7, 2.

34. Gao, X., Deng, P., Xu, Z.C. and Chen, J. (2011). Moderate traumatic brain injury causes acute dendritic and synaptic degeneration in the hippocampal dentate gyrus. PloS one 6, e24566.

35. Rubovitch, V., Ten-Bosch, M., Zohar, O., Harrison, C.R., Tempel-Brami, C., Stein, E., Hoffer, B.J., Balaban, C.D., Schreiber, S., Chiu, W.T. and Pick, C.G. (2011). A mouse model of blast-induced mild traumatic brain injury. Exp. Neurol. 232, 280-289.

36. Kamnaksh, A., Kwon, S.K., Kovesdi, E., Ahmed, F., Barry, E.S., Grunberg, N.E., Long, J. and Agoston, D. (2012). Neurobehavioral, cellular, and molecular consequences of single and multiple mild blast exposure. Electrophoresis 33, 3680-3692.

37. Foley, L.M., Hitchens, T.K., Melick, J.A., Bayir, H., Ho, C. and Kochanek, P.M. (2008). Effect of inducible nitric oxide synthase on cerebral blood flow after experimental traumatic brain injury in mice. J. Neurotrauma 25, 299-310.

38. Dalle Lucca, J.J., Chavko, M., Dubick, M.A., Adeeb, S., Falabella, M.J., Slack, J.L., McCarron, R. and Li, Y. (2012). Blast-induced moderate neurotrauma (BINT) elicits early complement activation and tumor necrosis factor alpha (TNFalpha) release in a rat brain. J. Neurol. Sci. 318, 146-154.

39. Kovesdi, E., Gyorgy, A.B., Kwon, S.K., Wingo, D.L., Kamnaksh, A., Long, J.B., Kasper, C.E. and Agoston, D.V. (2011). The effect of enriched environment on the outcome of traumatic brain injury; a behavioral, proteomics, and histological study. Frontiers in neuroscience 5, 42.

40. Tompkins, P., Tesiram, Y., Lerner, M., Gonzalez, L.P., Lightfoot, S., Rabb, C.H. and Brackett, D.J. (2013). Brain injury: neuro-inflammation, cognitive deficit, and magnetic resonance imaging in a model of blast induced traumatic brain injury. J. Neurotrauma 30, 1888-1897.

41. Valiyaveettil, M., Alamneh, Y., Wang, Y., Arun, P., Oguntayo, S., Wei, Y., Long, J.B. and Nambiar, M.P. (2013). Contribution of systemic factors in the pathophysiology of repeated blast-induced neurotrauma. Neurosci. Lett. 539, 1-6.

42. Cho, H.J., Sajja, V.S., Vandevord, P.J. and Lee, Y.W. (2013). Blast induces oxidative stress, inflammation, neuronal loss and subsequent short-term memory impairment in rats. Neuroscience 253, 9-20.

43. Sosa, M.A., De Gasperi, R., Paulino, A.J., Pricop, P.E., Shaughness, M.C., Maudlin-Jeronimo, E., Hall, A.A., Janssen, W.G., Yuk, F.J., Dorr, N.P., Dickstein, D.L., McCarron, R.M., Chavko, M., Hof, P.R., Ahlers, S.T. and Elder, G.A. (2013). Blast overpressure induces shear-related injuries in the brain of rats exposed to a mild traumatic brain injury. Acta neuropathologica communications 1, 51.

44. Armulik, A., Genove, G., Mae, M., Nisancioglu, M.H., Wallgard, E., Niaudet, C., He, L., Norlin, J., Lindblom, P., Strittmatter, K., Johansson, B.R. and Betsholtz, C. (2010). Pericytes regulate the blood-brain barrier. Nature 468, 557-561.

45. Higashida, T., Kreipke, C.W., Rafols, J.A., Peng, C., Schafer, S., Schafer, P., Ding, J.Y., Dornbos, D., 3rd, Li, X., Guthikonda, M., Rossi, N.F. and Ding, Y. (2011). The role of hypoxia-inducible factor-1alpha, aquaporin-4, and matrix

metalloproteinase-9 in blood-brain barrier disruption and brain edema after traumatic brain injury. J. Neurosurg. 114, 92-101.

46. Yokota, H., Naoe, Y., Nakabayashi, M., Unemoto, K., Kushimoto, S., Kurokawa, A., Node, Y. and Yamamoto, Y. (2002). Cerebral endothelial injury in severe head injury: the significance of measurements of serum thrombomodulin and the von Willebrand factor. J. Neurotrauma 19, 1007-1015.

47. De Oliveira, C.O., Reimer, A.G., Da Rocha, A.B., Grivicich, I., Schneider, R.F., Roisenberg, I., Regner, A. and Simon, D. (2007). Plasma von Willebrand factor levels correlate with clinical outcome of severe traumatic brain injury. J. Neurotrauma 24, 1331-1338.

48. Kobeissy, F., Mondello, S., Tumer, N., Toklu, H.Z., Whidden, M.A., Kirichenko, N., Zhang, Z., Prima, V., Yassin, W., Anagli, J., Chandra, N., Svetlov, S. and Wang, K.K. (2013). Assessing neuro-systemic & behavioral components in the pathophysiology of blast-related brain injury. Frontiers in neurology 4, 186.

49. Kim, N., Kim, J.Y. and Yenari, M.A. (2015). Pharmacological induction of the 70-kDa heat shock protein protects against brain injury. Neuroscience 284, 912-919.

50. Adachi, M., Liu, Y., Fujii, K., Calderwood, S.K., Nakai, A., Imai, K. and Shinomura, Y. (2009). Oxidative stress impairs the heat stress response and delays unfolded protein recovery. PloS one 4, e7719.

51. Stancu, I.C., Ris, L., Vasconcelos, B., Marinangeli, C., Goeminne, L., Laporte, V., Haylani, L.E., Couturier, J., Schakman, O., Gailly, P., Pierrot, N., Kienlen-Campard, P., Octave, J.N. and Dewachter, I. (2014). Tauopathy contributes to

synaptic and cognitive deficits in a murine model for Alzheimer's disease. FASEB J. 28, 2620-2631.

52. Shankar, G.M. and Walsh, D.M. (2009). Alzheimer's disease: synaptic dysfunction and Abeta. Molecular neurodegeneration 4, 48.

53. Scheff, S.W., Price, D.A., Hicks, R.R., Baldwin, S.A., Robinson, S. and Brackney, C. (2005). Synaptogenesis in the hippocampal CA1 field following traumatic brain injury. J. Neurotrauma 22, 719-732.

54. Geddes, D.M., LaPlaca, M.C. and Cargill, R.S., 2nd (2003). Susceptibility of hippocampal neurons to mechanically induced injury. Exp. Neurol. 184, 420-427.

55. Anderson, K.J., Miller, K.M., Fugaccia, I. and Scheff, S.W. (2005). Regional distribution of fluoro-jade B staining in the hippocampus following traumatic brain injury. Exp. Neurol. 193, 125-130.

56. Igarashi, T., Potts, M.B. and Noble-Haeusslein, L.J. (2007). Injury severity determines Purkinje cell loss and microglial activation in the cerebellum after cortical contusion injury. Exp. Neurol. 203, 258-268.

57. Nawashiro, H., Shima, K. and Chigasaki, H. (1995). Selective vulnerability of hippocampal CA3 neurons to hypoxia after mild concussion in the rat. Neurol. Res. 17, 455-460.

Figure 1

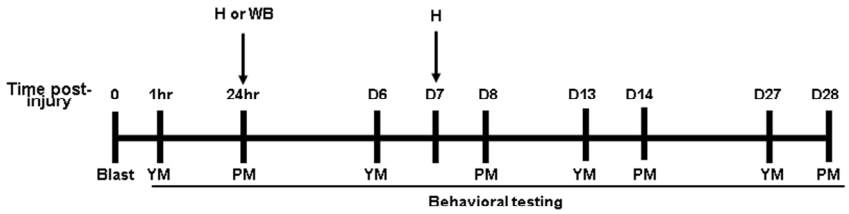

Figure 1. Experimental design and timeline
Detailed timeline of behavioral tests and end points of experimental procedures starting on study day 0 (blast exposure). YM, Y-maze test; PM, Plus-maze test; H, Histology, WB, western blots.

254x190mm (96 x 96 DPI)

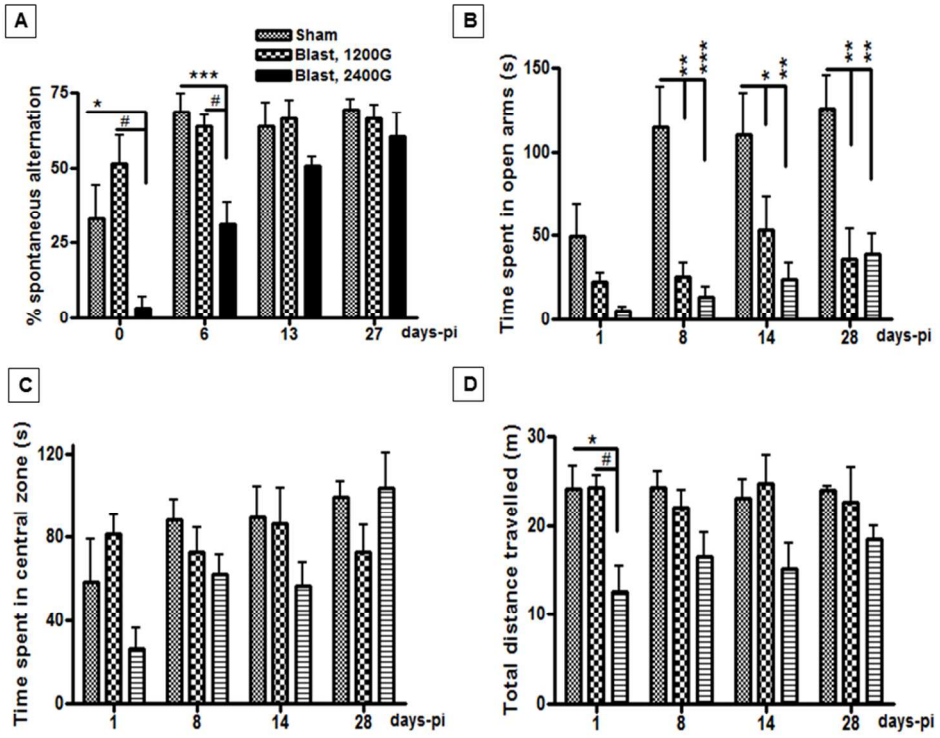

Figure 2. Behavioral outcomes after underbody blast
(A) Y-maze test results demonstrating significantly lower spontaneous alternation among maze arms by 2400G blast rats than shams or rats exposed to 1200G acceleration force (*,#p < 0.05 for day 0-pi and #p < 0.05, **p < 0.01 for day 6 post-injury (pi) respectively). (B) Plus maze test demonstrating that rats exposed to either 1200 or 2400G blasts spent significantly less time in the open arms on days 8, 14 and 28-pi compared to shams (*p < 0.05, **p < 0.01 and ***p < 0.001). There were no significant differences in the time spent in the central area (C) and in the total distance travelled (D) among blast and sham rats (p > 0.05), except on day 1 post-injury when 2400G blast rats travelled significantly less distance than sham and 1200G blast animals (*,#p < 0.05).

254x228mm (96 x 96 DPI)

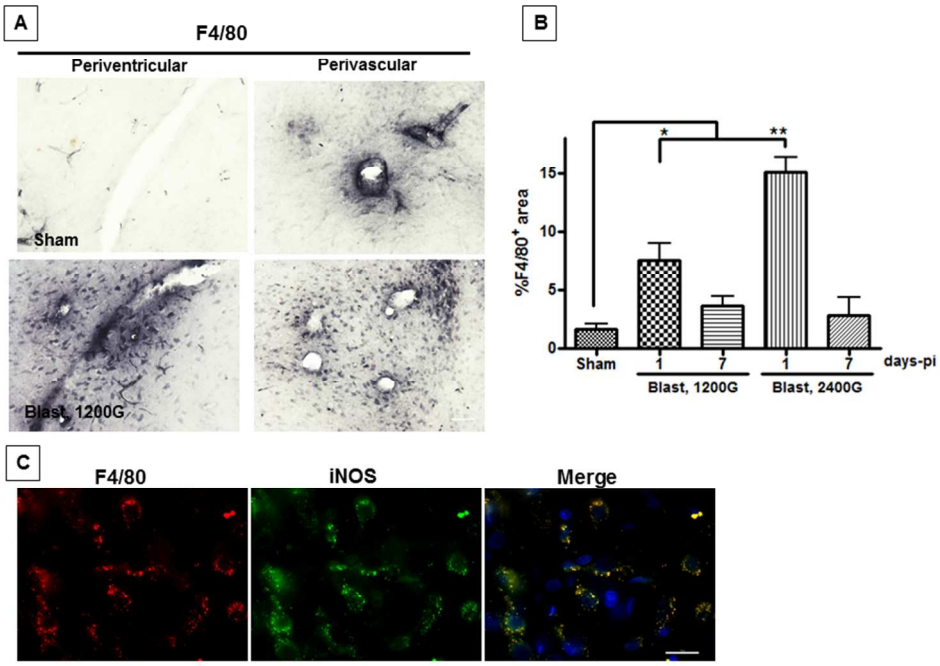

Figure 3. Accumulation of inflammatory cells in the brain
(A) Representative microphotograph exhibiting F4/80 immuno-positive cells in the perivascular and periventricular regions of blast rats. (B) Quantification of the percent of F4/80 immuno-reactive area indicating a significant increase in microglia/macrophage accumulation in the brain of 1200G and 2400G blast rats compared to shams 24 hr post-trauma (*$p < 0.05$ and **$p < 0.01$ respectively). (C) F4/80 immunopositive cells (Red) co-expressed the pro-inflammatory enzyme iNOS (Green); and DAPI 29 used as counterstain.

254x190mm (96 x 96 DPI)

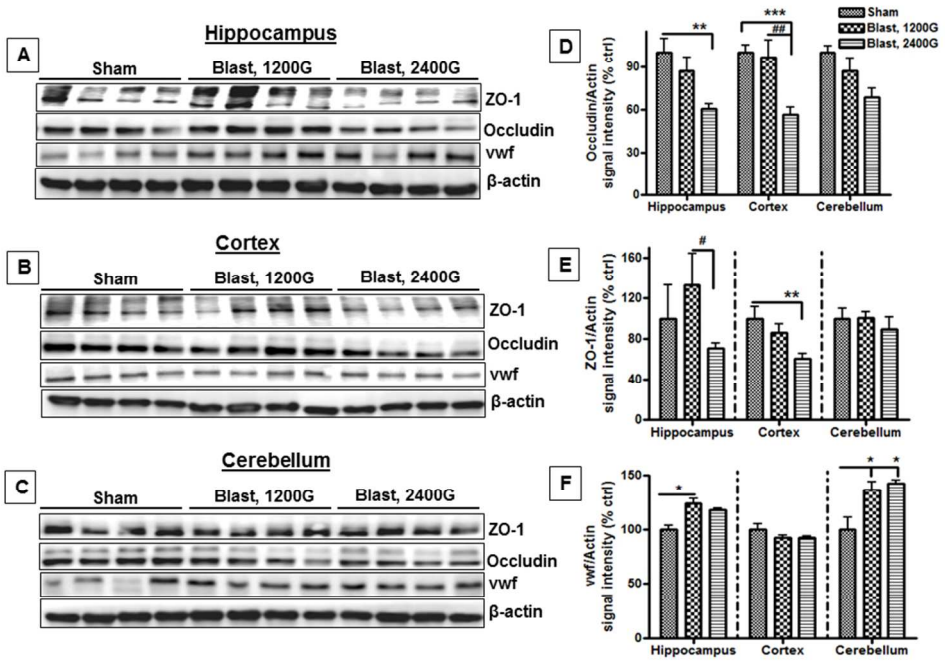

Figure 4. Vascular injury biomarkers
(A-C) Representative immunoblots illustrating the expression of Occludin, ZO-1, VWF and beta actin in the hippocampus, cortex and cerebellum 24 hr post-injury. Quantification of proteins bands indicating that (D) Occludin expression was significantly reduced in the hippocampus and cortex of 2400G blast rats compared to shams (**p < 0.01 and ***p < 0.001 respectively). (E) ZO-1 expression was significantly decreased in the cortex of 2400G blast rats compared to shams (**p < 0.01). In contrast, ZO-1 levels were significantly lower in the hippocampus of 2400G blast rats compared to 1200G blast rats (#p < 0.05). (F) Expression levels of VWF in the hippocampus were significantly higher in 2400G blast rats versus shams (*p < 0.05). In addition, VWF levels were also significantly higher in the cerebellum of 1200G and 2400G blast rats compared to shams (*p < 0.05).

254x190mm (96 x 96 DPI)

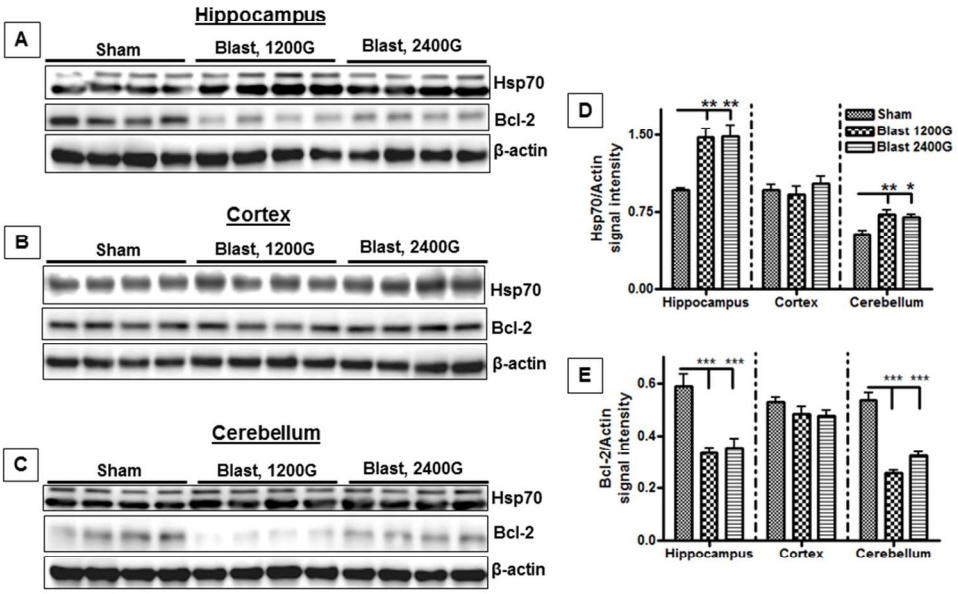

Figure 5. Reciprocal changes in the levels of Hsp70 stress response protein and Bcl-2 anti-apoptotic protein in different brain regions following blast exposure

(A-C) Representative immunoblots describing the expression of Hsp70, Bcl-2 and beta actin in the hippocampus, cortex and cerebellum. Quantification of proteins bands signal intensity indicated that (D) Bcl-2 expression was significantly reduced in the hippocampus and cerebellum of rats exposed to 1200G blasts (***$p < 0.001$) as well as 2400G blasts (***$p < 0.001$), respectively, versus shams. (E) Conversely, the expression of Hsp70 was significantly increased in the hippocampus and cerebellum of 1200G blast rats (**$p < 0.01$) and 2400G blast rats (**$p < 0.01$ and *$p < 0.05$), respectively, compared to shams.

254x190mm (96 x 96 DPI)

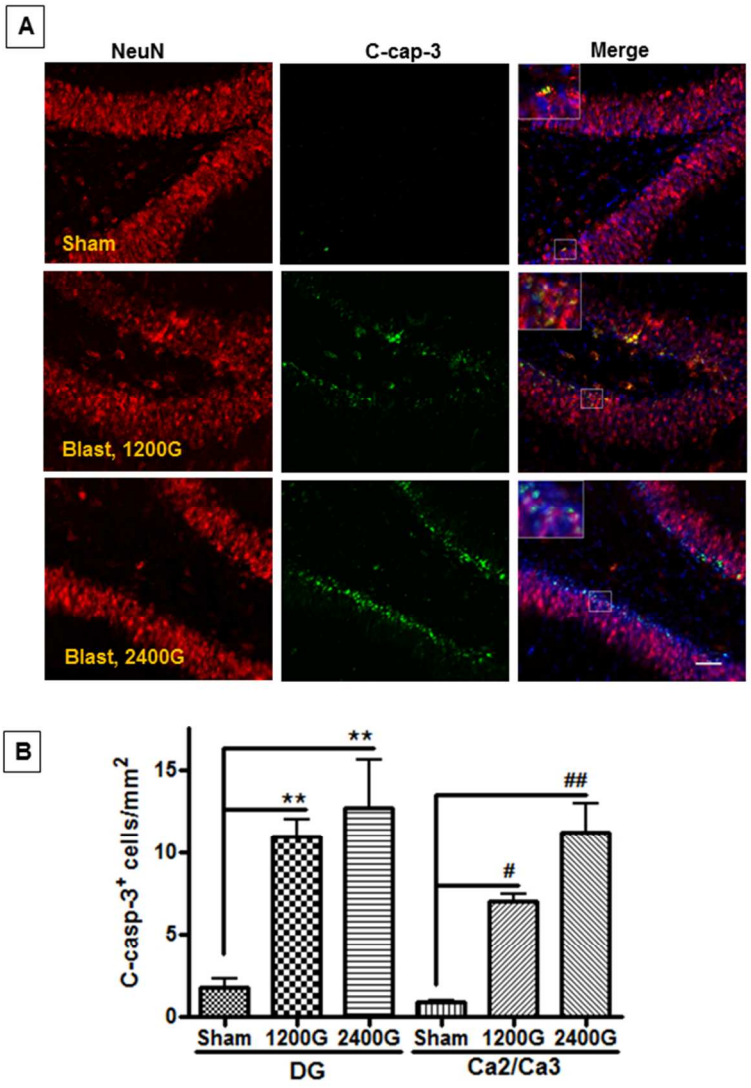

Figure 6. Cleaved caspase-3 immunoreactive cells present in rat hippocampus
(A) Representative fluorescent image showing the expression of cleaved caspase-3 (Green) in DG cells that overlap with NeuN positive cells (Red) and DAPI. (B) Quantification of cleaved-caspase-3 immunopositive cells 24hr post-insult indicated a significant increase in positive cells in the DG and Ca2/Ca3 area of both 1200G (**p < 0.01 and #p < 0.05) and 2400G (**p < 0.01 and ##p < 0.01) blast rats, respectively, compared to shams.

190x254mm (96 x 96 DPI)

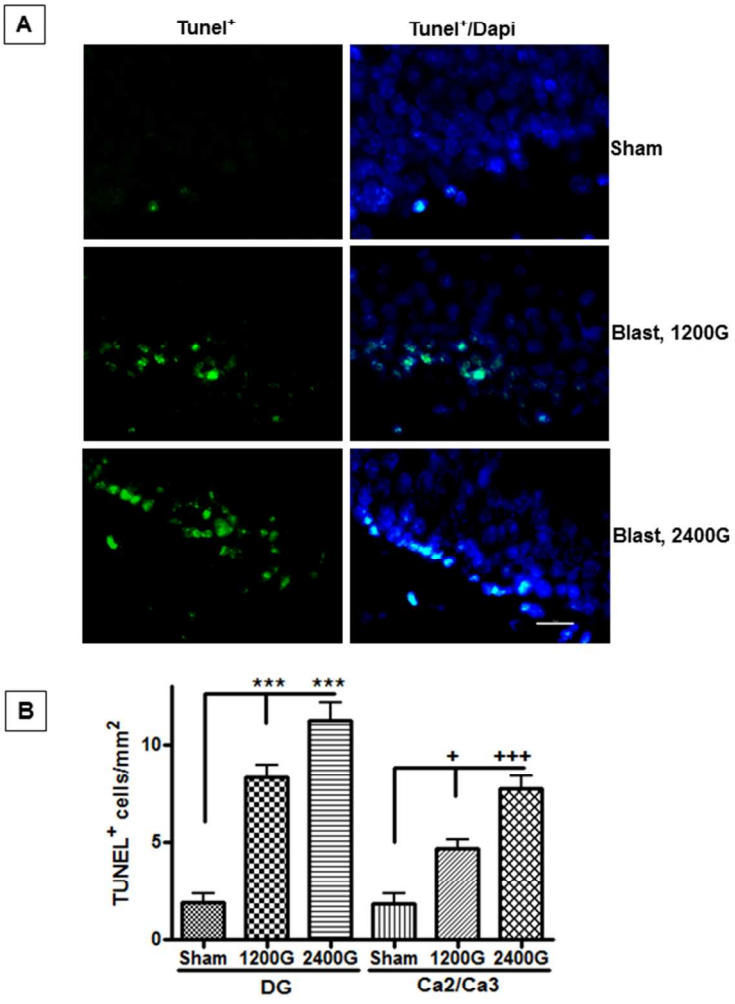

Figure 7. TUNEL positive cells in rat hippocampus
(A) Representative fluorescent image demonstrating the presence of TUNEL positive cells (Green) and DAPI-stained nuclei 29 in the DG. (B) In comparison with shams, there was a significant increase in TUNEL positive cells 24hr post-insult in the DG and Ca2/Ca3 areas of 1200G (***$p < 0.001$ and +$p < 0.05$) and 2400G blast animals (***$p < 0.001$ and +++$p < 0.001$) respectively.

215x254mm (96 x 96 DPI)

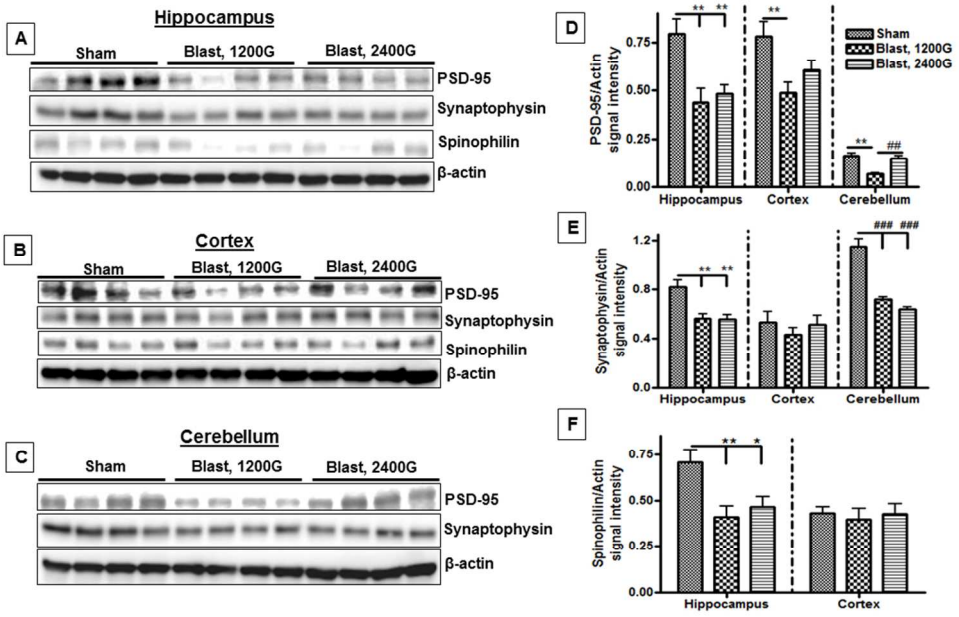

Figure 8. Brain region selective reduction in the expression of synaptic proteins following exposure to blasts (A-C) Representative immunoblots illustrating the expression of PSD-95, synaptophysin, and spinophilin in the hippocampus, cortex, and cerebellum. (Spinophilin was not detectable in the cerebellum). Quantification of proteins bands indicate that (D) PSD-95 expression was significantly reduced in the hippocampus, cortex and cerebellum of both 1200G and 2400G blast animals (**p < 0.01). Conversely, PSD-95 expression was only significantly affected in the hippocampus of rats exposed to 2400G blast (**p < 0.01). (E) Synaptophysin expression was dramatically reduced in the hippocampus and cerebellum of 1200G (**p < 0.01 and ###p < 0.001) and 2400G blast rats (**p < 0.01 and ###p < 0.001), respectively, in comparison with shams. (F) Spinophilin expression was only significantly affected in the hippocampus of 1200G and 2400G blast rats (**p < 0.01 and *p < 0.05 respectively).

279x190mm (96 x 96 DPI)

Figure legends

Figure 1. Experimental design and timeline

Detailed timeline of behavioral tests and end points of experimental procedures starting on study day 0 (blast exposure). YM, Y-maze test; PM, Plus-maze test; H, Histology, WB, western blots.

Figure 2. Behavioral outcomes after underbody blast

(A) Y-maze test results demonstrating significantly lower spontaneous alternation among maze arms by 2400G blast rats than shams or rats exposed to 1200G acceleration force ($^{*,\#}p < 0.05$ for day 0-pi and $^{\#}p < 0.05$, $^{**}p < 0.01$ for day 6 post-injury (pi) respectively). (B) Plus maze test demonstrating that rats exposed to either 1200 or 2400G blasts spent significantly less time in the open arms on days 8, 14 and 28-pi compared to shams ($^{*}p < 0.05$, $^{**}p < 0.01$ and $^{***}p < 0.001$). There were no significant differences in the time spent in the central area (C) and in the total distance travelled (D) among blast and sham rats ($p > 0.05$), except on day 1 post-injury when 2400G blast rats travelled significantly less distance than sham and 1200G blast animals ($^{*,\#}p < 0.05$).

Figure 3. Accumulation of inflammatory cells in the brain

(A) Representative microphotograph exhibiting F4/80 immuno-positive cells in the perivascular and periventricular regions of blast rats. (B) Quantification of the percent of F4/80 immuno-reactive area indicating a significant increase in microglia/macrophage accumulation in the brain of 1200G and 2400G blast rats compared to shams 24 hr

post-trauma (*p < 0.05 and **p < 0.01 respectively). (C) F4/80 immunopositive cells (Red) co-expressed the pro-inflammatory enzyme iNOS (Green); and DAPI [29] used as counterstain.

Figure 4. Vascular injury biomarkers

(A-C) Representative immunoblots illustrating the expression of Occludin, ZO-1, VWF and beta actin in the hippocampus, cortex and cerebellum 24 hr post-injury. Quantification of proteins bands indicating that (D) Occludin expression was significantly reduced in the hippocampus and cortex of 2400G blast rats compared to shams (**p < 0.01 and ***p < 0.001 respectively). (E) ZO-1 expression was significantly decreased in the cortex of 2400G blast rats compared to shams (**p < 0.01). In contrast, ZO-1 levels were significantly lower in the hippocampus of 2400G blast rats compared to 1200G blast rats ($^{\#}$p < 0.05). (F) Expression levels of VWF in the hippocampus were significantly higher in 2400G blast rats versus shams (*p < 0.05). In addition, VWF levels were also significantly higher in the cerebellum of 1200G and 2400G blast rats compared to shams (*p < 0.05).

Figure 5. Reciprocal changes in the levels of Hsp70 stress response protein and Bcl-2 anti-apoptotic protein in different brain regions following blast exposure

(A-C) Representative immunoblots describing the expression of Hsp70, Bcl-2 and beta actin in the hippocampus, cortex and cerebellum. Quantification of proteins bands signal intensity indicated that (D) Bcl-2 expression was significantly reduced in the hippocampus and cerebellum of rats exposed to 1200G blasts (***p < 0.001) as well as

2400G blasts (***p < 0.001), respectively, versus shams. (E) Conversely, the expression of Hsp70 was significantly increased in the hippocampus and cerebellum of 1200G blast rats (**p < 0.01) and 2400G blast rats (**p < 0.01 and *p < 0.05), respectively, compared to shams.

Figure 6. Cleaved caspase-3 immunoreactive cells present in rat hippocampus

(**A**) Representative fluorescent image showing the expression of cleaved caspase-3 (Green) in DG cells that overlap with NeuN positive cells (Red) and DAPI. (**B**) Quantification of cleaved-caspase-3 immunopositive cells 24hr post-insult indicated a significant increase in positive cells in the DG and Ca2/Ca3 area of both 1200G (**p < 0.01 and $^{\#}$p < 0.05) and 2400G (**p < 0.01 and $^{\#\#}$p < 0.01) blast rats, respectively, compared to shams.

Figure 7. TUNEL positive cells in rat hippocampus

(A) Representative fluorescent image demonstrating the presence of TUNEL positive cells (Green) and DAPI-stained nuclei [29] in the DG. (B) In comparison with shams, there was a significant increase in TUNEL positive cells 24hr post-insult in the DG and Ca2/Ca3 areas of 1200G (***p < 0.001 and $^{+}$p < 0.05) and 2400G blast animals (***p < 0.001 and $^{+++}$p < 0.001) respectively.

Figure 8. Brain region selective reduction in the expression of synaptic proteins following exposure to blasts

(A-C) Representative immunoblots illustrating the expression of PSD-95, synaptophysin, and spinophilin in the hippocampus, cortex, and cerebellum. (Spinophilin was not detectable in the cerebellum). Quantification of proteins bands indicate that (D) PSD-95 expression was significantly reduced in the hippocampus, cortex and cerebellum of both 1200G and 2400G blast animals (**$p < 0.01$). Conversely, PSD-95 expression was only significantly affected in the hippocampus of rats exposed to 2400G blast (**$p < 0.01$). (E) Synaptophysin expression was dramatically reduced in the hippocampus and cerebellum of 1200G (**$p < 0.01$ and $^{###}p < 0.001$) and 2400G blast rats (**$p < 0.01$ and $^{###}p < 0.001$), respectively, in comparison with shams. (F) Spinophilin expression was only significantly affected in the hippocampus of 1200G and 2400G blast rats (**$p < 0.01$ and *$p < 0.05$ respectively).

APPENDIX 10

UNDERBODY BLAST DEVICE: REDUCTION IN G FORCE AND LUNG INJURY BY COMPRESSIBLE CANS LOCATED BETWEEN A DOUBLE HULL.

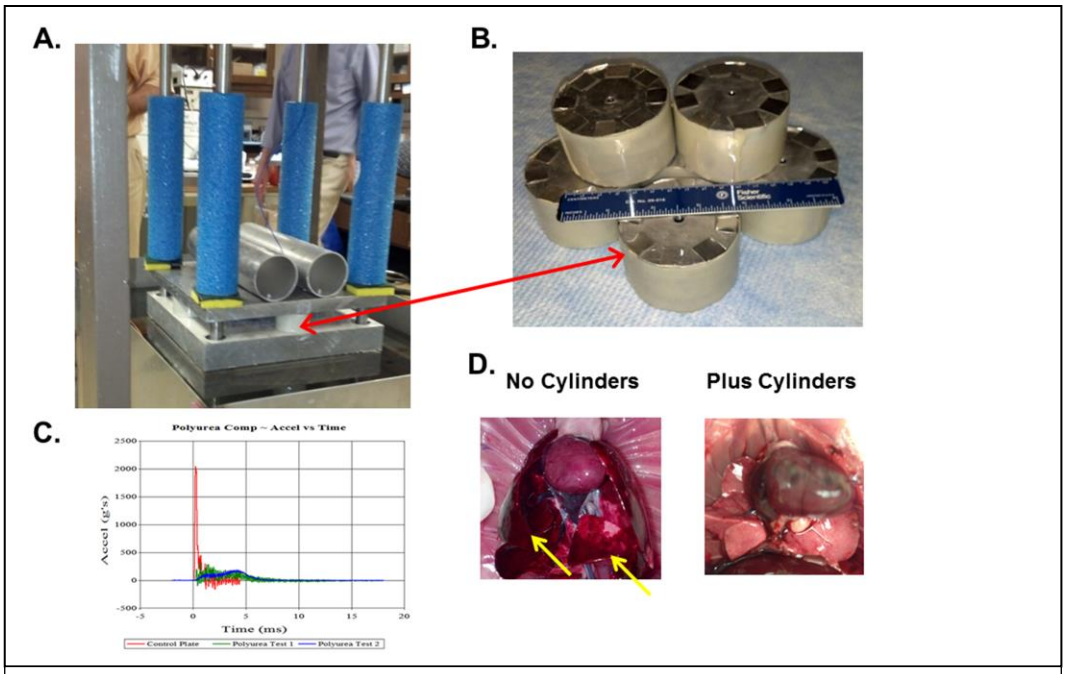

Underbody blast device: Reduction in G force and lung injury by compressible cans located between a double hull. A. Double hull with rat restraints. B. Polyurea-coated compressible cylinders. C. Reduction in G force on top hull from 2000 to 200G by inclusion of compressible cans. D. Massive lung hemorrhaging in rat that died immediately after 2800G blast.

APPENDIX 11

Pre-test and Post- tests pictures of mitigation by buckling.

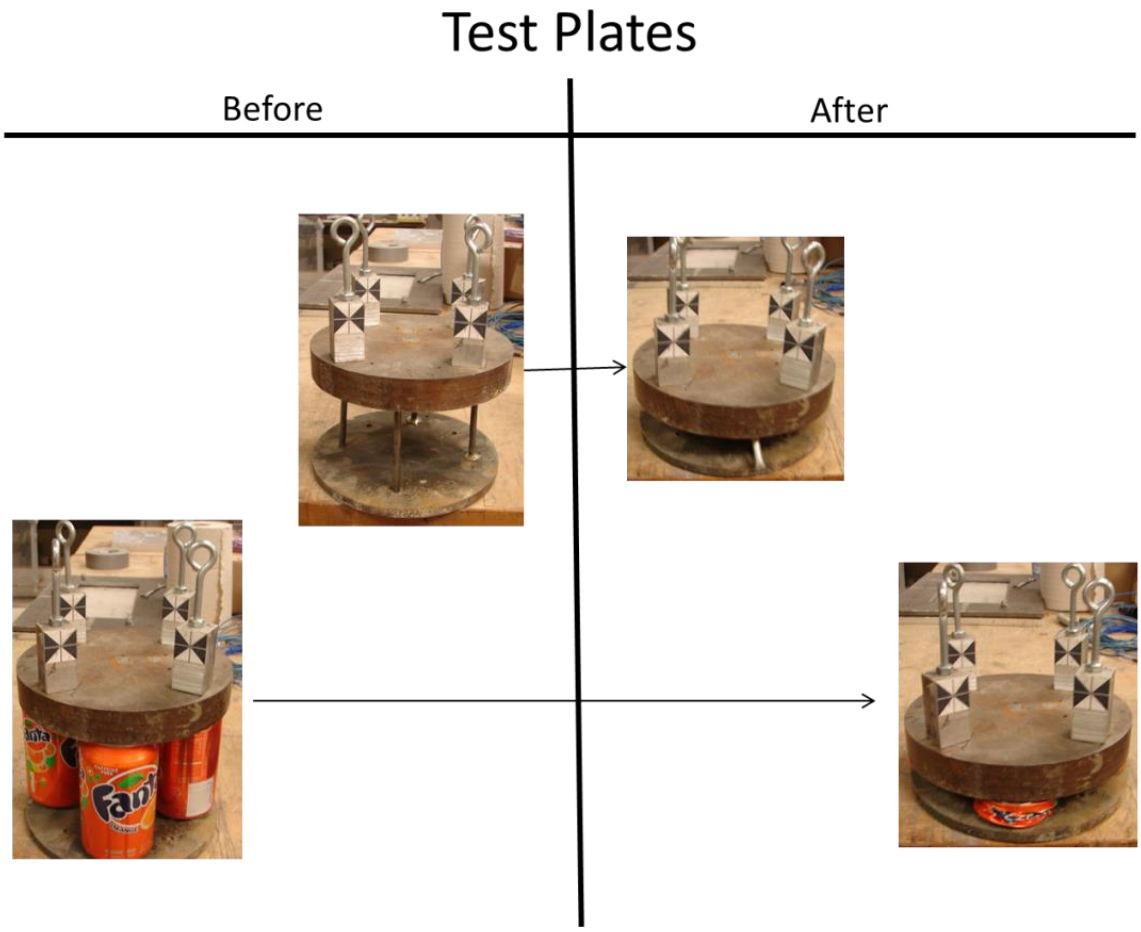

APPENDIX 12

Typical acceleration signal measured for blast with double hulls and no buckling devices

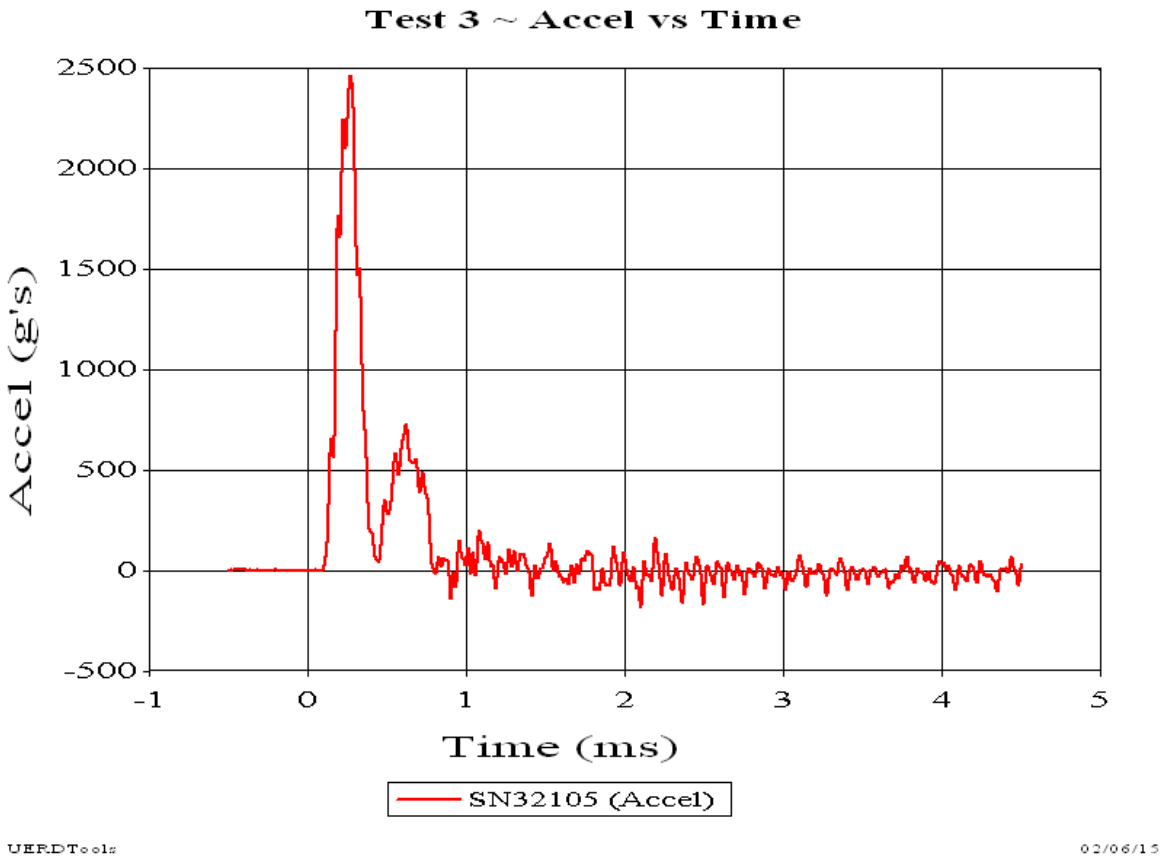

APPENDIX 13

Peak acceleration using different mitigation methods

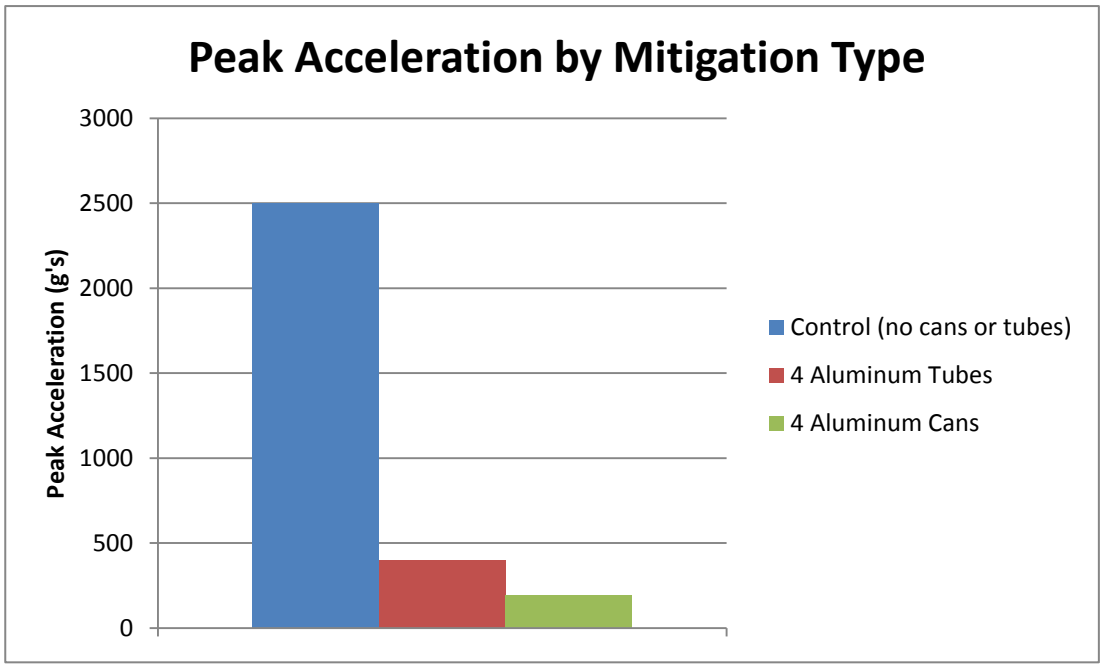

APPENDIX 14

Peak acceleration versus can polyurea coating mass ratio

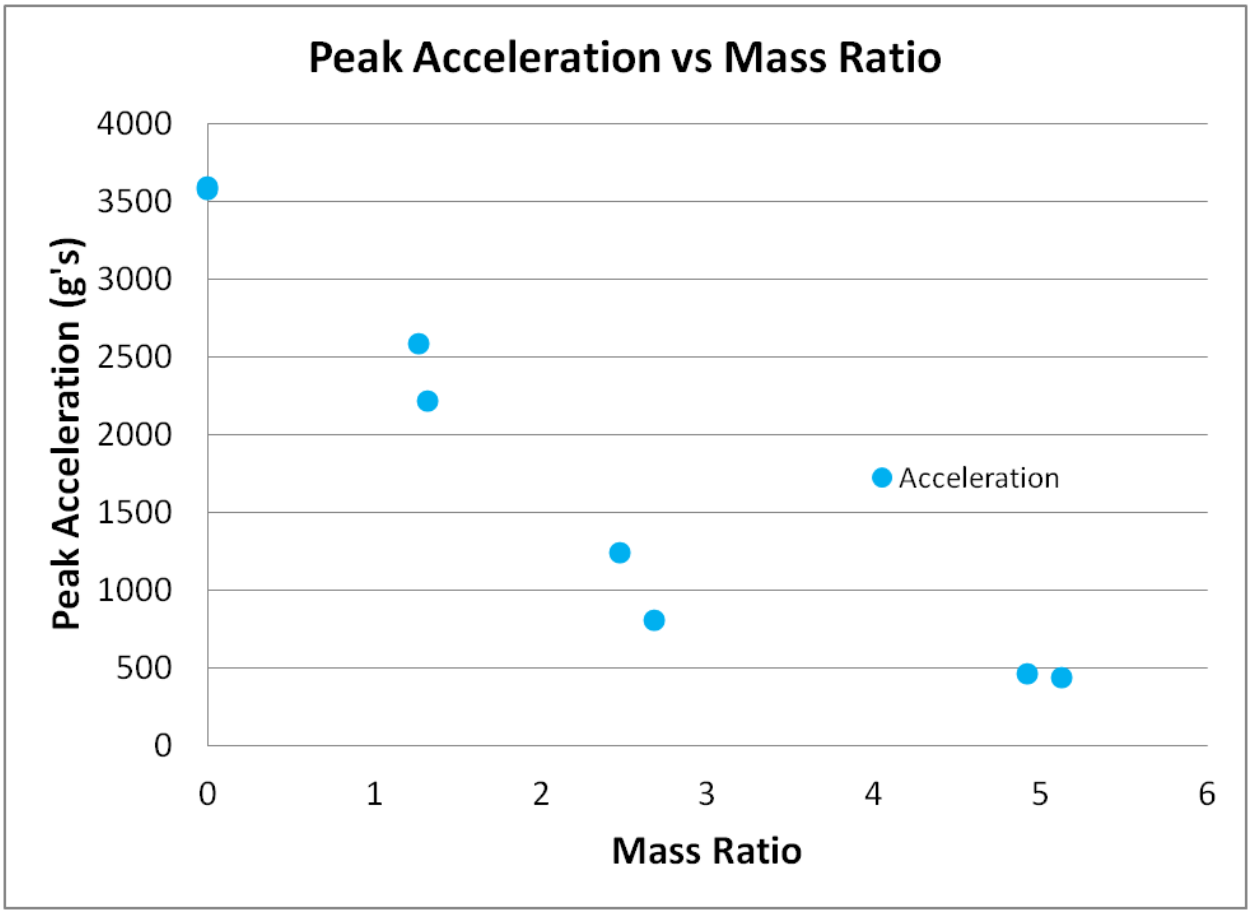

APPENDIX 15

Double hulls with rigid connections using a flat or V-shaped bottom hull

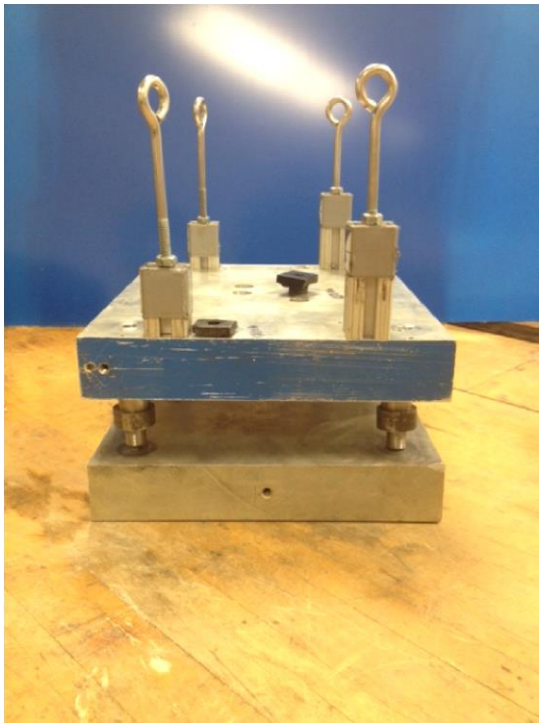

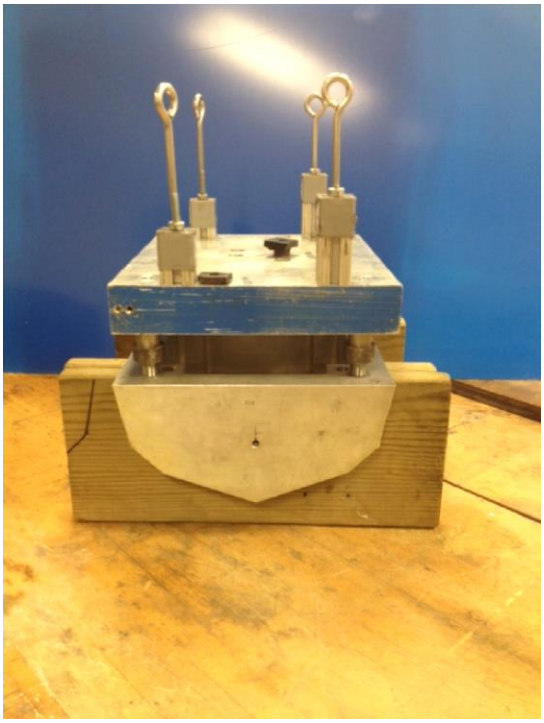

APPENDIX 16

Peak acceleration by hull design and charge location.

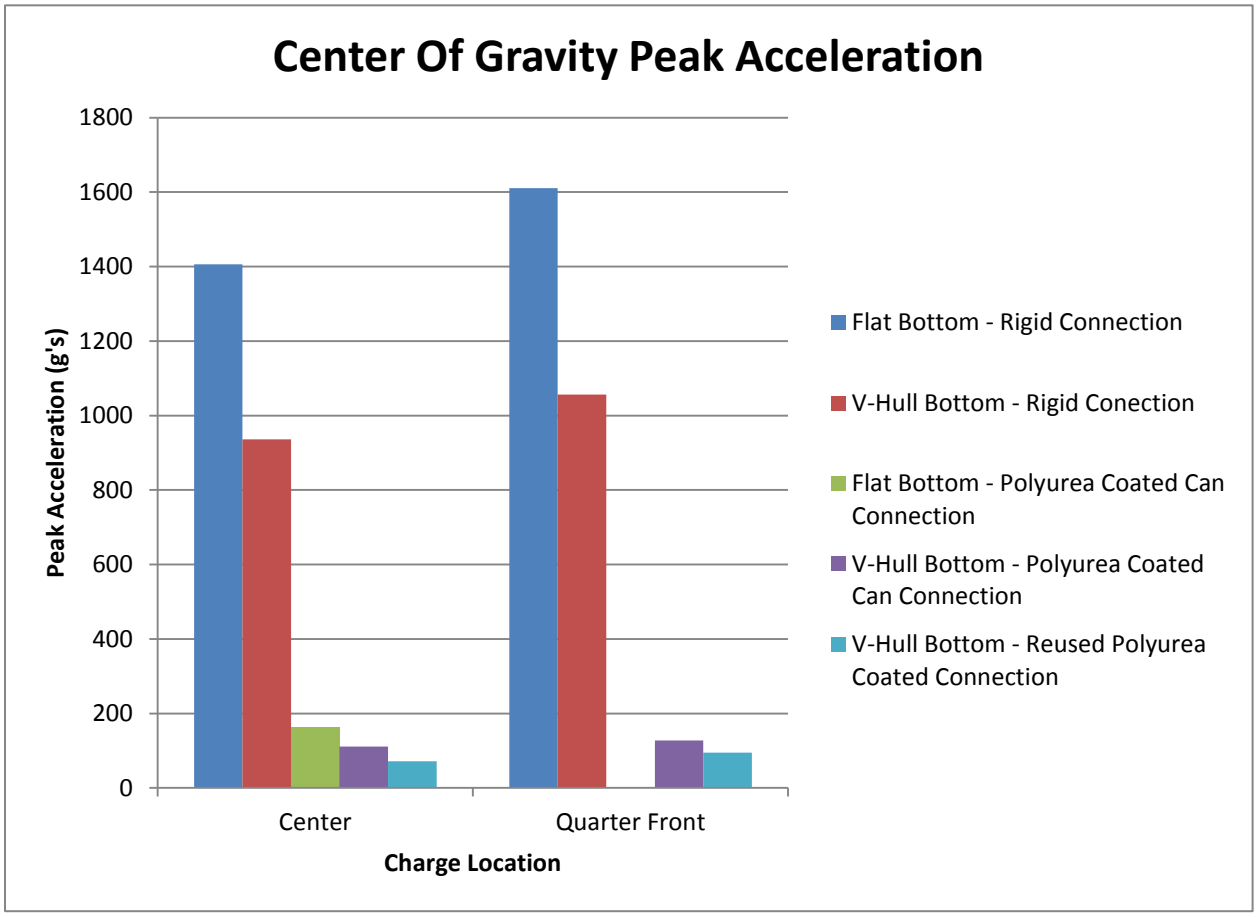

APPENDIX 17

Total Energy by hull design and charge location.

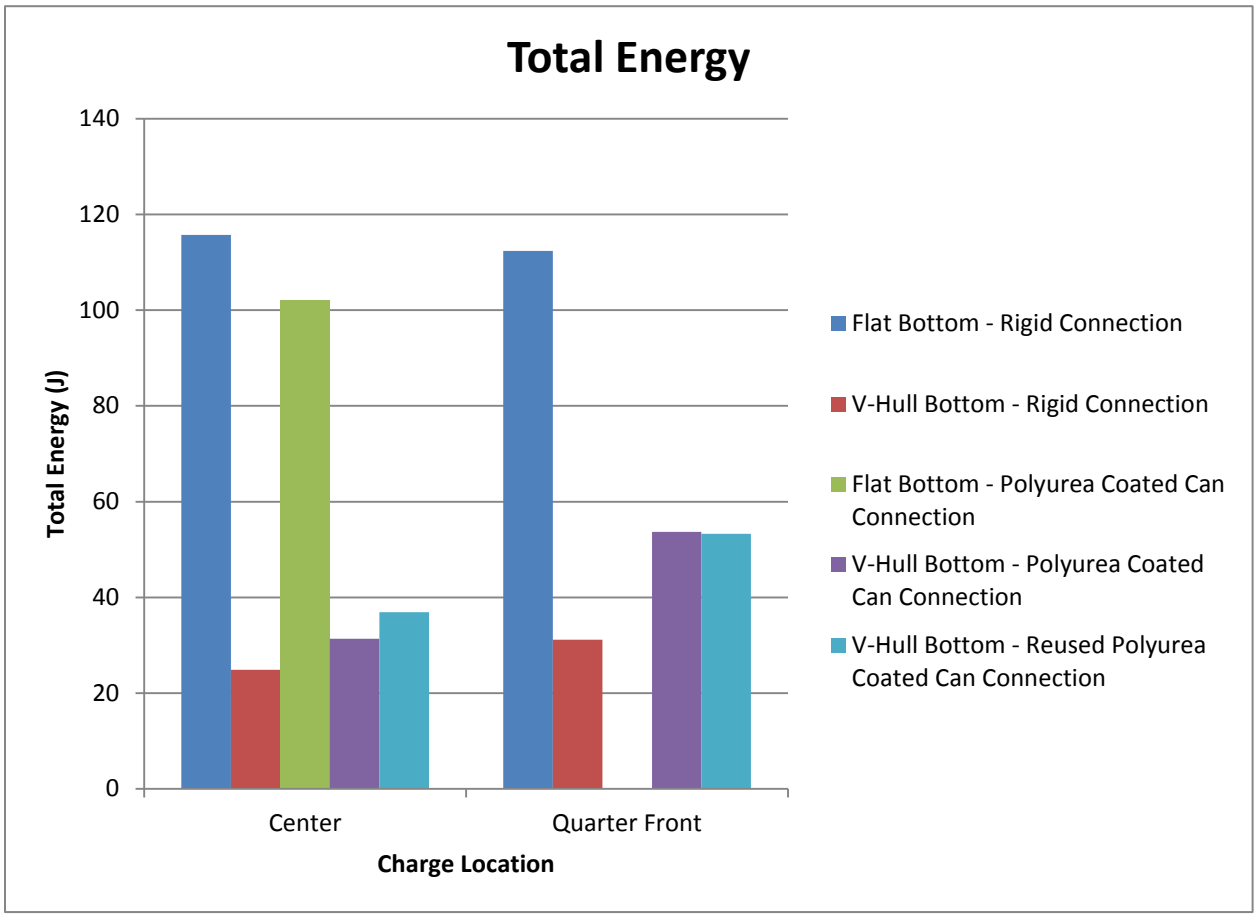

APPENDIX 18

Poster presented at 2015 MHSRS meeing

Underbody Blast-Induced Traumatic Brain Injury: Reduction of Acceleration Dependent Neurologic Impairment and Mortality by Advanced Vehicle Hull Designs

Flaubert Tchantchou[1], Yi-Chun Hsieh[1], Julie Proctor[1], William Fourney[2], Ulrich Leist[2], Joshua Vaughan[1], Adam Puche[1], Parisa Rangghran[1], and Gary Fiskum[1]

[1]University of Maryland Schools of [1]Medicine and [2]Engineering, Baltimore and College Park, MD

BACKGROUND

Among approximately 300,000 U.S military personnel victims of TBI in the wars in Iraq and Afghanistan over the last decade, more than 50% of casualties were due to explosive blast exposure, including those targeting military vehicles and their occupants. We developed a rat model of under-vehicle, blast induced TBI that at relatively low blast intensity (50 G acceleration force), displays histopathological evidence of diffuse axonal injury and astrocytes activation, but no evidence of neuronal cell loss and behavioral deficits (Proctor et al., 2014). Here, we assessed the impact of blast intensities that induced accelerative forces of 700 – 2800 G on neuronal cell death, inflammation, behavioral impairments and lethality. We also tested the hypothesis that advanced vehicle hull designs can dramatically mitigate the blast-induced force on occupants, resulting in improved survival and reduced TBI.

METHODS

1. Exposure of Rats to Underbody Blasts

Adult male Sprague-Dawley rats were isofluorane-anesthetized for 5 min, placed in restraint on the top of two platforms (hulls) separated by either a 3 mm thick rubber pad or by aluminum cylinders coated with polyurea. 0.75 – 1.5 g of pentaerytritol tetranitrate (DETA SHEET) explosive was located in the water tank under the platforms and detonated electrically after the rats were fully concsious. The platforms and the restrained rats were propelled vertically at G forces ranging from 100 to 4000 Gs, as measured with accelerometers attached to the top platform.

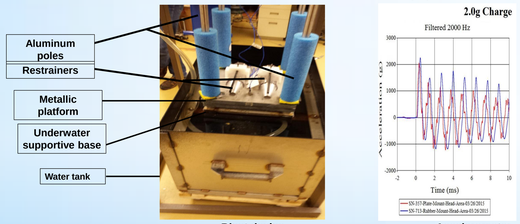

Figure 1. Underbody blast device with sample accelerometer recordings

2. Behavioral testing

- Immediately after blast experiment, animals were visually assessed for signs of physical damage and bleeding, returned to their cage and subjected to behavioral testing
- The elevated Plus maze (figure 3) was used to assess anxiety-like behavior was performed on study days 1, 8, 14 and 28.

3. Histology

- Blast-injured and sham animals were anesthetized and transcardially perfused or were decapitated 30 min, 24hrs, 7 days post-injury and brain tissues were collected and processed for immunostaining or western blot analysis.
- Brain sections were immunostained for the presence of apoptotic cells, inflammatory cells, and caspase 3 and TUNEL positive cells in the hippocamplus and cerebellum using standard nickel-DAB or fluorescence, while brain homogenates were electrophoresed by SDS-page followed by standard immunoblotting,.

4. Quantitation and statistical analysis

F4/80 immuno-reactivity and immunoblots signal intensity were quantified using NIH imageJ 1.48v software and the number of cleaved caspase-3 and Tunel positive cells using the Stereo Investigator 11 software (MBF, VT). Statistical analyses were performed by ANOVA using Graphpad Instat3.1 software (GraphPad Sft Inc., CA). *p < 0.05, **p < 0.01; and ***p < 0.001.

Figure 3. Elevated Plus Maze for anxiety measurements

RESULTS

1. Acceleration caused by exposure to underbody blasts results in long-term anxiety: Reduction in TBI and mortality by advanced vehicle hull designs

A. Persistent anxiety after blast TBI

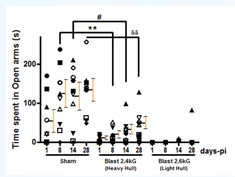

B. Max G-force, JERK and Mortality

	Heavy Hull[1]	Light Hull[2]	Light Hull Uncoated[3]	Light Hull 1 Coat[4]	Light Hull 2.5 Coats[5]
Max G Force	2436 ± 59[1]	2643 ± 118	2146 ± 160	1429 ± 55	563 ± 32
Time to Max	0.2 - 0.3 msec	0.2 msec	3.0 msec	3.0 msec	3.0 msec
JERK	1.2 - 1.4[1]	1.6 – 2.0	1.0 – 1.3	0.4 – 0.6	<0.1
Mortality	0/10	4/6	2/8	0/6	0/6

C. Polyurea coated cylinders reduce TBI

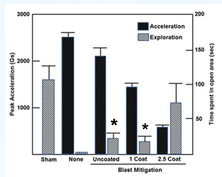

Figure 3. A. The time spent in the open in the plus maze was dramatically reduced at 1 day to as long as 28 days after 2400G underbody blast. The few animals that survived the 2600 G blast when secured to a light hull were essentially immobile. B. A 50% reduction in the weight of the top hull results in a large increase in JERK (dG/dt), resulting in 66% mortality due to pulmonary hemorrhaging. Placement of polyurea-coated cylinders between the two hulls dramatically reduces JERK and eliminates mortality. C. The amount of polyurea coated on the cylinders is related to reduction in G force and reduction in anxiety.

2. Underbody blast causes significant infiltration of activated microglia and macro-phages in the brain

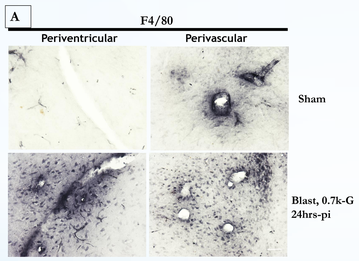

Figure 4. F4/80 immunostaining indicating that underbody blast causes a significant increase in activated microglia and microphages throughout the brain, mainly around perivascular ad periventricular regions.
(B) F4/80 quantitation (n = 6) indicating significant increase in microglia/microphages at 0.7 kG and 2.8kG in blast animals at 30 min and one day after blast.

3. Underbody blast causes cerebrovascular damage

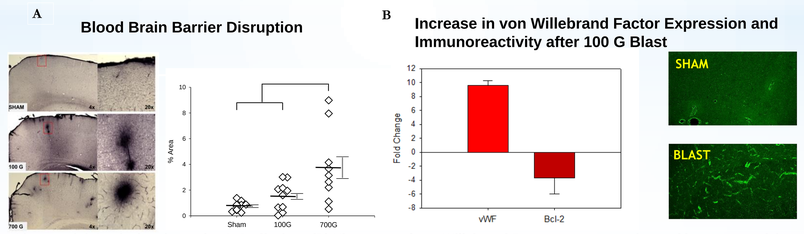

Figure 5. (A) Cortical perivascular IgG effusions (B) Hippocampal von Willebrand Factor gene expression and immunoreactivity (n = 4/group).

4. Underbody blast induced TBI caused significant increase in caspase-3 activation in the hippocampus

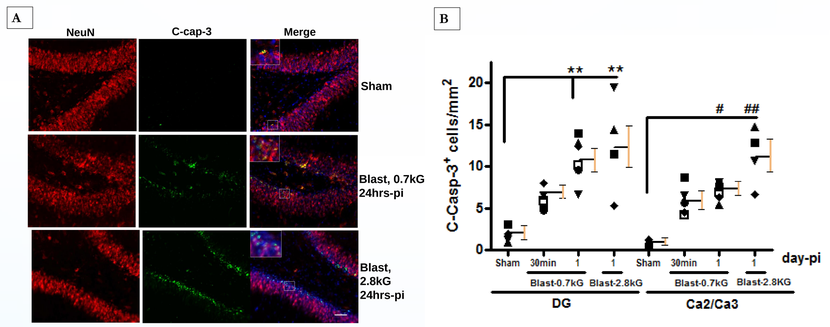

Figure 6. (A) Immunostaining for cleaved caspase 3 demonstrating a blast-induced increase in the hippocampus. Most cleaved caspase-3[+] cells overlapped Neun positive cells in the subgranular zone. (B) Quantitation of cleaved caspase 3 positive cells (n=6) indicating significant increase in apoptosis in the hippocampus dendate gyrus and Ca2/Ca3 areas.

5. Underbody blast induced brain injury increased Tunel positive cells in the hippocampus

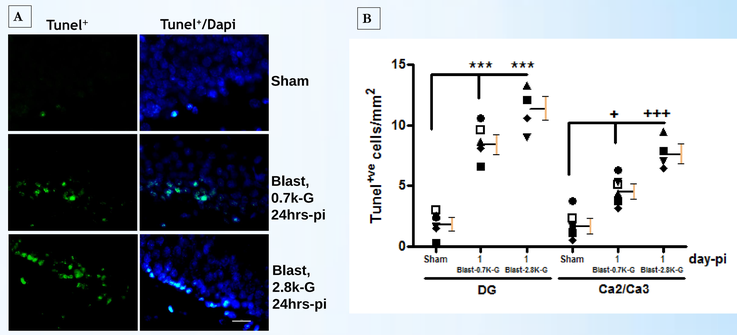

Figure 7. (A) Tunel staining demonstrating an increase of apoptotic cells in the dendate gyrus and Ca2 /Ca3 areas of the hippocampus of blast animals. (B) Quantitation of Tunel positive cells (n=4-6) indicated significant increases in apoptotic cells in the hippocampus dendate gyrus and Ca2/Ca3 areas of blast animals.

6. Blast induced brain injury decreased the expression of markers of synaptic transmission and anti-apoptotic protein Bcl-2

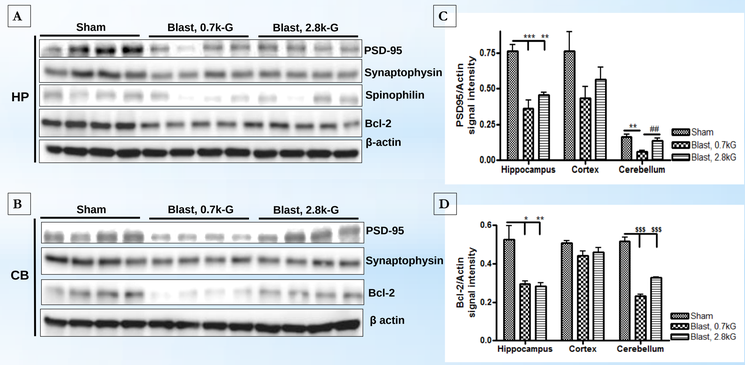

Figure 8. (A-B) Immunoblots showing the expression of synaptic transmission markers PSD-95, synaptophysin, and spinophilin and the expression of the anti-apoptotic protein Bcl-2 in the hippocampus and cerebellum of sham and blast rats. (C-D) Graphs indicating a significant decrease of Bcl-2 in the hippocampus and cerebellum of rats subjected to blast both at 0.7kG and 2.8kG, compared to sham animals. The post-synaptic marker PSD-95 is also significantly decreased at those two blast intensity in the hippocampus, but only at 0.7kG in the cerebellum. No significant change in the expression of those proteins was observed in cortical tissues.

CONCLUSIONS

- ***Underbody blasts cause mild but chronic anxiety in rats***
- ***Blast induced accelerations of 700 – 2500Gs result in brain inflammation, blood brain barrier disruption, induction of von Willebrand factor expression, an increase in caspase 3 activation, a small increase in neuronal cell death, a reduction in Bcl2, and a reduction in PSD95 levels, all within one day following the blast.***
- ***A novel double hull design incorporating shock-absorbing cylinders can reduce maximum acceleration by 80% and JERK by more than 90%, resulting in mitigation of both blast-induced TBI and mortality.***

REFERENCES

- Proctor, J.L., Fourney, W.L., Leiste, U.H., and Fiskum, G. (2014) Rat model of brain injury caused by under-vehicle blast-induced hyperacceleration. J. Trauma Acute Care Surgery 77: Suppl 2:S83-7
- Elder G.A. et al.(2015). Vascular and inflammatory factors in the pathophysiology of blast-induced brain injury. Front. Neurol. 6:48, 1-22

ACKNOWLEDGEMENTS

This study was supported by US Army grant W81XWH-13-1-0016 and US Air Force grant FA8650-11-2-6D04

APPENDIX 19

Poster presented at the 2015 National Capitol Brain injury symposium

A Rat Model of Underbody Blast-Induced Traumatic Brain Injury with Evidence of Neurobehavioral Deficits Associated With Neuronal Death and Inflammation

Flaubert Tchantchou[1], Joshua Vaughan[1], Parisa Rangghran[1], William Fourney[2], and Gary Fiskum[1]

[1]Anesthesiology Department and Shock, Trauma, Anesthesiology Research Center , University of Maryland School of Medicine, Baltimore, MD 21201

[2] Mechanical Engineering, University of Maryland College Park, College Park, MD 20740

BACKGROUND

Among approximately 300,000 U.S military personnel victims of TBI in the wars in Iraq and Afghanistan over the last decade, more than 50% of casualties were due to explosive blast exposure, including those targeting military vehicles and their occupants. We developed a rat model of under-vehicle, blast induced TBI that at relatively low blast intensity (50 G acceleration force), displays histopathological evidence of diffuse axonal injury and astrocytes activation, but no evidence of neuronal cell loss and behavioral deficits (Proctor et al., 2014). Here, we assess the impact of increased blast intensity on neuronal cell death, inflammation, behavioral impairments and lethality.

METHODS

1. Animal and Underbody blast induction

Sprague-Dawley rats (male, 300-350g), were isofluorane-anesthetized and restrained under anesthesia on a platform that was accelerated vertically at 700 Gs, 2800 Gs or 4000Gs in response to the detonation of a small explosive positioned at precise location under-platform standoff distances.

The device used for underbody blast induction consists of an aluminum water tank, an underwater supportive base carrying a metallic platform on which two animal restrainers and aluminum poles are attached to guide its movement during explosion-induced vertical acceleration (figure. 1).

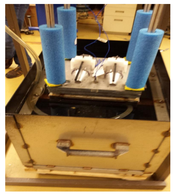

Figure. 1: Blast device

2. Behavioral testing

Immediately after blast experiment, animals were visually assessed for signs of physical damage and bleeding, returned to their cage and subjected to behavioral testing

- Continuous spontaneous alternation Y maze test

Y maze (figure 2) was used to test hipppocampus dependent working memory by measuring the % continuous spontaneous alternation of arms visits during 5 min exploration of the maze. Y maze tests were performed on study days 0, 6, 13, and 27.

- Elevated Plus maze

The Plus maze (figure 3) was used to assess anxiety-like behavior by determining the time rats spent in the open arm of the maze during 10 min exploration of the maze. Elevated plus maze test was performed on study days 1, 8, 14 and 28.

3. Histology

- Brain tissue collection and processing

Blast-injured and sham animals were anesthetized 30 min, 24hrs, 7 days post-injury, transcardially perfused glucose enriched and oxygenated PBS, fixed with 4% PFA and processed for sectioning. Brain sections of 40 µM thickness were cut and preserved in a cryoprotectant at -20ºC.

- Immunostaining

Brain sections were immunostained for the presence of apoptotic cells, inflammatory cells and purkinje cells in the cerebellum using standard nickel-DAB or fluorescence staining procedures

4. Quantitation and statistical analysis

F4/80 immunoreactivity was quantified using NIH imageJ 1.48v software and the number of cleaved caspase-3 positive cells using the Stereo Investigator 11 software (MBF, VT). Statistical analyses were performed by ANOVA followed with Turkey-Kramer Multiple Comparisons post test analysis using Graphpad Instat3.1 software (GraphPad Sft Inc., CA).

RESULTS

1. Underbody blast induced TBI significantly impaired hippocampus dependent working memory and increased anxiety-like behavior

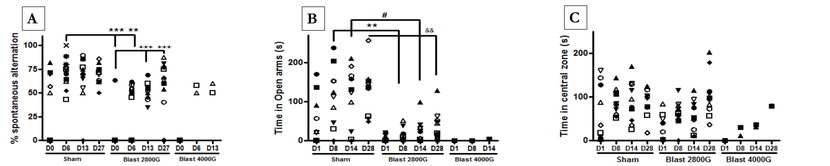

Figure 4. Illustration of the effect of blast induced injury on hippocampus dependent working memory and anxiety-like behavior
(**A**) Y maze test showed that underbody blast significantly impaired hippocampal performance on days 0 and 6 post-blast (n = 10). (**B**) Underbody blast caused a chronic increase of anxiety-like behavior to rats up to day 28 post-blast (n = 10). **(C)** However, there was no significant different in the amount of time spent by both blast and sham rats in the central zone of the maze. About 70% of rats subjected of blast explosion at 4000G died from blast-injuries within 1-4 hrs after blast resulting in fewer survivor for statistical analysis (**A,B,C**)

Figure 2. Y maze

Figure 3. Plus maze

2. Underbody blast caused significant infiltration of activated microglia and macrophages in the brain

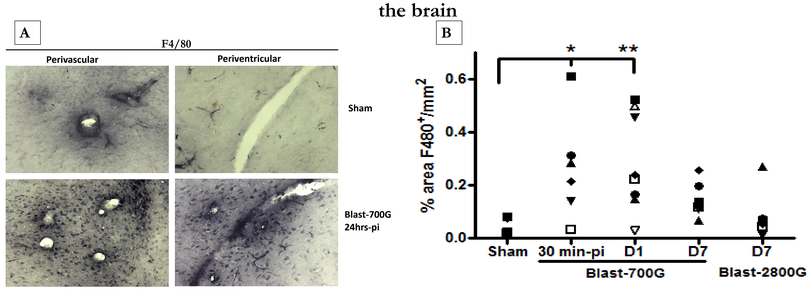

Figure 5. Representative micrographs and quantitation graph illustrating the effect of underbody blast induced brain injury on microglia and macrophages infiltration
(A) F4/80 immunostaining showed that blast induced injury caused a significant increase in activated microglia and macrophages throughout the brain, mainly around perivascular ad periventricular regions.
(**B**) F4/80 quantitation (n = 6) indicated significant increased microglia and macrophages infiltration at 700G in blast animals starting as early as 30 min after blast and reduced relatively 7 days after trauma.

3. Underbody blast induced TBI caused significant increase in caspase-3 activation in the hippocampus

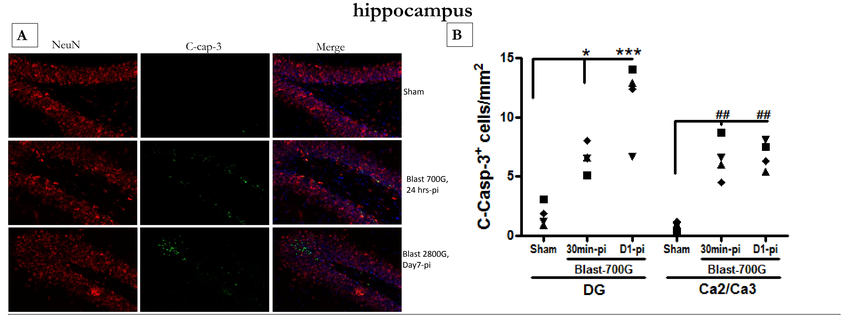

Figure 6. Representative micrographs and quantitation graph illustrating the effect of blast explosion on caspase-3 activation in the hippocampus
(A) Immunostaining for cleaved caspase 3 showed increase of caspase 3 activation in the hippocampus of blast animals at different study time points. Most cleaved caspase-3+ cells overlapped Neun positive cells in the subgranular zone (B) Quantitation of cleaved caspase 3 positive cells (n=4) indicated significant increases in apoptotic cells in the hippocampus dendate gyrus and Ca2/Ca3 areas.

4. Apoptotic hippocampus cell death was potentiated by increased presence of Tunel positive cells

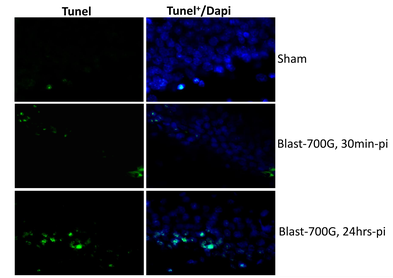

Figure 7. Representative micrographs illustrating the effect of underbody blast induced brain injury on apoptotic cell death
Tunel staining demonstrated an increase of apoptotic cells in the dendate gyrus, Ca2 /Ca3 areas of the hippocampus of blast animals.

5. Blast induced brain injury caused substantial reduction of purkinje cells in the cerebellum

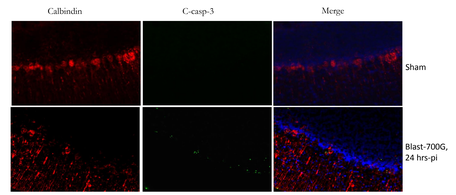

Figure 8. Representative micrographs showing the effect of underbody blast explosion on purkinje cells density
Blast injury substantially reduced the number of purkinje cells (calbindin immuno-positive) in the cerebellum

CONCLUSIONS

Our rat model of underbody blast showed a blast intensity dependent deficit in hippocampus dependent working memory and increased anxiety like behavior, and 67% blast-induced mortality at maximum blast intensity of 4000G force.

Behavioral impairments were associated with significant neuronal loss both in the hippocampus and cerebellum and an acute inflammation.

These findings suggest that our model may be an important tool to further close the gap in understanding the pathophysiology of blast induced TBI that closely reflects the real under-vehicle blast scenarios.

REFERENCE

Proctor, J.L., Fourney, W.L., Leiste, U.H., and Fiskum, G. (2014) Rat model of brain injury caused by under-vehicle blast-induced hyperacceleration. J. Trauma Acute Care Surgery 77: Suppl 2:S83-7

ACKNOWLEDGEMENTS

This study is supported by US Army grant W81XWH-13-1-0016

APPENDIX 20

Acceleration mitigation utilizing shape memory polymeric-coated metallic thin-walled cylinders

UNIVERSITY OF MARYLAND

CONFIDENTIAL

University of Maryland Intellectual Property Disclosure Form
(Patent, Copyright, Trademark and/or Tangible Research Property)

ATTENTION: If an invention is to be presented or published within a week, please contact the Office of Technology Commercialization (OTC) immediately (301-405-3947)

Guidelines and instructions for this form may be found at http://www.otc.umd.edu/documents/Guidelines and Instructions.doc
(Please review these instructions before signing the form)

Intellectual Property Disclosure Number: (to be assigned by OTC)

1. **Title of Invention/Work** Acceleration mitigation utilizing shape memory polymeric-coated metallic thin-walled cylinders

2. **Inventor/Creator Data** (*List inventors in order that they should appear on official documents; primary contact will be responsible for all communications regarding this invention.)*

Primary Contact Inventor/Creator Name: William Fourney

Inventor/Creator #1:
Dr. Name: William Fourney Percentage of Inventor Royalty (UM only) 50 %
Title: Professor Department: AE/ME U ID #: 104211647 Citizenship: USA
Full Business Address: 1131 U Martin Hall, University of Maryland, College Park, MD 20742
Full Home Address: 8710 Teresa Lane, Laurel, MD 20723
Direct Business Phone: 301 405 1129 Dept. Business Phone: Fax: Home Phone: 301 725 4108
Email: four@umd.edu UM Affiliation: ☒Faculty ☐Staff ☐Grad Student ☐Undergrad Student ☐Other
UM Appointment(s) at time of invention:
Institution Name: UMC 100% College Name: Engineering 100% Department Name: AE/ME 100%
Institution Name: % College Name: % Department Name: %

Inventor Signature: W Fourney **Date Signed:** 3/19/14

Inventor/Creator #2:
Dr. Name: Jarrod Bonsmann Percentage of Inventor Royalty (UM only) 50 %
Title: Lecturer Department: ME U ID #: 112043858 Citizenship: US
Full Business Address: 3181 Glenn L. Martin Hall, College Park, MD 20742
Full Home Address: 1115 Old Cedar Road, McLean, VA 22102
Direct Business Phone: 301-405-5339 Dept. Business Phone: Fax: Home Phone: 407-923-3554
Email: bonsmann@umd.edu UM Affiliation: ☒Faculty ☐Staff ☐Grad Student ☐Undergrad Student ☐Other
UM Appointment(s) at time of invention:
Institution Name: UMC 100% College Name: % Department Name: %
Institution Name: % College Name: % Department Name: %

Inventor Signature: [signature] **Date Signed:** 03-19-14

Inventor/Creator #3:
Dr. Mr. Ms. Mrs. Name: Percentage of Inventor Royalty (UM only) %
Title: Department: U ID #: Citizenship:
Full Business Address:
Full Home Address:
Direct Business Phone: Dept. Business Phone: Fax: Home Phone:
Email: UM Affiliation: ☐Faculty ☐Staff ☐Grad Student ☐Undergrad Student ☐Other
UM Appointment(s) at time of invention:

Institution Name: % College Name: % Department Name: %
Institution Name: % College Name: % Department Name: %

Inventor Signature: _____ Date Signed: _____

(Please attach extra page(s) with information on additional inventors)

3. **Date of Invention** *(Provide the date the invention was first conceived. This date should be documented in your lab records. Give reference numbers and physical location of the lab records, but do not enclose them.)* 08/08/2013

4. **Brief Description of Invention** *(attach description if necessary)* abstract attached

5. **Detailed Description of Invention** *(Please attach a complete enabling description of the technology describing the specific novelty of the invention. The description may be by reference to a separate document such as a copy of a report, preprint, grant application, manuscript and the like.)*

6. **Sponsorship**
Funding Source: ☒Federal ☐State ☐Corporate ☐UM ☐MIPS ☐Other: ☐ None

Contracting Agency/Commercial Entity	Grant/Contract Number	Funding Amt.	UM FRS#	MIPS #
UMB(USArmy Contract)	SR00002574	400K	4305830	

7. **Publication**
(a) Submitted to a Journal: ☐Yes ☐No Date: Journal Name:
(b) Published: ☐Yes ☐No Date: Journal Name:
(c) Oral Disclosure: ☐Yes ☐No Date: Location: Handouts? ☐Yes ☐No
(d) Poster Presentation: ☐Yes ☐No Date: Published Abstract: ☐Yes ☐No
(e) Thesis or Dissertation: ☒Yes ☐No Date:11/2014
(f) Other Disclosure: ☐Yes ☐No Date: Describe:

8. **Technology Significance** *(choose one)*
☐ Modification to existing technology ☐Substantial advancement in the art ☒Major breakthrough

9. **Technology Stage** *(choose one)*
☐Concept ☐Design ☒Prototype ☐Modification ☐Production Model
☐Used in current work ☐Ready to license final product

10. **Future Research Plans** What additional research is needed to complete development and testing of the invention?
(a) Is this research presently being undertaken? ☒Yes ☐No If yes, identify sponsor:
(b) Actively pursued by faculty/staff? ☒Yes ☐No If yes, identify faculty/staff:
(c) Actively pursued by corporate partner? ☐Yes ☐No If yes, identify corporate partner:
(d) Should corporate sponsorship be pursued, other than the corporate partner? ☐Yes ☐No
(e) Do you wish to form a "start-up" company based on this technology? ☐Yes ☒No

11. **Commercial Potential**
(a) List all products, processes and/or services you envision resulting from this invention and whether they can be developed in the near term (less than two years) or long term. -Vehicle protection systems, near term
(b) Software inventions: If this is a modification or improvement to an existing work or incorporates elements that are not original to the creator(s), please identify that work and its creator(s). n/a

12. **Competition and Potential Users and Manufacturers**
(a) Describe alternate technology or products, processes and/or services currently on the market of which you are aware that accomplish the purpose of this invention. Collapsible Bumpers
(b) Please identify any related technologies or devices which are used for other purposes.
(c) List any companies you believe may be interested in this technology. Provide contact(s), address(es) and phone number(s) for each, if available.

13. **Marketing**
Once the OTC staff accepts this disclosure, marketing of this technology will begin. Please acknowledge whether or not you believe the technology is ready for marketing to commence:
☒Begin marketing ☐Delay marketing until further notice (provide reason)
☐Company interested (identify company) ☐ Specifically contact persons and entities identified in 12(c)

Signatures All UM inventors must sign and date this Intellectual Property Disclosure Form which certifies that all information provided herein is complete to the best of the inventor's knowledge. Signatures further certify that inventors have reviewed and understand the University of Maryland Policy on Intellectual Property [IV-3.20 (A)]; Approved by the President on March 13, 2003, approved by the Chancellor on July 18, 2005 and the University of Maryland Intellectual Property Disclosure form General Guidelines and Information.

Completed Intellectual Property Disclosure Forms may be sent by email or mail to the Office of Technology Commercialization:
Postal Address: Office of Technology Commercialization, 2130 Mitchell Bldg., College Park, MD 20742
Email: otc@umd.edu

Incomplete Intellectual Property Disclosure forms cannot be processed and will delay the technology transfer process.

OTC Review and Acceptance of the Invention Disclosure (for OTC use only):

Printed Name: _____ Title:_____

Signature: _____ Date:_____

Guidelines and instructions for this form may be found at http://www.otc.umd.edu/inventors2/disclosures.html or contact the Office at Technology Commercialization at 301-405-3947

Acceleration mitigation utilizing shape memory polymeric-coated metallic thin-walled cylinders

Abstract

This paper investigates various means for mitigating acceleration experienced by passengers in vehicles subjected to blast loading. In order to complete this study, small-scale testing of simulated vehicles was used. The explosives designated for this research are exclusively buried in saturated sand, which will act as the loading media for the simulated vehicles. In addition to explosive testing, various tests were performed dynamically using a high-pressure gas gun. Test plates used in this study vary in both size and geometry. When necessary, simple plate geometries are employed to investigate various mitigation parameters. Ultimately, much of the testing was conducted on simplified scaled versions of vehicles likely to be subjected to attack. This paper focuses mainly on mitigation through crushing of thin-walled cylinders, but also investigates the advantages of applying polymeric coatings to dynamically loaded structures. Piezoelectric accelerometers are used in conjunction with high speed videography to collect test data. The ultimate goal of this research is to help create a vehicle that will increase the probability that the passengers will survive a blast event with minimal long-term damage to the brain.

Acceleration mitigation utilizing shape memory polymeric-coated metallic thin-walled cylinders

Introduction

Over the past decade, the increase in fatalities due to use of buried explosives has created a demand for expanded knowledge in the field of target response to blast loading. When a vehicle experiences a blast load from a buried explosive, it is speculated that the damage mechanisms for a passenger in the vehicle result from rapid accelerations [1] and large changes in momentum [2]. Blast loading results in traumatic brain injury (TBI) and violent injuries such as broken limbs due to rapid accelerations and large changes in momentum respectively. In recent years a growing number of people involved in buried explosive attacks have been diagnosed with TBI in what is speculated to have resulted from the rapid acceleration of the targeted vehicle. This research aims to help design vehicles that will minimize the amount of damage to a passenger traveling in a vehicle that undergoes explosive loading.

In order to accomplish the goals of the research, the primary experimental testing technique employed is small-scale explosive testing. This testing method is used to investigate means of acceleration mitigation including crushing of thin-walled cylinders. A number of geometric properties of thin-walled cylinders, such as height, wall thickness and outer diameter are all studied. In addition to geometric properties, the number of cylinders and to a minor degree, the cylinder material is also studied. The majority of the aforementioned tests were conducted on plates fabricated to be simplified scaled down versions of vehicles likely to undergo blast scenarios.

On top of using explosive testing to study mitigation properties of crushing of thin-walled cylinders, the mitigation properties of polymeric coatings of structures are also examined. Steel and aluminum bars coated with polyurea were tested dynamically using a pressurized gas gun to determine the effect of increasing the mass and thickness of polymeric coatings on acceleration. Thin-walled cylinders were also coated in polyurea and crushed by explosively loaded plates to determine the benefits of adding polyurea to the previously tested mitigation technique.

At the conclusion of the research it was determined that there are great benefits to using thin-walled cylinders to mitigate the acceleration of a passenger travelling in an explosively loaded vehicle. In addition to this, polymeric coatings were determined to be of use in the crushing of thin-walled cylinders and coated beams but the effects depend greatly on the amount of polyurea applied to the metallic structure.

Background

In answer to the demand for knowledge pertaining to vehicle response under blast loading, the Dynamic Effects Lab at the University of Maryland has spent much time and many resources investigating this event. Research has been conducted to better understand the mechanisms of the vehicle loading [3] and to determine various methods of reducing impulse and acceleration on these structures [4, 5]. The main mechanism of the vehicle loading for a buried charge is the impact on the vehicle bottom by the soil that is thrown up by the detonated charge. This soil has been

shown to be traveling in excess of Mach one, and when it is brought to rest on the bottom of the vehicle very large pressures develop [6].

As a result of the increased understanding of vehicle response to blast loading, the number of injuries and deaths as a consequence of buried explosive attacks has steeply declined as seen in Figure 1[7]. The most important development in vehicle design has been the utilization of Mine-Resistant Ambush-Protected vehicles which have angled bottoms that deflect the ejected soil in a sidewise direction.

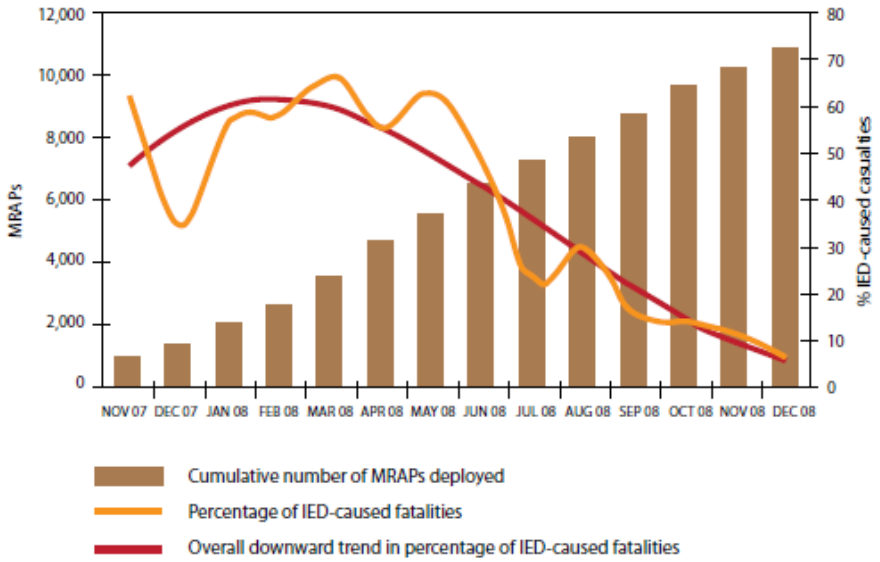

Figure 1: MRAPs deployed in the field versus IED casualties

By shaping the bottom of the blast loaded vehicles, violent injuries and deaths due to the change in the impulse have steeply declined. However, since the passenger of the vehicle is surviving beyond the initial blast, the incidences of TBI have risen. For this reason, further knowledge is needed in the area of acceleration mitigation on blast loaded vehicles.

The studies mentioned above place a good deal of emphasis on blast mitigation due to vehicle shaping. One of the primary focuses in this paper is to study the acceleration mitigation effects of localized buckling (crushing) of thin-walled cylinders. Thin-walled cylinders have long been studied in the field of energy absorption. There exists a plethora of research detailing the benefits of adding tubes to structures to absorb impact energy. For lower speed impacts both Alghamdi and Yuen et al. give an overview of a multitude of collapsible structures for use as energy absorbers [8, 9]. A number of studies have been performed characterizing the benefits of crushing tubes laterally for impact protection [10, 11]. Quite a few studies have been conducted to classify the energy absorption of composite tubes [12, 13, 14]. Additionally there have even been some studies, both numerical and experimental, where tubes or thin-walled structures of multiple geometries made of various materials (both metallic and composite) have been studied for use as sacrificial claddings for structures that undergo blast loading [15, 16, 17]. All of this research points to the fact that thin-walled structures, in a variety of geometrical patterns made

of all kinds of materials, have numerous benefits to offer when it comes to protecting structures from blast loads. There is a dearth of information, however, involving the benefits of using thin-walled cylinders as a technique for mitigating acceleration.

Much effort has been spent [18, 19] in researching the mechanical behavior of polymeric materials used for coatings in blast applications, especially the material polyurea. It has been found that under very high strain rates the polymer loses its "rubbery" mechanical behavior and begins acting more like leather. This characteristic allows the polymer to increase toughness under high strain rates, making it more effective at absorbing blast loads. In addition to characterizing the high strain rate mechanical properties of polyurea, the polymeric coating has been applied to panels that undergo blast loading in order to determine what benefits it has as a protective layer to prevent deformation and damage to structures. Major benefits in protection of structures due to polymeric or elastomeric coatings have been found when applied to composite structures [20]. On the contrary, when applied to steel plates, keeping the areal density constant, it was found that plain steel plates absorb the blast more efficiently than those coated with polyurea [21]. Finally, some preliminary work has been performed in previous years in the Dynamic Effects Lab that shows that coating the hull of a vehicle that undergoes blast loading is an effective means for acceleration mitigation, though it should be noted that the areal density of the plate was not kept constant in this study [22].

Small-Scale Testing

The testing facilities at the University of Maryland are equipped to perform small-scale explosive testing. Small-scale testing has a number of advantages over large-scale testing, costing less in both time and money to perform. In addition to these advantages, it has been shown [23, 24] that small-scale testing can accurately represent the response of a target to an explosion.

The scaling factor is determined by taking the cubed root of the ratio of the full-scale mass of the explosive over the small-scale mass of the explosive.

$$SF = \left(\frac{mass_{full-scale}}{mass_{small-scale}}\right)^{\frac{1}{3}}$$

In this work a geometry that will scale to 4.536 kilograms of explosive was used. In the majority of the research in this paper, the small-scale tests use an explosive mass of 4.4 grams, resulting in a scaling factor of approximately ten. All length and time dimensions are scaled using this factor. The small-scale lengths and times are determined by dividing the full-scale values by this factor while the small-scale accelerations are determined by multiplying the full-scale values by this factor.

Test Equipment

In order to perform a successful explosive experiment, a wide array of equipment is needed. Instrumentation to obtain measurements of acceleration, displacement, and time are all required to generate the data necessary for proper analysis. On top of that, equipment is needed for the blasting itself. In addition to the blasting apparatus,

equipment necessary for conducting dynamic testing using a pressurized gas gun is also required.

The accelerometers used in this series of tests were manufactured by PCB Piezotronics Inc. The accelerometers chosen were model 350B04 with a measurement range of ±5000g's. A PCB Piezotronics Inc. signal conditioner, model 483A and two LeCroy oscilloscopes, model numbers 9314AM and 9315AM, were employed alongside the accelerometers for data acquisition.

For obtaining displacement and time data for the blast tests, a Phantom v12.1 high speed camera equipped with a Tamron 28-75mm variable focus lens was used. The video was analyzed in the Phantom software. Microsoft Excel was used to create displacement versus time plots.

To create the blast, plastic explosive sheet (Deta Sheet from Omni Explosives) is used in conjunction with an Exploding Bridge Wire Detonator manufactured by Teledyne Technologies. The detonator has a small amount of explosive located inside of it that, when combined with the plastic deta sheet, sums up to a total mass of explosive reported for each test. The plastic explosive charge is formed and placed in a plastic sleeve to insure repeatability in charge geometry from test to test. The firing system responsible for detonation is connected to the explosive, high speed camera and oscilloscopes so that when the firing system is discharged each of the recording devices trigger so that they may record the explosive event simultaneously.

The actual blast test takes place in a tank constructed to outer dimensions of 1.5 meters long by 1.5 meters wide by 0.6 meters deep. The tank is filled with sand and is capable of being flooded with water from the bottom up. A schematic of the blast testing equipment is shown in Figure 2.

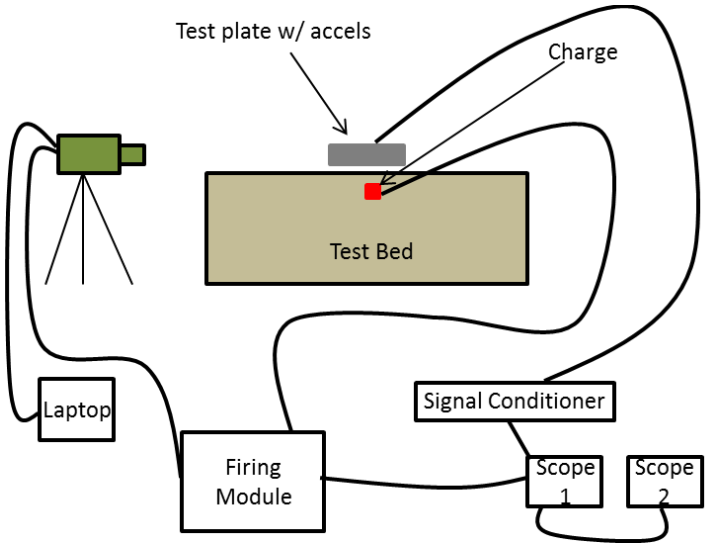

Figure 2: Schematic detailing blast test equipment set-up

Specific equipment is also necessary for dynamic testing using a pressurized gas gun. A high-pressure gas gun from a Split-Hopkinson bar is used in this research to provide dynamic loading to cantilevered beams. In addition to the gas gun, a cantilever support is created capable of providing a true cantilever boundary condition to a beam.

Blast Test Set-Up

There are a number of steps that must be taken in order to prepare for each blast test. Because the small-scale nature of the test, test preparation is performed with the utmost care as a small variation in any value may result in large variation in the test data. Each of the steps mentioned in the next paragraph are explained in more detail in previously published papers [29, 30].

The initial sand bed preparation consists of creating a 1.2 meter by 1.2 meter elevated and compacted sand platform in the center of the test bed. The height and compaction of the sand bed is controlled and repeatable. Once created, the explosive charge is buried in the sand platform at a location directly under the center of any specific test plate.

For all of the tests in this study a depth of burial (DOB) corresponding to ten centimeters large-scale is used. The small-scale DOB is ten millimeters since, as previously mentioned, the scaling factor for this series of tests was determined to be approximately ten. DOB is defined here as the distance between the top surface of the charge and the surface of the sand.

The next step is to locate the plate and set its stand-off distance (SOD). SOD is defined as the distance between the top of the sand and the bottom of the target plate. Depending on the plate characteristics, the test plate may either be placed on a set of blocks that are machined to have the exact height of the specified SOD, (Figure 3), or suspended above the sand on chains attached to the ceiling.

Once prepared, the test bed is saturated from the bottom up. The water height is controlled and repeatable. The final test set-up for a blast test is shown in Figure 3.

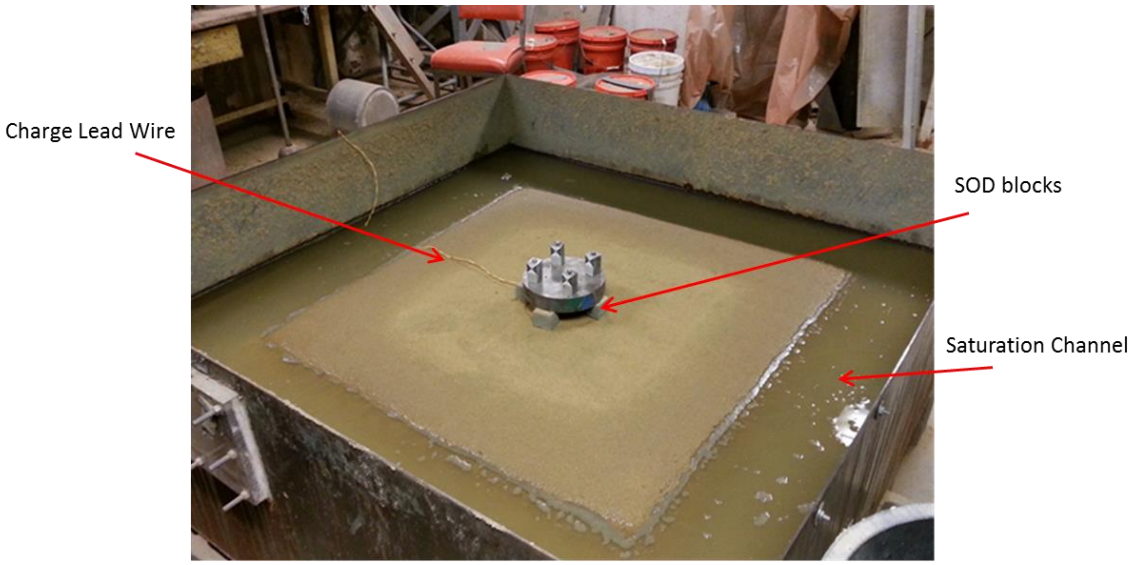

Figure 3: Fully prepared blast test sand bed

Once the bed has saturated fully, the accelerometer cables are connected to each accelerometer on the plate. The high speed camera is set-up and the image adjusted, following which a dummy charge is fired to make sure all data acquisition systems are functioning properly. After the dummy round, the charge lead wires are connected to the firing module and the charge is detonated. Upon detonation the video is examined and saved using the Phantom software. The acceleration signal is downloaded from the scopes and viewed in the UERDTools program to ensure proper recording; the signals are then saved and analyzed.

Gas Gun Test Set-Up

The cantilever beam tests are set-up by first placing a beam in the cantilever support mentioned in the section on gas gun test equipment. Care is taken to place the center of the beam in line with the striker projectile path. The beam is clamped such that it cannot move in the support.

Once the beam has been placed in the testing position, the gas gun projectile is loaded and the pressure chambers primed. For the beam testing the pressure is in the neighborhood of 75 kilopascals, and will be described in more detail later. Once the gun is pressurized, the oscilloscopes and high speed camera are made ready and are triggered simultaneously by the firing of the gas gun. The data is then downloaded from the oscilloscopes and saved for processing using the Phantom high speed camera software.

Mitigation Study on Small-Scale Vehicle Shapes

Ideally, the plates under study should reflect the geometric properties of the vehicles that are regularly targeted by explosive devices. As such, for the upcoming portion of this research, rectangular plates having the scaled down dimensions of some of those vehicles are used. Specifically, each plate has outer dimensions of 45.72 centimeters by 30.48 centimeters.

This series of tests utilizes a hull/frame combination to represent the vehicle. The hull, or bottom, of the simulated vehicle is responsible for capturing all of the ejecta. The frame, or top, of the simulated vehicle represents where the passengers of an actual vehicle would sit; this is where the accelerometers and tracking targets are placed, as this is the portion of the vehicle for which the mitigation needs to have the most effect. The hull to frame mass ratio is kept close to one. If the mass of the hull is much greater than the mass of the frame, it can be postulated that that the acceleration of the frame will be very high. On the other hand, if the frame is much more massive than the hull, this set-up might result in unrealistically low acceleration values.

Before going into any detail regarding the test series, it is necessary to describe the general test set-up used for the mitigation study. As previously mentioned, this series of tests employed a hull/frame combination small-scale vehicle. In between the hull and frame, there is at any given time either a series of thin-walled cylinders made from metal of various geometric properties, or air. The combination of the hull and frame resulted in a vehicle mass in the neighborhood of 15 kilograms.

It was mentioned previously that there are two methods for setting the SOD of a test plate – the stand-off blocks and hanging the plate from chains. The chains are normally used for heavier plates. For the mitigation tests, a combination of the two methods was used. The first portion of the mitigation study involved creating baseline data where the only air separates the hull and the frame. For these tests, the hull rested on stand-off blocks and the frame hung on the chains a specific distance away from the hull. In later tests when mitigation was added in between the hull and the frame only one of two SOD scenarios is used.

The first and most common set-up involves attaching the thin-walled cylinders only to the hull. In this situation, as in the air gap tests, the hull rests on the blocks and the frame is lowered on the chains until the frame just makes contact with the thin-walled cylinders. This set-up prevents the stand-off block from supporting too much weight – causing them to sink in the saturated sand and changing the SOD. For a few tests, the thin-walled cylinders are attached to both the hull and the frame. These tests only require the use of the chains to set the SOD of the test plate.

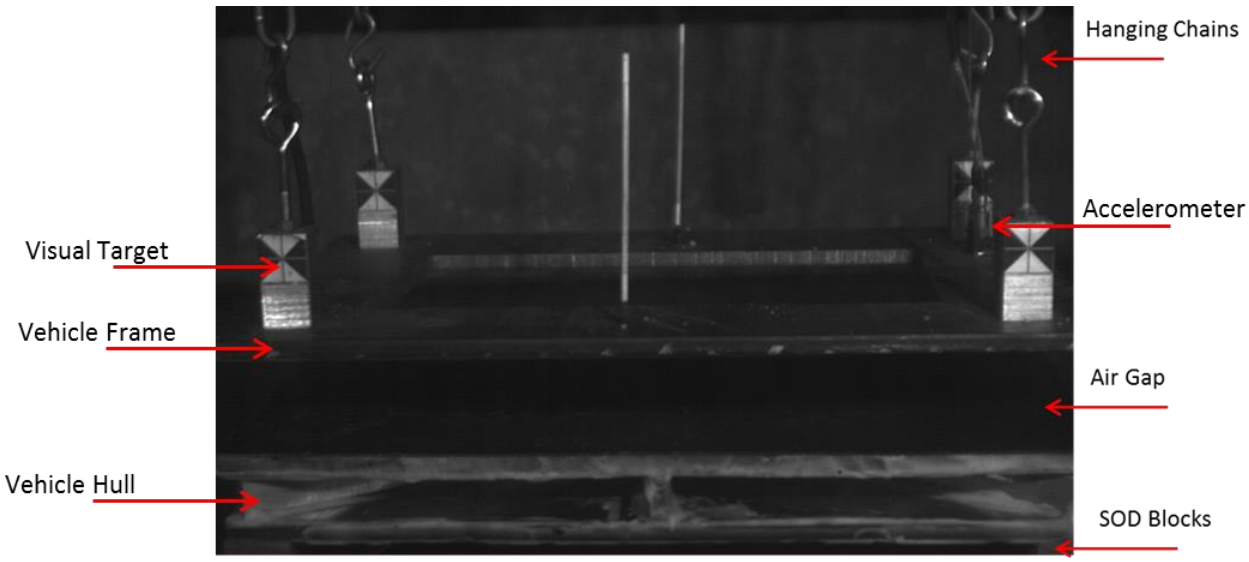

Figure 4: Test set-up for no mitigation tests

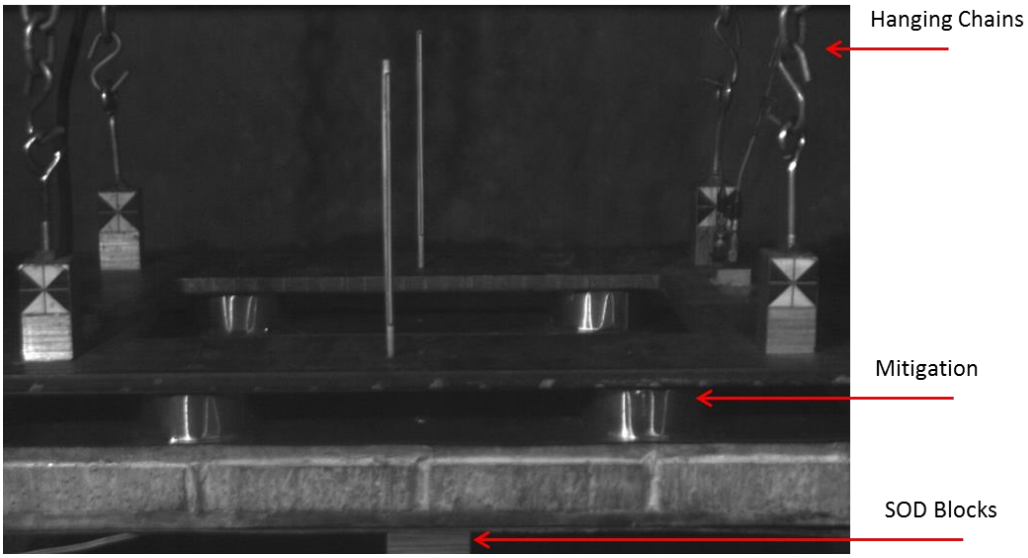

Figure 5: Test set-up with mitigation attached to hull only

A couple of minor things need to be mentioned in this section. The first is that each test plate will have four targets attached to the frame. One target will be located on each corner of the frame so that it may be tracked using the high speed camera. The second is that each test frame, much like those in the previous studies, will have two or three accelerometers located along a diagonal line connecting the left front portion of the frame with the rear right portion. These acceleration signals are averaged to give the final readings reported in the results section. The accelerometers and the visual targets can all be seen in Figure 4, Figure 5.

Height of Target Study

The first series of complete tests run to study the effect of adding thin-walled cylinders to mitigate acceleration was executed to determine how changing the height of the cylinders changes the peak acceleration recorded on the frame. The initial tests

in this series were conducted with no mitigation between hull and frame. Following this, four tests were run with standard aluminum beverage cans separating the hull and the frame by distances of 25, 38, and 50 millimeters.

The cylinders for the first round of mitigation tests were attached only to the hull. The second round of mitigation tests consisted of the same geometry cans tested with the cans attached to both the frame and the hull, resulting in an accordion type stretching following the initial crushing. One test was repeated to demonstrate test repeatability. The test matrix can be seen in Table 1.

Table 1: Test matrix for HOT test study

Test Number	Charge Mass (g)	DOB (mm)	SOD (mm)	# of Cylinders	Cylinder Material	Cylinder OD (mm)	Cylinder ID (mm)	Height of Target (mm)
1	4.4	10	40	-	-	-	-	50
2	4.4	10	40	-	-	-	-	25
3	4.4	10	40	-	-	-	-	38
4	4.4	10	40	4	Aluminum	66	65.8	50
5	4.4	10	40	4	Aluminum	66	65.8	25
6	4.4	10	40	4	Aluminum	66	65.8	38
7	4.4	10	40	4	Aluminum	66	65.8	25
8*	4.4	10	40	4	Aluminum	66	65.8	25
9*	4.4	10	40	4	Aluminum	66	65.8	38
10*	4.4	10	40	4	Aluminum	66	65.8	50
Note: Test numbers with an * were conducted with the cylinders attached to both frame and hull								

Height of Target Study Test Results

At the end of the test series described in Table 1, the acceleration signals were analyzed and averaged for each test. It is of interest to view how the acceleration signal changes from a test with no mitigation, to mitigation attached the hull only, to mitigation attached to both the hull and the frame. A plot of this can be seen in Figure 6. This plot compares the signals from the accelerometers from the tests for each scenario at a HOT of 25 millimeters. Following this plot, a full summary is given of how the acceleration changes with HOT for the three different test scenarios: No mitigation, mitigation attached to the hull, and mitigation attached to the hull and the frame. This plot is presented in Figure 7. A zoomed in view of the benefit of attaching the cylinders to the frame and the hull can be seen in Figure 8.

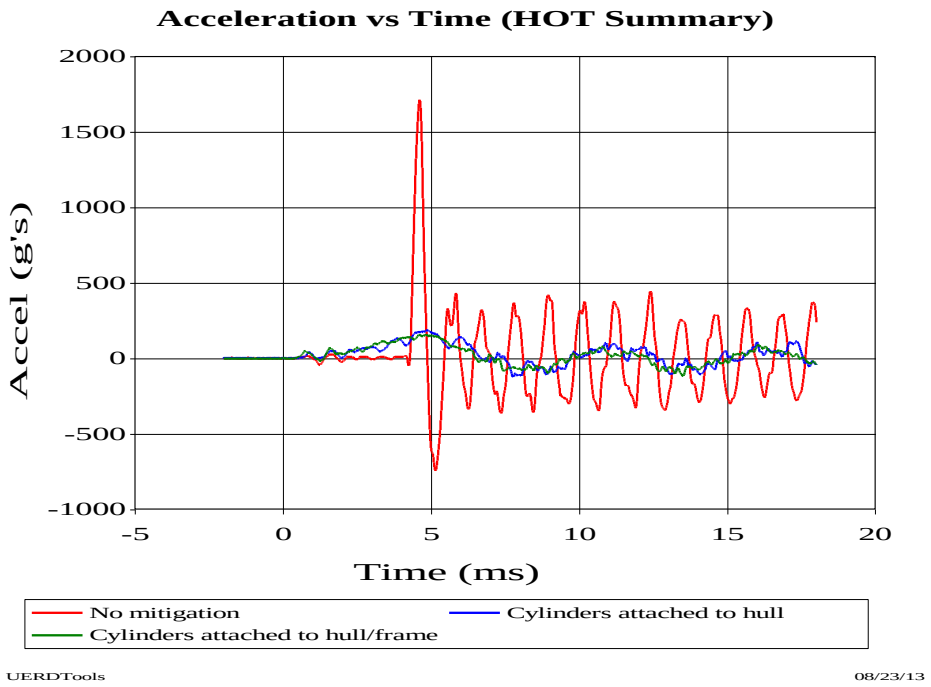

Figure 6: Comparison of acceleration signals for HOT study

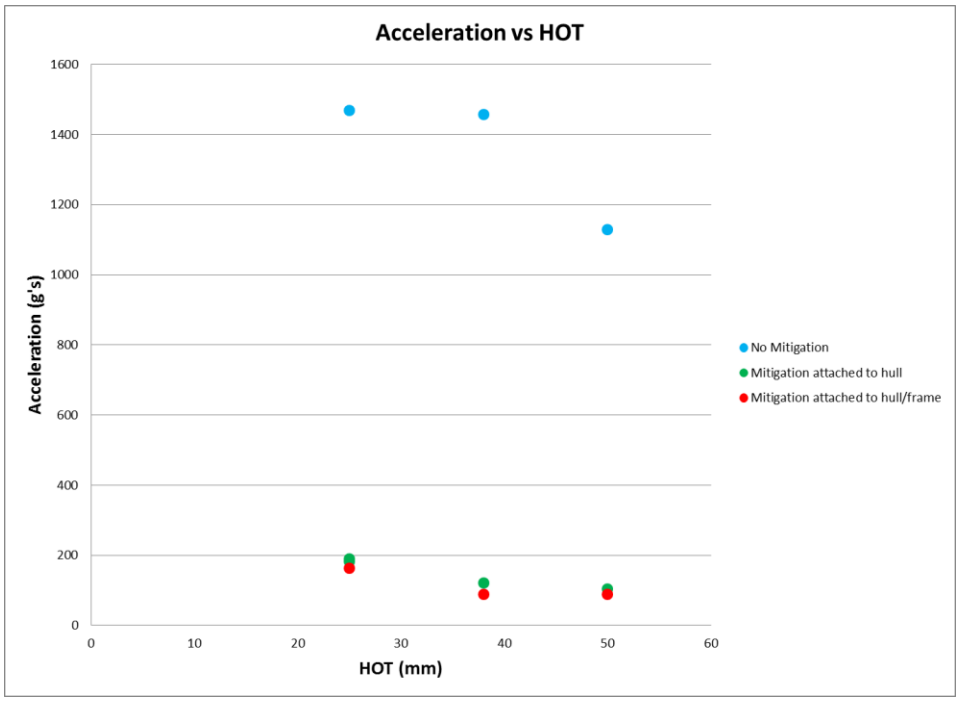

Figure 7: Acceleration versus height of target for no mitigation and mitigation

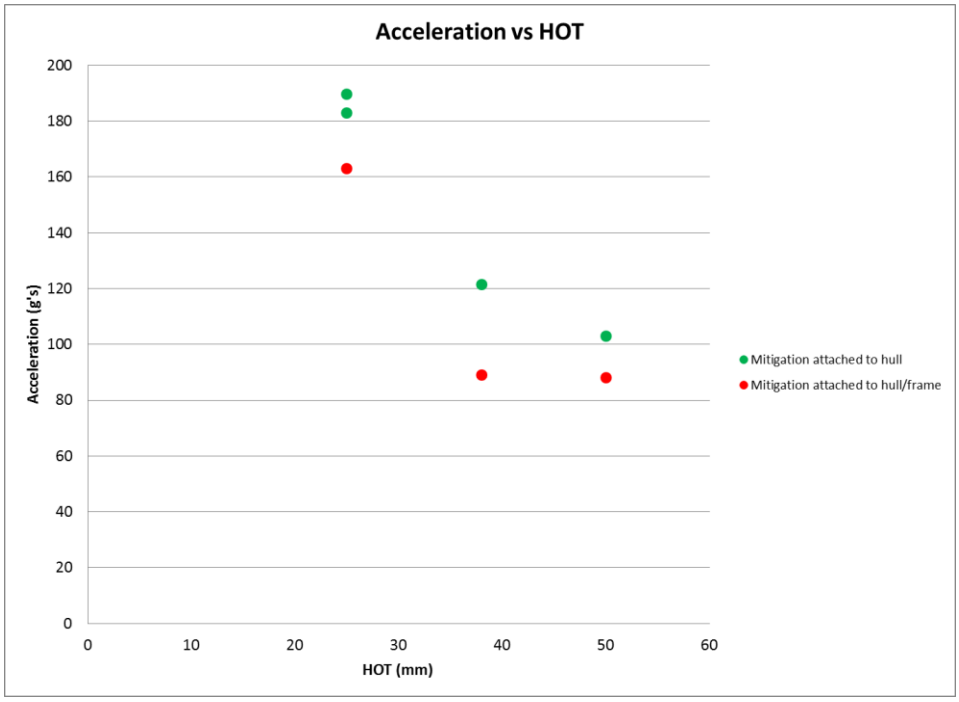

Figure 8: The effect of attaching cylinders to the hull and the frame

The first and primary take-away from the graphs in this section is that the crushing of thin-walled cylinders as a source of mitigation of acceleration can have a tremendous effect. At a height of target of 25 millimeters, the peak frame acceleration is decreased from close to 1500g's to around 190g's. Going a step further, if the cylinder height is increased by a factor of two, and the accordion stretching of the cans is added to the initial crushing by attaching the can to the frame, the acceleration level can be decreased to around 90 g's.

To put this into perspective, using the cube-root scaling law and scaling this result up to full-scale, for this series of testing, in the worst case scenario (no mitigation, 25 centimeter HOT full-scale) a passenger would experience an acceleration of 150g's – a fatal level. Using the hull/frame attached cans at a HOT of 50 centimeters full-scale, a passenger in the vehicle would experience around 9g's. This is around the same level of acceleration experienced by a fighter pilot in an ejection seat.

Number of Thin-Walled Cylinders Study

In order to determine the effect of adding more cylinders between the hull and the frame, a test series was run for four different scenarios. Initially a control test containing no cylinders was run. After which the number of cylinders was increased to four, then six, then eight. A summary of the important test parameters is listed in Table 2. Each test will be run with the cylinder attached only to the hull.

Table 2: Test matrix for the number of thin-walled cylinder study

Test Number	Charge Mass (g)	DOB (mm)	SOD (mm)	# of Cylinders	Cylinder Material	Cylinder OD (mm)	Cylinder ID (mm)	Height of Target (mm)
Control	4.4	10	40	0	-	-	-	25
1	4.4	10	40	4	Aluminum	66	65.8	25
2	4.4	10	40	6	Aluminum	66	65.8	25
3	4.4	10	40	8	Aluminum	66	65.8	25

As can be seen in Table 2, the thin-walled cylinders used for this study are of the same outer diameter and wall thickness of the cylinders used for the HOT study. Namely, a typical aluminum beverage can is used. It was decided to test the worst-case HOT in every instance for this study. This decision was made for two reasons. The primary reason for determining that a 25 millimeter height of target should be used comes as the fact that vehicles in the field face situations where vehicle roll-over is a very real concern. To combat this, it is often desired that the vehicle center of gravity be as low as possible. By testing the 25 millimeter high cylinders, a determination of the effectiveness of the mitigation techniques for a low center of gravity vehicle can be made.

Another reason for testing the 25 millimeter cylinders comes as the fact that the acceleration levels of the 50 millimeter HOT tests are simply too low to be easily measured. Upon examining the acceleration signals from the 50 millimeter HOT tests (Figure 9) it is not too difficult to imagine that the peak acceleration comes from the low frequency vibrations of the frame as opposed to a sharp acceleration peak resulting from hull to frame contact. Because of the extremely low acceleration levels of the 50 millimeter HOT, a more effective study of the effect of increasing the number of cylinders can be made at the 25 millimeter HOT. A comparison of the two different HOT test accelerations can be seen in Figure 9.

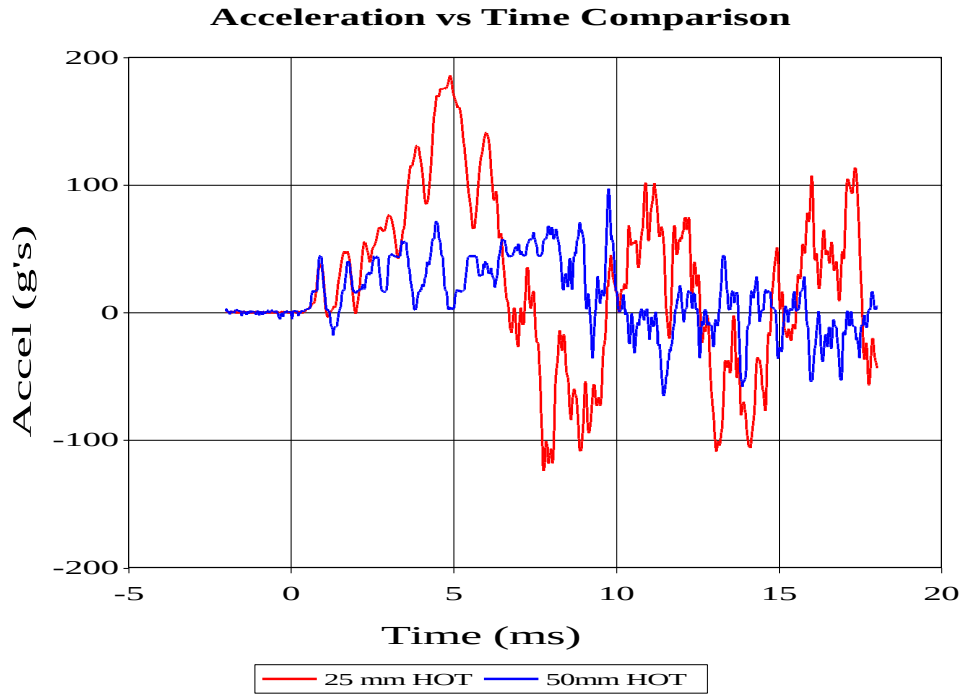

Figure 9: Comparison of acceleration signals for 25mm HOT and 50mm HOT

Number of Thin-Walled Cylinders Study Test Results

One of the initial interesting results coming from increasing the number of cans happens to be the general shape of the acceleration pulse. From looking at the test with four cylinders separating the hull and the frame, it appears as if there is a strong element of low frequency frame vibration that adds an element to the acceleration signal. When the cylinder number increases, that low frequency vibration seems to be eliminated. An illustration of this is seen in Figure 10. The red signal represents the four can test, with the blue and green signals representing six and eight cans respectively. After the initial peak acceleration, the four can test has a substantial vibration signal at a defined frequency. This vibratory characteristic does not appear in either of the other tests.

The overall effect of increasing the number of cylinders is also presented here. As in other tests, the average peak acceleration for each test is determined and plotted versus number of cans. The results can be seen in Figure 11.

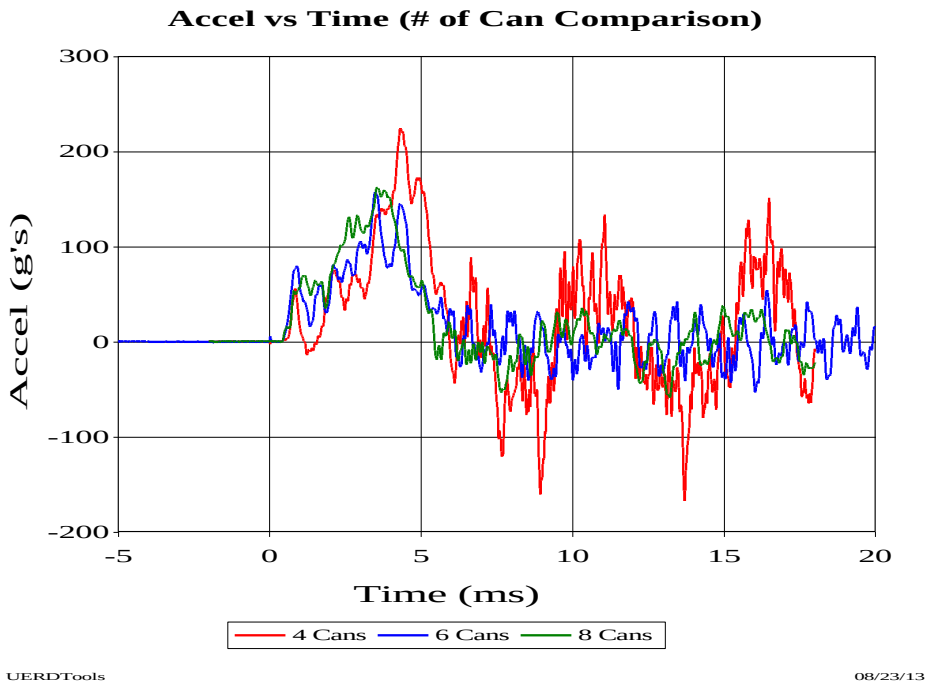

Figure 10: Comparison of acceleration signals for four, six, and eight cans

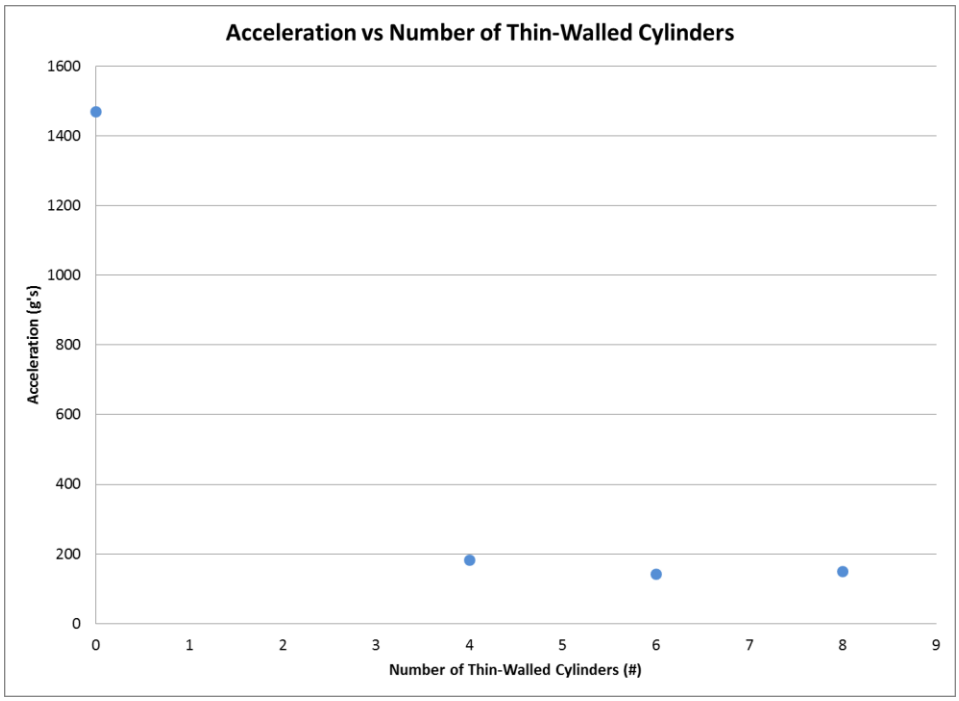

Figure 11: Acceleration versus number of thin-walled cylinders

From looking at Figure 11 some general remarks should be made. It appears as if there is a slight benefit to be realized in peak acceleration by increasing the number of cylinders to six and eight. Full-scale acceleration levels decrease from around 18 g's to somewhere in the neighborhood of 14 to 15 g's. While not a drastic drop the benefit is definitely there. Additionally, as mentioned previously, it looks like

increasing the number of cans may damp out low frequency frame vibration; significantly reducing the duration of time a passenger might experience high levels of acceleration.

Outer Diameter Study

To study the effect of an increased and decreased outer diameter of the mitigating cylinders, a series of four tests was run. In this series, in addition to the control test where no mitigation was present, tests were run with the outer diameter varying from 53 to 73 millimeters. The cylinders used for this test are beverage containers having the same wall thickness made from the same material, but of different outer diameters. The test matrix can be viewed in Table 3.

Table 3: Test matrix for outer diameter study

Test Number	Charge Mass (g)	DOB (mm)	SOD (mm)	# of Cylinders	Cylinder Material	Cylinder OD (mm)	Cylinder ID (mm)	Height of Target (mm)
Control	4.4	10	40	0	-	0	0	25
1	4.4	10	40	4	Aluminum	66	65.8	25
2	4.4	10	40	4	Aluminum	73	72.8	25
3	4.4	10	40	4	Aluminum	53	52.8	25

As in the number of thin-walled cylinder study, a height of target of 25 millimeters is used for this series of tests; for the same reasons as listed in that section. From examining Table 3, it should also be noted that only four cylinders were used in each of these tests. The final note before discussing test results is that the cylinders were only mounted to the hull.

Outer Diameter Study Test Results

As in the previous series of tests, a comparison between the actual acceleration signals is presented (Figure 12) along with the trend of acceleration versus outer diameter (Figure 13). When comparing the three tests with cylinders it is seen that each acceleration signal has the same low frequency vibrations present. This backs up the previous hypothesis that, when excited from the four points of contact of the thin-walled cylinders, the frame vibrates at a low frequency resulting in a relatively high acceleration level. The red line represents the smallest outer diameter, the blue line represents the middle outer diameter size, and the green line portrays the acceleration of the simulated vehicle frame that utilized the cans with the largest outer diameter.

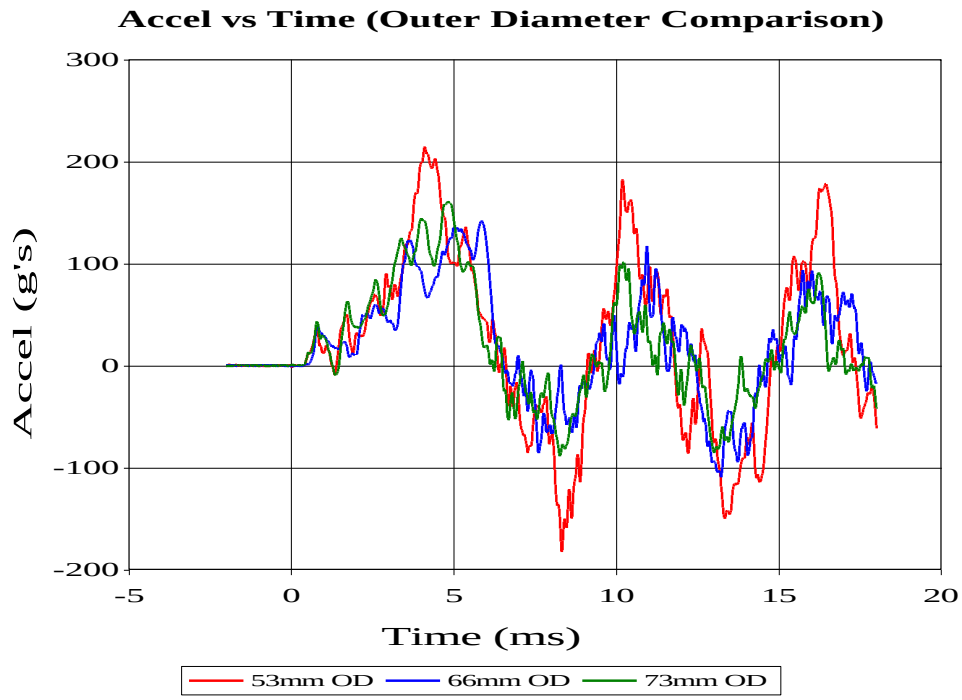

Figure 12: Acceleration signal comparison for outer diameter study

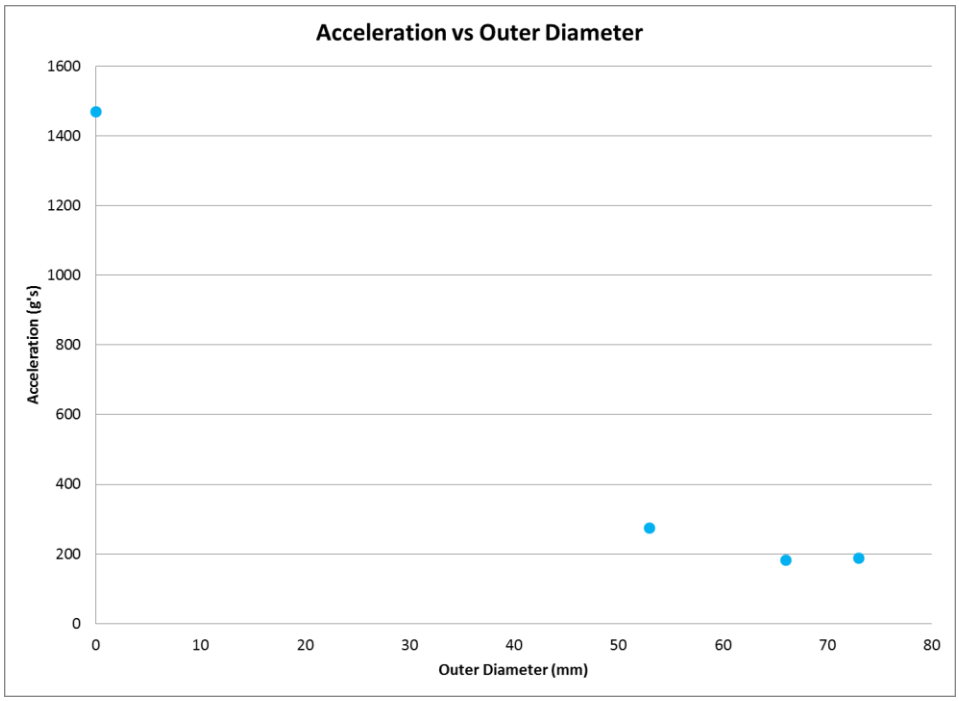

Figure 13: Acceleration versus outer diameter of mitigation cylinders

After examination of Figure 13 a few observations are in order. Starting with the graph displaying acceleration, it is seen that at the 53 millimeter outer diameter, the acceleration of the frame decreases from the baseline value of 1470 g's to around 275 g's. The sharp decline of acceleration continues at 66 millimeter outer diameter where the acceleration drops to around 180 g's. After which it appears as if the

acceleration value levels off somewhat, and a drastic change is not noted when moving from a 66 millimeter outer diameter to a 73 millimeter outer diameter..

Wall Thickness Study

To test the effect of wall thickness on acceleration, the test preparation is a bit more involved. In previous tests, beverage cans with the necessary geometric characteristics were used as the mitigation material. This provided a cylinder, uniform in wall thickness, with a seamless construction. Beverage cans of varying wall thicknesses could not be found, so thin-walled cylinders of varying wall thicknesses had to be constructed out of shim stock.

The initial test of this series involved replicating a previously performed test, but this time performing the test with a shim stock cylinder as opposed to a commercially produced cylinder. In addition to this comparison, two additional tests were completed with different wall thicknesses from the original test. The test matrix for the wall thickness study can be seen in Table 4.

Table 4: Test matrix for wall thickness study

Test Number	Charge Mass (g)	DOB (mm)	SOD (mm)	# of Cylinders	Cylinder Material	Cylinder OD (mm)	Cylinder Wall Thickness (mm)	Height of Target (mm)
Control	4.4	10	40	0	-	0	0	25
1	4.4	10	40	4	Aluminum (commercial)	66	0.1	25
2	4.4	10	40	4	Aluminum (shim)	66	0.1	25
3	4.4	10	40	4	Aluminum (shim)	66	0.15	25
4	4.4	10	40	4	Aluminum (shim)	66	0.2	25

From the test matrix note that these test were performed at a height of target of 25 millimeters; done for previously stated reasons. Also, for each of the tests only four thin-walled cylinders were used for mitigation. The cylinders were only attached to the hull and not the frame.

Wall Thickness Study Test Results

Before delving into the effects of wall thickness on acceleration, the results from the two tests comparing commercially produced aluminum cans to the shim stock cans will be analyzed. It was observed that there was no splitting of the shim stock cans at the seam. The cans crumpled as effectively as a commercially produced can as well. The test results for acceleration and velocity from the first integration of the acceleration are shown in Table 5.

Table 5: Test results for commercial versus shim stock cylinders

Test Number	# of Cylinders	Cylinder Material	Cylinder OD (mm)	Cylinder Wall Thickness (mm)	Height of Target (mm)	Avg Peak Accel (g's)	Avg Peak Velocity (m/s)
1	4	Aluminum (Commercial)	66	0.1	25	183	4.225
2	4	Aluminum (Shim)	66	0.1	25	182.75	4.235

From looking at Table 5 it is very clear that the thin-walled cylinders produced from shim stock perform the same as the commercially produced, seamless cans. As such, the test series studying the effects of wall thickness can be directly compared to the tests studying the effects of height of target, number of cans, and outer diameter. It is also beneficial in that, as will be seen later, cylinders from other materials might be made in a similar method and compared to the earlier mitigation studies.

The next graph will highlight the differences in the acceleration signal. Similar to the instance when the number of cylinders was increased, as the wall thickness increases, the low frequency frame vibration seems to diminish. Though not as drastic of a damping effect as increasing the number of cans, it is still recognizable. The easiest way to highlight this low frequency frame vibration damping effect is to study the Fourier Spectra for each of the three wall thicknesses. Refer to Figure 14 to witness the weakening of the low frequency frame vibrations as the walls of the cylinder become thicker.

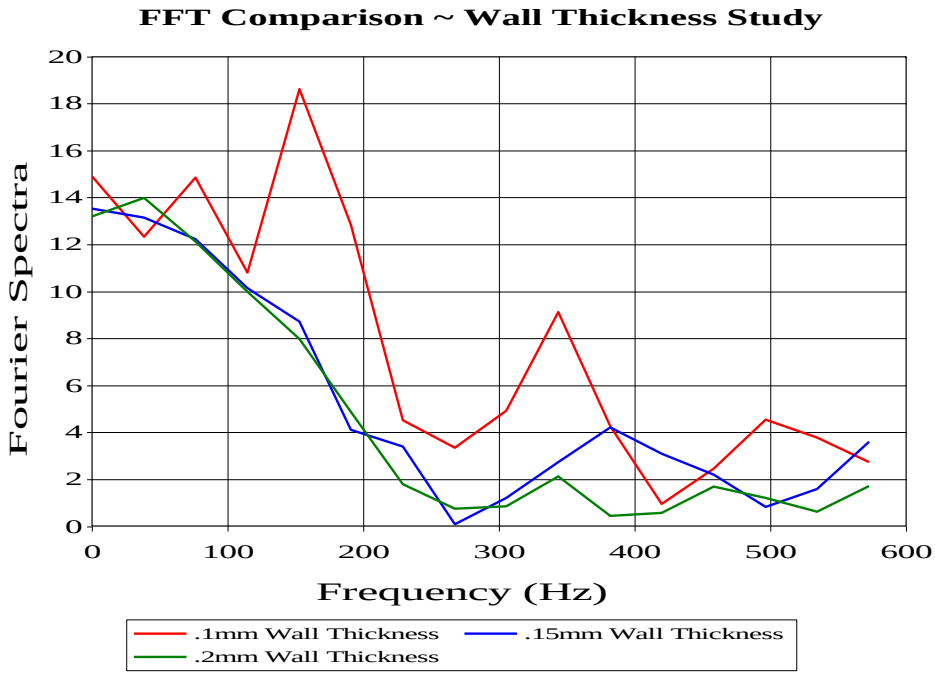

Figure 14: Fourier Spectra comparison for tests in the wall thickness study

In addition to the dampening of the low frequency frame vibrations, it appears as if increasing the wall thickness of the mitigation cylinders hold other benefits as well. To illustrate, the plots showing the acceleration of the frame for all of the tests

performed are reported here. Figure 15 displays the three test outputs as a function of increasing wall thickness of each mitigation cylinder.

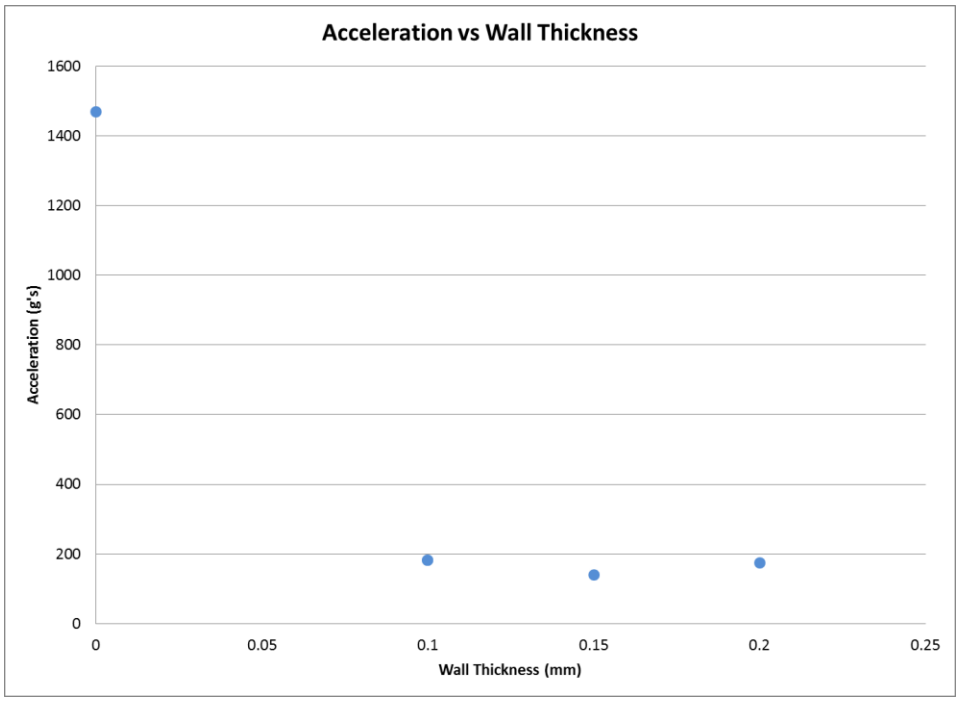

Figure 15: Acceleration versus wall thickness of mitigation cylinders

The initial indication from viewing Figure 15 is that the cylinder wall thickness has little notable effect. A minor decrease in acceleration accompanying the increase in wall thickness from .1 to .15 millimeters is directly followed by an increase of the same magnitude with an increase in wall thickness from .15 to .2 millimeters.

The final result stemming from the wall thickness study comes as a visual observation. After each test the cylinders are inspected to make sure no tearing of the can occurred. At this point it was noted that the cans crushed in significantly different ways as the wall thickness increased. Pictures of each platform of cylinders (post-test) are shown in Figure 16. From these photos it is noted that the .1 millimeter thick cylinders crushed completely with many folds in the material. The .15 millimeter can underwent semi-complete crushing with nice folds in the material as well. At the point when the wall thickness reached .2 millimeters, it is noted that the cylinder does not undergo complete crushing and that there are a few larger areas on the surface of the can that show little or no plastic deformation.

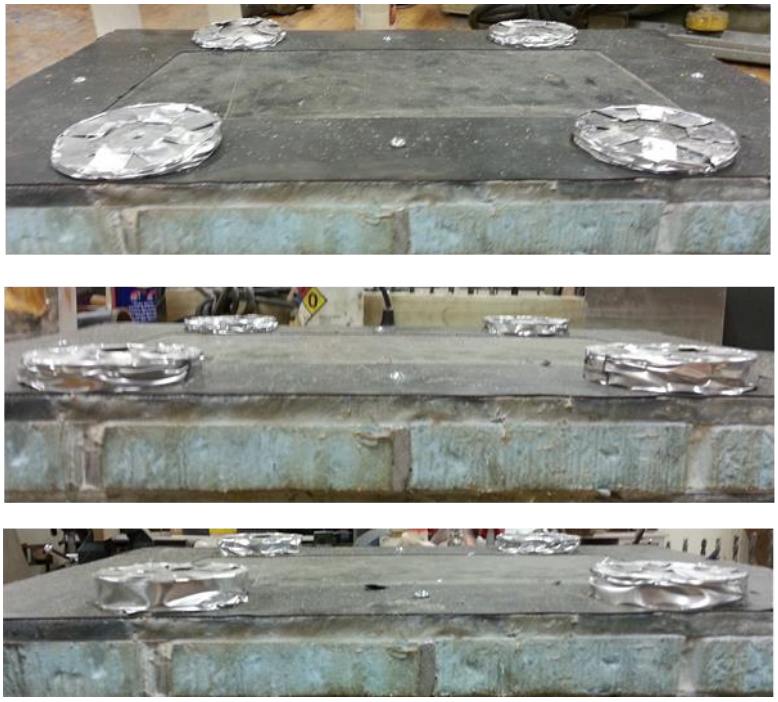

Figure 16: Crushing characteristics of .1mm (top) .15mm (middle) and .2mm (bottom) wall thickness cylinders

Cylinder Material Study

The next series of tests conducted was very brief. The series aimed at viewing the effects of changing the metal material of the thin-walled cylinders. To achieve this, steel cylinders with the same wall thickness and outer diameter as the aluminum cylinders were created. The test results are shown below in Table 6.

Table 6: Test results for cylinder material study

Test Number	# of Cylinders	Cylinder Material	Cylinder OD (mm)	Cylinder Wall Thickness (mm)	Height of Target (mm)	Avg Peak Accel (g's)	Avg Peak Velocity (m/s)
1	4	Aluminum (shim)	66	0.1	25	183.0	4.2
2	4	Steel (Shim)	66	0.1	25	203.3	3.8

From viewing the results in Table 6, it is seen that the difference between the two types of cylinders is minor. Due to the fact that the steel cylinders did not make a remarkable difference, for better or for worse, it was decided to spend effort studying other areas as opposed to creating cylinders out of various other materials. This concludes the portion of the research involving using thin-walled cylinders for mitigation of acceleration on small-scale vehicles.

Effects of cylinder geometry and number of impulse and kinetic energy

Though not covered in detail in this paper, the change in kinetic energy and impulse of the target plate should be mentioned briefly.

Regardless of the various HOT scenarios tested, the impulse imparted to the frame saw a decline in the neighborhood of 15 percent when compared with the baseline (no mitigation) tests. Kinetic energy decreased by close to 30 percent, compared with the corresponding test with no mitigation present, for each HOT.

With six cylinders used as mitigation, the impulse decreased by approximately 25 percent of the value of impulse resulting from a test with no mitigation. A larger decrease in kinetic energy of approximately 50 percent occurred when using six cylinders as opposed to no mitigation.

The largest outer diameter cylinder had a decrease of 15 percent compared with the impulse value obtained with no mitigation. The kinetic energy of the simulated vehicle with the largest outer diameter cylinders declined by 30 percent compared to the kinetic energy from the test with no mitigation.

The final series of tests studied the effect of changing the wall thickness of the cylinders. The minimum impulse occurs at a wall thickness of .2 millimeters and dropped 27 percent in relative to the maximum value of impulse when no mitigation is present. Similarly, the kinetic energy is lowest for a cylinder wall thickness of .2 millimeters and reduced the value of the no mitigation case by 48 percent.

Coated Cylinder Blast Test Study

To better understand the dynamic effects of coating structures with polyurea, a number of thin-walled cylinder crushing tests were run. Since crushing of thin-walled cylinders has already been proven to be an effective means of mitigation using small-scale vehicle shapes, a more practical means of comparison between non-coated and coated cylinders was developed. This series of tests utilized a single thin-walled cylinder in between two circular aluminum plates. The aluminum plates are termed the hull (bottom) and the frame (top); the same as the scaled vehicle testing. The plate characteristics are listed in Table 7.

Table 7: Polyurea coated cylinder test plate characteristics

Frame Material	Frame Diameter (cm)	Frame Thickness (cm)	Frame Mass w/ Targets and accels (kg)	Hull Material	Hull Diameter (cm)	Hull Thickness (cm)	Hull Mass (kg)	Total Plate Mass (kg)
Alum 6061	16.51	2.74	1.43	Alum 6061	16.51	2.82	1.27	2.74

The thin-walled cylinder was created from aluminum shim stock with a polyurea coating applied onto the outer walls. A specific mass of polyurea for each test is mixed and applied to the prepared shim stock surface using a small paint brush. Each test was conducted with a pre-determined mass ratio of polyurea to aluminum substrate.

The polyurea used for this portion of the research is manufactured by Specialty-Products, Inc. and is designated HM-VK. It is an ultra-high strength hand-mixable polyurea elastomer. This specific polyurea was chosen for its high gel-time of 18 minutes and lower viscosity. These two properties allow the polyurea to be used in a mold to accurately create test specimens for this study. A description of the dry

properties of the polyurea (as obtained from the HM-VK technical data sheet) is shown in Table 8.

Table 8: Polyurea dry properties for HM-VK [27]

DRY PROPERTIES @ 125 mils (1.67 mm)*	
Tensile Strength ASTM D412	6671 PSI (46.36 mpa) Average
Elongation ASTM D412	506% Average
Hardness (Shore A) ASTM D2240-81	95 (0s)
Hardness (Shore D) ASTM D2240-81	48 (0s)
Modulus 300% ASTM D412	1395 psi (9.7 mpa)
Service Temperature	-30°F - +250°F (-34°C - +121°C)

Tests for this study are conducted using stand-off blocks set to 40 millimeters in height. A 2.2 gram charge is buried at ten millimeters in a saturated sand bed prepared as previously described. The thin-walled cylinders are connected to the hull only, and the frame is equipped with four targets for high speed video tracking and two accelerometers on opposite sides of the plate. A sample test plate is seen in Figure 17.

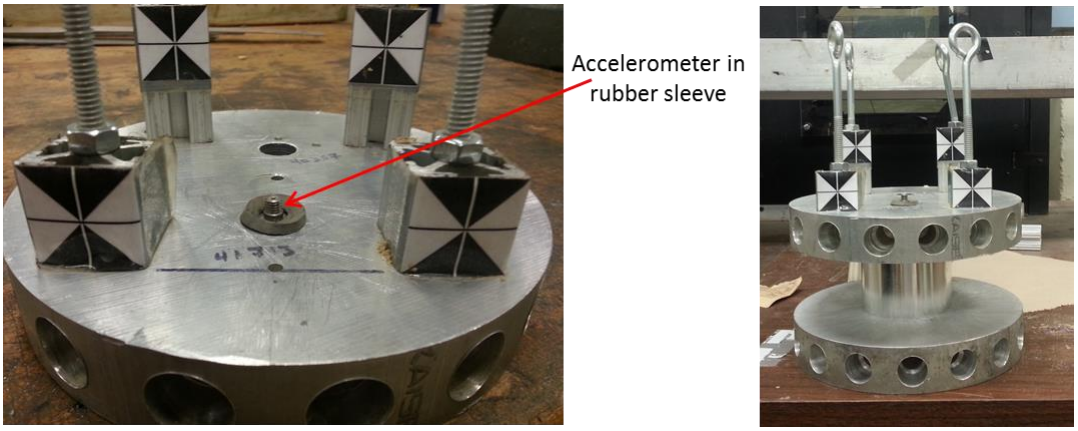

Figure 17: Accelerometer placement (left) and plate set-up (right) for coated can tests

Before describing the tests conducted for this study it should be noted that this series of tests aims only at describing the differences in acceleration of the frame that arise from coating thin-walled cylinders with polyurea. The charge mass has been decreased to result in manageable acceleration signals but the other test characteristics have remained the same. As such the test results are not meant to be indicative of full-scale levels experienced by a passenger in a vehicle that experiences blast loading. The variable that changed and is reported here is the mass ratio of polyurea applied to the thin-walled cylinder. The test matrix for this study is seen below in Table 9.

Table 9: Test matrix for polyurea coated can study

Test Number	Charge Mass (g)	DOB (mm)	SOD (mm)	# of Cylinders	Cylinder Material	Cylinder OD (mm)*	Cylinder ID (mm)*	Cylinder Height (mm)*	Cylinder Mass (g)*	Polyurea Mass (g)	Mass Ratio (Poly/Alum)
2	2.2	10	40	1	Aluminum	66	65.8	38.1	3.07	0	0.00
3	2.2	10	40	1	Aluminum	66	65.8	38.1	2.89	0	0.00
4	2.2	10	40	1	Aluminum	66	65.8	38.1	6.95	3.88	1.27
5	2.2	10	40	1	Aluminum	66	65.8	38.1	7.1	4.03	1.32
6	2.2	10	40	1	Aluminum	66	65.8	38.1	10.65	7.58	2.48
7	2.2	10	40	1	Aluminum	66	65.8	38.1	11.28	8.21	2.68
10	2.2	10	40	1	Aluminum	66	65.8	38.1	18.12	15.05	4.92
11	2.2	10	40	1	Aluminum	66	65.8	38.1	18.75	15.68	5.12

*Note: Values reported with an * denote those takes of the shim stock cylinder before the coated in polyurea

Coated Cylinder Study Test Results

Similar to the mitigation studies conducted with the thin-walled cylinders, the initial test for test validity is the comparison of the displacement curve developed from the tracking of the targets using high speed video with that of the double integrated acceleration signal. It should be mentioned that due to the small size and weight of the test plate, slight offsets in charge location or plate placement resulted in significant rotation of the frame. As such the accelerometer displacement was plotted alongside all four target displacement curves to make sure it fell in among them. Samples of the acceleration signal along with the displacement curve comparison are shown in Figure 18 and Figure 19. The displacement signals from the high speed camera and the accelerometer match very nicely. This same level of agreement is required for the test results to be considered valid and worthy of reporting.

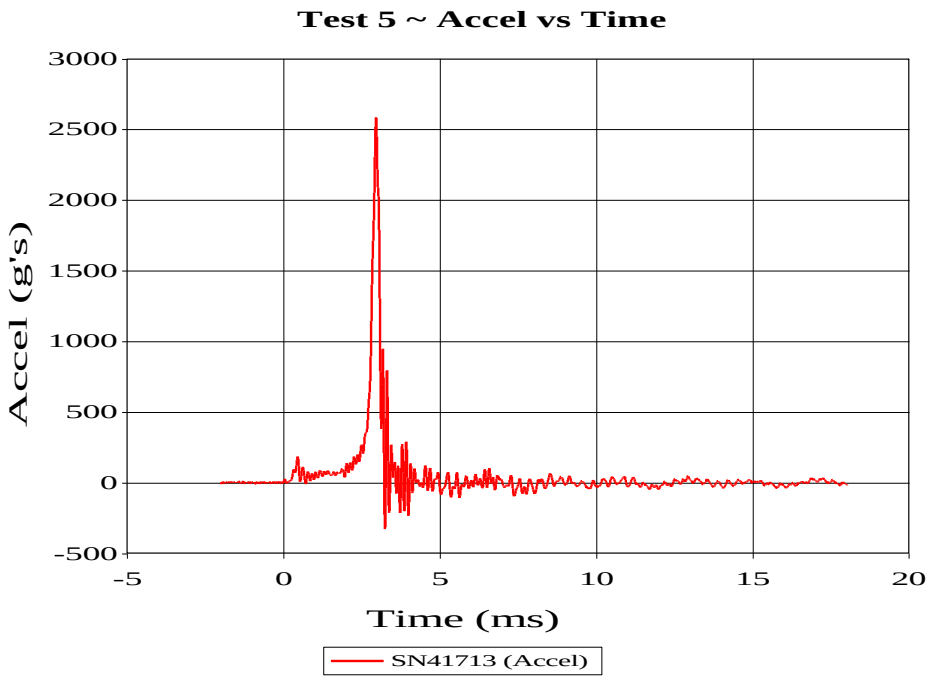

Figure 18: Acceleration signal from a polyurea coated cylinder test

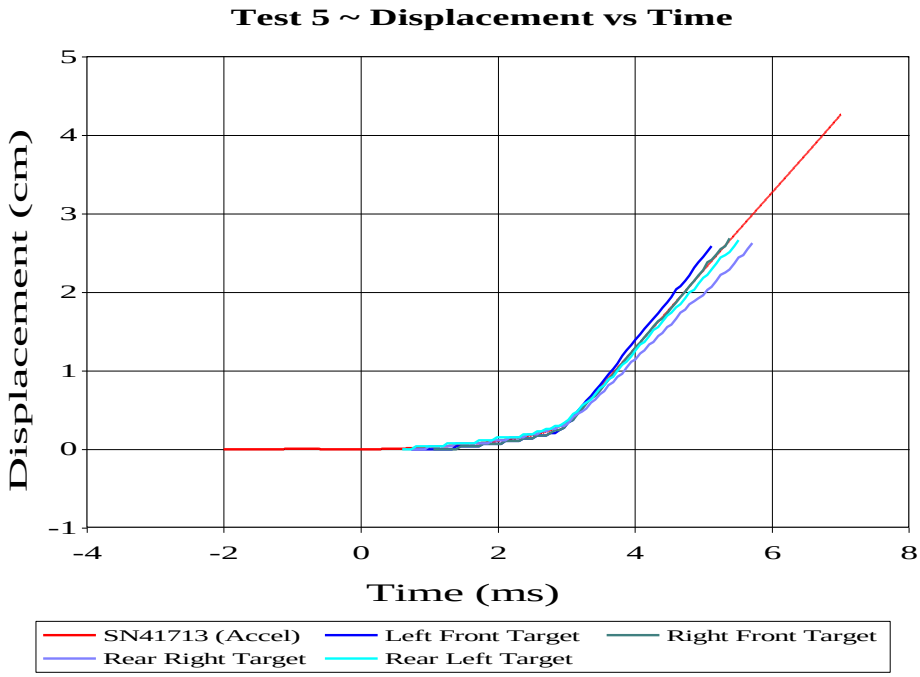

Figure 19: Accompanying displacement versus time curve comparison for accelerometer and camera data

Another area of interest is viewing how the acceleration signal changes with the increasing mass of polyurea applied to the thin-walled cylinder. To this end a sample

signal from one accelerometer for four testing scenarios is plotted on the same graph. The result is shown in Figure 20.

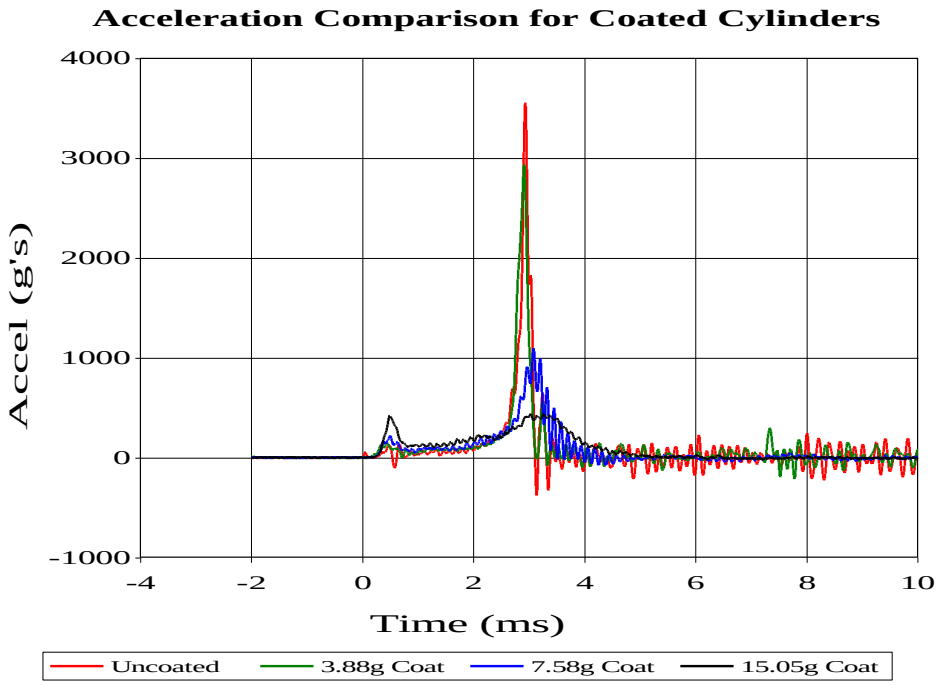

Figure 20: Acceleration signal comparison for various coatings

From studying Figure 20 a couple of observations can be made. The first and most obvious is how the peak acceleration decreases as the mass of polyurea applied to the cylinder increases. The second is that the time over which the acceleration pulse is delivered stretches out as the mass of the coat increases. So though the acceleration signal is lower it is delivered over a significantly larger period of time.

It might be helpful to view the final deformed state of each of the testing scenarios. At the end of each test, the cylinder was detached from the hull and compared with the other test cylinders. It was noted that as the mass of the polyurea coating increased, the recovered height of the cylinder also increased. A visual of the final cylinder deformations (post-test) is presented in Figure 21.

Figure 21: Front view of crushed cylinders increasing in polyurea mass from left to right

From Figure 21 it is clearly seen that as the mass of polyurea applied to the aluminum base increases, the final deformation of the can decreases. It should be noted that each cylinder underwent severe crushing in every test. After the initial crushing, the cylinders with the polyurea coating rebounded and recovered a portion of their initial

height. There was no delamination of polyurea from the metal substrate noted in the thinner coats, and only minor delamination of the polyurea from the aluminum as the mass of the polyurea increased. A measurement of the height of the crushed cylinder was made in each scenario and averaged to determine how much height each cylinder recovered after the blast event. These results are shown in Table 10.

Table 10: Recovered height of blast-tested polyurea-coated cylinders

Test Number	Approximate Mass Ratio (Polyurea/Aluminum)	Initial Cylinder Height (mm)	Post-Test Cylinder Height (mm)
2 & 3	0	38	6.7
4 & 5	1.3	38	16
6 & 7	2.5	38	31
10 & 11	5	38	35

Finally a comparison between the acceleration is made by plotting against the mass ratio of polyurea to aluminum of each cylinder. This plot is shown in Figure 22.

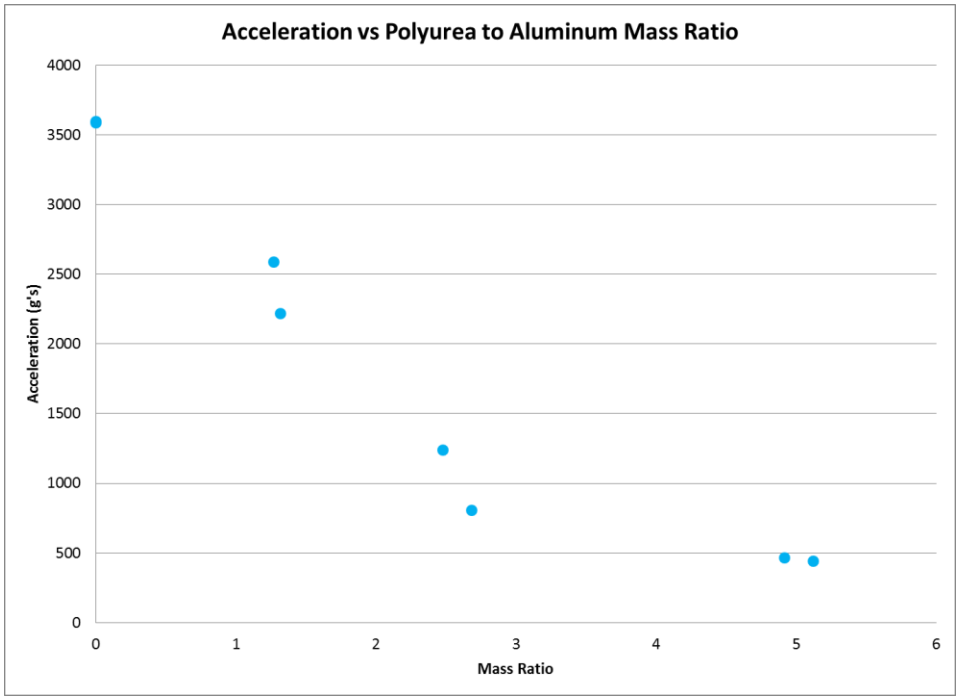

Figure 22: Acceleration versus mass ratio for coated cylinders

From viewing the graph a few observation can be made. The first and most important is how much of a decline in acceleration is obtained through coating thin-walled cylinders with polyurea. Studying Figure 22 it is noted that by adding the mass of the metal substrate in the form of a polyurea coating (resulting in a 1:1 mass ratio), the acceleration levels of the frame can be reduced by 30 percent of the value experienced by the frame that utilized only an uncoated cylinder. In the wall thickness study it was noted that only marginal gains were made by doubling the wall thickness, and thus the cylinder mass. Also it should be noted that the mass of the cylinders is negligible compared to the mass of the hull/frame combination. Though

not reported in detail here it was found that increasing the mass ratio on the thin-walled cylinders did not affect the impulse and kinetic energy of the frame.

Polyurea Coated Cantilevered Beam Test Study

This section of this research aims at developing a better understanding of the effects of polyurea coatings structures subjected to dynamic loading. Cantilevered beams coated in polyurea were tested using a high-pressure gas gun. Beams with varying thicknesses and mass ratios of polyurea were all tested.

In addition to being viewed by high speed camera, each beam test was conducted with an accelerometer mounted to the end of the beam for data collection purposes. A photograph of the final beam configuration is seen in Figure 23.

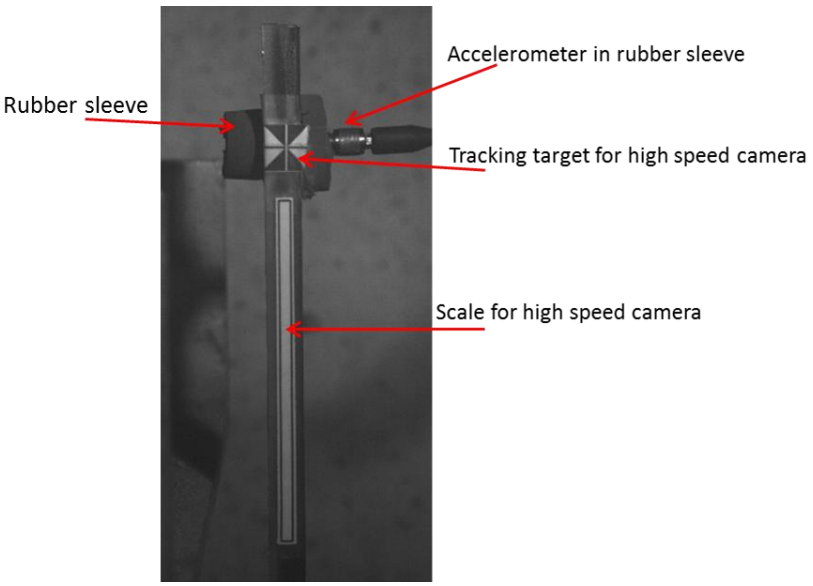

Figure 23: Beam set-up for cantilever beam tests

By mounting the accelerometer in the rubber sleeve as shown in Figure 23, the accelerometer moves with the neutral axis of the beam and does not incur any transverse motion during the test. As a result, it was discovered that the displacement curves determined from the accelerometer and high speed camera match perfectly (Figure 24). In order for test results to be reported, the displacement versus time curves developed from the double integrated accelerometer data and the high speed camera must match similarly.

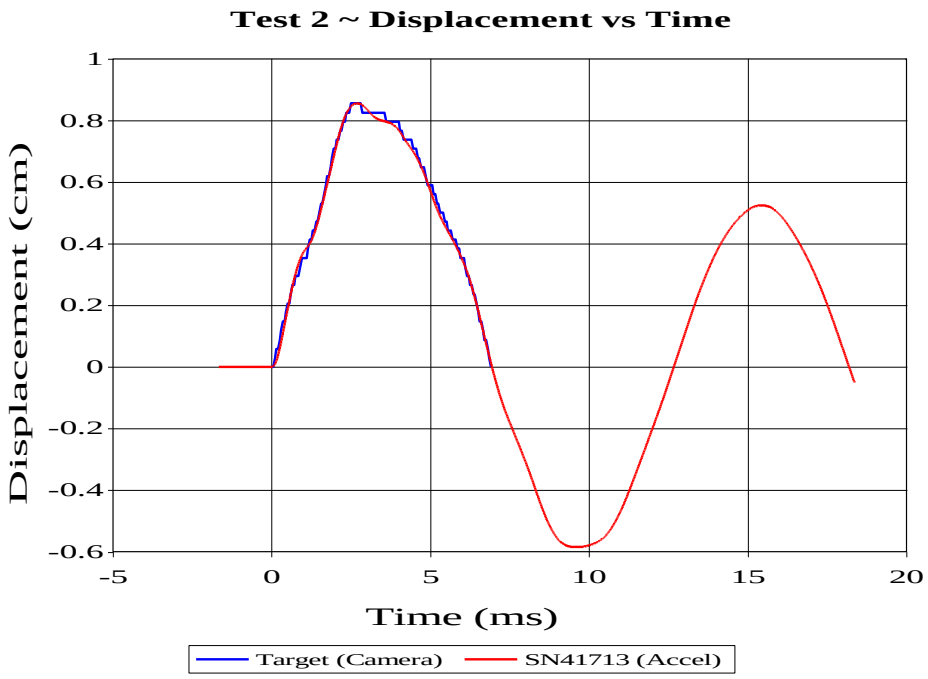

Figure 24: Example of a displacement versus time comparison for rubber mounted accelerometer

Preliminary Polyurea Beam Tests

Before going into each specific series of tests for the polyurea coated beams, it is necessary to specify how each beam will be placed in the cantilever support in relation to the oncoming projectile. The first item of note is that each beam is 25.4 centimeters long with the first 2.54 centimeters being secured in the cantilever support. The axis of the accelerometer is placed 2.54 centimeters below the tip of the beam. Each beam is placed such that the projectile fired from the gas gun hits the tip of the beam in the center of the beam width so that the beam does not twist upon impact.

A number of beam set-ups were tested to determine which face of the bar (the metal side or the polyurea side) should be contacted with the projectile. Three different scenarios were tested: projectile contacting the steel (polyurea in compression), projectile contacting the polyurea (polyurea in tension), and the polyurea at the area of contact ground off so that the projectile contacted the steel but still put the polyurea in tension. The situation of these preliminary tests is shown in Figure 25.

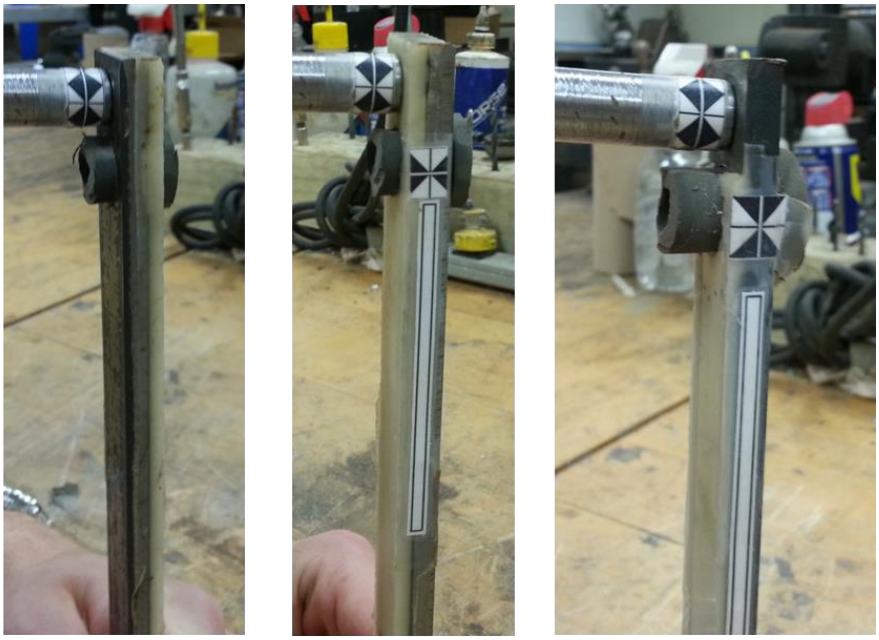

Steel side contact | Polyurea side contact | Steel contact on polyurea side

Figure 25: Contact configuration for preliminary polyurea tests

Preliminary Beam Test Results

Only the peak acceleration will all be reported for each test. The results of situating the beam in the cantilever for the three scenarios portrayed in Figure 25 are displayed in Figure 26. Each configuration was tested twice to determine test scatter. The blue bars show the values for the initial tests and the red bars give the value for the repeat test for each scenario.

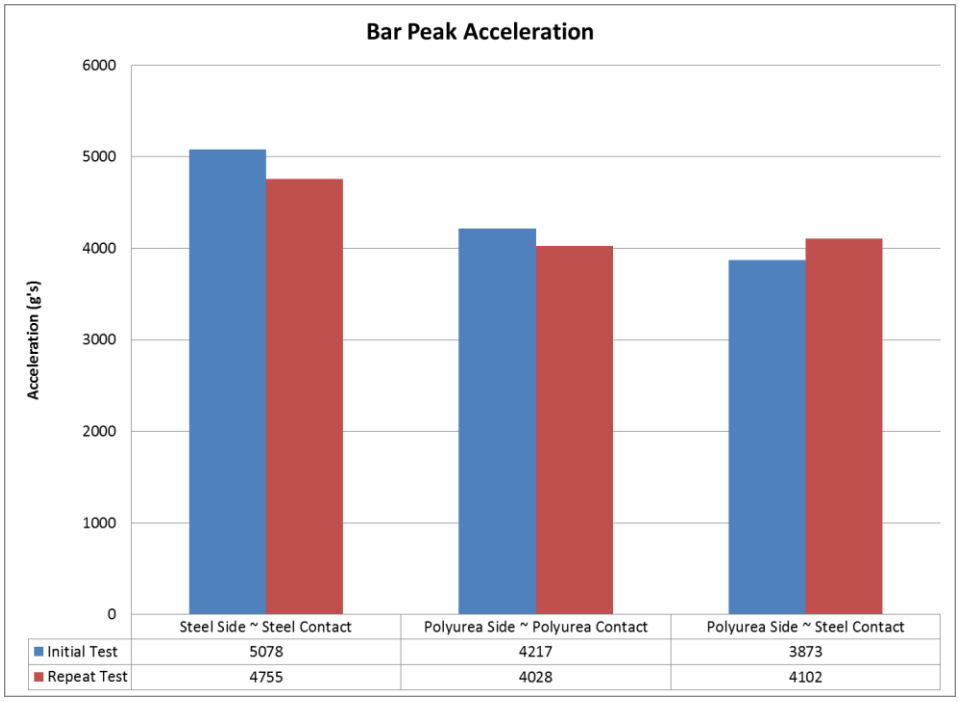

Figure 26: Peak acceleration for preliminary polyurea beam tests

From looking at the figure it is noted that situation of the polyurea side to the oncoming projectile only has a slight effect on acceleration. The slight benefit in acceleration values results from the bar being placed so that upon initial deflection of the beam, the polyurea is put into tension. There does not appear to be any effect on any test output when the polyurea at the tip of the beam is removed, resulting in a projectile to steel interaction. As such, each of the cantilevered beam tests in what follows were conducted with the polyurea side facing the projectile, without removing the polyurea from the tip of the beam.

Cantilevered Beam General Study

The first series of tests run for polyurea coated bars studied the effects of increasing polyurea thicknesses on steel beams of the same outer dimensions. Baseline tests were run with two different bare steel beams to determine the variance in behavior for two different beams of steel cut from the same bar. After these initial tests, three different thicknesses of polyurea were applied to steel beams and tested.

As a quick note, looking at Figure 25, it is seen that there is a target taped to the end of the projectile. For each test the projectile is tracked for an inch of travel using high speed video. The slope of the displacement versus time curve for the projectile is determined to be the velocity of the projectile for each test, and must be in the range of 8.4-8.6 meters per second in order for the test to be accepted. The outline of the tests for the general study is seen in Table 11. Each test is performed twice to display data scatter and repeatability.

Table 11: Test matrix for general polyurea thickness study

Test Number	Bar Number	Steel Mass (g)	Polyurea Mass (g)	Total Mass (w/ accel) (g)	Bar Thickness (mm)	Polyurea Thickness (mm)	Total Thickness (mm)
4	3	302.6	0	314.1	6.22	0.00	6.22
6	3	302.6	0	314.1	6.22	0.00	6.22
8	1	300.3	0	312.5	6.20	0.00	6.20
9	1	300.3	0	312.5	6.20	0.00	6.20
17	2	301.5	12.6	326.8	6.23	1.58	7.81
18	2	301.5	12.6	326.8	6.23	1.58	7.81
24	1	300.3	18.3	329.7	6.20	3.11	9.30
25	1	300.3	18.3	329.7	6.20	3.11	9.30
27	3	302.6	21.4	334.6	6.22	4.76	10.97
28	3	302.6	21.4	334.6	6.22	4.76	10.97

General Study Test Results

At the conclusion of the general study series of tests, as in the preliminary tests, peak acceleration was analyzed and plotted. The graph is shown in Figure 27. The figure shows a very interesting and unexpected result. The tip acceleration of bars coated in polyurea increases with polyurea thickness, and at the final thickness (with the polyurea about two millimeters thinner than the steel) the acceleration level is around 1000g's higher than the baseline steel bar.

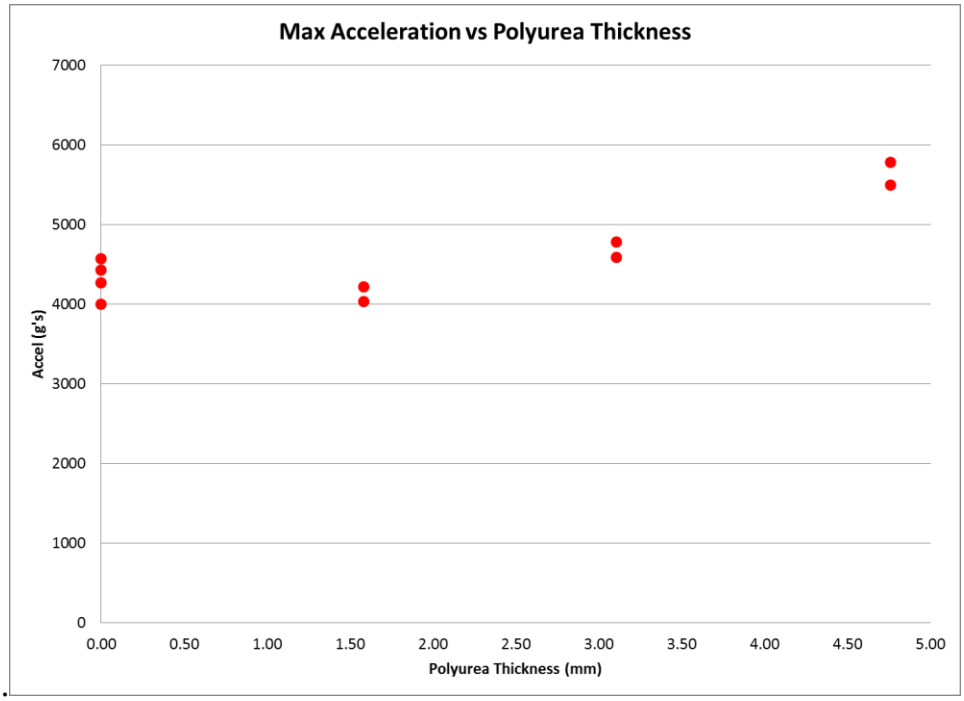

Figure 27: Peak acceleration versus polyurea thickness

Cantilevered Beam Mass Study

After having seen the unexpected trend in polyurea coated beams, it was determined that a series of tests should be run to further explore this behavior. To this end a set of tests was conducted where the mass of each bar was kept constant as the polyurea mass increased. This was performed by using a mill to shave specific thicknesses of metal off of steel beams. A polyurea coat having the same mass as the removed steel was then applied to each beam. The mass of the each beam was kept at the mass of the baseline beam from the first series of tests. The tests were run in the same configuration as the previous series of tests. The matrix of tests is seen in Table 12.

Table 12: Test matrix for polyurea beam mass study

Test Number	Bar Number	Steel Mass (g)	Polyurea Mass (g)	Total Mass (w/ accel) (g)	Mass Ratio (Polyurea/Steel)	Bar Thickness (mm)	Polyurea Thickness (mm)	Total Thickness (mm)
a	3	302.6	0	314.1	0.000	6.22	0	6.22
b	3	302.6	0	314.1	0.000	6.22	0	6.22
c	1	300.3	0	312.5	0.000	6.20	0	6.20
d	1	300.3	0	312.5	0.000	6.20	0	6.20
12	6	281.8	23.4	316	0.083	5.88	3.49	9.37
15	6	281.8	23.4	316	0.083	5.88	3.49	9.37
17	4	273.9	25.8	310.2	0.094	5.68	4.33	10.01
18	4	273.9	25.8	310.2	0.094	5.68	4.33	10.01
19	5	265.2	37.8	313.8	0.143	5.46	5.88	11.34
20	5	265.2	37.8	313.8	0.143	5.46	5.88	11.34
21	5	265.2	37.8	313.8	0.143	5.46	5.88	11.34

Mass Study Test Results

As with the other two cantilever beam studies the acceleration was analyzed at the end of each test. These values were then plotted as a function of the polyurea to steel mass ratio. The results can be seen in Figure 28. It is seen that the acceleration of the beam tip increases for increasing mass ratio, though not as smoothly as it did for the general study.

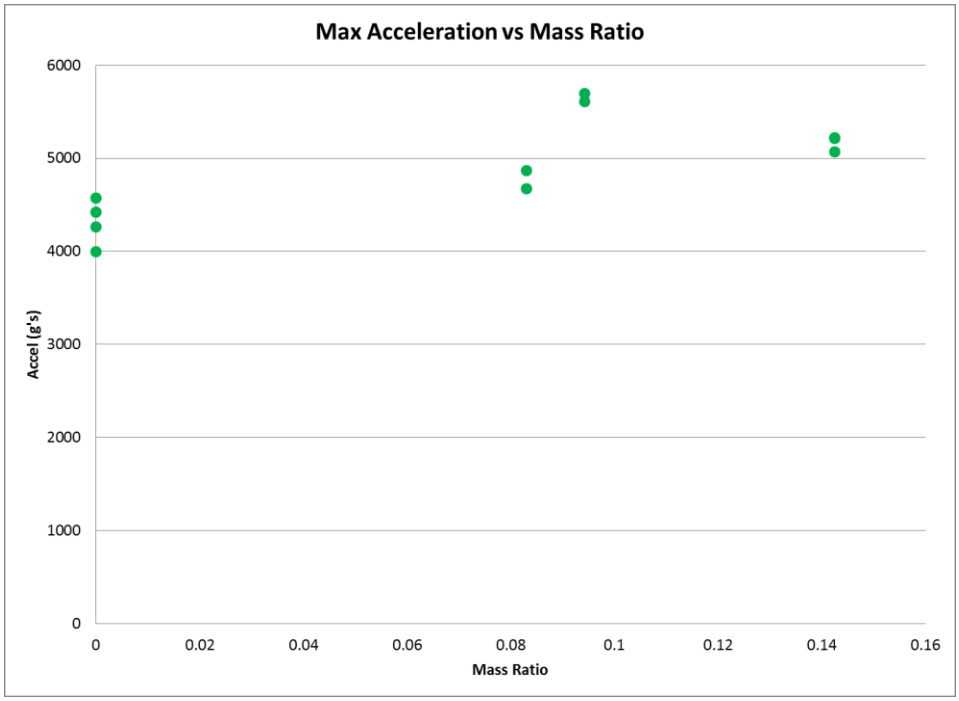

Figure 28: Peak acceleration versus polyurea to steel mass ratio

Similar Mass Ratio Cantilever Beam Study

After the completion of the polyurea-coated cylinder tests in which two plates were explosively loaded, it was seen that by coating an aluminum thin-walled cylinder with polyurea, significant benefits in the peak acceleration are realized. Referring to the results of the polyurea to steel mass ratio study performed with cantilevered beams, this positive impact of the polyurea coating on the cylinders may come as a surprise. It is seen in Figure 28 that a general increase in acceleration is expected as the polyurea to steel mass ratio of a coated beam increases.

In hopes of clarifying this result, a final series of cantilever beam tests were carried out. It was noted that the mass ratios of the beam tests and the cylinder tests were not equivalent with the beams having a polyurea to steel mass ratio in the neighborhood of .08-.15 while the cylinders had a mass ratio anywhere from one to five. To create a more equivalent series of tests, it was necessary to process cantilever beams with a mass ratio in the same neighborhood as that of the cylinders.

These beams were created by cutting the mass of the metal base of the beam by switching the metal from steel to aluminum, and also by decreasing the thickness of the metal from 6.2 millimeters to 3.18 millimeters. An uncoated beam was tested in addition to two beams with mass ratios in the desired range. The test matrix can be seen in Table 13. Each beam was tested twice to show data scatter and repeatability.

Table 13: Test matrix for similar mass ratio cantilever beam study

Test Number	Beam Number	Beam Thickness (mm)	Beam Mass (g)	Polyurea Thickness (mm)	Polyurea Mass (g)	Beam Length (cm)	Beam Total Mass w/ accel (g)	Polyurea/Steel Mass Ratio
1	1	3.18	54.81	0	0	25.4	65.93	0
2	1	3.18	54.81	0	0	25.4	65.93	0
3	2	3.18	54.81	7.77	48.1	25.4	65.93	0.88
4	2	3.18	54.81	7.77	48.1	25.4	65.93	0.88
5	3	3.18	53	14.01	95.5	25.4	159.3	1.80
6	3	3.18	53	14.01	95.5	25.4	159.3	1.80

Similar Mass Ratio Cantilever Beam Study Test Results

At the conclusion of the tests mentioned in Table 13, the acceleration is studied as a function of mass ratio. Two tests are conducted for each beam, and these results are shown in Figure 29.

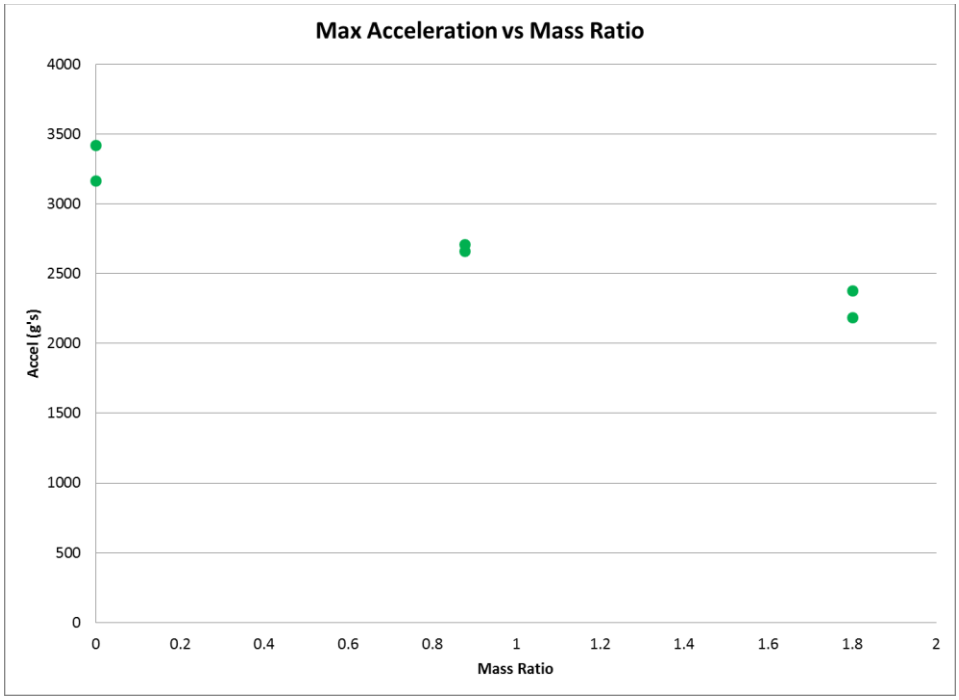

Figure 29: Peak acceleration versus mass ratio for aluminum cantilever beam tests

From viewing the previous figure and comparing it with the trends developed in the steel cantilevered beam tests, it is apparent that a completely different trend has emerged. Whereas the beams with a mass ratio much less than one see increases in the peak acceleration, the beams with mass ratios greater than one see decreases in the same parameter

To develop a better understanding of how all of the polyurea coating results line up, the acceleration values for each series of tests were normalized by setting the acceleration of the uncoated bar or cylinder as the baseline value, and dividing each acceleration value in the series by the acceleration of each test series' respective baseline value. By doing this, a plot was developed that directly compares the effect on acceleration of coating structures in polyurea. This plot is shown in Figure 30.

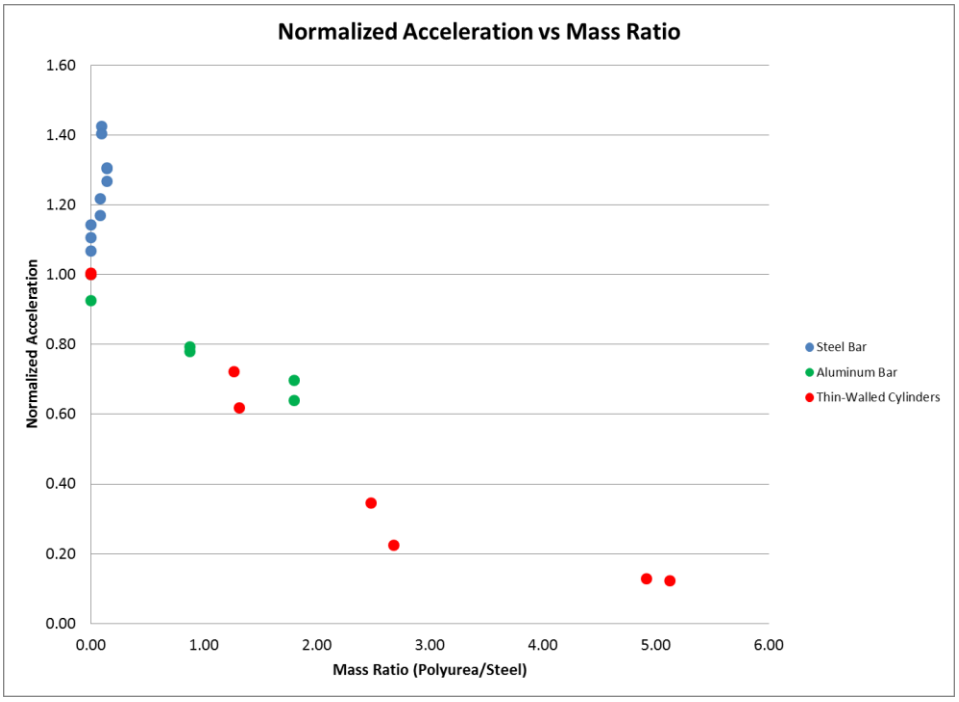

Figure 30: Normalized acceleration versus mass ratio for three test series

In Figure 30, blue is the cantilevered beam tests conducted with steel bars, the red represents the thin-walled cylinders which were blast tested, and green shows the acceleration value of the aluminum cantilevered beams. From this figure, the conclusion is made that the mass ratio of a coated structure has significant importance when considering the possibility of the coating to have an effect on peak acceleration of a structure. Very small mass ratios may indeed have a detrimental, or no, effect on the ability of a structure to effectively absorb a blast load, while a mass ratio greater than one has a positive effect. This result is of significant value as steel plates are a commonly coated material. In order for the coating to have positive effects, an extremely thick coating would have to be applied. On the other hand, when considering very light structures, such as the thin-walled cylinders used in this study, a small amount of polyurea may have a very large effect.

Polyurea-Coated Thin-Walled Cylinder Tests on a Simulated Vehicle

In this section two tests were run using the simulated vehicle set-up previously described. The first test involved connecting the hull of the vehicle to the frame with six aluminum columns. This test served as a "worse-case" scenario in which there was a rigid connection between the hull and the frame. Each column was connected to the hull and the frame. A blast test, using a 40 millimeter SOD and a ten millimeter DOB was performed in the saturated sand test bed described in the mitigation chapters.

The second and final test performed for this section used six thin-walled cylinders coated with polyurea as the connecting elements between the hull and the frame. Each thin-walled cylinder was created with .1millimeter aluminum shim-stock with a height of 38 millimeters and a 66 millimeter outer diameter. All six cylinders were coated with three grams of polyurea, resulting in an approximately one to one

polyurea to aluminum mass ratio. The cylinders were connected to both the hull and the frame so that the cylinders could crush and stretch during the test, maximizing the amount of acceleration mitigation they have to offer.

As in each of the previous simulated vehicle tests, a 4.4 gram charge is used to supply the blast load. Two accelerometers are embedded in rubber mechanical filtering mounts and four targets on the frame are used for high-speed video tracking. Pictures of the two plate set-ups can be seen in Figure 31 and Figure 32.

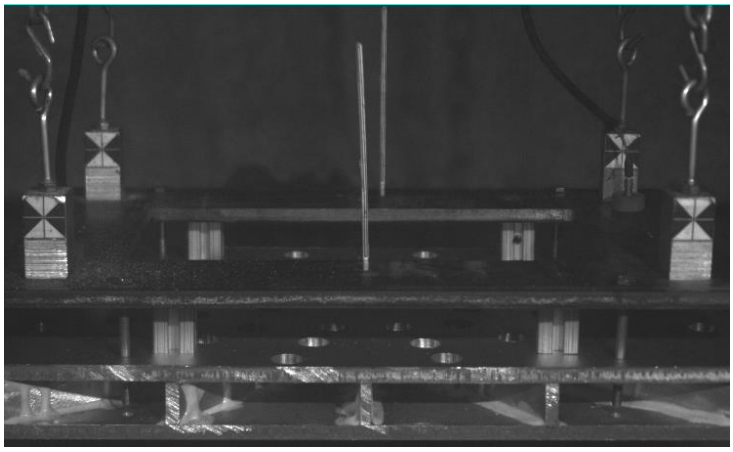

Figure 31: Plate set-up for solid column test

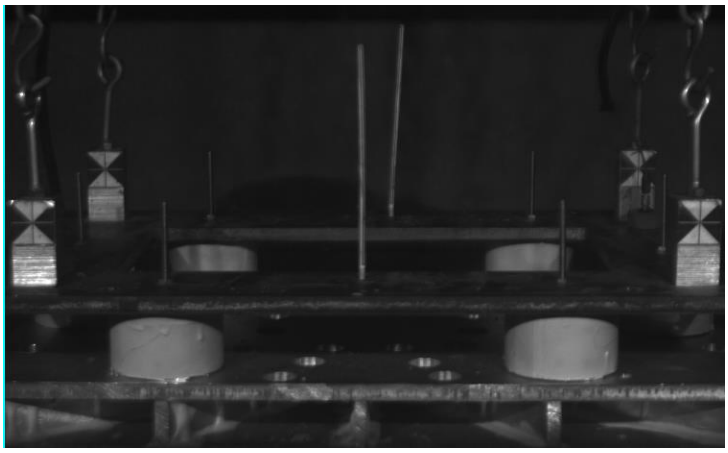

Figure 32: Plate set-up for polyurea-coated cylinder test

Polyurea-Coated Thin-Walled Cylinder Test Results

After completing each of the two tests, the initial data verification steps were taken by comparing the displacement curve developed from the high speed video to the double integrated acceleration signal. In order for the data to have been considered worthy of reporting, the two displacement signals must show strong correlation.

Once the acceleration data has been verified, it is of interest to compare the two acceleration profiles for each test. To this end, the acceleration profile was taken from the same accelerometer for each of the two tests and plotted on the same graph.

The comparison between the non-deforming column test and the polyurea-coated thin-walled cylinder test is shown in Figure 33.

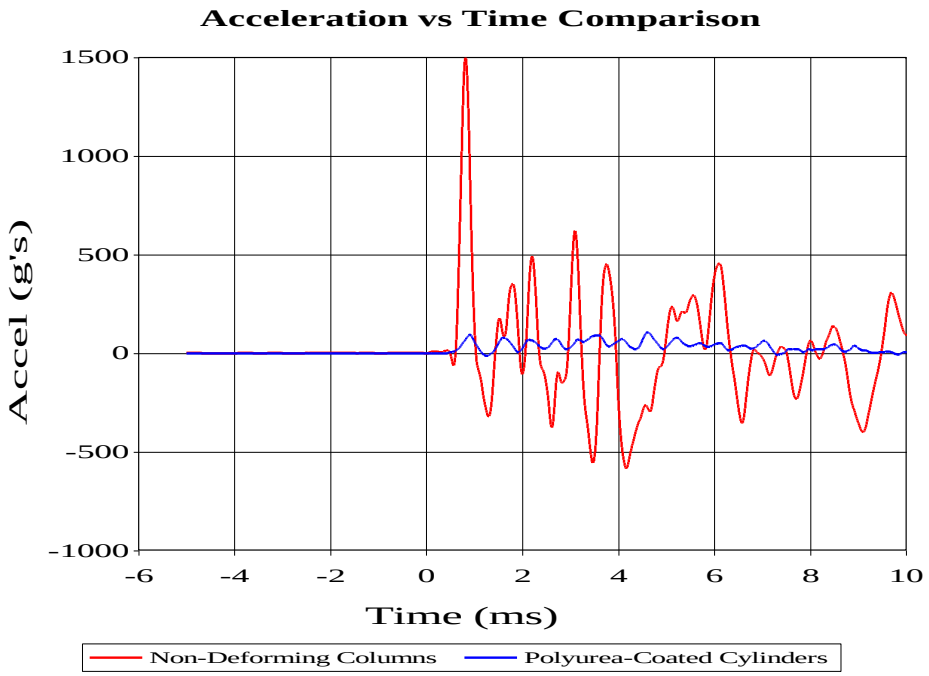

Figure 33: Acceleration versus time comparison for non-deforming columns and polyurea-coated cylinders

It is evident from viewing Figure 33 that an immense benefit comes from using thin-walled cylinders as a mitigation technique. This information however was already known from previous tests. Perhaps a more telling comparison can be made by studying how the accelerations of the simulated vehicle frame compare between the coated and uncoated cylinder tests. To perform this comparison, it is necessary to view a number of test results as a test with the cylinder number and geometry of the final test was not conducted previously in the mitigation study. As such, the information in Table 14 is presented so that a better understanding of the material may be obtained.

Table 14: Comparable test results for numerous simulated vehicle test studies

Connection Method	Number of Elements	HOT (mm)	Hull Attached	Frame Attached	Acceleration (g's)	Impulse (N-s)	Kinetic Energy (J)
Air	-	38	-	-	1458	70.56	178.00
Aluminum Cylinder	4	38	Yes	No	121.5	58.01	118.48
Aluminum Cylinder	4	38	Yes	Yes	89	51.27	89.40
Aluminum Cylinder	6	25	Yes	No	141.5	55.02	102.61
Solid Columns	6	38	Yes	Yes	1641	76.24	181.64
Coated Cylinder	6	38	Yes	Yes	108	52.96	87.65

Studying Table 14, a number of observations are made. Initially it is seen that by substituting non-deforming columns in the place of air as the material in between the hull and the frame, comparable values in terms of acceleration result. Moving

beyond these baseline comparisons, it is noted that while the polyurea coated cylinders perform admirably with extremely low acceleration, the drastic drop from the bare cylinder case is not realized. According to the tests conducted with the reduced circular plates, a 20-40 percent drop in acceleration should have occurred between the bare cylinder and the coated cylinder tests.

While slightly unexpected, the above results are not discouraging for a couple of reasons. The first reason for enthusiasm with regards to polyurea coated cylinders is due to the fact that while the bare aluminum thin-walled cylinders crushed completely during the blast tests (see Figure 16), the polyurea coated cylinders crushed approximately one-half of their height during the initial blast, and recovered over 90 percent of their initial height by the end of the blast event (see Figure 34). The relatively small initial deformation will be treated later, but at this point, the fact that the polyurea coated cylinders recover such a large percentage of their initial shape may result in a vehicle that is structurally able to drive away from a blast event.

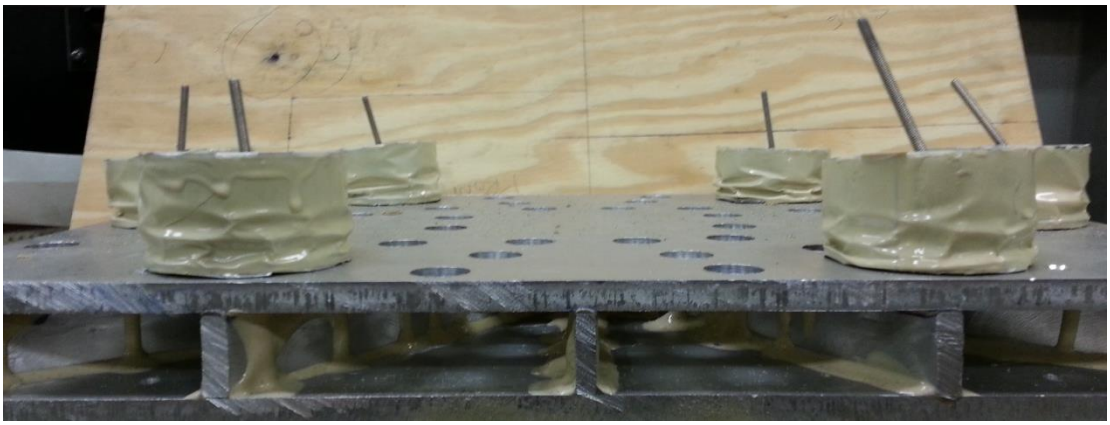

Figure 34: Recovered height of the polyurea-coated cylinders after blast testing

Looking at Figure 34, it is clearly seen that deformation of the coated cylinder occurs primarily at the lower half of the cylinder. This fact will be used in conjunction with information from the small circular plate tests to realize a further advantage of using polyurea coated cylinders as opposed to bare aluminum cylinders as a mitigation technique. The statement that needs to be made about the coated cylinder tests using the reduced-sized circular plates is that the acceleration of the baseline (uncoated cylinder) tests was dramatically greater than that of the simulated vehicle baseline (uncoated cylinder) tests. Comparing acceleration values from Figure 22 and Table 14, it is seen that the acceleration of the bare cylinder test using the circular plates and a single cylinder is in the neighborhood of 3500g's while the acceleration using bare cylinders on the simulated vehicle plates lies in the area of 100-150g's.

The increased level of loading of the smaller plates is backed up by the high speed video, in which the polyurea coated cylinders crush completely before recovering some of their height. In the case of the simulated vehicle tests, it was pointed out that the cylinders crush only partially before recovering almost all of their height. It was initially curious that a 20-40 percent acceleration drop between uncoated and coated cans did not appear in the simulated vehicle test. However, after looking at the data in its entirety, it is not that surprising, as the acceleration levels in the simulated

vehicle using bare cylinders might not be sufficient to bring out the full benefit of coating the cylinder with polyurea. The next section of the paper will study the non-linear mitigation behavior of polyurea coated thin-walled cylinders.

Nonlinear Acceleration Mitigation Benefit of Polymeric Coated Thin-Walled Cylinders

In order to tease out the previously hypothesized nonlinear acceleration mitigation benefit of polymeric coated thin-walled cylinders, a series of blast tests was run where the polyurea to aluminum mass ratio was kept constant (along with the other test parameters such as SOD and DOB) while the charge mass was varied. Tests with coated and uncoated cylinders were run to compare how the acceleration varied between the coated and uncoated cylinders as the charge size changes. The test matrix for this series of tests is shown in Table 15.

Table 15: Test matrix for nonlinear study

Test Number	Charge Mass (g)	DOB (mm)	SOD (mm)	# of Cylinders	Cylinder Material	Cylinder OD Before Coat (mm)*	Cylinder ID (mm)*	Cylinder Height (mm)*	Cylinder Mass (g)*	Polyurea Mass (g)	Mass Ratio (P/S)
1	2.2	10	40	1	Aluminum	66	65.8	38.1	5.37	2.37	0.79
2	2.2	10	40	1	Aluminum	66	65.8	38.1	5.58	2.58	0.86
3	1.75	10	40	1	Aluminum	66	65.8	38.1	5.75	2.75	0.92
4	1.75	10	40	1	Aluminum	66	65.8	38.1	5.02	2.02	0.67
5	1.25	10	40	1	Aluminum	66	65.8	38.1	5.63	2.63	0.88
6	1.25	10	40	1	Aluminum	66	65.8	38.1	5.27	2.27	0.76
7	0.75	10	40	1	Aluminum	66	65.8	38.1	5.46	2.46	0.82
8	0.75	10	40	1	Aluminum	66	65.8	38.1	5.47	2.47	0.82
9	0.75	10	40	1	Aluminum	66	65.8	38.1	3	0	0.00
10	0.75	10	40	1	Aluminum	66	65.8	38.1	3	0	0.00
11	1.25	10	40	1	Aluminum	66	65.8	38.1	3	0	0.00
12	1.25	10	40	1	Aluminum	66	65.8	38.1	3	0	0.00
13	1.75	10	40	1	Aluminum	66	65.8	38.1	3	0	0.00
14	1.75	10	40	1	Aluminum	66	65.8	38.1	3	0	0.00
15	2.2	10	40	1	Aluminum	66	65.8	38.1	3	0	0.00
16	2.2	10	40	1	Aluminum	66	65.8	38.1	3	0	0.00

A total of 16 tests were run, eight tests with cylinders having a polyurea to aluminum mass ratio of about 0.75 and eight tests with uncoated cylinders. Two tests were run for each type of cylinder at charge sizes of 0.75 grams, 1.25 grams, 1.75 grams, and 2.2 grams of explosive. The simplified hull/frame plate combination used in conjunction with a single cylinder was used to collect data. As in the other studies, in order for the data to be reported, the displacement profiles obtained from the high speed camera and the accelerometer must match.

Nonlinear Effect Results

At the conclusion of the test series to determine the non-linear acceleration mitigation effect on coating thin-walled cylinders with polyurea, two plots were created that show the effect quite clearly. In Figure 35 , the difference between the peak acceleration of the coated cylinder and non-coated cylinder is plotted for each charge mass. Figure 36 shows the final recovered height of the cylinder.

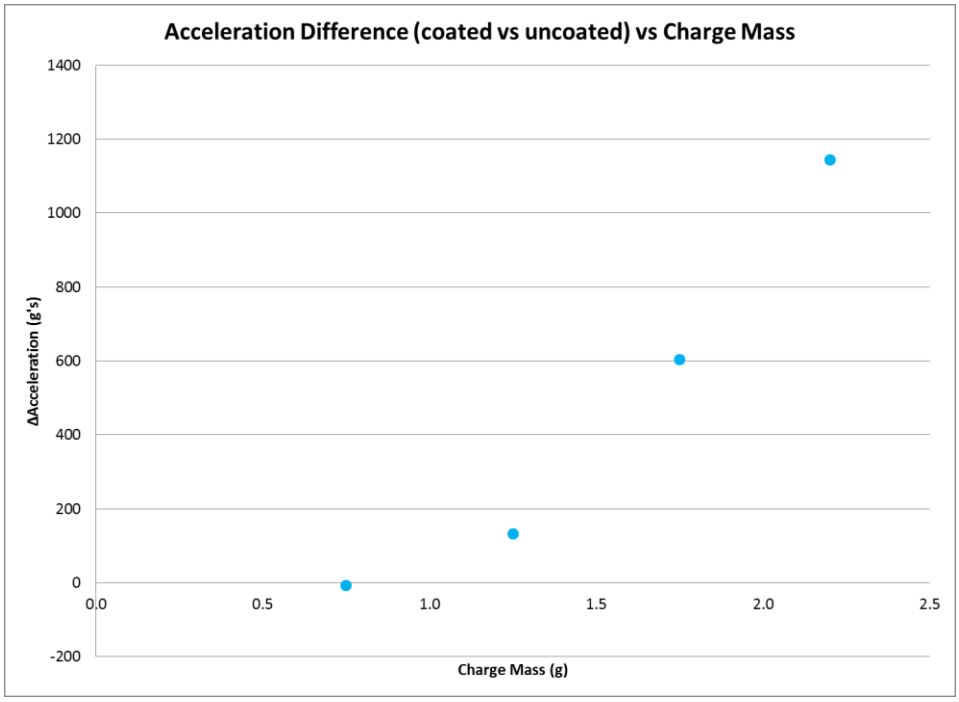

Figure 35: Difference in peak acceleration between coated and uncoated cans versus charge mass

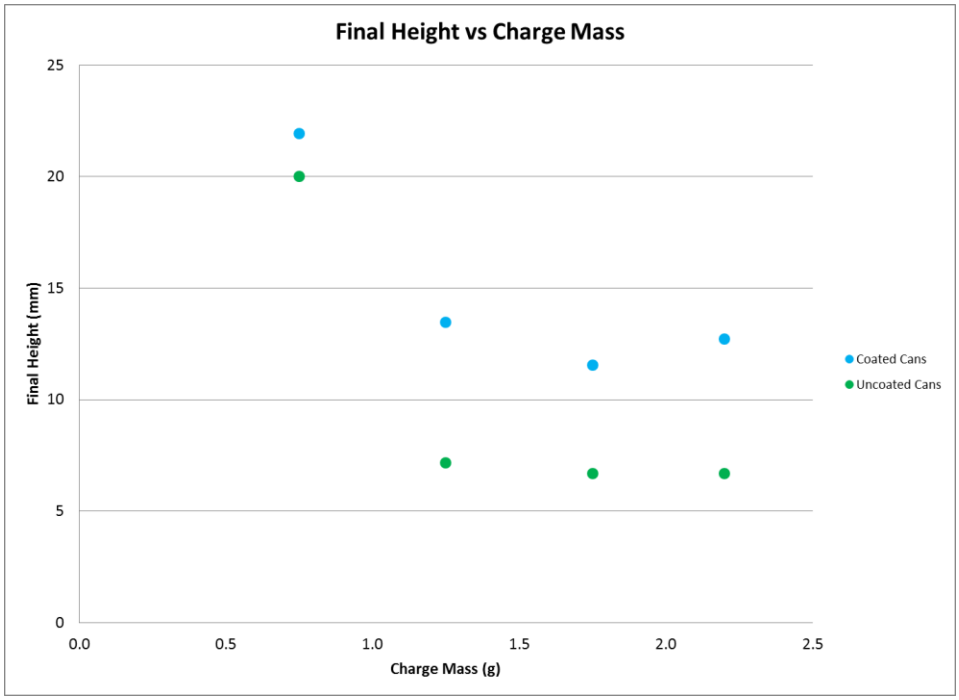

Figure 36: Final recovered height of the blast loaded cylinder versus charge mass

Looking at the previous two figures a complete picture of the non-linear effect of polymeric coatings on peak acceleration can be determined. It is seen that as charge mass increases, the recovered height of the polymeric cylinder is steadily greater than the uncoated can. It seems that during maximum crushing scenarios, coated cylinders

will recover to around a 13 millimeter height as compared with uncoated cylinders which only recover to around a seven millimeter final height. In terms of acceleration, it is seen that at smaller charge sizes, the acceleration profiles of coated and uncoated cylinders are essentially the same. However as the charge mass increases, the polyurea cylinder acts to better mitigate the acceleration of the frame.

Conclusions

At the outset of this research program a couple of broad goals were laid out. Initially it was desired to develop an effective means of acceleration mitigation for use on explosively loaded vehicles. To achieve these goals, small-scale explosive testing was conducted in saturated sand. Simulated vehicles and more simply shaped plate combinations were utilized to study the effects of various mitigation techniques.

It was shown in this paper that acceleration levels, reported at full-scale values, can be decreased from 150 g's to levels around 10 g's by application of thin-walled cylinders alone. With the addition of a polyurea coating to the thin-walled cylinders, at very high acceleration levels, an 80-90 percent decrease in acceleration may also obtained. Furthermore, numerous geometric properties of thin-walled cylinders were experimented with showing marginal differences to the baseline acceleration mitigation. It is believed that some combination of all of the best-case scenarios for each geometric condition, in addition to a polyurea coating, applied to the cylinders would result in a mitigation technique that would allow for complete survivability of an explosive event.

It was also found, though not reported in depth, that significant improvements in impulse and kinetic energy may also be made through the use of thin-walled cylinders. Previous research has been conducted in the Dynamic Effects Lab that used shaped hulls to decrease impulse on simulated vehicles to safe levels. In addition to using shaped hulls, the thin-walled cylinders may give further aid in preventing impulse related injuries to passengers in blast-loaded vehicles.

It was also desired that a greater understanding of the effects of polyurea applied to structures be developed. Some basic research was performed through the use of polyurea coated steel and aluminum cantilever beams. The cantilever beams were tested dynamically through the use of a high-pressure gas gun, and produced information leading to the following conclusion; that in the elastic range of material response to dynamic loading, bare steel has lower levels of acceleration, velocity, peak displacement, and half-wavelength time than steel bars coated with a thin layer of polyurea. For the beneficial effects of polyurea coatings to appear, the mass ratio of polyurea to metal must be increased to the order of magnitude of one or higher. It was found that at higher mass ratios, the acceleration of cantilever beams and explosively loaded plates both show similar decreasing trends as the mass ratio of the polyurea to metal increases.

Finally, a very important conclusion was made with regard to coating thin-walled cylinders with polyurea. It was seen that at low acceleration levels, polyurea coated and uncoated cylinders both mitigate acceleration equally well even if the deformation of the coated cylinder was significantly less. This minimal deformation would result in a vehicle being structurally sound enough to drive away from an

explosive event. In addition to this powerful fact, the data from a multitude of tests was used to come to the conclusion that as the explosive event becomes more violent, the polyurea coated cylinders can be expected to act to mitigate more of the acceleration, creating non-linearity in the mitigation of acceleration a vehicle by using polyurea coated thin-walled cylinders.

Bibliography

[1] Fiskum, G., Hazelton, J., Gullapalli, R., Fourney, W.L. "Animal Model of Mild Brain Injury Caused by Blast-Induced Hyper-Acceleration Relevant to IED-Targeted Military Vehicles."

[2] Nelson, N.W., Lamberty, G.J., Sim, A.H., Doane, B.M. "Blast from the Past and Present: A Review of Blast-Related Injury in Military Personnel and Veterans." *Neuropsychological Practice with Veterans* (2012): 145.

[3] Fourney, W. L., Leiste, U., Bonenberger, R., Goodings, D. J. "Mechanism of Loading on Plates Due to Explosive Detonation." Fragblast, Vol. 9, No. 4, December 2005.

[4] Genson, K. (2006). "Vehicle Shaping for Mine Blast Damage Reduction." University of Maryland: College Park.

[5] Benedetti, R., Fourney, W.L. (2010) "Mitigation of Loading on Floorboards in Light Armored Vehicles Subjected to Explosive Loading." University of Maryland: College Park.

[6] Leiste, U. (2012). "Experimental Studies to Investigate Pressure Loading on Target Plates." University of Maryland: College Park.

[7] Lamb, C., Schmidt, M., Fitzsimmons, B. "MRAPS, Irregular Warfare, and Pentagon Reform." Institute for National Strategic Studies National Defense University. Volume 6, June 2009.

[8] Alghamdi, A.A.A. "Collapsible Impact Energy Absorbers: An Overview." Thin Walled Structures, Vol. 39, No. 2, February 2001.

[9] Yuen, S.C., Nurick, G.N. "The Energy-Absorbing Characteristics of Tubular Structures with Geometric and Material Modifications: An Overview." Applied Mechanics, Vol. 69, No. 2, March 2008.

[10] Gupta, N.K., Sekhon, G.S., Gupta, P.K. "Study of lateral compression of round metallic tubes." Thin Walled Structures, Vol. 43, No. 6, December 2005.

[11] Shim, V.P.W, Stronge, W.J. "Lateral crushing in tightly packed arrays of thin-walled metal tubes." International Journal of Mechanical Science, Vol. 28, No. 10, June 1986.

[12] Gupta, N.K., Velmurugan, R. "An analysis of axial crushing of composite tubes." Journal of Composite Materials, Vol. 31, No. 13, July 1997.

[13] Palanivelu, S., Paepegem, W.V., Degrieck, J., Vantomme, J., Kakogiannis, D., Ackeren, J.V., Hemelrijck, D.V., Wastiels, J. "Comparison of the crushing performance of hollow and foam-filled small-scale composite tubes with different geometrical shapes for use in sacrificial cladding structures." Composites Part B: Engineering, Vol. 41, No. 6, September 2010.

[14] Palanivelu, S., Van Paepegem, W., Degrieck, J., Van Ackeren, J., Kakogiannis, D., Van Hemelrijck, D., Wastiels, J., Vantomme, J. "Experimental study on the axial crushing behavior of pultruded composite tubes." Polymer Testing, Vol. 29, No. 2, April 2010.

[15] Palanivelu, S., Van Paepegem, W., Degrieck, J., Reymen, B., Ndambi, J.M., Vantomme, J., Kakogiannis, D., Wastiels, J., Hemelrijck, D.V. "Close-range blast loading on empty recyclable metal beverage cans for use in sacrificial cladding structure." Engineering Structures, Vol. 33, No. 6, June 2011.

[16] Theobald, M.D., Nurick, G.N. "Numerical investigation of the response of sandwich-type panels using thin-walled tubes subject to blast loads." International Journal of Impact Engineering. Vol. 34, No.1, January 2007.

[17] Theobald, M.D., Nurick, G.N. "Experimental and numerical analysis of tube-core claddings under blast loads." International Journal of Impact Engineering. Vol. 37, No.3, March 2010.

[18] Yi, J., Boyce, M.C., Lee, G.F., Balizer, E. "Large deformation rate-dependent stress-strain behavior of polyurea and polyurethanes." Polymer, Vol. 47, No.1, January 2006.

[19] Roland, C.M., Twigg, J.N., Vu, Y., Mott, P.H. "High Strain Rate Mechanical Behavior of Polyurea." Polymer, Vol. 48, No.2, January 2007.

[20] Tekalur, S.A., Shukla, A, Shivakumar, K. "Blast resistance of polyurea based layered composite materials." Composite Structures, Vol. 84, No.3, July 2008.

[21] Ackland, K., Anderson, C., Ngo, T.D. "Deformation of Polyurea-Coated Steel Plates under Localized Blast Loading." Impact Engineering, Vol. 51, January 2013.

[22] Brodrick, T.J. "Mitigation of Frame Acceleration Induced by a Buried Charge." Diss. 2010.

[23] Fourney, W. L., Leiste, U., Bonenberger, R., Goodings, D. J. "Explosive Impulse on Plates." Fragblast, Vol. 9, No. 1, December 2005.

[24] Taylor, L.C., Skaggs, R.R., Gault, W. "Vertical Impulse Measurement of Mines Buried in Saturated Sand." Fragblast, Vol. 9, No.1, March 2005.

[25] PCB Piezotronics, Shock ICP Model: 350B04. (2013). Retrieved August 20, 2013 from <http://www.pcb.com/products.aspx?m=350B04#.UhOiuZLVAsI>

[26] RP-501 Economy EBW Detonator. (2011). Retrieved August 20, 2013 from <http://www.teledynerisi.com/products/0products_1ebw_page28.asp>

[27] HM-VK Ultra high strength handmix polyurea elastomer. (2013). Retrieved August 26, 2013 from <http://www.specialty-products.com/pdf/tech-data/polyurea/HM-VK%20Preliminary.pdf>

[28] Plunkett, R. Lee, C.T. (1968) "Length Optimization for Constrained Viscoelastic Layer Damping." Minnesota University Minneapolis Department of Aeronautics and Engineering Mechanics: Minneapolis.

[29] Bonsmann, J.M. “Small Scale Testing to Study Mitigation of Acceleration on Simulated Vehicles.” Diss. 2013.

[30] Bonsmann, J.M., Fourney, W.L. “An Examination of the Factors Affecting the Loading on a Vehicle Subjected to the Detonation of a Buried Mine.” Blasting and Fragmentation, Vol. 6, No. 3, December 2012.